Synthesis of ^{13}C-Labelled 2-Pyrones: Towards Imaging in Biomedical Applications.

Mary Paymwa Luka-Anzah Kagoro

PhD

University of York

Chemistry

July 2018.

Abstract

The project examines the synthesis of antimicrobial ^{13}C-labelled 3/5-alkyl-6-styryl-2-pyrone based on the known pharmacological activities exhibited by this class of compounds. The compounds were designed to be employed as hydrogenative 'hyperpolarizable' imaging agents in cell-based assay to characterise their interaction with their cellular receptor in bacterial cells. The targeted compounds would therefore be potential drug candidates and also imaging agents and were therefore screened for *in-silico* druglikeness. They exhibited good to excellent physicochemical, solubilities and toxicological properties. Their binding affinity profile was evaluated employing the same protein (human tyrosyl-DNA phosphodiesterase) and it was found that 5-decyl-6-styryl-2-pyrone **133e** had a higher binding affinity than 5-benzyl-6-styryl-2-pyrone **133d**. 5-Pentyl-6-styryl-2-pyrone **133c** was less effective than both **133e** and **133d**. Hence 5-decyl- and 5-benzyl-6-styryl-2-pyrone were selected as potential imaging agents.

The selected potential imaging agents were synthesized in five steps employing [^{13}C-1,3]-diethyl malonate, haloalkane (benzyl chloride and 1-bromodecane) and methyl propiolate leading to an overall yield of 17%. Beside the labelled compounds, the optimization procedure led to the synthesis of several new compounds in moderate to good yields. The key step in the synthetic route is the Sonogashira cross-coupling between 3-alkyl-6-chloro-2-pyrone-^{13}C-2 and phenyl acetylene to afford the targeted imaging agents **168/169a-b** in yields ranging from 52-69%. The project led to the discovery of a novel room temperature Pd/Cu-catalysed (1,5)-sigmatropic shift of the phenylacetylene moiety. Furthermore, the targeted compounds were evaluated for their proton signal enhancements on hydrogenation using parahydrogen in the presence of a cationic Rh catalyst. An enhancement of 92-100% was observed with a relaxation time of 140 seconds. Polarization transfer from parahydrogen to the ^{13}C-isotopically labelled carbon at low fields of (50 and 100 gauss) were observed. Therefore, the designed and synthesized ^{13}C-isotopically labelled imaging agents can be employed both as ^{1}H and ^{13}C imaging agents.

Table of Contents

List of Figures

List of Schemes

List of Tables

Acknowledgements

I would like to thank my two supervisors, Ian Fairlamb and Simon Duckett, for giving me the opportunity to be part of this project. It was a pleasure to work under their joint supervision and I am hugely grateful for the insightful help and advice, and for giving me the chance to work independently and creatively.

I must thank all the fantastic people in both the Fairlamb and SBD groups who I have been lucky enough to work with and who have made my time in York so enjoyable. I would especially like to thank the members of the Fairlamb group in particular: Josh, Alan and Kate (for showing me the way things are done), Charlotte (for keeping things running smoothly), Evans, Anders, George Platt (for being a friend), Neil, and George Clark.

For the invaluable technical help and support I have received throughout this project, warm thanks must go to Heather Fish, Pedro Aguilar and Alex Heyam (NMR), Karl Heaton (MS), Adrian Whitwood (XRD), and Graeme McAllister (CHN).

I feel fortunate for the support of my family particularly my Kids (Kuyet and Martin) that I had to leave back in my country; due to financial constraints. I would also like to appreciate my friends and colleagues: Talatu Dashal, Dr. A. M. Lohdip, Dr. J. J. Gongden and a host of others too numerous to mention here. I will also want to appreciate the family I made in York; Peter, Joy and their kids and Pastor Reuben and all the members of Hope Centre Church. I feel highly favoured to have met you people and how you helped shaped my growth. To my sisters and brothers, I would not have been able to complete this study without you going out of your ways to make it easier for me to study by looking after my kids and joining me in prayers always. I particularly appreciate for Mr & Mrs. Sunday Adelaiye for your sacrifices and patience in taking care of Kuyet and Martin Luther.

Finally, I would like to appreciate Schlumberger Foundation Faculty for the Future for sponsorship without which this study would have been impossible.

Author's Declaration

The work presented in this thesis is my own except where referenced or clearly indicated in the body of the text. The work was carried out at the University of York between August 2014 and December 2017 and has not previously been presented for an award at this or any other university.

Mary Paymwa Luka-Anzah Kagoro

MSc. Organic Chemistry

July 2018

1.1 Introduction to Drug Discovery

Worldwide, one death in every three is caused by infectious and communicable diseases such as HIV/AIDS, tuberculosis (TB) and malaria.[1] In 2010, a total of 52.8 million deaths occurred globally with TB killing 1.2 million and HIV/AIDS killing 1.5 million people.[2] Some of these deaths could have been prevented with existing drugs. There is therefore an urgent need to develop new antibiotics to replace the ones been knocked off by antimicrobial resistance. However, the process of bringing a new antibiotic medication to the market is challenging, cost-intensive and takes on the average eight to twelve years (**Figure 1**).

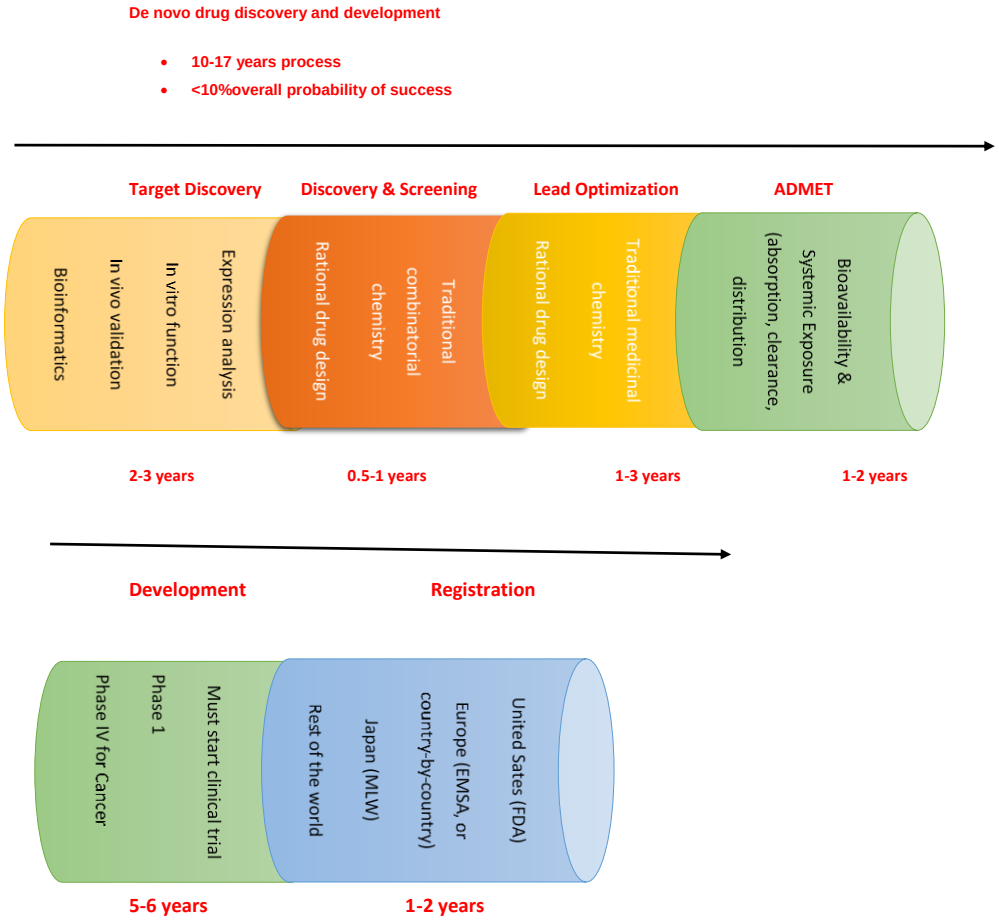

Figure 1: Drug discovery cycle.[3]

Data has showed that it is only one in five-ten thousand screened compounds make it to approval.[3] A common trend in the development of new drugs, hence the need to adopt new strategies to make the drug discovery process more efficient. The drug discovery process begins with the identification of a vital protein essential for the pathogens existence and the screening of many compounds to find hits. These hits are further optimized to improve drug properties such as potency, safety and bioavailability. The lead compounds are then further subjected to clinical trials.

For just a moment 'imagine seeing a specific molecular target in a live animal, following a drug's distribution in the same animal and quantitating the drug's direct effect on the target, all in a matter of minutes.[4] Though a hard concept to imagine three decades ago is now made more possible by new enabling imaging modalities and molecular probes.[5] The imaging modalities are radiography, magnetic resonance imaging, ultrasound, elastography, tactile imaging, thermography, medical photography and nuclear medicine functional imaging techniques as positron emission tomography (PET) and single-photon emission computed tomography (SPECT).[6] None of the several imaging modalities can effectively answer all the questions and different imaging techniques are complementary rather than competitive.

1.2 Introduction to Image-guided Drug Discovery

MI is now a very attractive tool in biomedical research ranging from preclinical research to early clinical trials. Molecular imaging techniques detect, identify and characterize biologic events at molecular level using a remote sensing device without perturbing the system being imaged.[1,8] The cellular events imaged could be a biomarker of a disease, drug metabolite, protein—protein interaction, protein-small molecule interaction and even gene interaction when cells meet each other. Most MI procedures are carried out by first introducing the molecular probe (a small molecule) into the living subject which enables the visualization of the molecular target by acting as a ligand, possibly modifying the target and enabling it to be directly visualized using the ligand assay (**figure 2**).[9] In some cases, the probe could be a pharmaceutical agent providing a link with pharmacology. A probe (the ligand) must bind preferentially to the intended cellular receptor and be detected by the

ligand assay; these probes are referred to as imaging agents, tracers, radiopharmaceuticals, radiotracers, and smart probes. The assay detects the complex formed between the probe and the intended target.

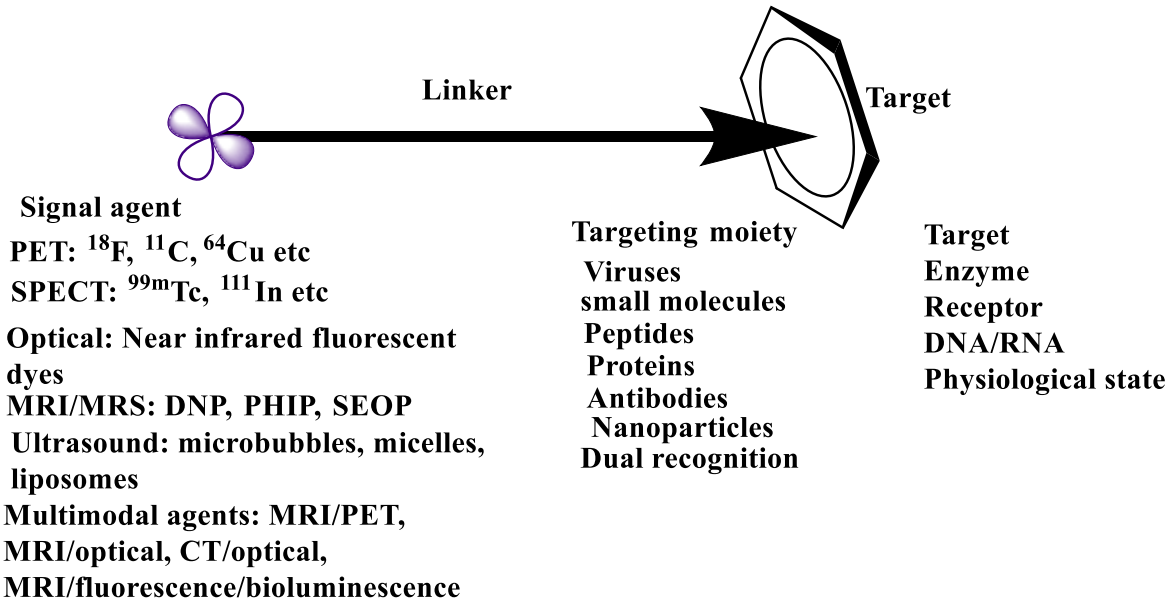

Figure 2: Schematic representation of molecular imaging probe.[9]

Molecular imaging is an attractive modality aimed at the early detection of diseases such as cancer,[10] inflammations,[11] and neurodegenerative disorders,[12] and therapeutic response.[13] The field emerged because of a paradigm shift in healthcare that is all inclusive for the prediction and prevention of diseases. By this approach biomedical researchers can now visualize molecular events noninvasively, repeatedly and continuously in a living system using molecular contrast agents, reporters or probes. MI agents could provide answers to complex biological, physiological and pathological events in live organisms.[14]

In drug discovery, any technique that will provide information on whether the drug has effectively reached its target, the dose required to achieve the right biological effect and how the target is expressed, is very important in early drug development as illustrated in **Figure 3**.

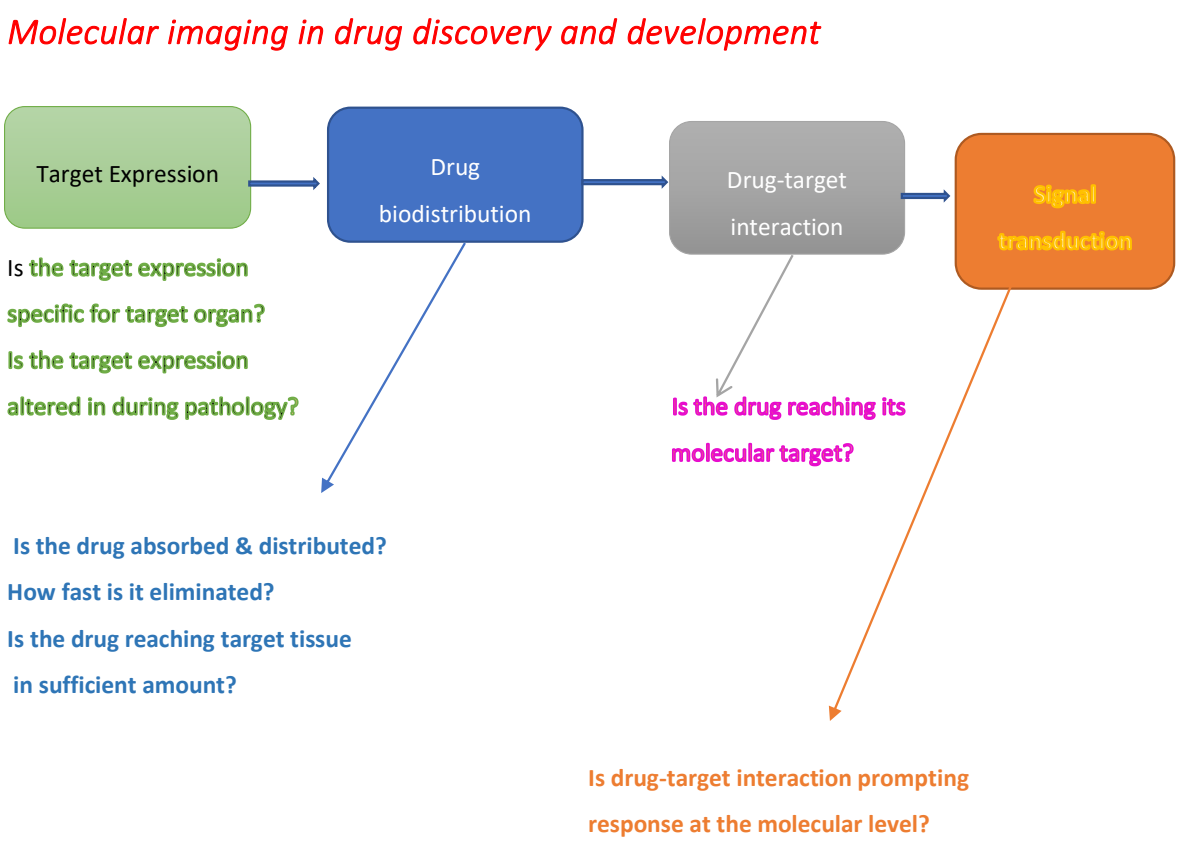

Figure 3: Information relevant for drug discovery and development provided by molecular imaging.[15]

MI provides data that aids drug candidate choice, lower risks of failure and assist in dose regimen choices. The use of MI in drug discovery was expected by pharmaceutical industries to reduce the number of compounds failing in late phases of drug discovery (lower attrition rates) and hence reduce cost.

1.2.1 Radionuclide Imaging and Drug Discovery

Nuclear molecular imaging techniques of positron emission tomography (PET) and single photon emission computed tomography (SPECT), allow visualization and quantification of a variety of pathophysiological processes. It is employed primarily in validating drug targets, safety, and efficacy. They provide information on biomarkers of diseases that allow the evaluation of drug response in the brain and other organs.

The measurement of the pathway of a radiolabelled drug provides data on the pharmacokinetics and pharmacodynamics parameters of the drug. It also

provides data on efficacy and fractional occupancy of a specific target by the drug.

Receptor-based probes make up sixty percent of all SPECT and PET agents in the database of the Molecular Imaging and Contrast Agent Database (MICAD).[16] Example is ^{18}F labelled thymidine radiotracers used to study tumour cell growth (**Figure 4)**. ^{11}C-labelled amino acids (**Figure 4**) are been investigated as biomarkers of proliferating cells.[17]

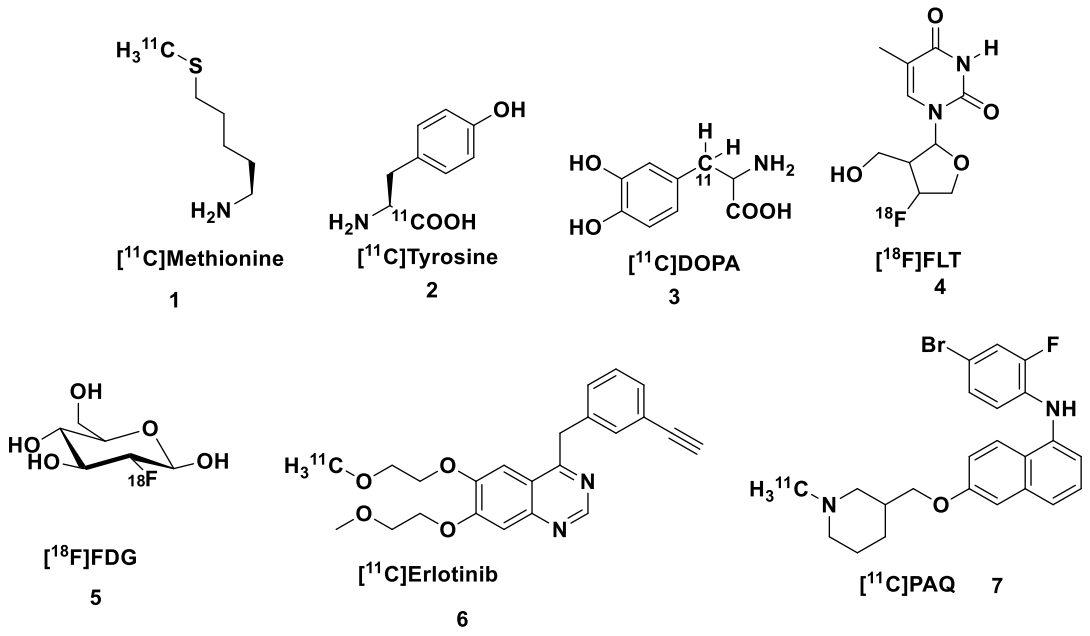

Figure 4: Examples of PET MI Probes.

Angiogenesis, the formation of new blood vessels is critical to tumour growth and initiation of metastasis.[18] The development of drugs that target angiogenic agents are useful for visualization of angiogenic process in live organisms. ^{99m}Tc-labelled growth factor protein over expression in tumour cells are biomarkers of tumour cells in mice.

Apoptosis is programmed cell death on treatment certain anticancer drugs. Annexin V and other anticancer drugs that function in a similar manner bind to phosphatidylserine (PS). Radionuclide imaging of SPECT and PET labelled Annexin V or similar drugs are employed to visualize the onset of apoptosis after anticancer treatment.[19]

1.2.2 Optical Molecular Imaging and Drug Discovery

Optical MI technique uses light to assess optical properties of cells and tissues. It measures pre-defined wavelength when the fluorescent/bioluminescent probes are introduced into the cells/tissues are excited by light or chemical reaction that produces light. Fluorescence optical MI techniques is limited by tissue autofluorescence and the use of near-infrared fluorescent (NIRF) tag is the solution and examples of NIRF agents are shown in **figure 5**.[20]

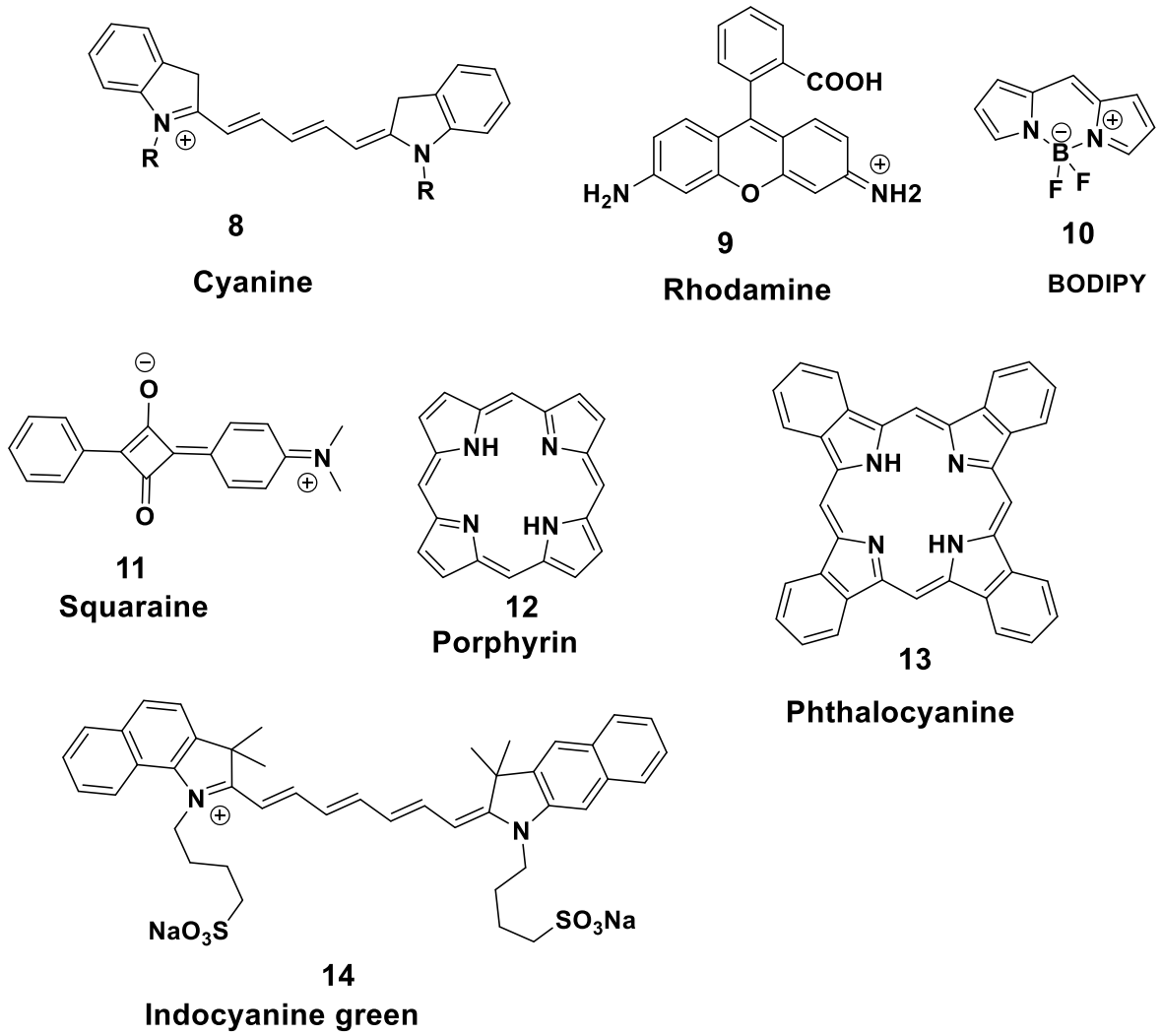

Figure 5: Selected examples of NIRF dyes.

Fluorescent reporter tags have been employed to visualize numerous endogenous components. An example is the turn-on-and-off fluorescent tag based on azidocoumarin **15** (**Scheme 1**). This tag has been used to label antibodies, and proteins.

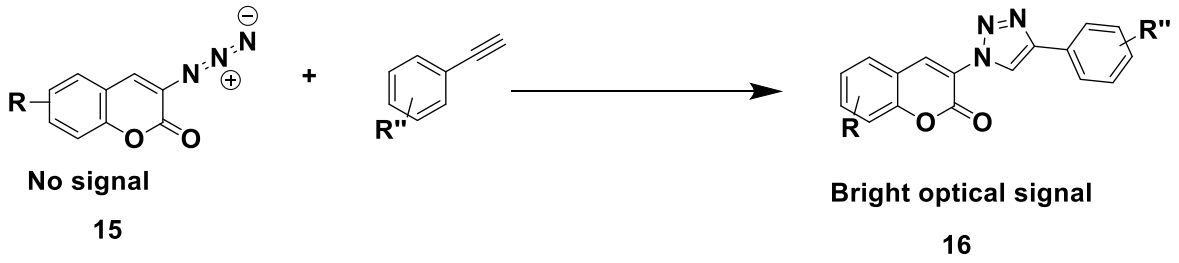

Scheme 1: Turn-on-and-off optical imaging agent, **15/16**.

In bioluminescence imaging (BLI), sensitivity is high due to low background bioluminescence in contrast to fluorescence. The oxidation of luciferin from firefly takes place in the presence of magnesium, ATP and oxygen to form an unstable electronically excited oxyluciferin (**Scheme 2**).[21] When the excited oxyluciferin relaxes it release energy in the form of light.[22] BLI is widely used to observe the biological processes *in vivo and in cellulo* like disease progression, certain gene expression, tumour growth, and metastasis and evaluate the effect of certain treatments. The main disadvantage it has not yet being employed in humans.

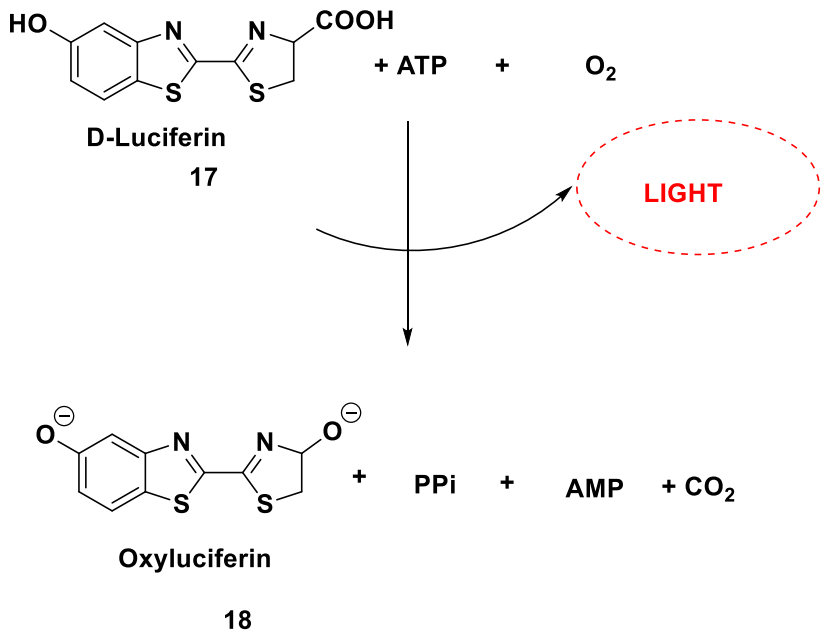

Scheme 2: Oxidation of luciferin by light, ATP and O_2.

The design of imaging agents based on bioluminescence is performed based on the understanding that the BLI agents must have a signalling molecule (the bioluminescent core), a linker (or spacer) and a reactive group which enables the

attachment to the desired target (**Figure 6**). A few researchers have designed imaging agents that target proteases.[23-25]

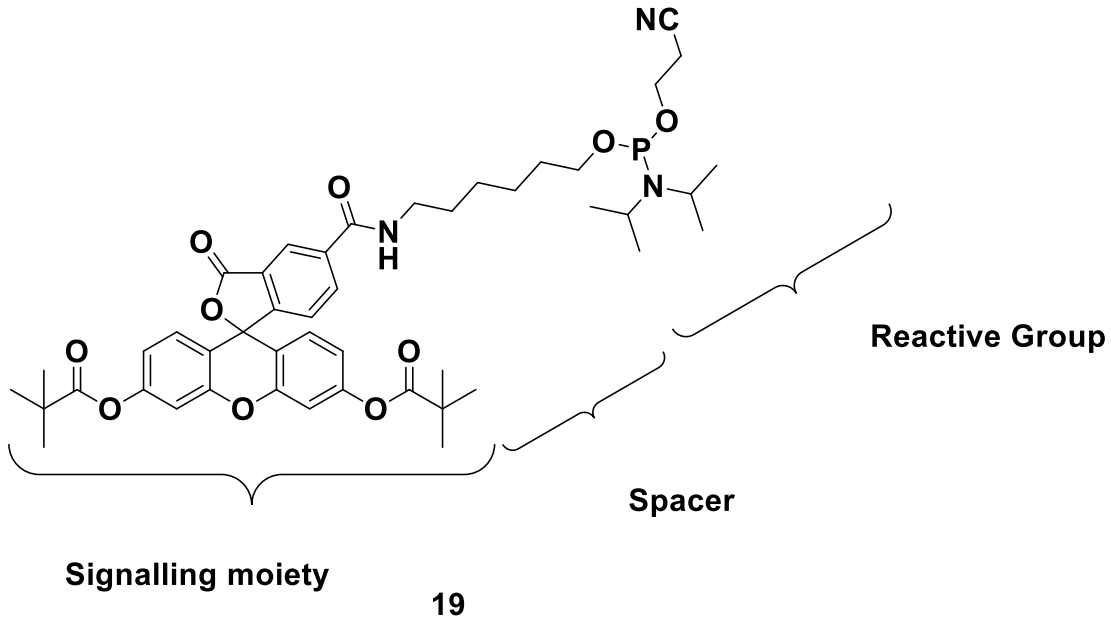

19

Figure 6: Component of a labelling tag- a general strategy employed in the field.

Photodynamic therapy (PDT) is a cancer treatment that employs drugs that produce cytotoxic species (reactive oxygen species) on photoexcitation by a photosensitizer (PS) on exposure to a specific wavelength of light (**Figure 7**). This treatment option is producing better results than traditional treatment methods.[32-36]

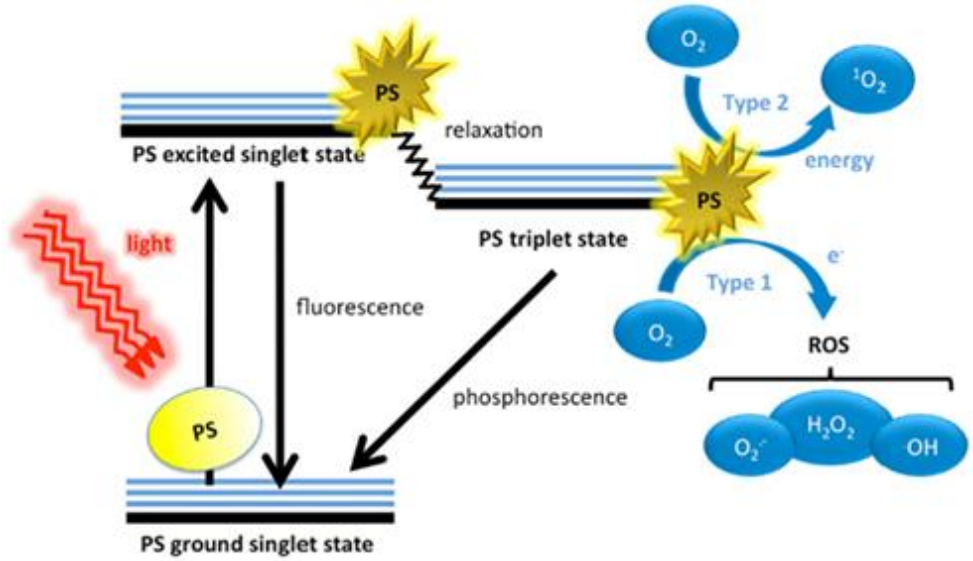

Figure 7: Illustration of the photoprocesses involved in photodynamic therapy. Key: PS = Photosensitizer, ^{1}PS = singlet excited state of photosensitizer, ^{3}PS =

triplet excited state of photosensitizer, type 1 = type 1 photoprocess: which involves electron and hydrogen-transfer reactions; type II = type II photoprocess, involves, electron spin exchange; $^1O_2$ = singlet excited state of oxygen and $^3O_2$ = triplet excited state of oxygen).

Several photosensitizers (PSs) have been developed for PDT, including photofrin, Visudyne, temoporfin, foscan, methylene blue, and various derivatives of amino levulinic acid (**Figure 8**). The next step for PDT is the development of various PS that target different tissues and cells with new target motifs.

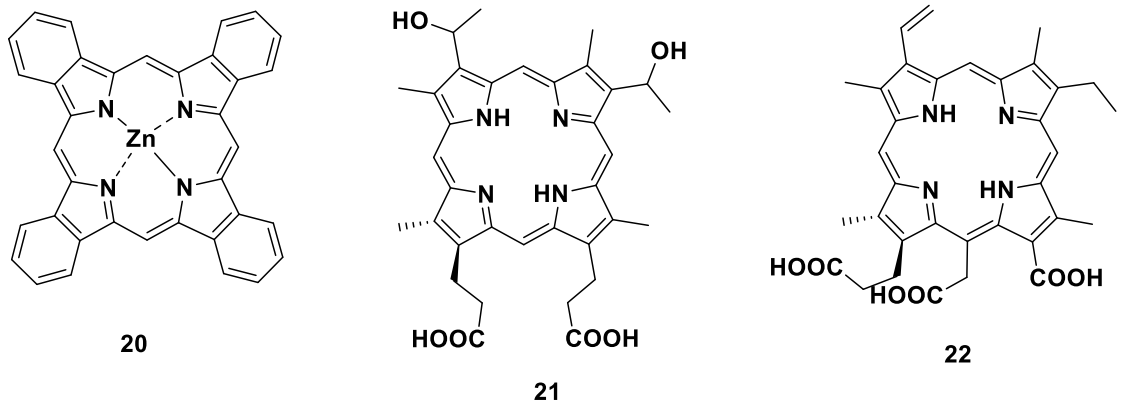

Figure 8: Selected examples of photosensitizers in cancer therapy.

In some cases, near infrared fluorescent (NIRF) probes would enhance the efficiency of photodynamic thermal therapy (PTT) when the cancer cells are incubated with PS in addition to (NIRF).

1.2.3 Nuclear Magnetic Resonance in Drug Discovery

Drug discovery and development is a challenging process marked by high attrition rates because of poor solubility and poor pharmacokinetic and pharmacodynamics properties during clinical studies. Drugs function by binding to biomolecules selectively and this interaction produces a biological/clinical effect. The structure of these biomolecules at the atomic level is essential and the way that they interact are important to enable the design of drug candidates that can target them. NMR spectroscopy is a versatile tool in drug design and development as it provides information on the molecular structure of biomolecules, small molecule and how

they interact in addition to the contaminants they may contain.[26] Drugs are either natural or synthetic compounds.

NMR screening methods are subdivided into techniques that detect target peaks and those that detect ligand peaks, **Figure 9**. In target screening methods chemical shift perturbation are evaluated. Ligand screening methods the change in ligand peaks as a result of binding is studied. The methods employed here include saturation transfer difference (STD), WaterLOGSY, relaxation-edited, and diffusion-edited.

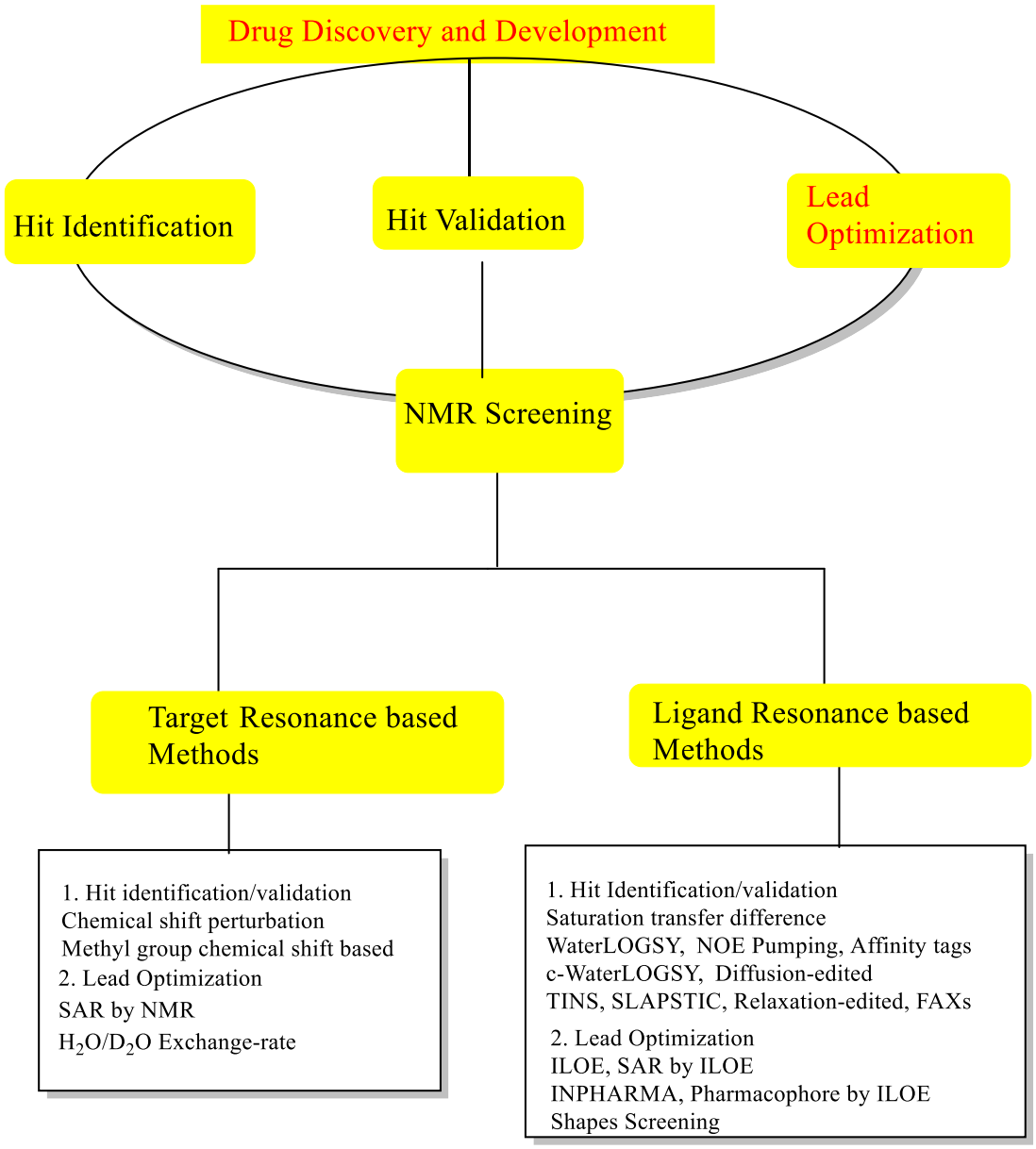

Figure 9: An overview of application of NMR spectroscopy in drug discovery and development.

Solid state (SS) NMR studies elucidate the structure of non-crystalline molecules and this is complementary to X-ray crystallographic data.[25-26] Lange *et al.* studied the binding of scorpion toxin; kaliotoxin to K1 channel proteins (KcsA-Kv1.3).[27-28] They determined the chemical shifts perturbation and $^{`1}H–^{1}H$ distances and from the result they concluded that SS NMR could be employed to screen protein-ligand interaction. Rotational-echo double-resonance (REDOR) NMR is a technique of SS NMR technique which was employed to characterise protein-protein binding drug mode. Olsen *et al*.[29] investigated protein interaction using ssNMR via ^{31}P-^{19}F REDOR experiments to study the interaction between an 11-residue peptide (an HIV regulating peptide) and a 29-mer RNA sequence.[30]

In-cell NMR spectroscopy is important because it characterises molecular structures and interactions at physiological conditions making it the most desirable technique in drug discovery and development.[31] By using in-cell NMR spectroscopy the structure of the target protein and drug candidate can be inferred through uniform and/or selective isotopic labelling, and both can be monitored simultaneously using differential isotopic labelling; in addition, structural changes because of protein maturation or post-translational modifications (PTMs) can be analysed. Non-specific interaction can be distinguished through concentration-dependent chemical shift analyses and signal broadening, which also helps identify the binding epitope and the affinity of the interaction approximated. To detect specific interactions by in-cell NMR spectroscopy, the interactor molecules must be present in stoichiometric ratio with the target protein so that the bulk of the population is bound. Arnesano et al.[32] utilized liquid state and in-cell NMR spectroscopy to investigate the binding between drug cisplatin (cis-$[PtCl_2(NH_3)_2]$) with Atox1, a human copper chaperone protein that mediates Cu(1) delivery to copper-transporting P-type ATPases).[32-33] In order to identify the residues of Atox1 involved in Pt coordination $^{1}H\{^{15}N\}$-Heteronuclear Single Quantum Correlation (HSQC) NMR spectra were collected on purified [U-^{15}N]-Atox1 in the absence and presence of unlabelled cisplatin.

1.3 Antimicrobial Resistance and Urgent Need for New Antibacterials.

Antimicrobial resistance [AMR] is a serious public health problem with the impact of generating untreatable infections reminiscent of the pre-antibiotic era.[34] Most infectious pathogens develop resistance fast and in unexpected ways leading to

the difficulty to characterise or treat by public health institutions. They develop this resistance through contact with other resistant species of the same kind or belonging to different species.[34] Antimicrobial resistance is a cause for concern as diseases that were once readily cured by drug therapy are either difficult or impossible to treat. Therefore, there is a continuing need for new drugs to combat the current generation of resistant pathogens.[35]

The use of antibiotics among animals has led to the spread of multidrug-resistant strains (MDR), among human populations.[36] The most commonly identified MDR bacteria are methicillin-resistant *Staphylococcus aureus* (MRSA) and vancomycin-resistant Enterococci (VRE), *Escherichia coli* and *Pseudomonas aeruginosa* resistant to fluoroquinolones, *Klebsiella pneumoniae* resistant to ceftazidime and multidrug-resistant (MDR) *Acinetobacter baumannii*.[37-38] The pathogenic bacteria, *Neisseria gonorrhoeae* is re-emerging as a threat to public health with a majority being multidrug resistant.[39] Widespread resistance to current TB drugs is a problem with one solution the development of new drugs.[40]

The mechanisms for this acquired antimicrobial resistance include enzymatic cleavage of drugs; by-pass mechanism of target proteins, and increased efficiency amongst efflux families of proteins rendering the membrane impermeable to antibiotics. The molecular targets of drugs and their resistance mechanisms are illustrated in **figure 10**.

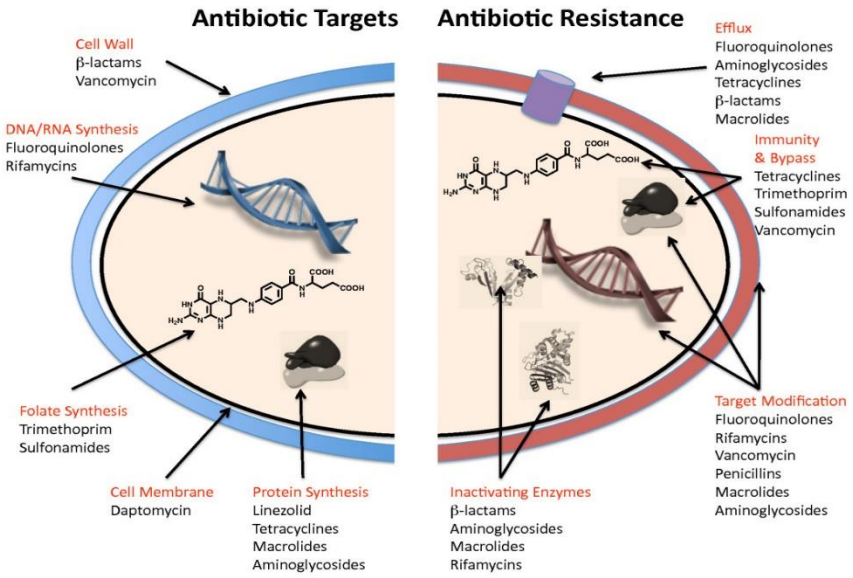

Figure 10: Pathways for Acquiring Antimicrobial Resistance. Adapted with permissions from Wright GD. BMC Biology 2010, 8:123 http://www.biomedcentral.com/1741-7007/8/123. Wright; licensee Biomed Central Ltd 2010.[40]

Persister cells are bacteria cells that survive high concentration of certain antibiotics due to a natural selection process.[41] These persister cells are produced via a natural selection that ensures the survival of the bacteria despite harsh environmental factors. Thus, antibiotic therapy is deemed inefficient in the presence of such persistent cells.

There is therefore a need to change the drug discovery process and make it more efficient and reduce late stage attrition. Pharmaceutical industries have reckoned that the introduction of MI into drug discovery and development has the potential to reduce duration, reduce cost and provide answers to complex biological questions.

1.4 Natural Products-based Antibacterial Drugs

Natural products (NP) represent about 60% of current drugs in the market.[42-44] NP is the source of unique structural diversity responsible for consistently providing novel platform for drug discovery. Between 2000 and 2011, twenty new antibiotics were launched worldwide (**Figure 11**), of which eleven (55%) were natural products-derived (NP-derived) and nine (45%) were synthetically-derived. The NP-derived antibiotics belong to six different classes of drugs whilst the synthetically-derived belong to just two classes (quinolone (eight belong to this class) and one novel class, oxazolidinone). Among the NP-derived antibiotics are daptomycin **23** and retapamulin **24**, and doripenem **28** (**Figure 11**).[45-46]

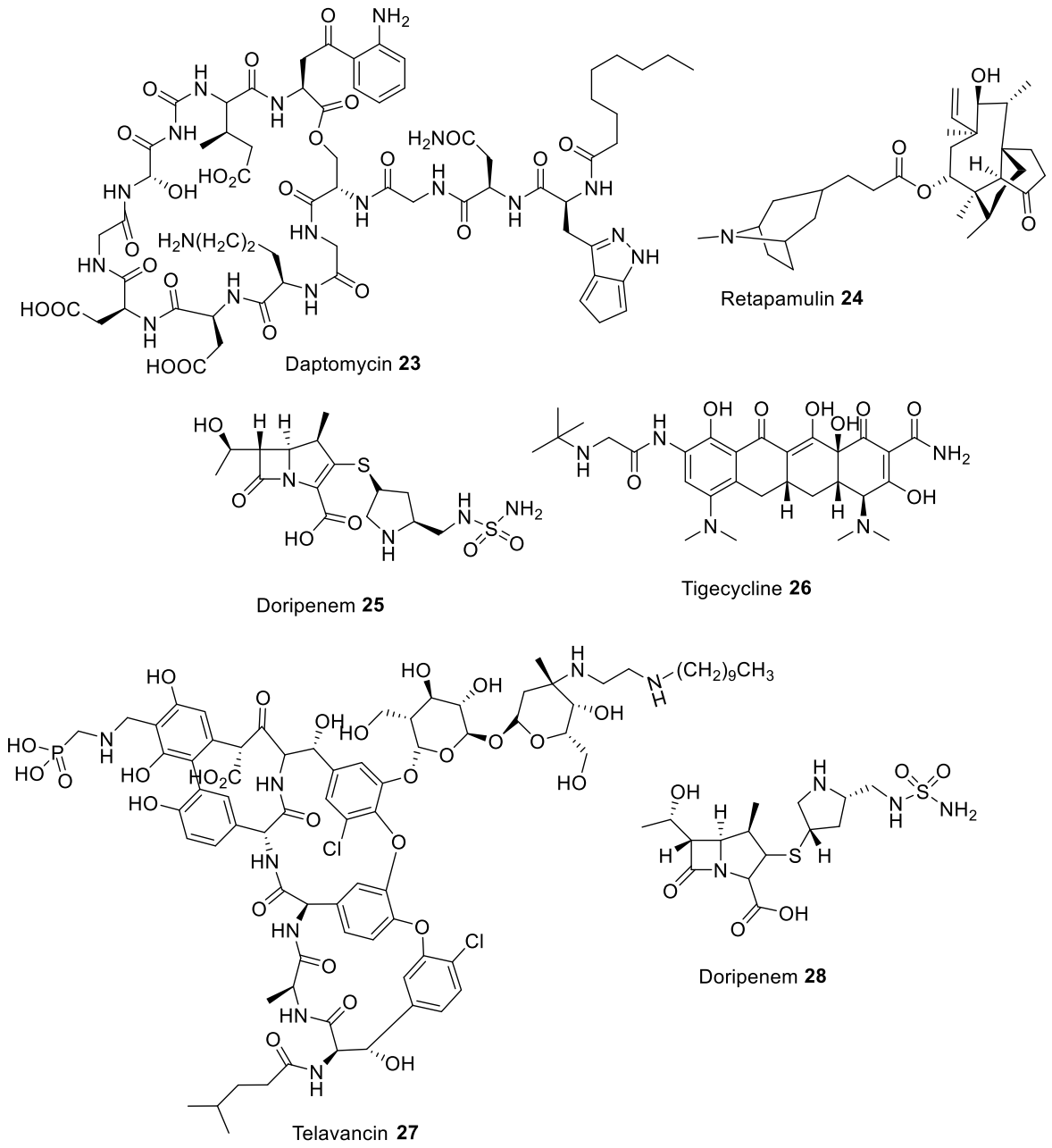

Figure 11: Selected NP-derived drugs approved between 2000 and 2011.

NP has been the source of drugs for centuries and it contains a reservoir of unique structures that push the boundary of science all the time and hence will continue to play a route in drug discovery.

1.4.1 2-Pyrone compounds in Medicine and Drug Discovery

NPs in drug discovery dates to when medicinal teas were brewed from willow bark to treat fevers. NPs are usually isolated in trace amount from a large amount of biological material. The trace amount is insufficient to meet the needs of the world hence the development of the field of natural product synthesis. Styrylpyrones are ubiquitous in nature and were first isolated in 1889 and identified in 1961. Hispidin **29** and bisnoryangonin **30** are common examples of styrylpyrones. From labelling experiments in cultures of microorganisms it was discovered that the styryl scaffold is derived from cinnamic acid, p-coumaric acid and caffeoyl-CoA pathways. The 2-pyrone system is biosynthesized from acetate.[47-49] The biosynthetic route to 2-pyrone is generally accepted to be via the polyketide pathway though Serrano-Carreon et al.,[50-51] reported another possible route via C-18 linoleic acid which is cleaved to a C-10 intermediate **31** (5-hydroxy-2,4-decenoic acid) which upon lactonization afforded 6-pentyl-2-pyrone (**Scheme 3**). Numerous styrylpyrone compounds have been isolated from plants, microorganisms and marine sources. These include hypholomines A-B **33-34**, fasciculines A-B **35-36**,[52-53] phelligridimer A **37**,[54] squarrosidine **38** and pinillidine **39** (**Figure 12**), and phelligridins A-J **40-49** (**Figure 13**).[55-56]

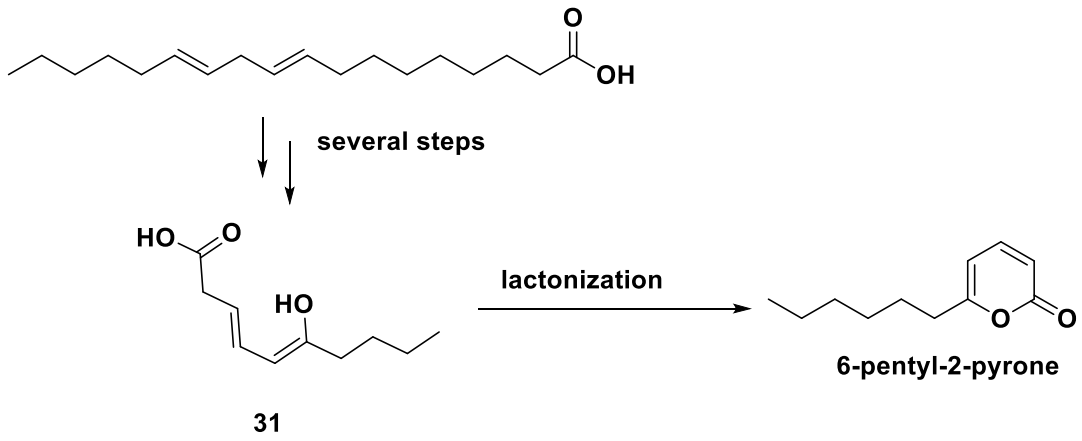

Scheme 3: Proposed biosynthetic route via linoleic acid.[50-51]

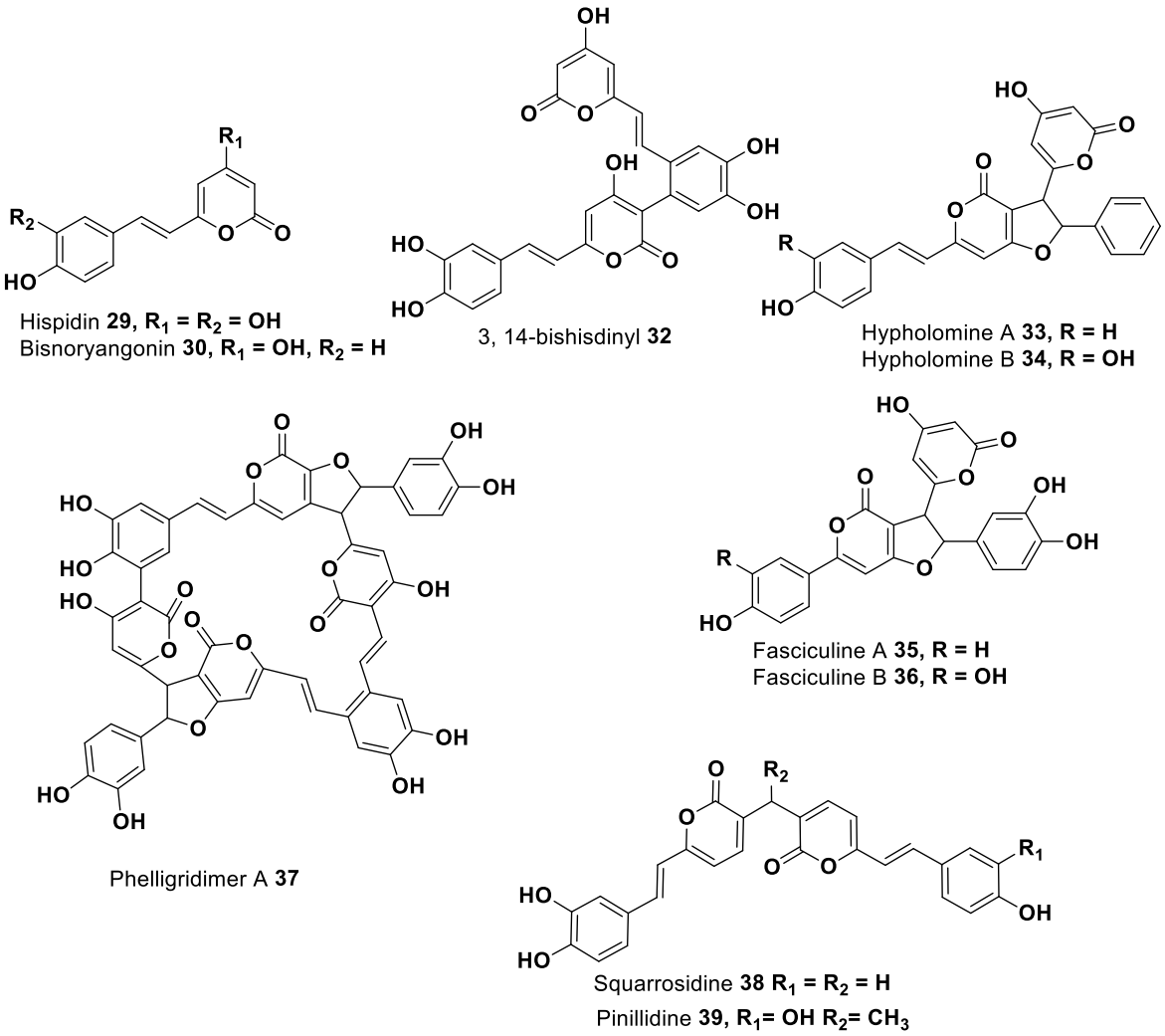

Figure 12: Structures of hispidin **29**, bisnoryangonin **30** and their dimeric compounds **32-39**.

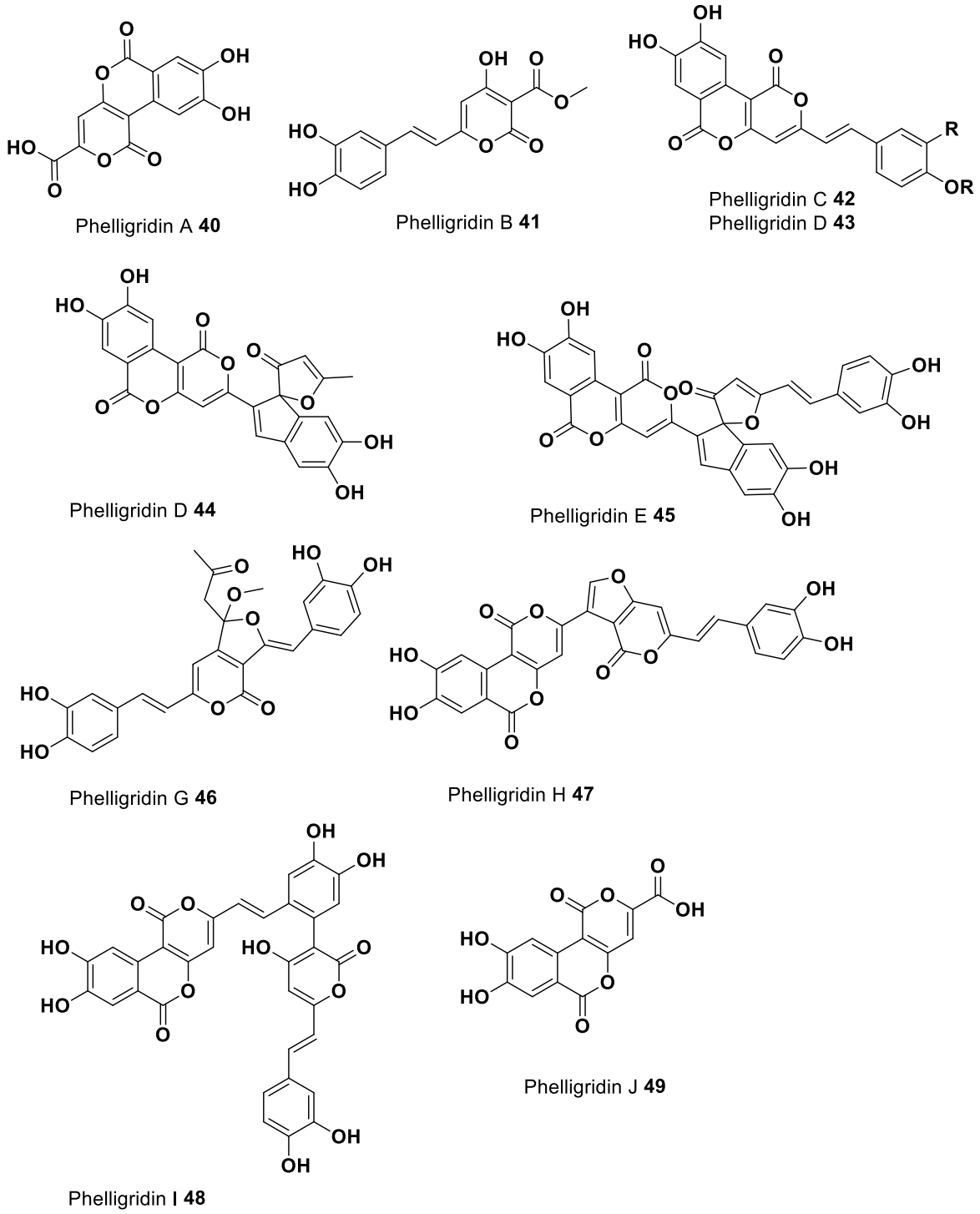

Figure 13: Structures of phelligridin compounds **40-49**.

A recent report showed that hispidin **29,** bisnoryangonin **30** and other polycyclic compounds such as **32**-**35** and **44** were bioluminescent fungal natural products.[57] Styrylpyrone have diverse range of biological activities attributed to them. Hispidin **29** and bisnoryangonin **30** are free radical scavengers. Free radical scavengers

have been implicated in anticancer and anti-inflammatory activities. Hispidin has also exhibited anti-HIV against HIV-1 integrase and activity against amyloid plaques associated with Alzheimer's.[58-59]

Some synthetic 6-styryl-2-pyrone **50-52**(**Figure 14**) have been synthesized by Copp *et al*.[60] and they also exhibited *in vitro* antimalarial and antitubercular activities. Ndom *et al.*[61] reported the isolation of 6-styryl-2-pyrone **53-54,** and three others containing sugar moiety at position 11 from *Senecio manii* Hook (Asteraceae) used in the traditional treatment of bacterial and fungal diseases in Africa.

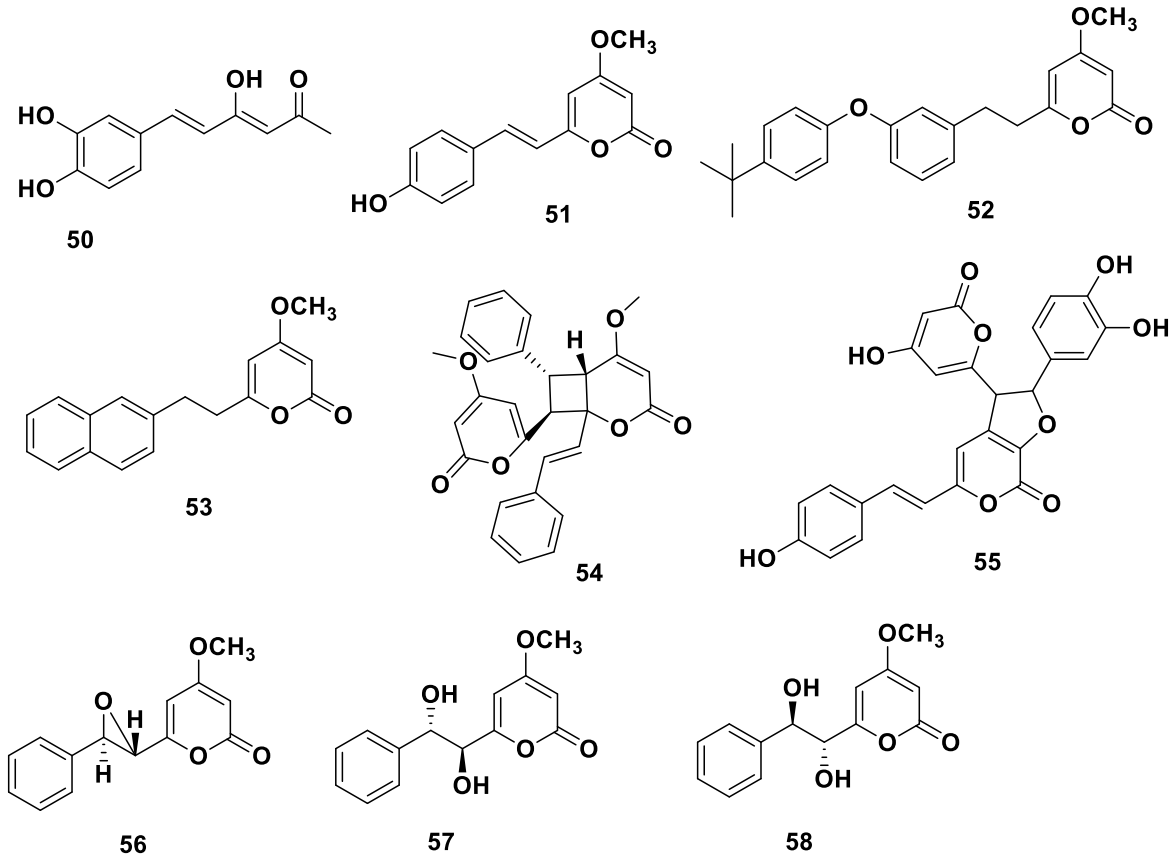

Figure 14: Selected synthetic and natural 6-styryl-2-pyrones.

Compounds **56-58** (**Figure 14**) were isolated from the root barks of *Sanrafaelia ruffonammari* and *Opherypetalu*m *odoratum* and reported to exhibit both cytotoxic and significant antifungal activity against *Candida albicans* was suggested for further drug development.[62] Nonetheless, despite these series of activity reported for these compounds not much is reported on their mechanism of action. This

research therefore intends to synthesize a hydrogenative hyperpolarizable contrast agent (hPHIP) based on 6-styryl-2-pyrone motif.

2-Pyrone compounds have been of interest in the Fairlamb research group and in 2015, Fairlamb and co-workers had synthesised a macrocyclic 2-pyrone **59** from *Phacelocarpus spp*. and its aromatic mimic **60** (**Figure 15**) and this total synthesis led to the elucidation of the correct stereochemistry around the enoyl ether of the natural product.[63]

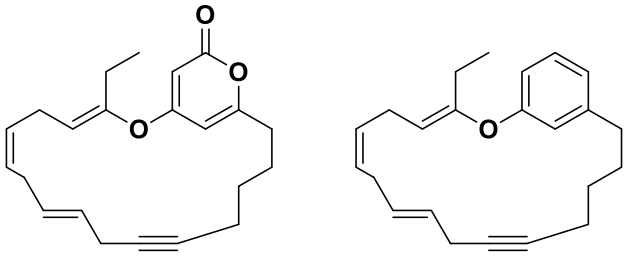

59 **60**

Figure 15: Phacelocarpus 2-pyrone A and aromatic mimetic.

1.4.2 Anti-Tuberculosis potential of 2-pyrone Compounds

Tuberculosis (TB) is an infection caused by *Mycobacterium tuberculosis* that affects the lung, and all other major organs and tissues of the body. TB is characterised by inflammation and granulomas. At least 2.3 billion people worldwide are infected with this bacterium. In recent years, the control of TB has led to increase in the prevalence of multi-resistant (MDR) and extensively drug-resistant (XDR) TB. The challenges with current TB drugs, is the long period of drug regimen, raising cases of resistant TB including the recent report of totally resistant TB (TR-TB) and the coinfection of TB and HIV. To address these challenges, efforts have been directed towards TB drug discovery. Brachmann *et al*.[64] identified a class of 2-pyrone (photopyrones **61-68, Figure 16**) that are involved in cell-cell signalling in prokaryotic cells and are opined to be the reason for the recent renewed interest in designing 2-pyrone-based drug molecules as it can be transported into the cytoplasm.[65] This is important as *M. tuberculosis* is known to have advance efflux pumps that function synergistically to expel most drugs.[7]

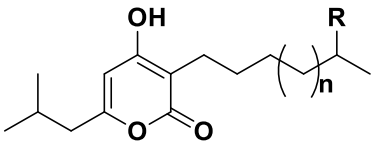

R = H, n = 1; photopyrone A **61**
R = CH_3, n = 1**;** photopyrone B **62**
R = H, n = 3; photopyrone C **63**
R = CH_3,n = 3**;** photopyrone D **64**
R = H; n = 5**;** photopyrone E **65**
R = CH_3, n = 5**;** photopyrone F **66**
R = H, n = 7**;** photopyrone G **67**
R = CH_3, n = 7**;** photopyrone H **68**

Figure 16: Cell-cell signalling molecules, **61-68**.

The antituberculosis (anti-TB) activity of 2-pyrone compounds are known and some selected examples are shown in **figure 17**. Ferulenol **69**, a 2-pyrone based coumarin showed inhibitory activity against *M. Tuberculosis* (**Figure 17**). Screening of a combination of ferulenol **69** with isoniazid, an approved drug for TB led to a drop in the minimum inhibitory concentration (MIC) of both drugs.[66] A synthesised analogue without the isoprenoid chain retained the antimycobacterial activity.

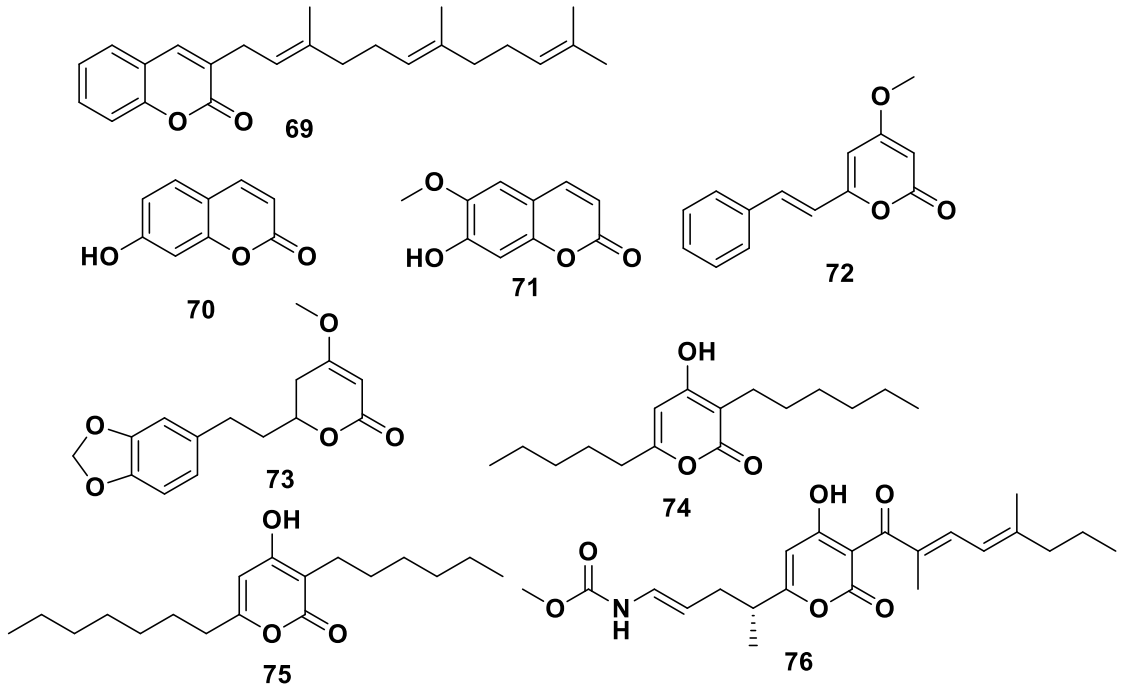

Figure 17: Selected anti-TB 2-pyrone compounds **69-76**.

Demethoxyyangonin **72** and 5,6-dehydro-7,8-dihydromethysticin **73** have both exhibited anti-TB activity. Copp et al.,[60] synthesise a selected number styrylpyrone

compounds and evaluated for antimalarial and anti-TB activity and reported that the compounds did not exhibit any significant antiTB property. Pseudopyronines A **74** and B **75** (**Figure 18**) were screened and found to have anti-TB activities against *M. tuberculosis* H37Rv.[67] Myxopyronin (Myx) **76** isolated from marine source also exhibited anti-TB activity against *M. tuberculosis* and showed no acute toxicity in mice.[68]

As a further proof of the antiTB potential of 2-pyrone compounds; **77** and **78** have activity against TB with compound **78** approved for the treated for HIV/TB coinfection whilst **79** is an HIV-1 protease inhibitor. [69-74]

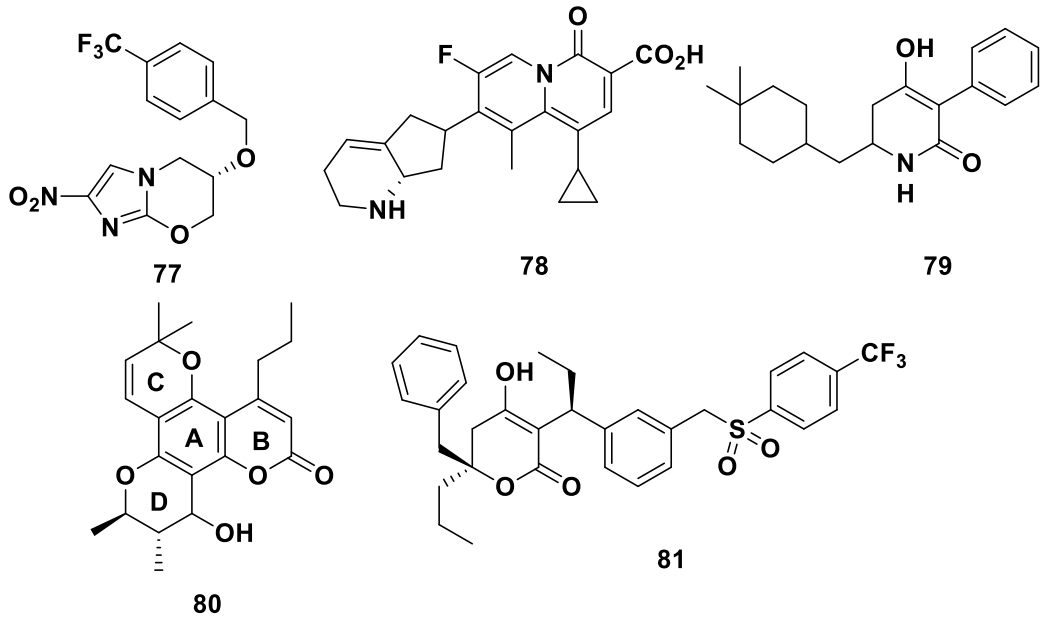

Figure 18: Selected 2-pyrone-based anti-TB and anti-HIV drugs.

1.5 2-Pyrone Compounds and Chemistry

Pyrone compounds are abundant in nature with diverse biological activity attributed to this class of compounds. We therefore decided to design 2-pyrone-based antibacterial small drug molecule with NMR molecular imaging capability. Pyrone exist in two isomeric forms, 2-pyrone **82** (α-pyrone) and 4-pyrone **83** (γ-pyrone) (**Figure 19**).

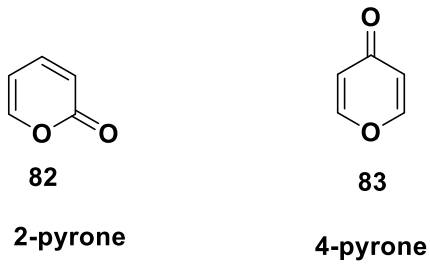

Figure 19: 2-Pyrone and 4-pyrone ring systems.

The 2-pyrone ring has been synthesized employing several strategies such as cyclization, condensation/cyclization and metal-catalysed strategies.[75] Most synthetic strategy to 2-pyrone involved metal-catalysed processes but an interesting synthesis was reported by Dobler and Reiser (2016),[76] which involved a thermal rearrangement of furfural **84** to cyclopentenone **85**, a Diels-Alder reaction with cyclopentadiene to give the cycloadduct **86** which reacted with several aldehydes in the presence of alkyl phosphine as catalyst in a Baylis-Hilman reaction to afford the enone **88** which was oxidise with hydrogen peroxide to give the epoxide **89**. A reduced pressure thermal cleavage of the epoxide led to a retro-Diels-Alder reaction eliminating cyclopentadiene and affording substituted 2-pyrone **90-91** in good yield (**Scheme 4**). The reaction works well with both aromatic and aliphatic aldehydes.

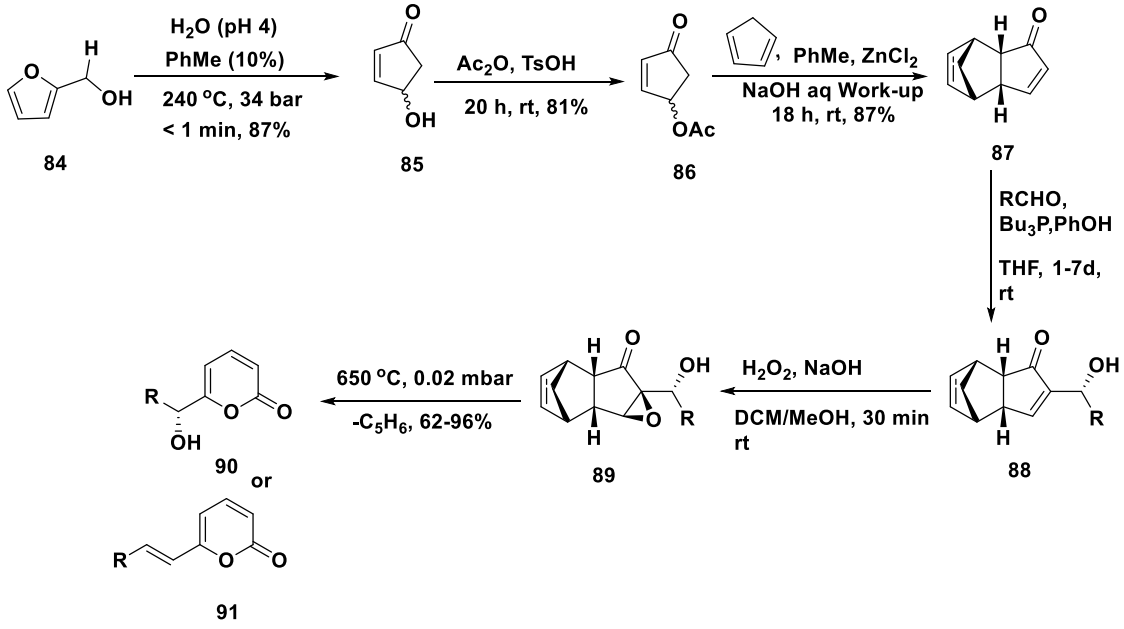

Scheme 4: 2-Pyrone synthesis via furfuryl hydroxide, a renewable reagent.

The above synthesis was designed based on the premise that 2-pyrone compounds are known to undergo electrocyclic ring opening (ERO) reaction to give a vinylketene. At temperatures above 550°C, 2-pyrone compounds are known to undergo rearrangement by reversible ERO to a vinylketene aldehyde **93** (**Scheme 5**).[77]

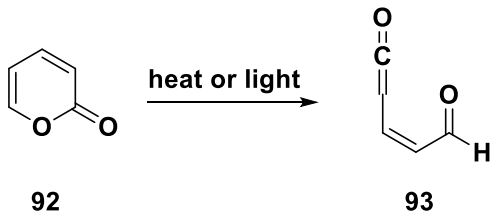

92 **93**

Scheme 5: Photochemical and thermal induced ERO of 2-pyrone to vinylketene.

Photochemical irradiation of 2-pyrone in ether affords bicyclo[2.2.0]pyran-2-one **94**,[78] which underwent photodecarboxylation to cyclobutadiene; a very reactive intermediate not readily observable except when trapped (**Scheme 6**).[79] This cyclobutadiene was observed trapped in a supramolecular matrix.[78-79]

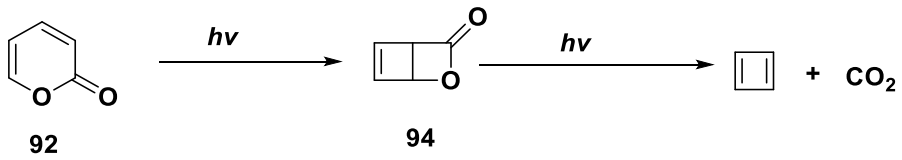

92 **94**

Scheme 6: Photochemical-induced intramolecular [2+2] cycloaddition of 2-pyrone.

McMahon and Menke,[80] reported irradiation at λ ≥ 299 nm, of the 2-oxo-2H-pyran-5-carbonitrile **95** and its conversion to a bicyclic, Dewar-benzene-like, lactone **97** and ketene derivative such as **96.** Upon further irradiation, at λ ≥ 200 nm of the lactone afforded cyanocyclobutadiene **98** via a retro [2+2] cycloaddition and subsequent extrusion of CO_2 (**Scheme 7**). They observed the formation of the bicyclic **97** and ketene **96** via matrix-isolated IR spectroscopy.

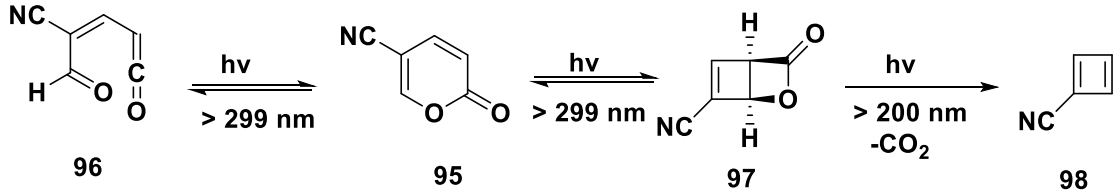

Scheme 7: Intramolecular [2+2] cycloaddition, retro [2+2] cycloaddition leading to cyclobutadiene derivatives.

Other 2-pyrone compounds have been reported to undergo similar reactions, 3/5-deuterated-2-pyrone, and other isotopically labelled 2-pyrone compounds (^{13}C,[81] and ^{18}O[82]) whereby a rearrangement that interconverts the regioisomers is observed via the intermediacy of the ketene and subsequent [1,5]-sigmatropic shift of hydrogen, chlorine and fluorine but not methyl group (**Scheme 8**).[83-84] The reaction depicted in **IV** and **V** was carried and found that though the 3-substituted compound rearranged to give the 5-substituted via the intermediacy of ketene **100/101** and these ketenes were observed via matrix-isolation. However, the 5-substituted did not lead to the rearranged product and what was observed was a trace amount of the Dewar-benzene-like lactone and the unrearranged starting material.

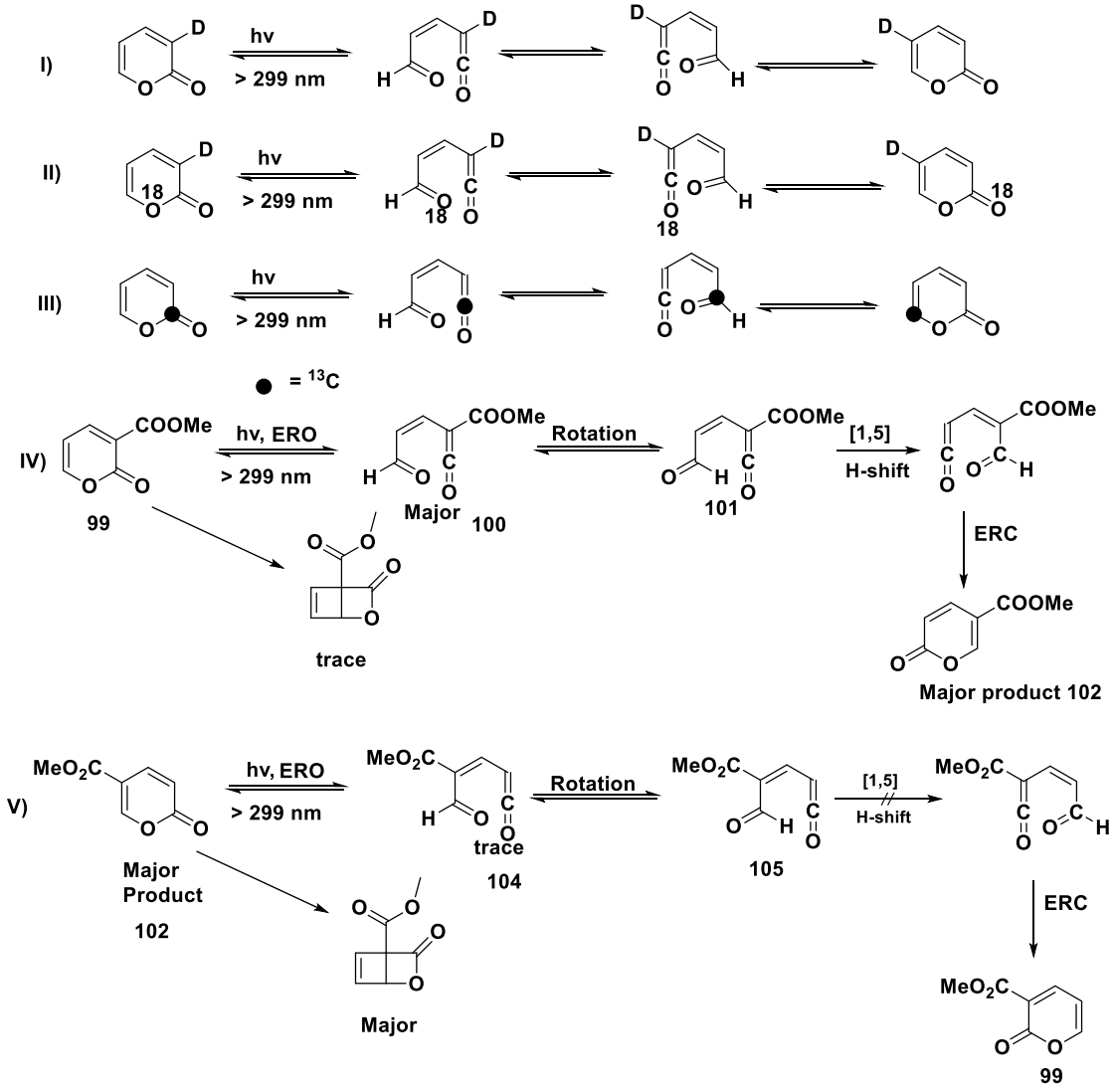

Scheme 8: Ketene formation and [1,5]-sigmatropic rearrangement of 2-pyrone compounds. ERO = electrocyclic ring opening and ERC = electrocyclic ring closure.

Meanwhile, the metal catalysed 2-pyrone synthesis include those catalysed by silver(I), gold(I), palladium, ruthenium and rhodium (**Scheme 9**). The Ru(I) catalysed reaction involve homo/heterodimerization and subsequent cyclization to the 2-pyrone compound **107, 110-111**.[85-86]

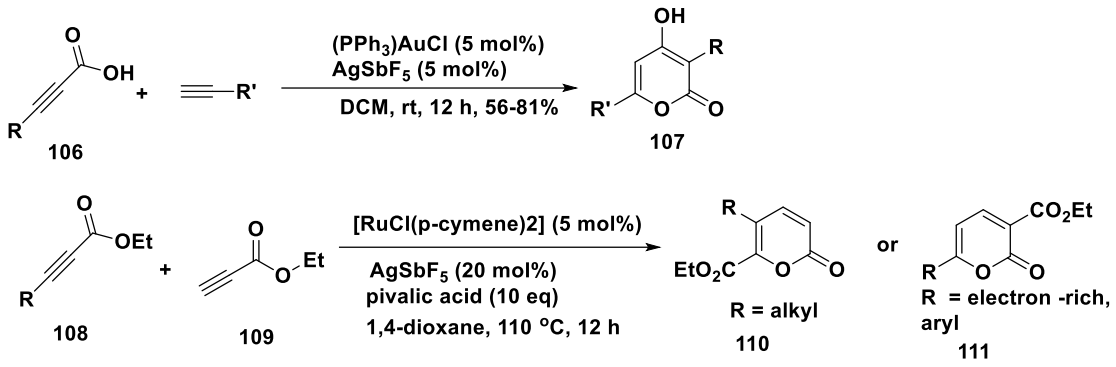

Scheme 9: Gold (1) and ruthenium-catalysed 2-pyrone synthesis.

Another synthetic route to substituted 2-pyrone is the [3+2+1]-cyclization catalysed by thiazolium salt **115** as shown in **Scheme 10**.[87]

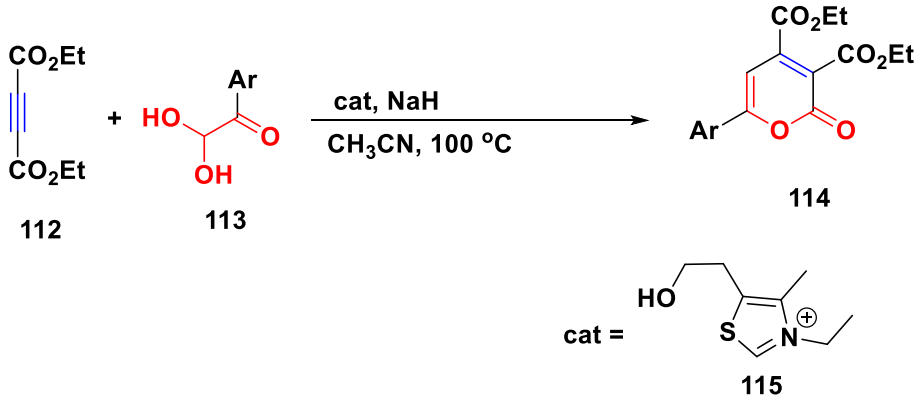

Scheme 10: Organic salt catalysed [3+2+1]-cyclization leading to substituted 2-pyrone.

A 2014 paper reported the synthesis of 4,6-subsituted 2-pyrone via the reaction of enone **116** with diethyl cyanoethyl phosphonate **117** to give penta-2,4-dienenitriles **118** which underwent an intramolecular condensation to afford the 2-pyrone **119** (**Scheme 11**).[88]

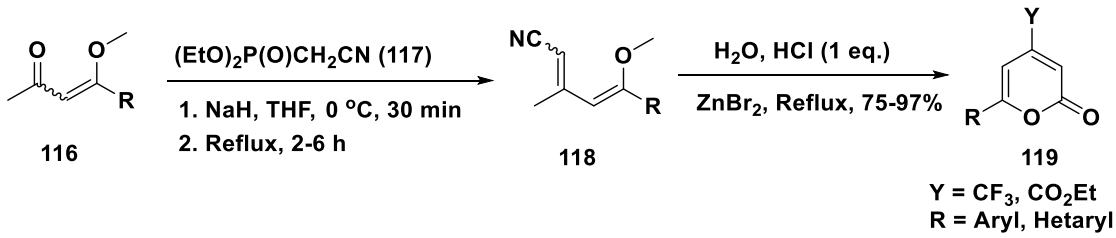

Scheme 11: Intramolecular cyclization of penta-2,4-dienenitriles to substituted 2-pyrone.

1.6 Aim and Objectives

The aim of this research is to design and synthesise a biological activity-based 3-alkyl-[6-^{13}C]-6-(phenylethynyl)-2-pyrone as a hydrogenative hyperpolarizable (hNMR) NMR imaging agent for cell imaging. However, the high cost of the isotopically labelled reagents required the optimization of the whole synthesis using unlabelled reagents. The design of a potential small drug molecule implies the requirement for analysing the *in-silico* drug-like property of the designed compounds. The research therefore has the following objectives.

- To evaluate the *in-silico* drug-like properties of the 2-pyrone-based designed small drug molecule and molecular simulation to protein receptors (Chapter 2).
- To design, optimise and synthesise 2-pyrone-based antibacterial hPHIP NMR imaging agents (Chapter 3).
- To carry out a protein binding assay employing saturation transfer difference (STD) NMR and preliminary signal enhancement studies (Chapter 4).
- Summary and Future work from the results obtained (Chapter 5).

Chapter Two: Virtual-based Screening of 2-Pyrone compounds and Molecular Simulation.

2.1 Introduction

In the design of small drug molecule or molecular imaging agent, it has now become imperative that all the designed compounds go through *in silico* drug discovery procedure.[91] This implies the subjection of the designed compounds through various software and thereafter, making an informed decision based on what compounds have the best predicted absorption (A), distribution (D), metabolism (M), excretion (E) and toxicity (T) and affinity for the target receptors before the synthesis is done.[91]

The medicinal scaffold chosen is the 2-pyrone motif, this is in line with Fairlamb group's longstanding interest in 2-pyrone compounds and their chemistry. The imaging agents were designed based on the pharmacological activities of 6-substituted 2-pyrone **120-123** and 6-styryl-2-pyrone **124-127** (**Figure 20**) as discussed in Chapter One. 2-Pyrone compounds are ubiquitous compounds in nature and exhibit diverse range of biological activities and a simple change in substitution pattern leads to a change in activity.[92-93]

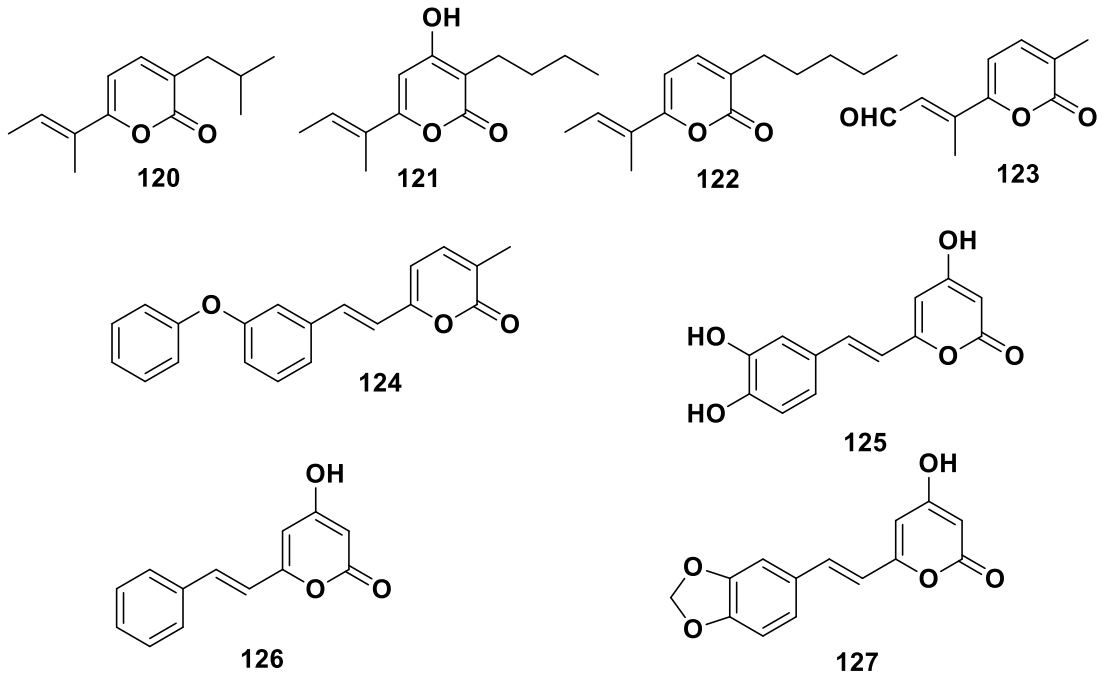

Figure 20: Generic structures showcasing potential 2-pyrone target structures.

Scientists with interest in designing molecular imaging agents are known to design new imaging agents based on other successful imaging agents or based on some approved drug structure. An example in this area include the design of a radionuclide imaging agent based on (^{18}F-Glu), (^{11}C-Glu) and (^{99m}-Glu) agents each containing different radionuclide.[94]

This research designed imaging agents based on NMR imaging protocol and designed the agents based on the slow relaxation of ^{13}C=O motif whereby the signal enhancement of parahydrogen added to a 6-alkynyl-2-pyrone can be transferred to the carbonyl functionality either through space or through bond and subsequently used to image the cellular interaction between the imaging agent and their cellular receptor in live bacterial cells. The design of a drug candidate that is also an imaging agent has the potential of making drug discovery process more efficient as first it will undergo approval process once and also be employed for real time monitoring of drug effects. Secondly, it can be employed to non-invasively quantitate the drug response, and receptor occupancy in real time.

The designed chemical structures are synthetically available from Pd-catalysed Sonogashira cross-coupling reactions between **128a-e** and phenylacetylene (Scheme 12). This would be discussed in Chapter Three. Compounds **128a-e** are interesting as they are reported to be inhibitors of chymotrypsin, elastase and other serine-type enzymes. Therefore, in silico-based analyses of **128a-e** is a good place to start and its binding to bovine protein trypsin will be explored using saturation transfer difference (STD) NMR see Chapter Four.

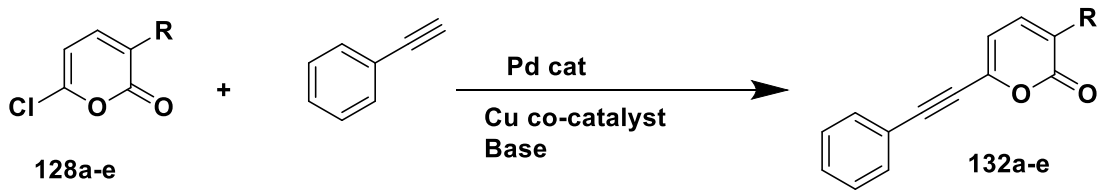

Scheme 12: Pd-catalysed Sonogashira cross-coupling of **128a-e** and phenylacetylene.

There are several software packages available to the medicinal chemists to ensure the accuracy of the result obtained. They include BioSolve, SwissADME, SwissSimilarity, SwissTarget, PyRx, PyMol, admetSAR, and Fragmentscore.

2.2 Virtual Screening of Designed Compounds

Medicinal chemistry is concerned with the effect of chemical structure on biological activity and the mechanism by which these molecules exert their activity. Physicochemical properties govern the way molecules act and exert their influence *in vivo* or *in vitro*. The medicinal chemist is therefore concerned with the influence that chemical structures have on acidity, aqueous solubility, lipid solubility and, biological activity.

These properties affect the ADMET profile of these molecules. The contribution of each functional group to the overall physicochemical properties is important to drug discovery. More so, ADMET profiling and prediction depends on several molecular descriptors as defined by Lipinski's Rule of five (Ro5).[95] Multiple software packages are available for prediction of ADMET properties based on structural features of the molecules relative to other molecules with similar structure. Quantitative-structure-activity relationship (QSAR) models the effect of structure on activity.

Computer-aided drug discovery (CADD) provides insights on what structures to synthesise, by utilizing a set of reference structures collected from compounds known to interact with a target and analysing the interaction of any compounds based on the 2D and 3D structures of these reference and giving a scoring function for the binding affinity. It has been extended to predict physicochemical properties, absorption, distribution, metabolism, excretion and toxicity profiles of millions of compounds. CADD methods have been successful in optimizing a number of drugs.[96-97] CADD methods are subdivided into structure-based methods (SBDS) which employs simulation tools to dock libraries of compounds and ligand-based drug screening (LBDS), which matches ligands to either approved drugs or to literature data of biologically active drug molecules and makes use of QSAR, and matched molecular pairs (MMP).[98-99] Therefore, medicinal chemists can take advantage of all kinds of software and resources related to CADD during their routine work. It merges a wide range of area of research to stimulate each other to make drug discovery more efficient.

CADD in drug design is faster and cheaper than experimental procedures and many compounds can be optimized using in silico methodology before they are synthesized, and in vitro testing carried out.

2.3 Predicted physicochemical properties of 6-chloro-3-alkyl-2-pyrone, 128a-e.

The approach employed in this project is the combined use of SBDS and LBDS to choose a lead compound that is synthesized and employed as hydrogenative hyperpolarizable nuclear magnetic resonance (hNMR) imaging agent (this will be discussed in Chapter Three). The physicochemical properties of the synthesised compounds are shown in **Figures 25-29**. Based on Lipinski's definition only one compound had a value above the minimum of 250 Da and all others have values below this minimum value. The compounds designed here fit into the category of small drug molecule and therefore can be optimized further to improve any parameter that does exactly fit the profile to obtain a more efficacious drug/contrast agent with excellent ADMET parameters.

Aqueous solubility measures the concentration of drug in water at specified temperature.[100-101] Computational methods predict aqueous solubility based on group contributions,[102] thermodynamic calculations,[103] and structure-property relationships.[104-105] Two factors affect water or lipid solubility of a drug; the presence or absence of hydrogen-bond donors or acceptors. Lemke,[106] defined this criterion ''based on carbon-solubilizing potential of the functional groups in the drug''. If the solubility potential of the functional group exceeds the total number of carbon atoms present, then the drug molecule is water soluble: otherwise, it is water-insoluble. Another method predicts the water solubility based on partition coefficient (Log P) which is the ratio of the concentration of a drug in a hydrophobic solvent (usually octanol) to that in a hydrophilic solvent (water). **Figure 22** show that these molecules are relatively water soluble and are within the acceptable range for small drug molecules (Log P<5) except for **128e**, **130/131e** and **132/133e**.

128a-e **129a-e**

a) R = CH_3
b) R = $CH_2CH{=}CH_2$
c) R = C_5H_{11}
d) R = $PhCH_2$
e) R = $C_{10}H_{21}$

Figure 21. 3-Alkyl-6-chloro-2-pyrone **128a-e** and 5-alkyl-6-chloro-2-pyrone **129a-e**.

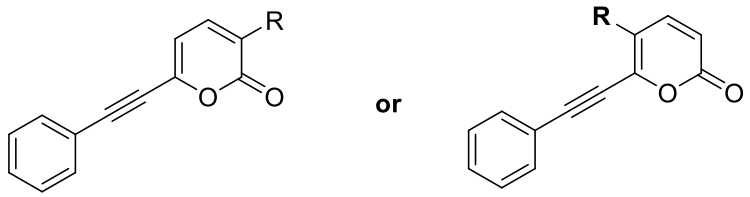

130a-e **131a-e**

a R = CH_3
b) R = $CH_2CH{=}CH_2$
c) R = C_5H_{11}
d) R = $PhCH_2$
e) R = $C_{10}H_{21}$

Figure 22. Generic structures of targeted imaging agents' **130/131a-e**.

Analysis of the molecular weight against logP for these compounds show that the carbon-solubilising potential of these compounds is in the order **128a**<**128b**<**128c**<**128d**<**128e**. More so, the number of hydrogen-bond acceptors are not up to 10 which is the upper limit whilst there are no hydrogen-bond donors in the designed molecule and log P not greater than 5. These properties suggest that 3-alkyl-6-chloro-2-pyrone **128a-d** have better drug-like properties compared to **128e** because of its long hydrocarbon chain. The long hydrocarbon chain though makes this compound ideal as a potential inhibitor for membrane receptors. As the hydrocarbon tail (or chain) would likely interact with the hydrophobic regions of the membrane receptor proteins possibly producing a more efficacious drug as has

been observed in other approved drugs such as telavancin (structure is given in chapter 1).[107-108]

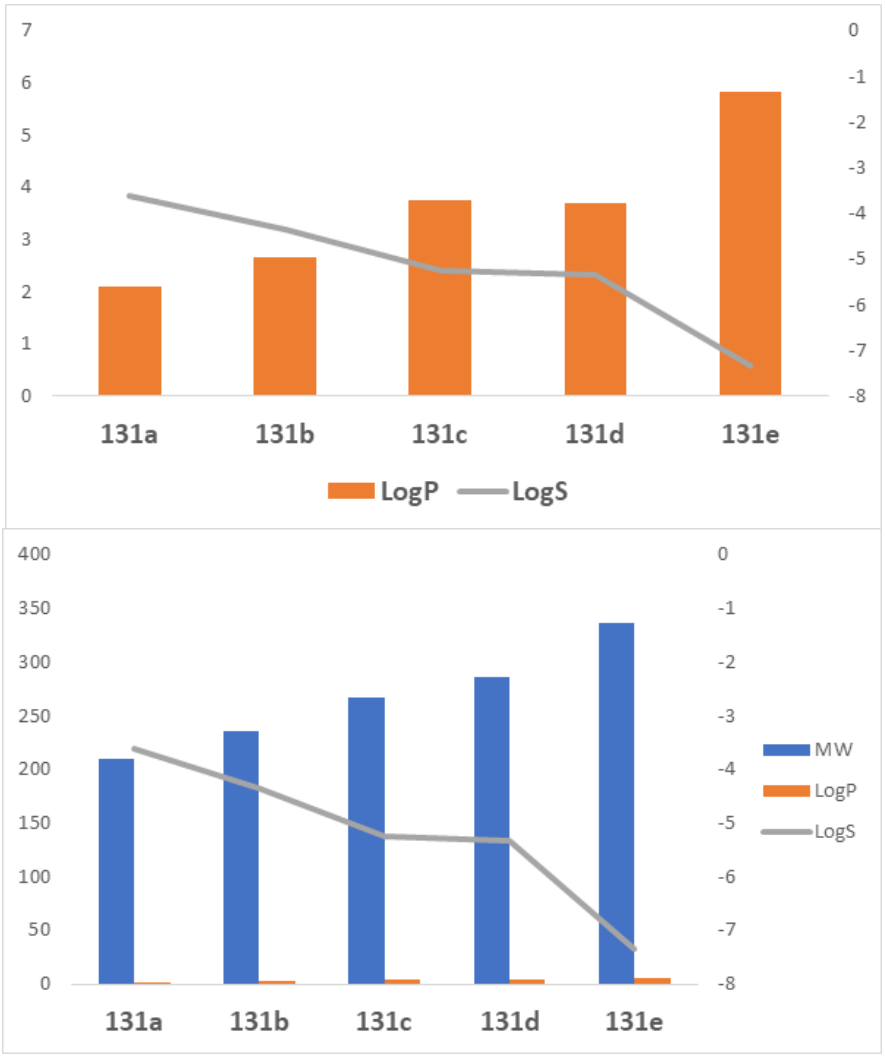

Figure 23: The graphs show the effect of increase in alkyl and aryl substituent on LogP and LogS.

The graph shows that to increase water solubility decreasing alkyl chain length is a factor to consider amongst compounds of the same molecular description and vice versa for lipid solubility. Similar trend was observed for **128a-e** and **131a-e** (**Figure 23**). As the length of the carbon chains increased so also did the LogS decreased and LogP increased.

The ideal physicochemical properties of this class of compounds as shown in **Figure 24-29** is indicated by the pink area and of all the designed compounds analysed here, **Figures 24-29** are those closest to the ideal properties. From these physicochemical properties the choice of decyl-, benzyl or pentyl as imaging agents

is rational, as these chemical structures possess good physicochemical and ADMET properties.

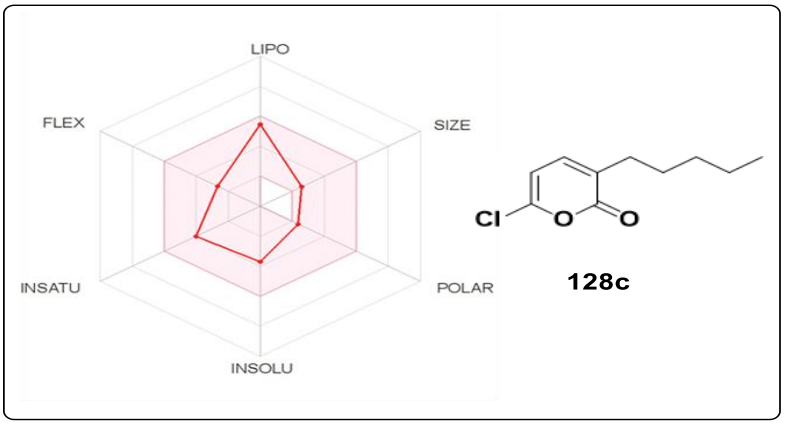

Figure 24: Fragment-based physiochemical properties of 6-chloro-3-pentyl-2-pyrone **128c**. The pink circle is the optimal property for an oral drug.

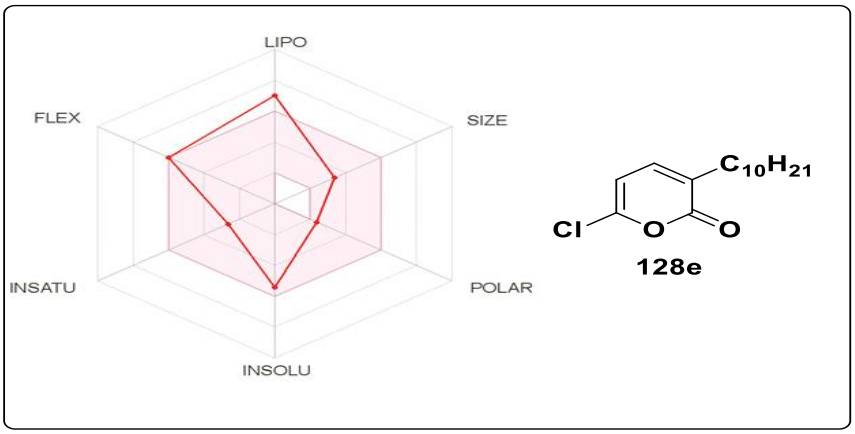

Figure 25: Fragment-based physiochemical properties of 6-chloro-3-decyl-2-pyrone **128e**. The pink circle is the optimal property for an oral drug.

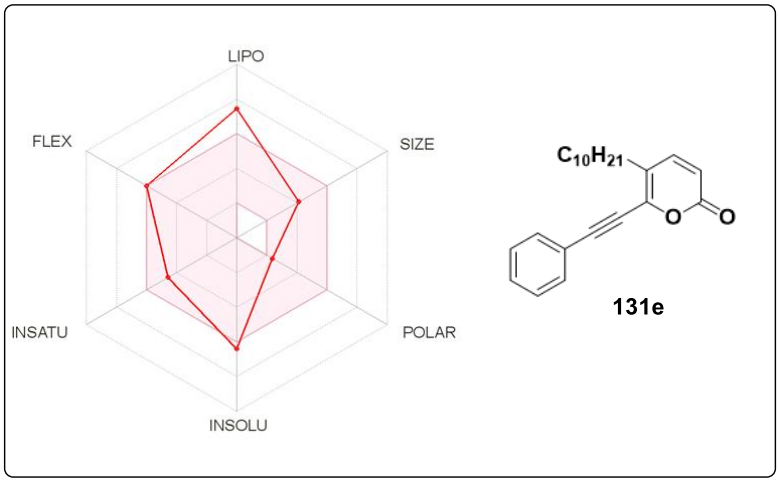

Figure 26: *In-silico* based physicochemical properties of 5-decyl-6-(phenylethynyl)-2-pyrone **131e**. The inner pink circle is the optimal property for oral drugs.

There is provision for improvement in polarity and molecular weight. In the light of this addition of polar molecules such as amine and sulfoxide groups as this will add to the weight and the polarity in addition, making the contrast agents more water soluble, a prerequisite for cellular imaging agents. There is also a requirement for additional unsaturated bonds in compounds **130c/131c**, **130c/131e**, **132c/133c** and **132e/133e**. The radar shows that optimum value for flexibility, but polar groups need be added to decrease lipophilicity and increase aqueous solubility. There is room for increasing molecular weight and number of saturation. The ideal thing to do is decrease flexibility by decreasing the number of rotatable bonds and decrease lipophilicity by adding polar groups which will also increase size. **Figure 23** but polar groups are needed to decrease lipophilicity and increase water solubility whilst **figure 29** show that optimization would have to be carried on all properties to obtain the optimum value.

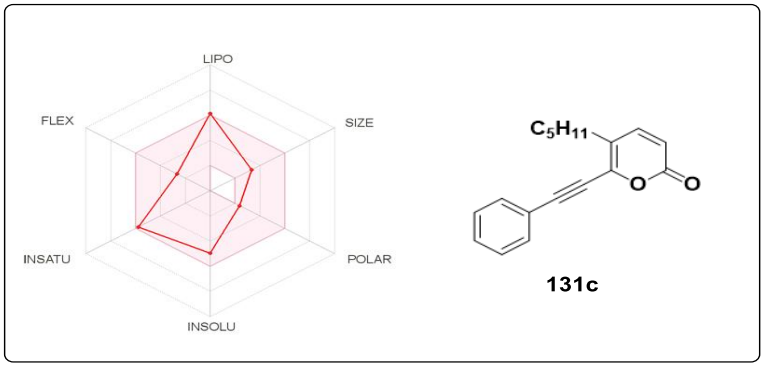

Figure 27: *In-silico* based physicochemical properties of 3-pentyl-6-(phenylethynyl)-2-pyrone **131c**. The inner pink circle is the optimal property for oral drugs.

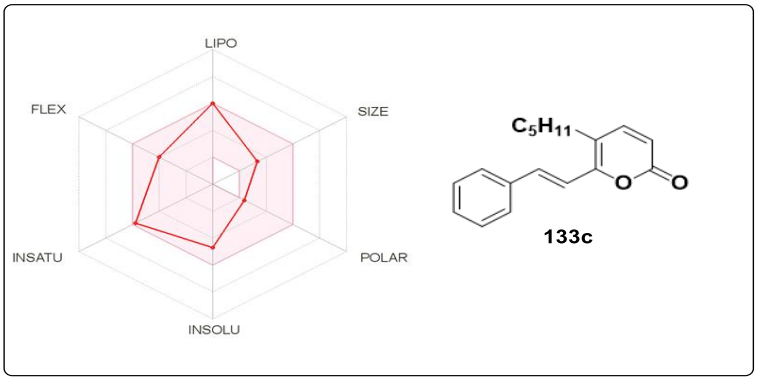

Figure 28: *In-silico* physicochemical parameters of 5-pentyl-6-styryl-2-pyrone **133c**. The pink circle is the optimal property for an oral drug.

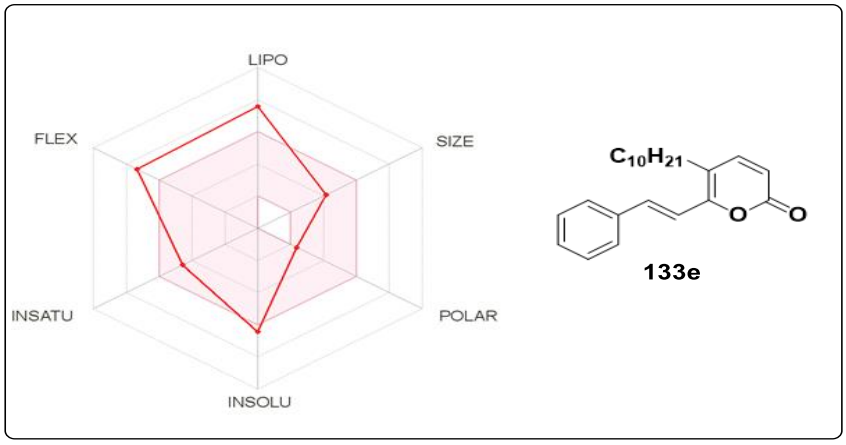

Figure 29: *In-silico* physicochemical parameters of 5-decyl-6-styryl-2-pyrone **133e**. The pink circle is the optimal property for an oral drug.

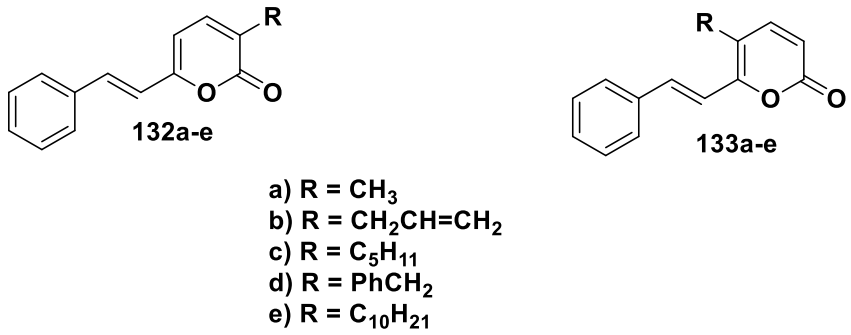

Figure 30. Targeted polarised imaging agents **132/133a-e**.

Poor solubility could be a liability in development. To improve solubility, certain modifications can be made, and these include reduction of molecular weight, introduction of ionisable groups, addition of hydrogen-bond forming groups and, in some cases, making the drug as a prodrug. Example Acyclovir is poorly absorbed, but many prodrugs have been developed to improve absorption and hence bioavailability as shown in **Figure 31**.

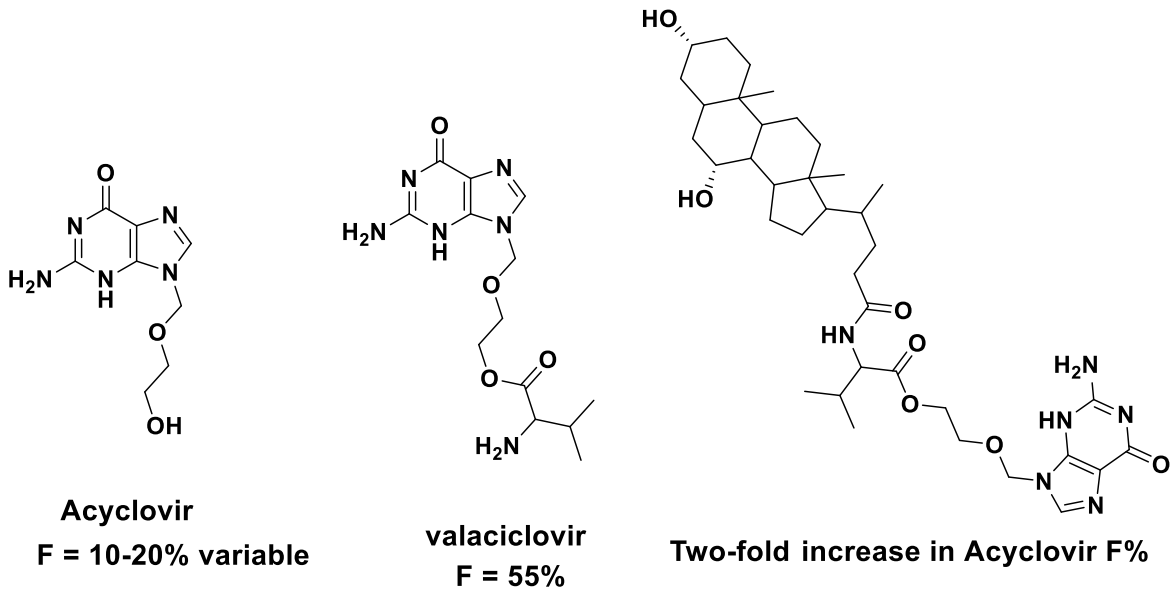

Figure 31: Prodrugs based on Acyclovir designed to improve metabolism and absorption.[109-110]

2.4 Predicted ADMET Parameters

2.4.1 Predicted ADMET Properties for the Designed Compounds.

CADD is currently indispensable in drug discovery and development. The computational medicinal chemists employ several software and resources to discover and optimise drugs. Drugs concentrations in tissues or cells is controlled by either diffusion or transporters and this determines drug effect. Lipid soluble drugs diffuse easily through cell membranes, but water-soluble drugs depend on transporters.[111] Transport proteins that move drugs through membrane barriers are important in the absorption, distribution and excretion of the drugs, while enzymes are critical for drug metabolism (**Figure 32**). The pharmacodynamic pathway is the drug receptor pathway of drug response. It involves drug receptors and biochemical events that occur after drug administration before drug effect is measured. The complex modular pharmacodynamic pathway can be simplified when all the biological approach and the many biochemical pathways between drug-receptor interaction and the drug response is linked (**Figure 32**).[112-113]

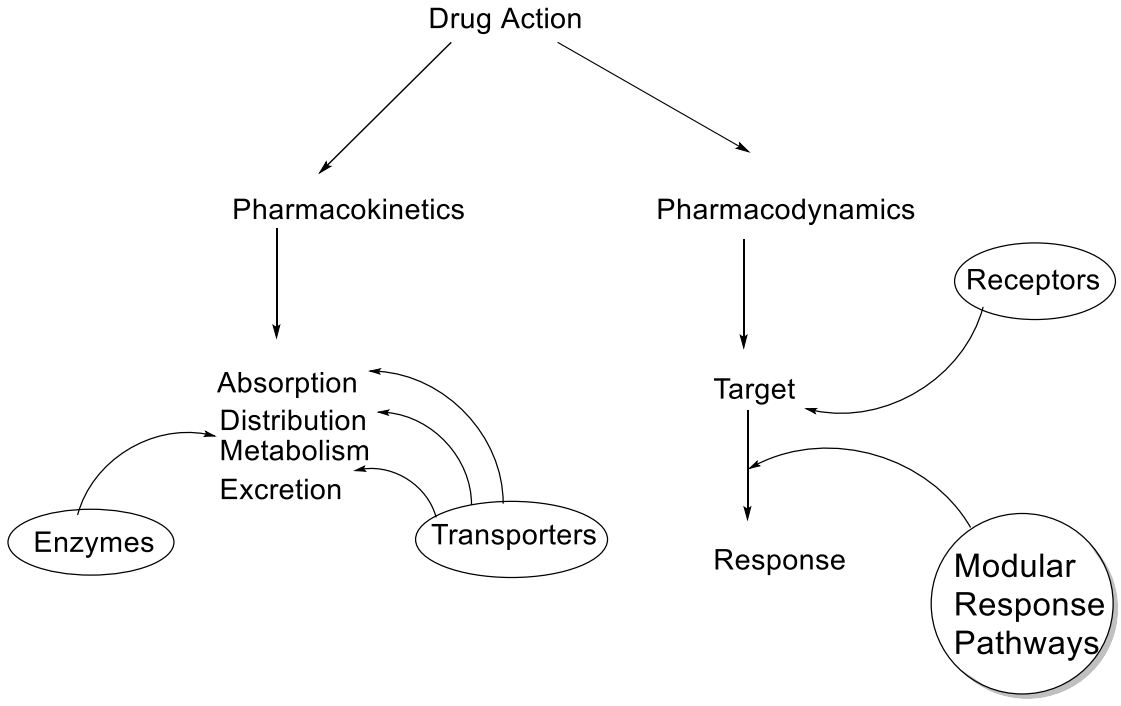

Figure 32: Schematic representation of the multigenic therapeutic drug pathway.[114]

Whilst drugs bind to cell membrane receptors, others bind to intracellular enzymes. However, it is the unbound drug that causes the pharmacological effect.[115] Direct measurement of drug concentrations in tissues is achieved by measuring blood or plasma drug concentration.[116]

Drug transporters play an important role in ADMET profile of both endogenous and exogenous compounds. Drug transporters function in controlling both drug effect and their toxicological effects in tissues and cells.[117] Drugs that are organic cations rely on transporters to move across cell membranes and several organic cation transporters are available in mammals.[118-120]

Drug absorption affects mode of administration, formulation and chemical properties of the drug. In silico models of drug absorption employs simple filters to evaluate the absorption of a drug based on some physicochemical properties, LogS, LogP, and acid dissociation constant (pKa).[121-122] Human Intestinal Absorption (HIA) determines the success of a drug candidate during development process and several in silico methods have been developed to predict it.[123-124]

Drug distribution is critical to pharmacodynamic and toxic effects and is usually predicted based on plasma protein binding (PPB) and blood brain permeation (BBB). The distribution of drug is affected by several factors, but PPB is the most critical. Compounds with low volume distribution (Vdss) are strongly bound to plasma proteins and have long plasma half-lives ($T_{1/2}$) (**Figure 33**).[125] High PPB has an impact on the drug effect.

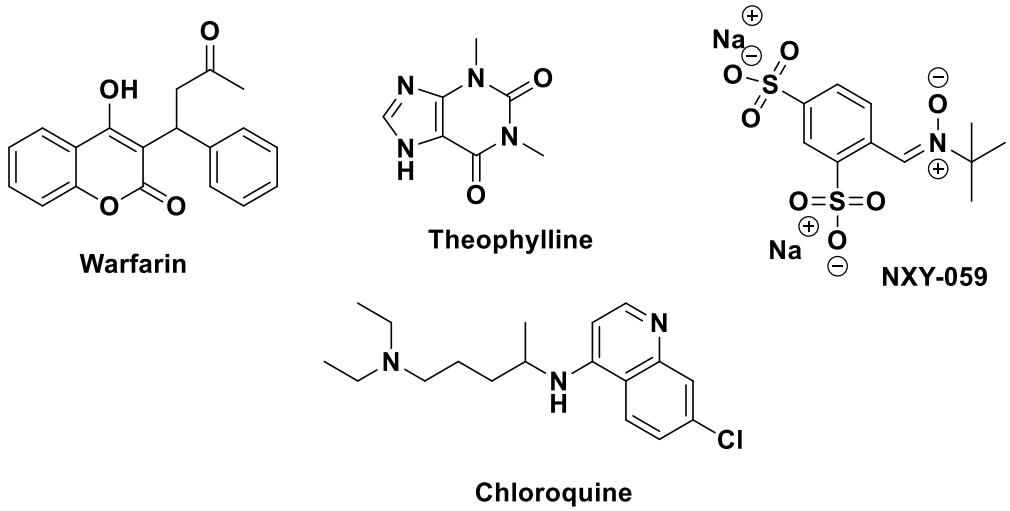

Figure 33: Selected drugs with variable PPB and Vdss.[126]

In general, lipid soluble drugs exhibit greater PPB. Plasma proteins include albumin, alpha-1-acid glycoprotein and lipoproteins. Acidic and neutral drugs bind to albumin, whilst basic drugs bind to alpha-1 acid glycoprotein or lipoproteins.[127] P-glycoprotein (P-gp) is involved in maintaining cells integrity by exporting hundreds of chemically unrelated toxins and has been implicated in multidrug resistance (MDR). Inhibitors of P-gp are widely used in preclinical and clinical studies for overcoming MDR. The compounds designed here are neither substrates nor inhibitors of P-glycoproteins. The implication been that they cannot be employed as possible drugs or inhibitors of multidrug resistance. They are predicted to enter the cellular spaces as indicated by their subcellular distribution into the mitochondria (Table 1 and 2), and are unlikely to be expelled by these glycoproteins, making they good contrast agent for cellular imaging.

Table 1: ADMET Predicted Profile of 5-decyl-6-styryl-2-pyrone **133e**.

ADMET Predicted Profile----------Classification

Model	Result	Probability
	Absorption	
Blood-brain Barrier	BBB+	0.97
Human Intestinal Absorption	HIA+	1.00
Caco-2 Permeability	Caco2+ cell	0.83
P-glycoprotein Substrate	Non-substrate	0.60
P-glycoprotein inhibitor	Non-inhibitor	0.54
	Inhibitor	0.57
Renal Organic Cation Transporter	Non-inhibitor	0.75
	Distribution	
Subcellular Localization	Plasma Membrane	0.55
	Metabolism	
CYP450 2C9 Substrate	Non-Substrate	0.71
CYP450 2D6 Substrate	Non-Substrate	0.81
CYP450 3A4 Substrate	Non-Substrate	0.56
CYP450 1A2 inhibitor	Inhibitor	0.74
CYP450 2C9 inhibitor	Inhibitor	0.55
CYP450 2D6 inhibitor	Non-inhibitor	0.86
CYP450 2C19 inhibitor	Inhibitor	0.82
CYP450 3A4 inhibitor	Non-inhibitor	0.65
CYP Inhibitory Promiscuity	High CYP inhibitory promiscuity	0.73
	Excretion/Toxicity	

Human-Ether-a-go-go Related Gene Inhibition	Weak inhibitor	0.57
	Non-inhibitor	0.73
AMES Toxicity	Non-AMES Toxic	0.93
Carcinogens	Non-carcinogens	0.92
Fish Toxicity	High FHMT	0.99
Tetrahymena Pyriformis Toxicity	High TPT	1.00
Honey Bee Toxicity	High HBT	0.62
Biodegradation	Non-Ready biodegradable	0.79
Acute Oral Toxicity	II	0.65
Carcinogenicity (Three-Class)	Non-Required	0.59
ADMET Predicted Profile-Regression		
Model	Value	Unit
Aqueous solubility	-4.23	LogS
Caco-2 Permeability	1.53	LogPapp, cm/s
	Distribution/Metabolism/Excretion, Toxicity	
Rat Acute Toxicity	1.98	LD_{50}, mol/Kg
Fish Toxicity	-0.14	pLC_{50}, mg/L
Tetrahymena Pyriformis Toxicity	1.96	$pIGC_{50}$, µg/L

Renal drug transporters can serve as the focus of drug-drug interactions (DDIs).[125-126] Such DDIs often lead to changes in drug pharmacokinetic profile and possibly lead to accumulation of drug causing renal toxicity.[130-131] Consequently, a considerable amount of effort has been made to develop in vitro tools to support screening of new molecular entities as renal drug transporter inhibitors. It has been reported that renal transporters are subject to substrate-dependent inhibition.[132] The

compounds designed (**128a-e**, **129a-e**) in this project are predicted to be non-inhibitors of renal organic cationic transporters as shown in Tables 1 and 2.

The brain is protected by the blood-brain barrier (BBB). Transporters are involved in the transportation of drugs in and out of the brain. Studies have shown that lipid solubility is vital to blood brain penetration.[133]

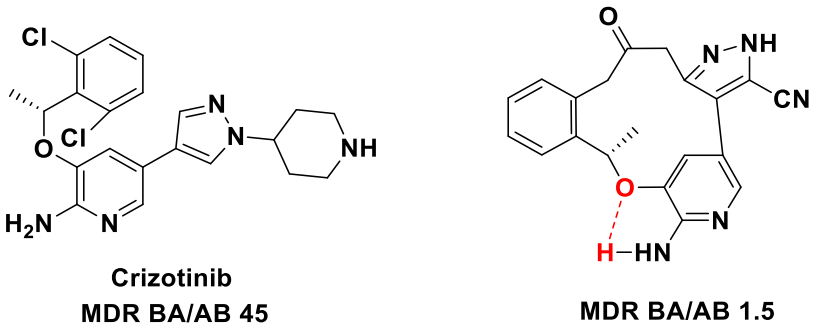

Figure 34: Selected TPSA and MDR P-gp binding

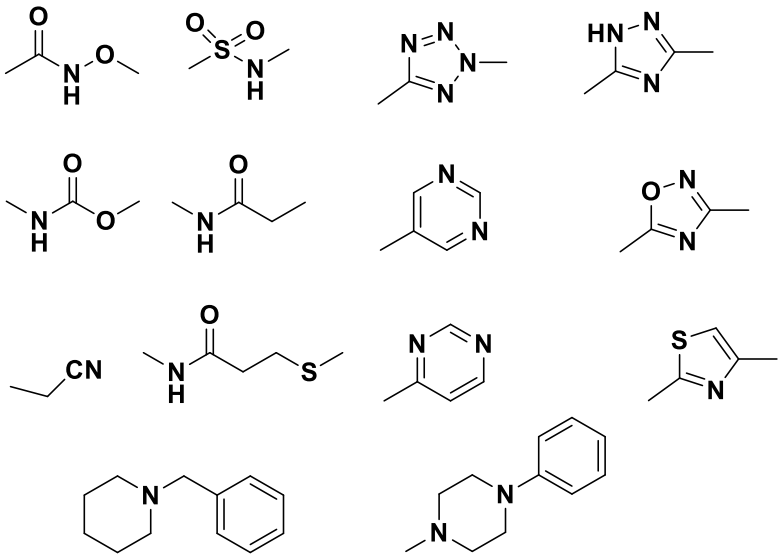

Figure 35: Functional groups associated with high P-gp activity.

The major cause of failure in drug discovery is currently toxicity and not pharmacokinetics.[134] This implies that every time drug design/discovery process is undertaken the chemical structures designed or discovered must first be subjected to *in silico*-based analyses to ensure that pharmacokinetics data is optimized and minimised as the cause of drug failure. Thus the reason for this Chapter is to ensure

that before any chemical structure is synthesized the best choice of 3/5-alkyl-2-pyrone is made.

Another factor that is vital in drug discovery is metabolism and is normally carried out by cytochrome P450 enzymes and are implicated in several drug-drug interactions (DDI), accumulations and clearance.[135-137] DDI is linked with promiscuous activities and adverse drug reactions (ADR). Therefore, understanding the molecular basis of drug promiscuity could help to design novel drugs with less ADR profiles in the early drug discovery process. Hepatotoxicity is the cause of withdrawal of several approved drugs though these effects are still poorly understood.[138-139] The result in Tables 1 and 2 showed that the synthesized 3-alkyl-6-chloro-2-pyrone compounds **128a-e** are inhibitors of CYP1A2 family of enzymes. The compounds **128a-e** are predicted to be inhibitors of CYP1A1 and CYP2C19 enzymes, but this does not necessarily preclude them from been involved in drug discovery. The fact they also inhibit CYP2C19 might produce DDI that will need be properly characterised before it reaches the market. However, DDI effects due to drug promiscuity can be reduced to a minimal by reducing their CYP2C19 inhibition from 91% to 3% by modifying the groups on the substituents (**Figure 36**).

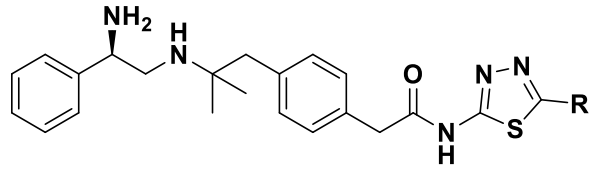

R = H CYP2D6 91% @3uM
R = Me CYP2D6 18% @3uM
R = CF3 CYP2D6 3% @3uM

Figure 36: Modification and its effect on CYP2D6 inhibition

Drug toxicity is a complex process. Models have been created that relates QSTR and toxicities of drugs to their chemical structure. Generally, two approaches are used to develop the QSTR models for diverse datasets: global models and local models.[140] Global models are based on different chemical classes and/or mechanisms of action; in contrast, local models are based on a specific chemical class and/or single mechanism of action.[141-142] These models have some drawbacks that can limit their application for regulatory purposes.

One of the toxicity tests used to determine the environmental impact of a molecule is an assay based on the concentration of growth inhibition (IGC_{50}) to Tetrahymena pyriformis (TP) ciliated freshwater. It is considered appropriate for toxicological testing and safety assessment of chemical components.[143] The designed compounds (**128d-e**) are predicted to have high TP toxicity, as shown in Tables 1 and 2.

The Ames test is a short-term bacterial reverse mutation assay detecting drugs that induce genetic damage and mutations.[144-146] From Tables 1 and 2 the designed compounds are predicted to be non-AMES toxic nor are they carcinogens. However, they have high honeybee, fish and Tetrahymena pyriformis toxicity. The lethal dose that is predicted to kill 50% of rats is 2.5937 mol/Kg and 1.9787 mol/Kg for 5-benzyl-6-styryl-2-pyrone **133d** and 5-decyl-6-styryl-2-pyrone **133e** respectively (Tables 1 and 2).

Table 2: ADMET Predicted Profile of 5-Benzyl-6-styryl-2-pyrone, **133d**.

ADMET Predicted Profile----------Classification

Model	Result	Probability
	Absorption	
Blood-brain Barrier	BBB+	0.98
Human Intestinal Absorption	HIA+	0.98
Caco-2 Permeability	Caco2+ cell	0.89
P-glycoprotein Substrate	Non-substrate	0.69
P-glycoprotein inhibitor	Non-inhibitor	0.62
Renal Organic Cation Transporter	Non-inhibitor	0.80
	Distribution	
Subcellular Localization	Mitochondria	0.76
	Metabolism	
CYP450 2C9 Substrate	Non-Substrate	0.74
CYP450 2D6 Substrate	Non-Substrate	0.88
CYP450 3A4 Substrate	Non-Substrate	0.72
CYP450 1A2 inhibitor	Inhibitor	0.51
CYP450 2C9 inhibitor	Inhibitor	0.65
CYP450 2D6 inhibitor	Non-inhibitor	0.86
CYP450 2C19 inhibitor	Inhibitor	0.85
CYP450 3A4 inhibitor	Non-inhibitor	0.75
CYP Inhibitory Promiscuity	High CYP inhibitory promiscuity	0.79
	Excretion/Toxicity	
Human-Ether-ago-go Related Gene Inhibition	Weak inhibitor	0.78
	Non-inhibitor	0.95
AMES Toxicity	Non-AMES Toxic	0.88
Carcinogens	Non-carcinogens	0.92
Fish Toxicity	High FHMT	0.88

Tetrahymena Pyriformis Toxicity	High TPT	0.99
Honey Bee Toxicity	High HBT	0.73
Biodegradation	Not Readily biodegradable	0.63
Acute Oral Toxicity	II	0.44
Carcinogenicity (Three-Class)	Not Required	0.51
ADMET Predicted Profile-Regression		
Model	Value	Unit
Aqueous solubility	-2.74	LogS
Caco-2 Permeability	1.70	$LogP_{app}$, cm/s
	Distribution/Metabolism/Excretion	
	Toxicity	
Rat Acute Toxicity	2.59	LD_{50}, mol/Kg
Fish Toxicity	0.13	pLC_{50}, mg/L
Tetrahymena Pyriformis Toxicity	1.10	$pIGC_{50}$, µg/L

2.5 *In-silico* Molecular Targets for the Designed Compounds

2.5.1 Similarity of Designed Compounds to Approved Drugs.

Drug-based similarity index (DBSI) measures the similarity of two drugs to each other and is a cheminformatics process that compares these drugs based on how similar they are in relation to their 2D and 3D structures. It uses bits to compare two structures '1' for positive similarity and '0' when it's absent. A Bit is a fragment that contains some functional group. Chemical fragments are building blocks of chemical structures and useful in modelling biological or physicochemical properties of chemicals. This is usually collated by the computer and using Tanimoto score (where T>0.7).[147] It is based on ligand—based screening methods that assumes that compounds that are structurally similar have the same activity. The same type of similarity measure is also assumed for receptors and proteins. This is a simple premise and is valid in some cases though not all.[147]

Similarity (or distance) metrics are employed in cheminformatics and several types exist (e.g. cosine coefficient, Euclidean distance, Tversky index,

fingerprints/Tanimoto coefficient). However, from the several studies carried out by Willet's group at the University of Sheffield has affirmed the popularity of Tanimoto coefficient.[148-156] Chen and Reynolds suggest the use of the Tanimoto index instead of the Euclidean distance for 2D Fragment-Based Similarity Searching.[157] Salim and coworkers though suggested that the use of 2-4 similarity index was superior to Tanimoto coefficient.[158] Though Willett still maintains that the Tanimoto coefficient is still the method of choice to compare similarities of molecules.[159] In 2013 Todeschini *et al.,* affirmed the better performance of Tanimoto coefficients among 51 similarity coefficients.[160-162]

Some researchers have collaborated the applicability of the Tanimoto coefficient, several of its weaknesses have also been reported by Flower.[163] More so, Tanimoto has a bias towards small molecules and reports a value of 0.33 for unrelated structures.[164-167] The implication of this is that the Tanimoto similarity index gives a good index of similarity of about 0.7.

2.5.2 Drug Discovery Based on Electroshape Similarity to Approved Drugs

The compounds designed here were analysed employing their electroshape similarity to approved FDA drugs and found to show high similarity to some of these drugs.[168] Electroshape characterise the similarity based on distance and charge distributions of the chemical compounds from four different points and has been opined as a better method for similarity measure than 3D similarity alone.[169] It is a five-dimensional OMICS tools employed in drug design that allows the design of drugs that act on multiple targets or disease pathways as well as evaluate adverse effects. Iophendylate is predicted to have Electroshape similarity to 6-chloro-3-decyl-2-pyrone **128e** (**Figure 37**). Iophendylate is a radiographic and magnetic resonance (MR) contrast agent for spinal cord.[170] Compound **128e** could serve as a good contrast agent for in a similar way to this analogue. Besides, the project is geared towards the design of compounds that can be used as contrast agents in cell-based imaging.

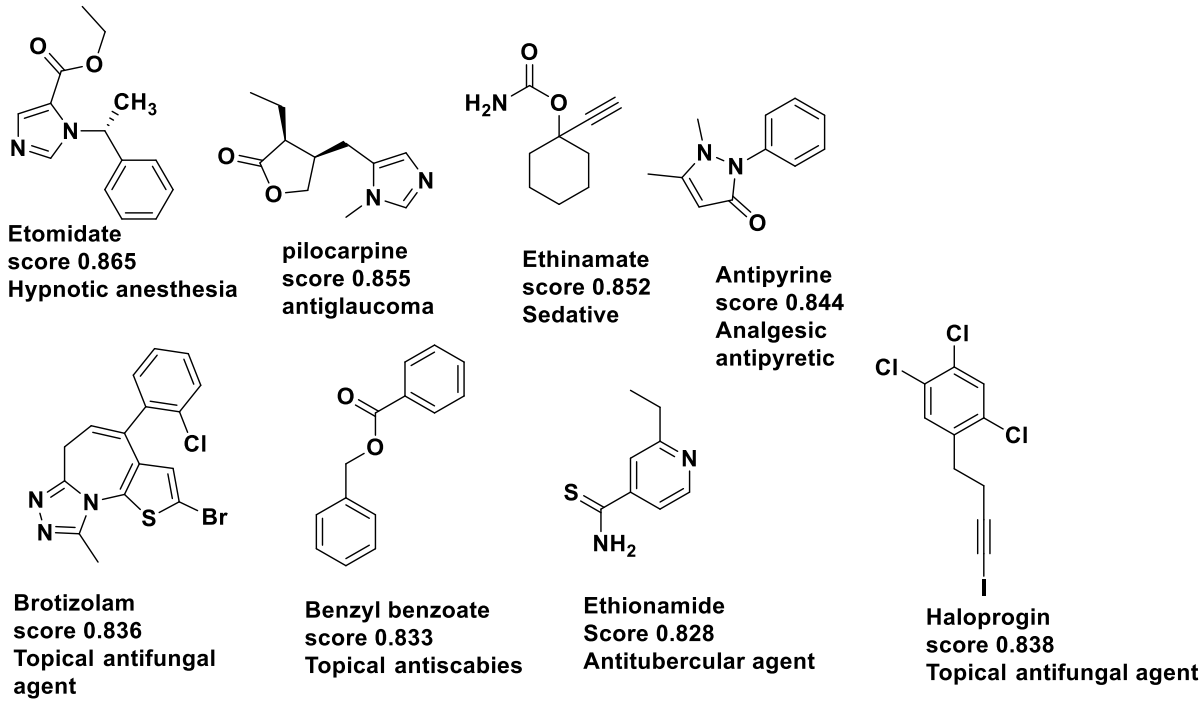

Figure 37: DBS for 3-benzyl-6-chloro-2-pyrone **128e** as ranked by SwissSimilarity software.

From the pharmacokinetic data as discussed above, the chemical structures with the best in silico data is n-pentyl, benzyl, and n-decyl derivatives. Comparative analyses of the chemical structures of **128c-e**, **131c-e** and **133c-e** to approved drugs will be carried out in this section. The next section would be to analyse what chemical structure to advance forward as the best imaging agent based on its physicochemical, pharmacokinetic and docking score to same target.

Ethionamide has Electroshape similarity to 3-benzyl-6-chloro-2-pyrone **128d** with a similarity score of 0.828 which is a good similarity to warrant a possible optimization of our test ligand to target the same protein (EtaR, PDB ID: 5f1J,151 **Figure 38**).[172] Ethionamide is an antiTB drug with a good similarity score (0.852) to 3-benzyl-6-chloro-2-pyrone and it has been employed in radionuclide imaging to examine its *in vitro* metabolites and found that it had inhibitory effect on *Mycobacterium tuberculosis*. Radiolabelled ETA was activated to 4-pyridylmethanol which is similar in structure to the metabolite of isoniazid another prominent anti-TB drug.[173] In line with our interest to design an anti-tuberculosis drug, this can potentially be achieved by optimizing 3-benzyl-6-chloro-2-pyrone **128d** as an anti-TB drug possibly by changing the cyclohexyl ring to a 2-pyrone and adding the appropriate substituents

as shown on the ethinamate molecule to obtain a molecule such as **130-131** (**Figure 39**).

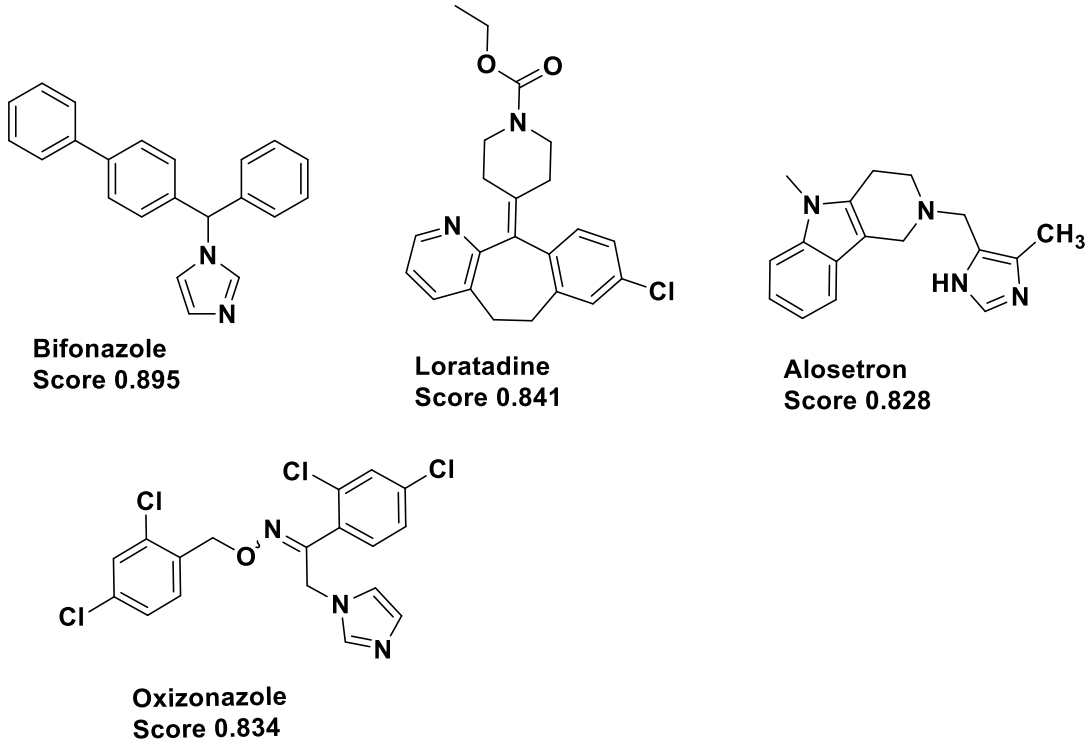

Figure 38: DBS for 5-benzyl-6-styryl-2-pyrone, **133d**.

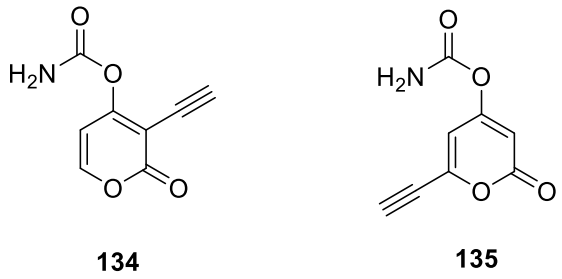

Figure 39: Proposed 2-pyrone based anti-TB drug.

Another approved drug with electroshape similarity to 5-benzyl-6-styryl-2-pyrone **128d** is oxiconazole nitrate (**Figure 38**) an antifungal drug which targets a cytochrome P450 51 enzyme vital to the survival of the fungi. Compound **128d** can be optimized as an antifungal drug that targets the same enzyme.[174-175]

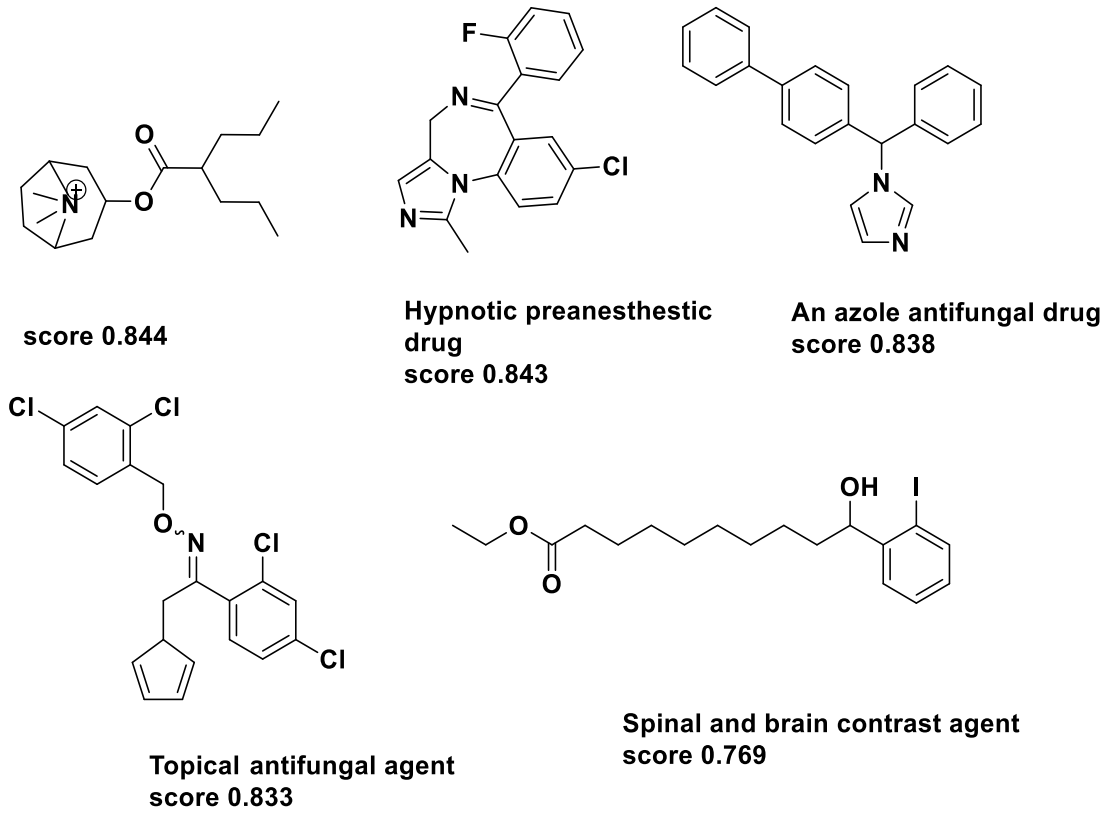

Figure 40: Drug-based similarity score to 6-chloro-3-decyl-2-pyrone, **128e**.

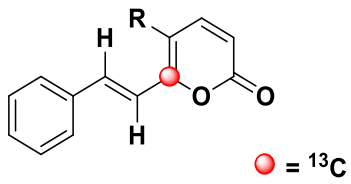

136a R = Bn
136b R = $C_{10}H_{21}$

Figure 41: Generic structure of the bioactive imaging agent **136a-b**.

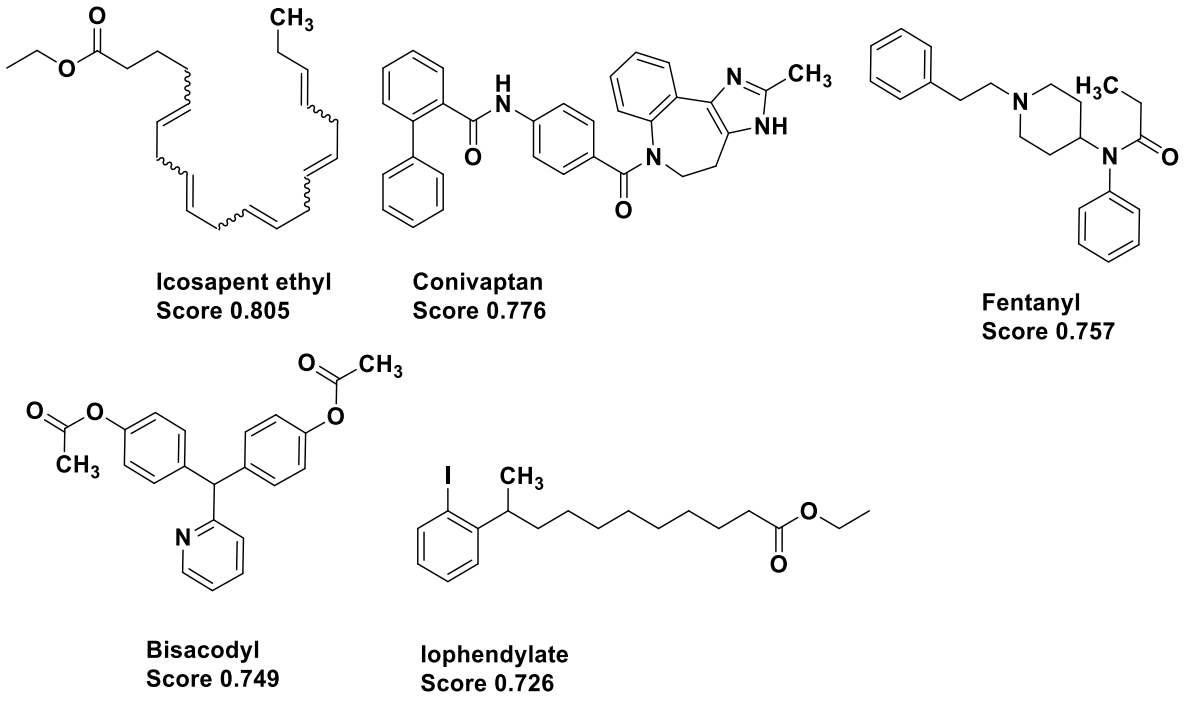

Figure 42: DBS for 5-decyl-6-styryl-2-pyrone **133e**.

Similarly, iophendylate (ethyl 10-(2-iodophenyl)undecanoate),[176] which is used as a contrast agent for locating spinal tumours has structural similarity to 5-decyl-6-styryl-2-pyrone **133e**. It is used as a contrast agent for diagnosing disc herniation. It is both a radiographic and magnetic resonance (MR) contrast agent for spinal cord imaging.[177-178] One of the best ways of attempting to design and synthesise contrast agents is to put your effort in designing agents based on other well-characterised imaging agents. The designed hNMR agents **128e/133e** have high molecularity similarity (0.826 and 0.726) to iophendylate which is a contrast agent for imaging disc herniations and spinal tumours. These molecules could be evaluated for use in this same manner.

2.5.3 *In silico* predicted target

An ideal drug target could be defined as a biomolecule (a protein) whose inhibition produces a biological response. In the past, drug design conception was based on "one drug-one target" approach but it was discovered that it is better based on multiple drug-multiple target approach.[180-181]

Table 3: Predicted target for 5-benzyl-6-styryl-2-pyrone **133d**. The result is ranked from top to bottom with the top being the most likely target.

S/No	Target	Uniprot ID	Gene code	ChEMBL ID	#sim. Cmpds (3D/2D)	Target Class
1	Tyrosyl-DNA phosphodiesterase 1	Q9NUW8	TDP1	CHEMBL1075138	293 / 2	Unclassified
2	Muscleblind-like protein 2 (by homology)	Q5VZF2	MBNL2		293 / 2	Unclassified
3	Muscleblind-like protein 3 (by homology)	Q9NUK0	MBNL3		293 / 2	Unclassified
4	Cannabinoid receptor 1	P21554	CNR1	CHEMBL218	264 / 9	Membrane receptor
5	Cannabinoid receptor 2	P34972	CNR2	CHEMBL253	205 / 7	Membrane receptor
6	NAD(P)H dehydrogenase [quinone] 1	P15559	NQO1	CHEMBL3623	5 / 26	Enzyme
7	Ribosyldihydronicotinamide dehydrogenase [quinone]	P16083	NQO2	CHEMBL3959	5 / 26	Enzyme
8	Prostaglandin D2 receptor 2	Q9Y5Y4	PTGDR2	CHEMBL5071	7./1	Membrane receptor
9	Cytochrome P450 2C9	P11712	CYP2C9	CHEMBL3397	7./1	Enzyme
10	Cytochrome P450 2C19	P33261	CYP2C19	CHEMBL3622	7./1	Enzyme
11	Cytochrome P450 2E1 (by homology)	P05181	CYP2E1	CHEMBL5281	7./1	Enzyme
12	Cytochrome P450 2C8 (by homology)	P10632	CYP2C8	CHEMBL3721	7./1	Enzyme
13	Cytochrome P450 2A6 (by homology)	P11509	CYP2A6	CHEMBL5282	7./1	Enzyme
14	Cytochrome P450 2B6 (by homology)	P20813	CYP2B6	CHEMBL4729	7./1	Enzyme

ChEMBL is an Open Data database containing information on bioactive and drug-like compounds. The database contains about five million bioactivity data for more than one million compounds and myriad number of proteins. Access is available at: https://www.ebi.ac.uk/chembldb.[182] The target prediction algorithm is opined to give accurate prediction in 92% of the cases and accurately predict the target family in 95% of the cases.[183]

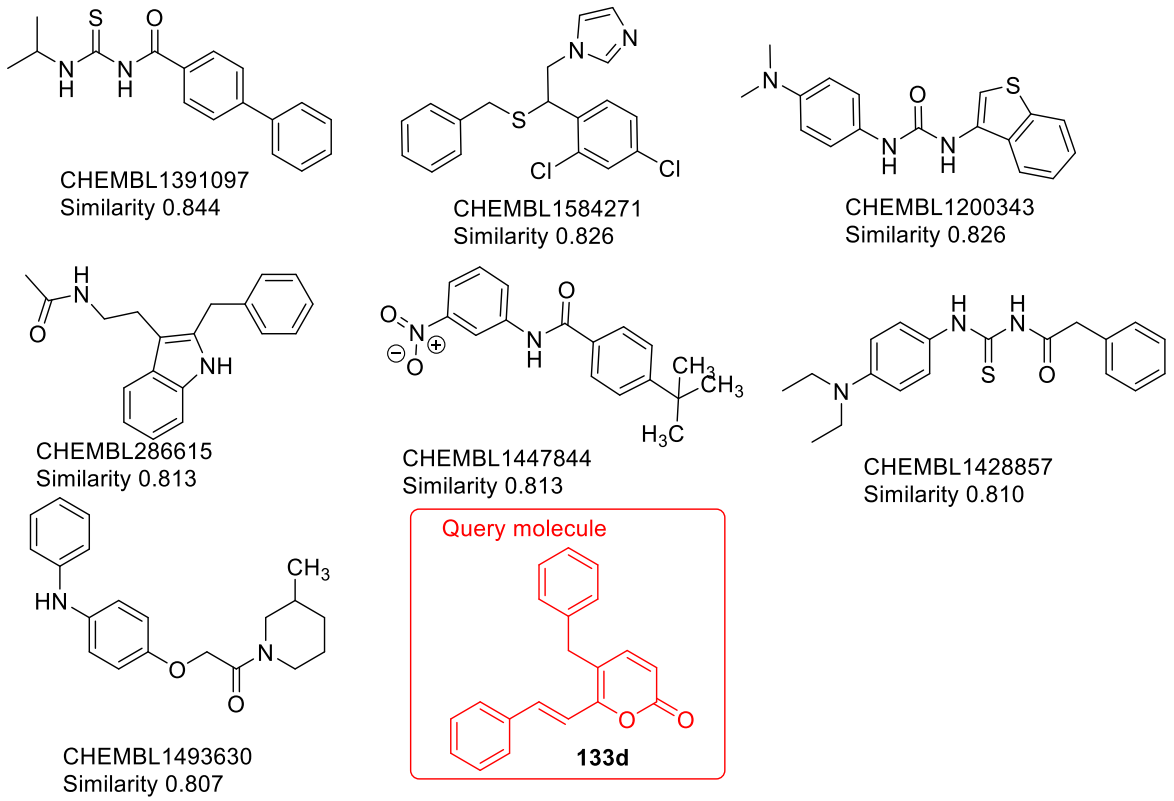

Figure 43: Ligands of tyrosyl-DNA phosphodiesterase 1 (TDP1) with 3D-based similarity to query molecule (red boxed molecule).

There is now a paradigm shift in drug discovery from single drug-single target to single drug-multiple target with effects in a complex neural network of enzymes and processes. Ligand-based methods predict the effect of new compounds based on the properties of compounds known to bind similar targets. A widely-recognized example is the QSAR method (Quantitative Structure Activity Relationship), which uses 2D topological fingerprints encoding atom types and their bond connectivity to infer activity and structure relationship. Molecular fingerprints of small molecules are employed as vectors to evaluate statistical relationships of numerous models and thereafter predict their binding activity towards specific target proteins.[184-187]

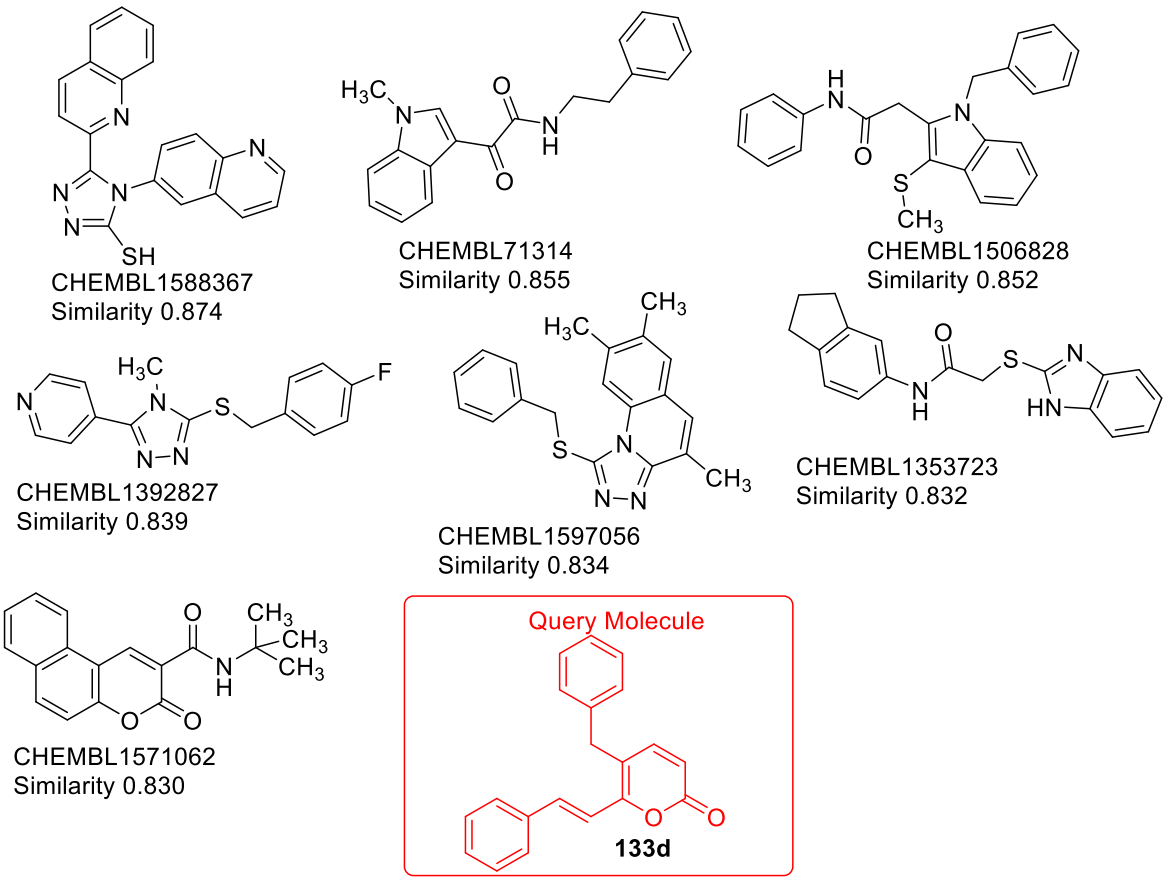

Figure 44: Ligands of muscleblind-like protein 1 (MBNL1) with 3D-based similarity.

Table 4: Predicted target for 5-decyl-6-styryl-2-pyrone **133e**. The result is ranked from top to bottom with the top being the most likely target.

S/no	Target	Uniprot ID	Gene code	ChEMBL ID	#sim. Cmpds (3D/2D)	Target Class
1	Tyrosyl-DNA phosphodiesterase 1	Q9NUWB	TDP1	CHEMBL107513	06./1	Enzyme
2	Thromboxane A2 receptor	P21731	TBXA2R	CHEMBL2069	3./1	Membrane receptor
3	Chymotrypsin-C	Q99895	CTRC	CHEMBL2386	1./1	Serine protease
4	Chymotrypsin-like elastase family member 2A (by homology)	P08217	CELA2A	CHEMBL2119	1./1	Serine protease
5	Chymotrypsin-like elastase family member 2B (by homology)	P08218	CELA2B	CHEMBL3887	1./1	Serine protease
6	Chymotrypsin-like elastase family member 3B (by homology)	P08861	CELA3B	CHEMBL4995	1./1	Serine protease
7	Chymotrypsin-like elastase family	PO9093	CELA3A	CHEMBL2809	1./1	Serine protease

	member 3A (by homology)					
8	Chymotrypsin-like elastase family member 1 (by homology)	Q9UN1	CELA1	CHEMBL3000	1./1	Serine protease
9	Cannabinoid receptor 1	P21554	CNR1	CHEMBL253	66/1	Membrane receptor
10	Cannabinoid receptor 2	P34972	CNR2	CHEMBL218	22./1	Membrane receptor
11	Carbonic anhydrase 1	P00915	CA1	CHEMBL261	22./1	Enzyme
12	Carbonic anhydrase 2	P00918	CA2	CHEMBL205	22./1	Enzyme
13	Carbonic anhydrase 7 (by homology)	P43166	CA7	CHEMBL2326	22./1	Enzyme
14	Carbonic anhydrase 3 (by homology)	P07451	CA3	CHEMBL2885	22./1	Enzyme
15	Carbonic anhydrase 5A, mitochondrial (by homology)	P35218	CA5A	CHEMBL4789	22./1	Enzyme

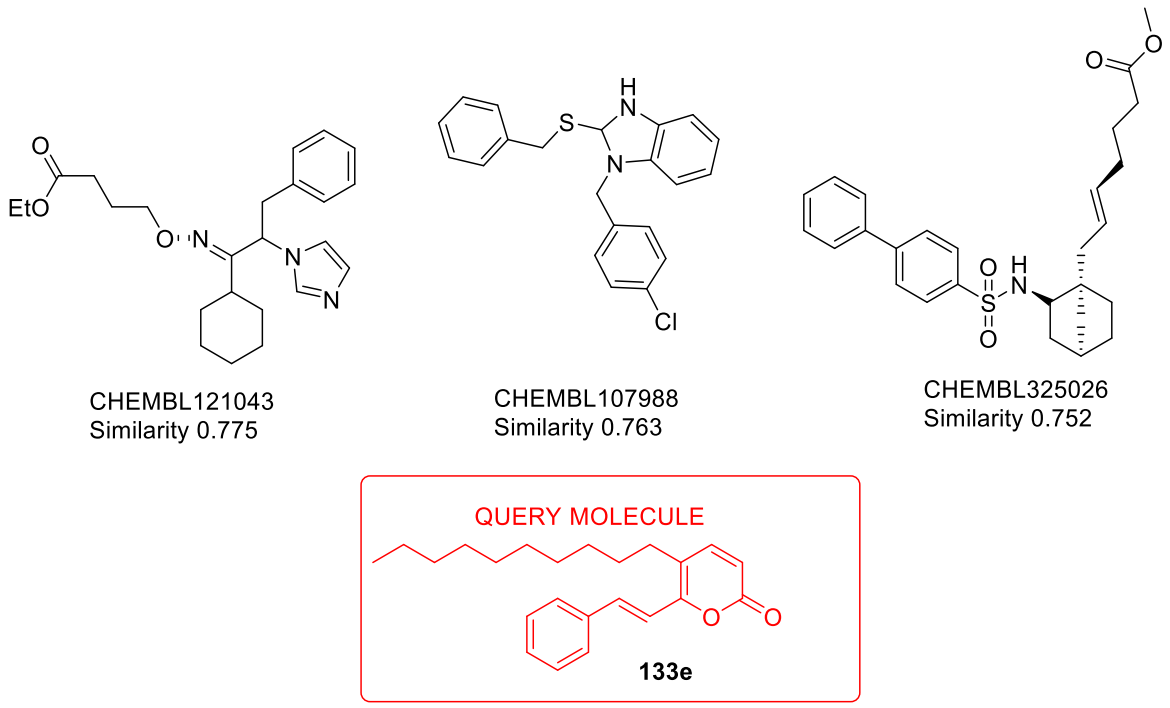

Figure 45: Ligands of thromboxane A2 receptor (TBXA2R) with 3D-based similarity to query molecule.

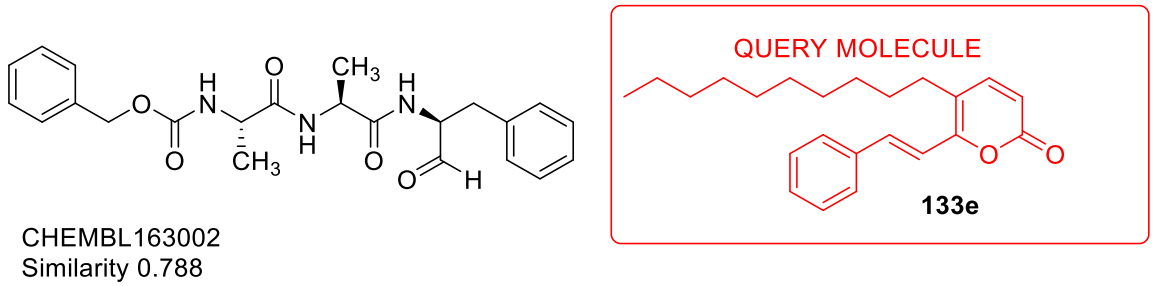

Figure 46: Ligands of chymotrypsin-C (CTRC) with 3D-based similarity to 5-decyl-6-styryl-2-pyrone **133e**.

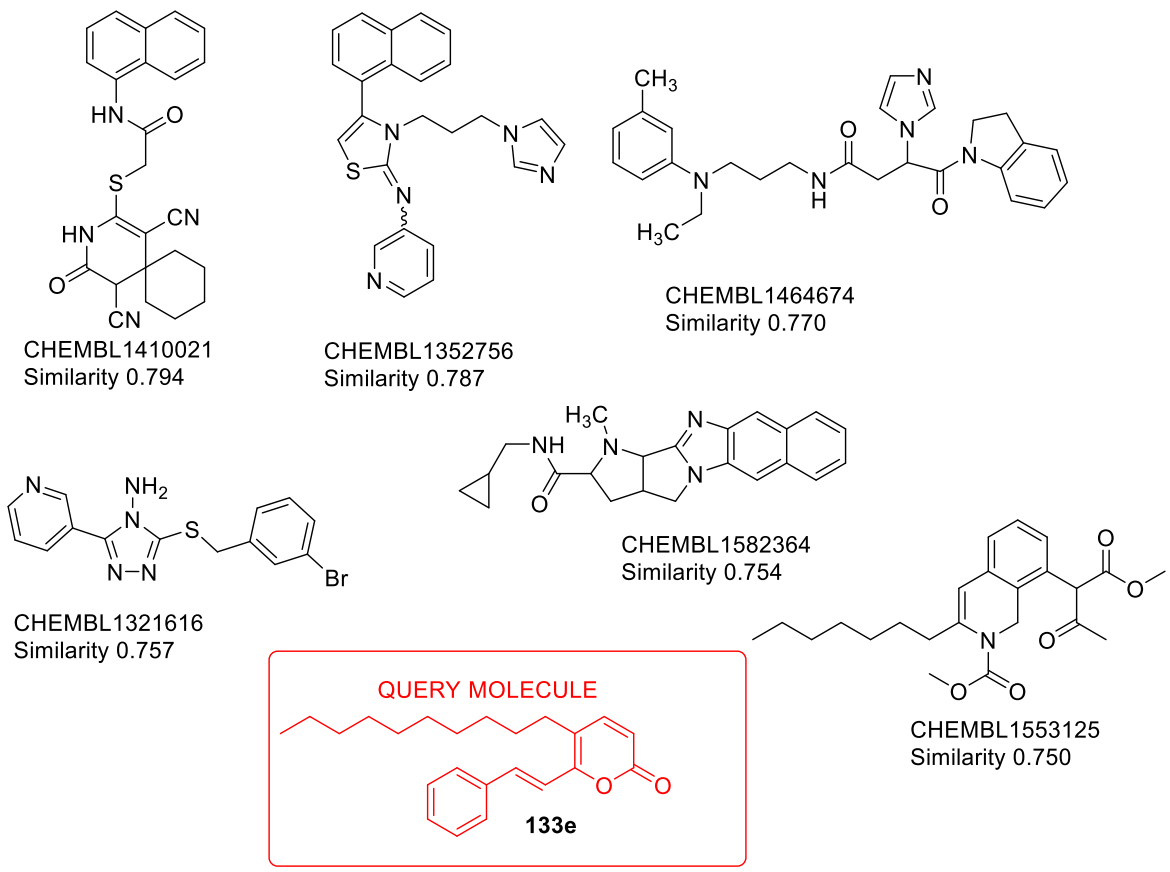

Figure 47: Ligands of tyrosyl-DNA phosphodiesterase 1 (TDP1) with 3D-based similarity to 5-decyl-6-styryl-2-pyrone **133e**.

Structure-based methods develop protein structural information associated with scoring functions to predict protein-ligand binding mode. The most extensively used form of structure-based target prediction methods is protein-ligand docking, which predicts interactions between drug candidates and their target proteins.[188] Structure-

based methods scores ligands based on how tightly they bind to their receptor.[189-190]

2.6 Molecular Docking

Molecular docking is a computational technique that predicts the way a ligand or drug binds its target and it prepares the binding poses of the ligand and the binding sites of the target and assign values based on the most favourable to the least favourable binding positions as shown in Figure 48-49.[191-193]

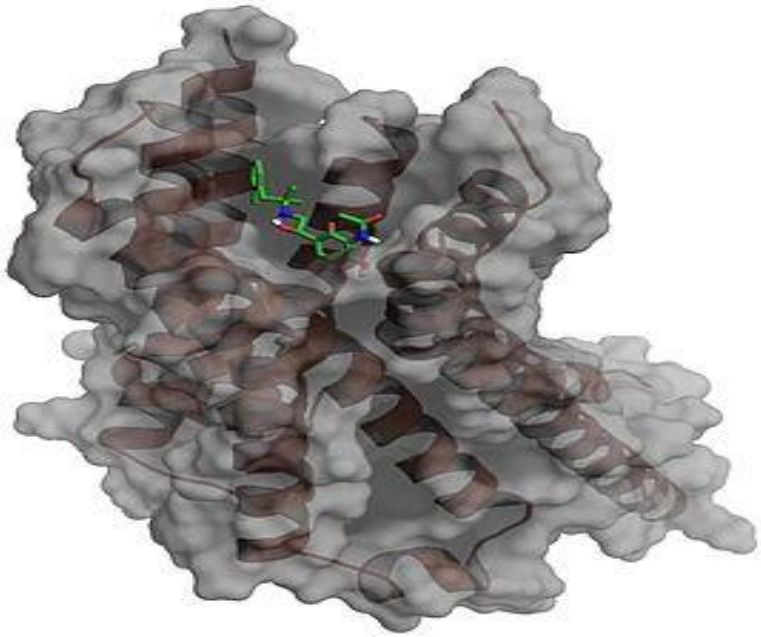

Figure 48: Docking of a small molecule (green) into the crystal structure of the beta-2 adrenergic G-protein coupled receptor (PDB: 3SN6).[194] This was adapted from ref.[195]

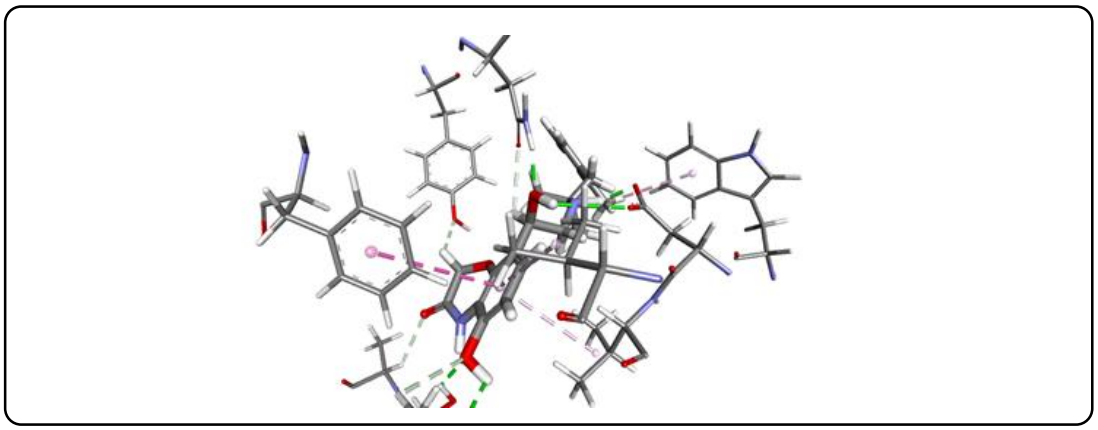

Figure 49: Expansion of the above docking to show the binding interaction between small molecule and the amino acids from the receptor; of beta-2 adrenergic G-protein coupled. The green dotted lines shows hydrogen-bond acceptor type interaction with oxygen, the pink dotted lines show hydrogen-bond donor-type interaction whilst the purple dotted indicate the pi-pi aromatic interaction as treated by PyMol.

The predicted targets for **133d** and **133e** are shown in Table 3-4 (PDB: ID: 5TVP,[196] 2MZ2,[197] 2E5C,[198]) was obtained from the protein data bank at Research Collaboration for Structural Bioinformatics (RSCB) Protein Database (PDB).[196] To study the scoring energy(s), root mean standard deviation (RMSD) and amino acid interactions and docking of the ligand would be carried out. The Protein Data Bank (PDB; http://www.rcsb.org/pdb/),[199] is the single worldwide archive of structural data of biomolecules (enzymes, proteins, genes). The rmsd gives the resolution of the target poses relative to the crystallographic data. Favourable poses have low values of rmsd and vice versa. This quantity is calculated between equivalent atoms in two structures, defined as

$$RMSD = \sqrt{\sum_i d_i^2/n} \quad \text{.....Eq. 1}$$

where d is the distance between each of the n pairs of equivalent atoms in two optimally superimposed structures. When rmsd is 0 for identical structures and the most favourable orientation of the protein. However, rmsd values depend on the number of amino acid sequence and the total number of atoms present. Whilst a rmsd value of 3 Å is significant for a protein with 50 residues is not so for one with 500 residues.[200-201]

2.6.1 METHODS

2.6.2 Docking Programs. In this study employed PyRx docking programs based on Autodockvina1.29 (ADV),[202] and OpenBabel.[203] ADV was developed by University of Cambridge. OpenBabel is part of the Rosetta's software suite for modelling small molecule structures. The receptors and ligands were prepared following the standard setup protocols using Gasteiger partial charges.[204] The grid sizes were set up to 25 Å × 25 Å × 25 Å in both programs, using as grid centre the centre of mass of the ligand provided by the DUD to localize the binding pocket. The global search exhaustiveness parameter was set to 8 (default value 8).

2.6.3 DockScore. This feature is given by the best docking score of the ligand poses. It represents the traditional approach, in which the docking score helps to provide enough information to discriminate an active molecule from an inactive one. Prior to analysis the docking scores were standardized as Z-scores.

2.6.4 DockLE. The ligand efficiency (LE) was computed as the quotient between the best ligand's score and the number of heavy atoms of the ligand.

2.7 Discussion

In lead optimization, one typically starts from a known inhibitor of a protein (often with a known binding mode) and modify it to attempt to improve binding.[202-203] Figure 47 shows the binding interaction between 6-chloro-3-decyl-2-pyrone **128e** with tyrosyl-DNA phosphodiesterase, a human protein. This same protein was predicted for 5-benzyl-6-chloro-2-pyrone **128d** as well as the 5-decyl derivative **128e.** The PyRx docking data showed several favourable hydrophobic bindings and a few hydrogen bonding interactions.

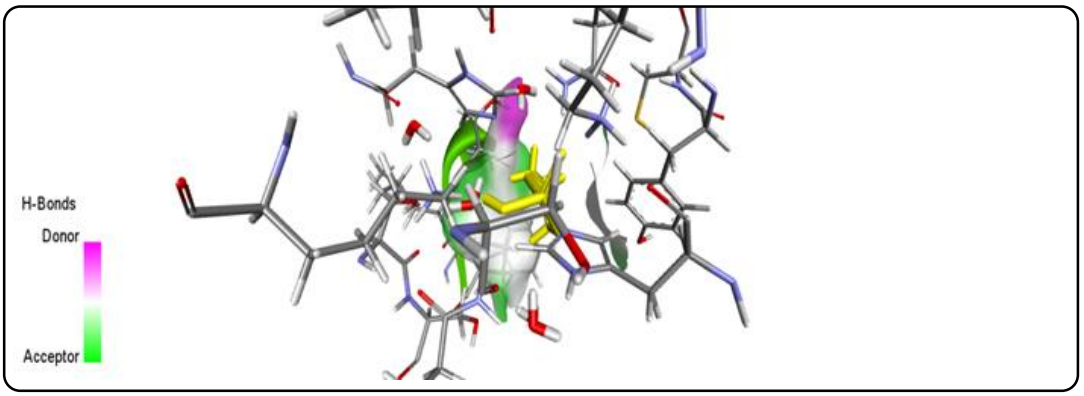

Figure 50: Showing the interaction between 6-chloro-3-decyl-2-pyrone **128e** (shown as in yellow colour) and a human protein (PDB ID: 1MU9),[210] a tyrosyl-DNA phosphodiesterase enzyme. This target is predicted for both 5-benzyl- and 5-decyl-6-chloro-2-pyrone **128d** and **128e**. The Vina search space was centred at X: 15.6269, Y: 100.521 and Z: 177.4974 and dimensions (Å) of X: 25.0000, Y: 25.0000 and Z: 25.0000.

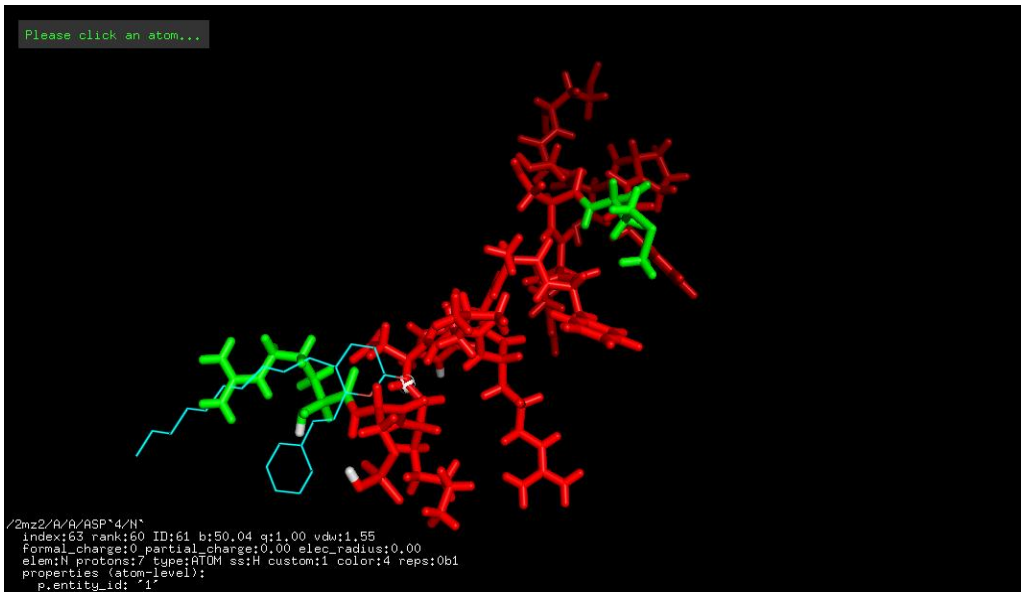

Figure 51: Muscleblind-like protein 1 (PDB: 2E5C,[208]) treated using PyMol software the 3rd predicted target for 5-benzyl-6-styryl-2-pyrone **133e**. The Vina search space was centred at X: 15.6269, Y: 100.521 and Z: 177.4974 and dimensions (Å) of X: 25.0000, Y: 25.0000 and Z: 25.0000.

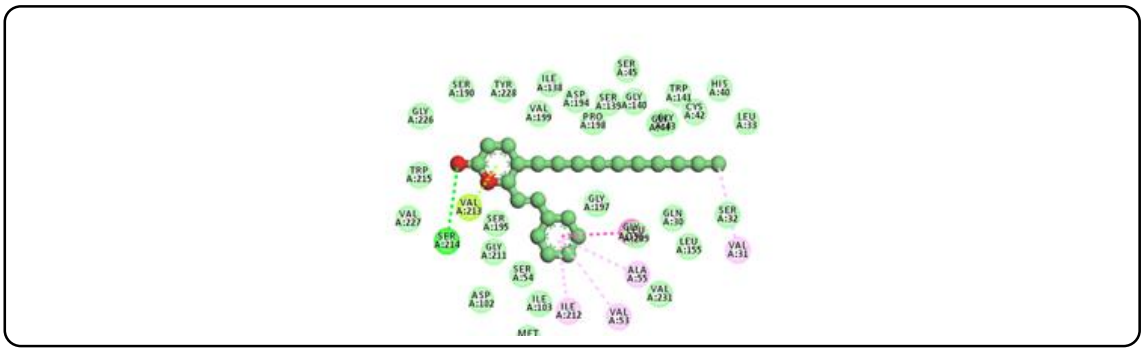

Figure 52: Molecular interaction between 3-benzyl-6-chloro-2-pyrone **128d** and bovine pancreatic protein, trypsin (PDB ID: 1AUJ,[211]) treated using BioSolve. The Vina search space was centred at X: 15.6269, Y: 100.521 and Z: 177.4974 and dimensions (Å) of X: 25.0000, Y: 25.0000 and Z: 25.0000. Interactions showing green-van der waals interaction, Bright green-hydrogen bond interaction, Lemon-green-Pi-lone pair interaction, Bright Pink-Amide-pi stacked interaction, Light Pink-Pi-Alkyl interaction

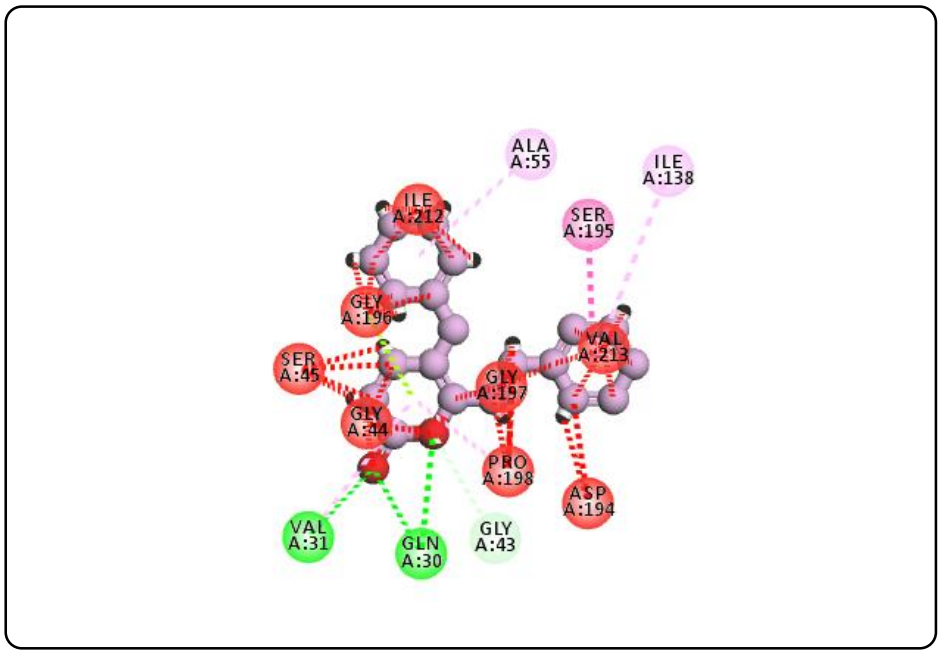

Figure 53: Illustrating the molecular interaction between 3-benzyl-6-chloro-2-pyrone **128d** and bovine pancreatic trypsin (PDB ID: 1AUJ,[211]) treated using BioSolve. The diagram shows the red dotted lines-unfavourable bumps, bright green-hydrogen bond, lemon-green dotted lines-π-lone pair interaction, pink dotted lines-Amide-π

stacked interaction and light pink dotted line-π-Alkyl interaction. The Vina search space was centred at X: 15.6269, Y: 100.521 and Z: 177.4974 and dimensions (Å) of X: 25.0000, Y: 25.0000 and Z: 25.0000.

The docking was carried out using AutoDock Vina software via the automated PyRx software. The structures of the targets were uploaded from the PDB data bank with PDB ID: 1QZQ,190 and PDB ID: 5TVP,[211] whilst those of the ligands were uploaded from ChemDraw as MDL SDF file and optimized automatically by OpenBabel in the PyRx software.

The docking using both 5-benzyl-6-styryl-2-pyrone **133d** and 5-decyl-6-styryl-2-pyrone **133e** indicated that the latter gave better binding energies of -48.95 to -47.70 KJ/mol with rmsd of 2.27 Å, whilst 5-benzyl-6-styryl-2-pyrone had free energies of binding between -34.73 to -33.89 KJ/mol with a lower structural similarity of 2.13 Å, as shown in Tables 5 and 11 respectively. The implication is that the 5-decyl-6-styryl-2-pyrone 1**33e** is a stronger binder than 5-benzyl-6-styryl-2-pyrone **133d**. Besides, the variability shown as indicated by the rmsd values (Tables 5 and 6) of 5-benzyl-6-styryl-2-pyrone **133d** is less so than those shown for the same target with 5-decyl-6-styryl-2-pyrone **133e**.

Table 5. Summary of free energy calculation results based on crystal structures. ΔG_{calc} is the calculated standard binding free energy. Reported are also the PDB files used. All values are in KJ.mol^{-1}. Docking Results for 5-decyl-6-styryl-2-pyrone **133e** with human tyrosyl-DNA phosphodiesterase 1(1QZQ).[210]

Entry	ΔG/ KJ/mol	Mode	rmsd/ Å
1	-48.95	0	0
2	-48.12	1	2.13
3	-47.7	2	20.26
4	-47.28	3	13.74
5	-46.86	4	20.24
6	-46.02	5	14.45
7	-45.61	6	15.38
8	-45.61	7	20.89
9	-43.51	8	12.17

Table 6. Summary of free energy calculation results based on crystal structures. ΔG_{calc} is the calculated standard binding free energy. All values are in KJ.mol^{-1}. Docking Results for 5-benzyl-6-styryl-2-pyrone **133d** with human tyrosyl-DNA phosphodiesterase 1(1QZQ).[210]

Entry	ΔG/ KJ/mol	Mode	rmsd/ Å
1	-34.73	0	0
2	-33.89	1	2.13
3	-32.64	2	20.26
4	-31.8	3	13.74
5	-31.38	4	20.24
6	-31.38	5	14.45
7	-31.38	6	15.38
8	-30.96	7	20.89
9	-30.12	8	12.17

The implication of 5-decyl-6-styryl-2-pyrone **133e** having a higher binding affinity implies it might have a higher affinity when employed as a target specific imaging agent. We therefore selected 5-decyl-6-(phenylethynyl)-2-pyrone **131e** as our initial cellular imaging structure to move forward to the synthesis stage. Its structural similarity to iophendylate is also good indication that this compound is a good choice to move forward towards optimization as a contrast agent.

2.8 Conclusion

The drug-like properties of the compounds for design and synthesis in the project have been analysed and some interesting features arose from this study. Firstly, the 6-chloro-3-decyl-2-pyrone **128e** has a better drug-like parameter than the other designed compounds. The molecular simulation docking score showed that for the same protein receptor (PDB ID: 1AUJ,[210] and 4h4f,[213]) 6-chloro-3-decyl-2-pyrone **128e** exhibited a better interaction. In the same light, the better pharmacokinetic and higher affinity was showed by 5-decyl-6-styryl-2-pyrone **133e,** followed by 5-benzyl-6-styryl-2-pyrone **133d**. Therefore, these two compounds should be synthesised as the imaging agents and the details can be found in the following chapters.

2.9 Antibacterial Screening of 3-Alkyl-6-chloro-2-pyrone

Concentration-dependent time-of-kill test is the most appropriate method for determining the bactericidal or fungicidal effect. The time-kill test reveals a time-dependent or a concentration-dependent antimicrobial effect.[214-215] For bacteria, this test has been well standardized and described in M26-A document of CLSI.[215-216] Bacterial growth was measured with turbidometric assay for antibacterial screening UV-Visible spectrum. *E. coli* was inoculated in 8 Falcon tubes at optical densities of 0.06 nm in LB medium at 3.12 mL final volume and incubated at 37 ^{o}C with agitation. OD was measured hourly for 6 h. A control sample was prepared identical to the test sample except for inclusion of the synthesised antimicrobial 2-pyrone compounds at a final concentration of 2.21 µg/ml for **131d**. The compounds tested showed antimicrobial activity against *E. coli* BT21. The concentration of 2.21 mg/mL was bactericidal to *E. coli.* However, with lower concentration the bacteria showed some recovery after 3 hours.

Chapter Three: Design, and Synthesis of Isotopically-labelled ^{13}C-2-Pyrone compounds.

3.1 Introduction

Given the requirement to synthesise imaging agents based on the 2-pyrone scaffold for use as contrast agent in cell-based NMR to characterise the binding interaction and/or biological effect of this small drug molecule in bacterial cell. It seemed appropriate to select 2-pyrones possessing broad spectrum antibacterial effect (discussed in Chapter 1). The compounds selected for synthesis were small molecule 2-pyrone compounds with good physicochemical, pharmacokinetic and good binding affinity as discussed in Chapter Two. The inhibitory effect of selected members of the target 2-pyrones against *E. coli* is discussed in Chapter 5.

NMR has demonstrated unique capabilities in providing useful information about the structural dynamics of binding between small drug molecules and proteins, protein-protein interactions. Thus, the decision to employ NMR as the biophysical method to measure the interaction between the designed imaging agent and their cellular receptors.

In-cell NMR is plagued by high concentration of water, lipids and other biomolecules present in the cells. One method of suppressing these interfering signals is the selective enrichment of an NMR-active nuclei. This research therefore designed molecules that their NMR signals can be enhanced on the catalytic addition of parahydrogen (the NMR-inactive nuclear spin state of molecular hydrogen). This will require the synthesis of a 2-pyrone containing alkyne motif, which on catalytic addition of parahydrogen (para-H_2) will give the desired imaging agent (a polarised alkene), our target will therefore be compounds such as **132a-e** (**Scheme 13**).

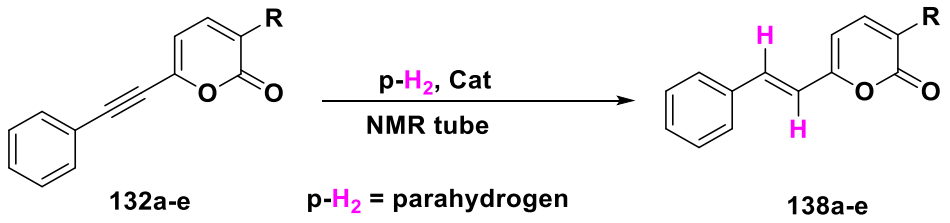

132a-e **p-H_2 = parahydrogen** **138a-e**

a) R = CH_3
b) R = $CH_2CH{=}CH_2$
c) R = C_5H_{11}
d) R = $PhCH_2$
e) R = $C_{10}H_{21}$

Scheme 13: Incorporation of para-H_2 into alkynyl-2-pyrones using a catalyst.

The application of such a compound (imaging agent) depends on the relaxation rate of the nuclei of interest. Protons relax too fast for efficient characterization of the interaction between the agent and analyte (e.g. the receptor). The average lifetime (T_1) of the excited state of any NMR-active nucleic is dependent on the magnetogyric ratio of the nucleus and its mobility. Hence, there is a requirement for isotopic labelling. This labelling requires enrichment above 95% because natural ^{13}C (1.11%) and ^{15}N (0.37%) (the other spin half NMR nuclei) levels make them less sensitive relative to hydrogen (100%). Therefore, the designed imaging agent must be Isotopically-labelled with a carbon-13 isotope which serves as the signalling motif. Carbonyl functional groups relax more slowly on the NMR timescale relative to other carbon centres hence the choice of enriching the carbonyl group within the 2-pyrone ring system (**Scheme 14**). This imaging agent **138** upon formation can transfer its signal enhancement to the signalling carbon nucleic either directly through bond or through space. The ^1H and ^{13}C NMR signal enhancement studies of the designed compounds will be discussed in Chapter 4.

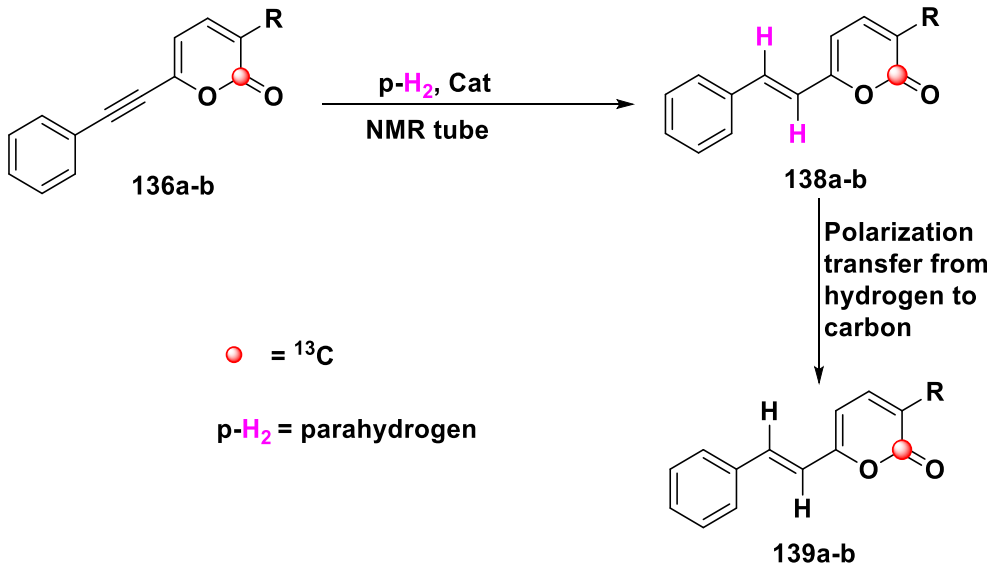

Scheme 14: Polarised generic target compound **138**.

3.2 Retrosynthetic analysis

The target compounds 2-pyrones can be accessed using a palladium-catalysed Sonogashira cross-coupling reaction. The reaction occurs between a nucleophilic fragment such as **140** and an electrophilic fragment such as **128** (**Scheme 15**). The nucleophilic fragment is commercially available, but fragment **128a-e** has to be synthesized. There are two major reports on the synthesis of 6-chloro-2-pyrone and their synthetic procedures will be explored and optimized using non-isotopically labelled reagents. Once an efficient synthetic sequence has been developed on the non-isotopically labelled materials, the optimized procedure can be applied to the isotopically-labelled analogues.

The proposed forward synthesis is shown in **Scheme 16**. Commercially available diethyl malonate can be alkylated with an appropriate alkyl halide **147a-e** and the resultant monoalkylated ester **145a-e** employed in an electrophilic addition with **143f-g** or **144**. This will afford a tri-ester with structure such as **148a-e**, on hydrolysis and consequent decarboxylation should afford **141a-e**. Diacid **141a-e** can be condensed using excess acetyl chloride to afford the appropriate chloropyrone **128a-e**.

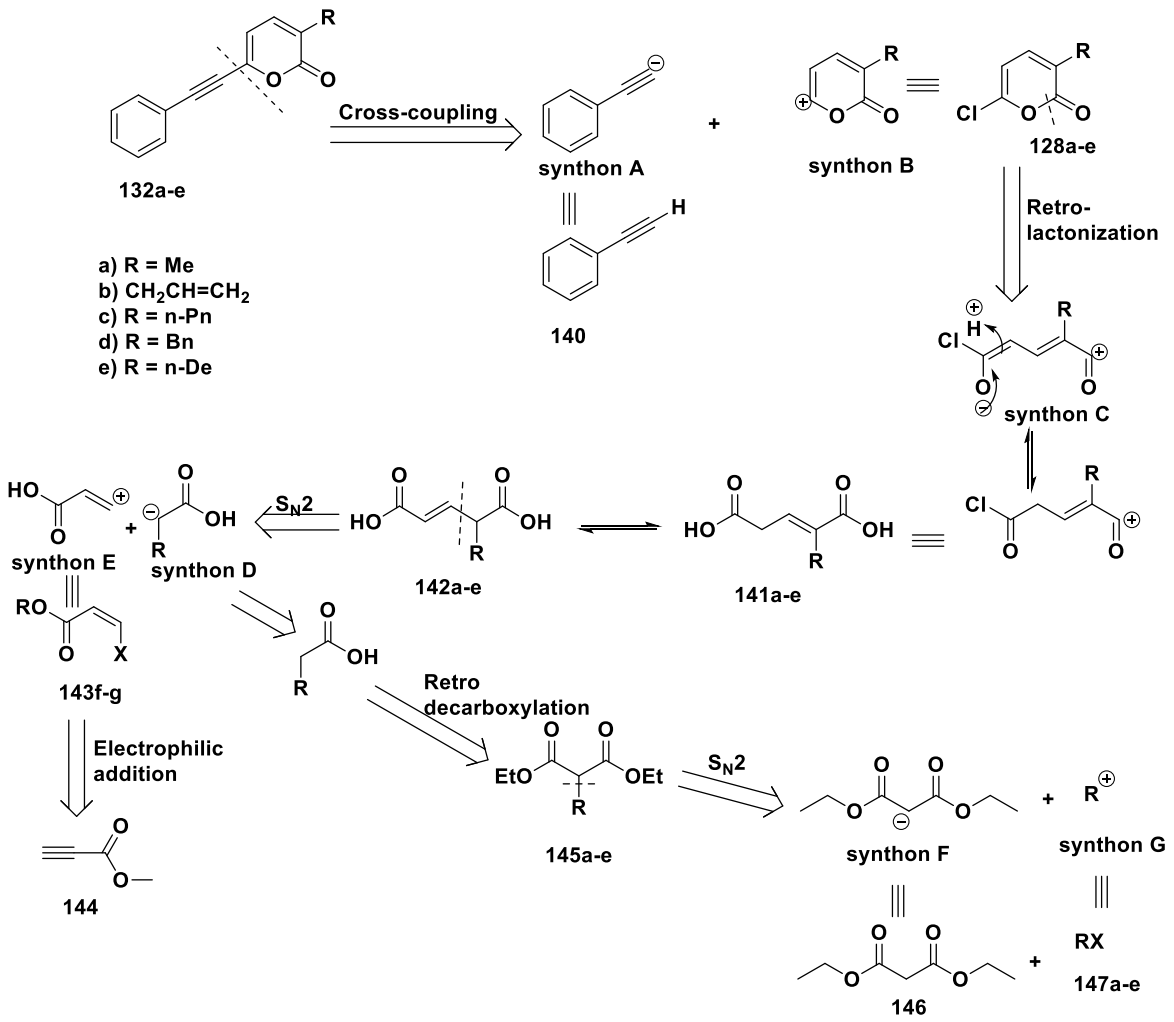

Scheme 15: Retrosynthetic analysis to compounds **132a-e**.

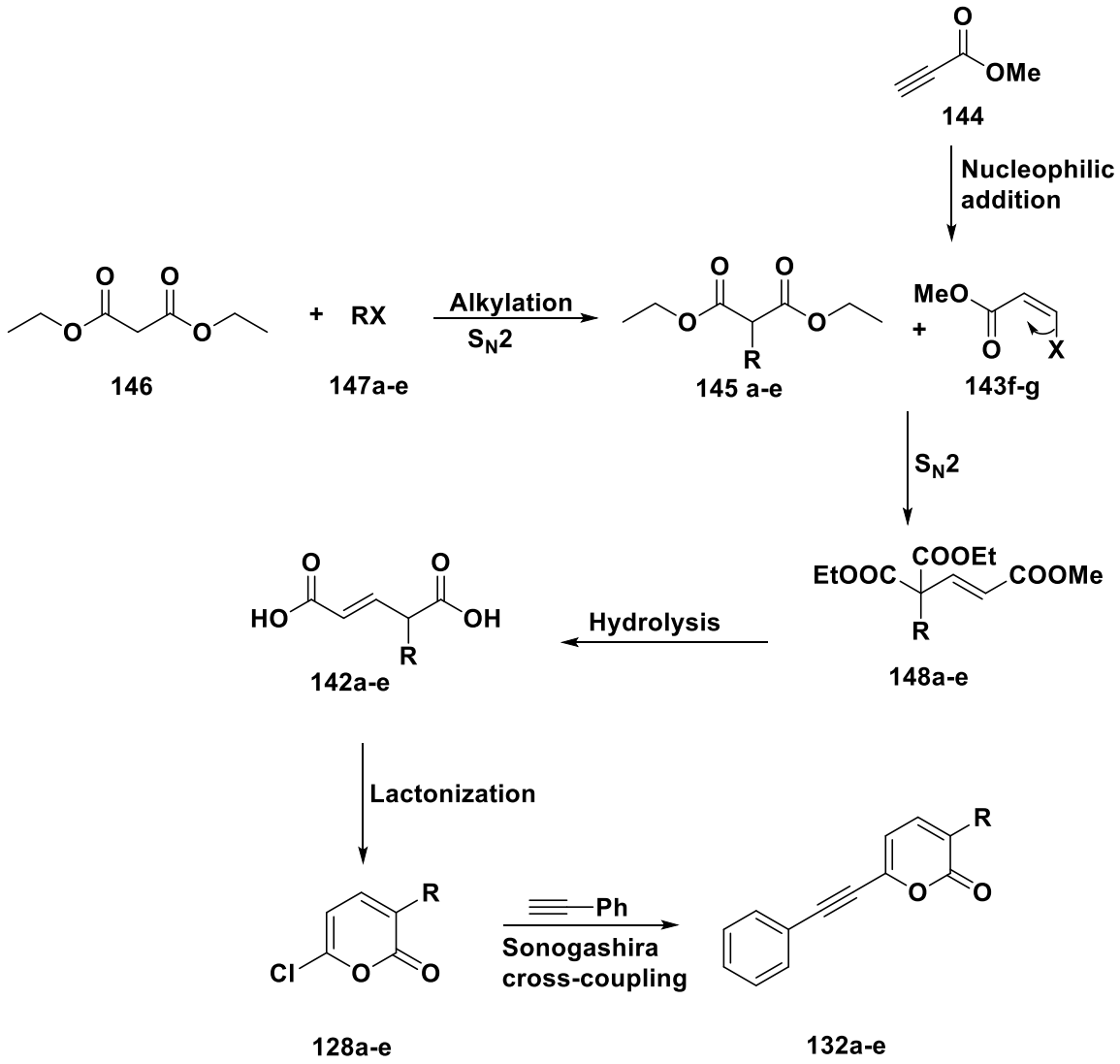

Scheme 16: Proposed forward synthesis of 6-alkynyl-2-pyrone **132a-e**.

3.3 Development and optimization of fragment 128a-e

The four step synthetic process, as reported by Gelb and Abeles (1983), afforded 180 mg/40 mg 3/5-benzyl-6-chloro-2-pyrone-2,6-^{13}C **153, 154** from 5.2 g of diethyl malonate-1-^{13}C, respectively as shown in **Scheme 17.**[211-212] The reaction involved two equivalent of diethyl malonate and one equivalent of chloroform.[213,217] They reported the yield for the final products in milligrams but none for the intermediate products.[210-211] The report of Westkaemper and Abeles,[217] employed a similar synthetic route to Gelb and Abeles,[211] and reported a yield of 140 mg and 80 mg respectively for the two regioisomers, though as the isotopically non-labelled analogue.

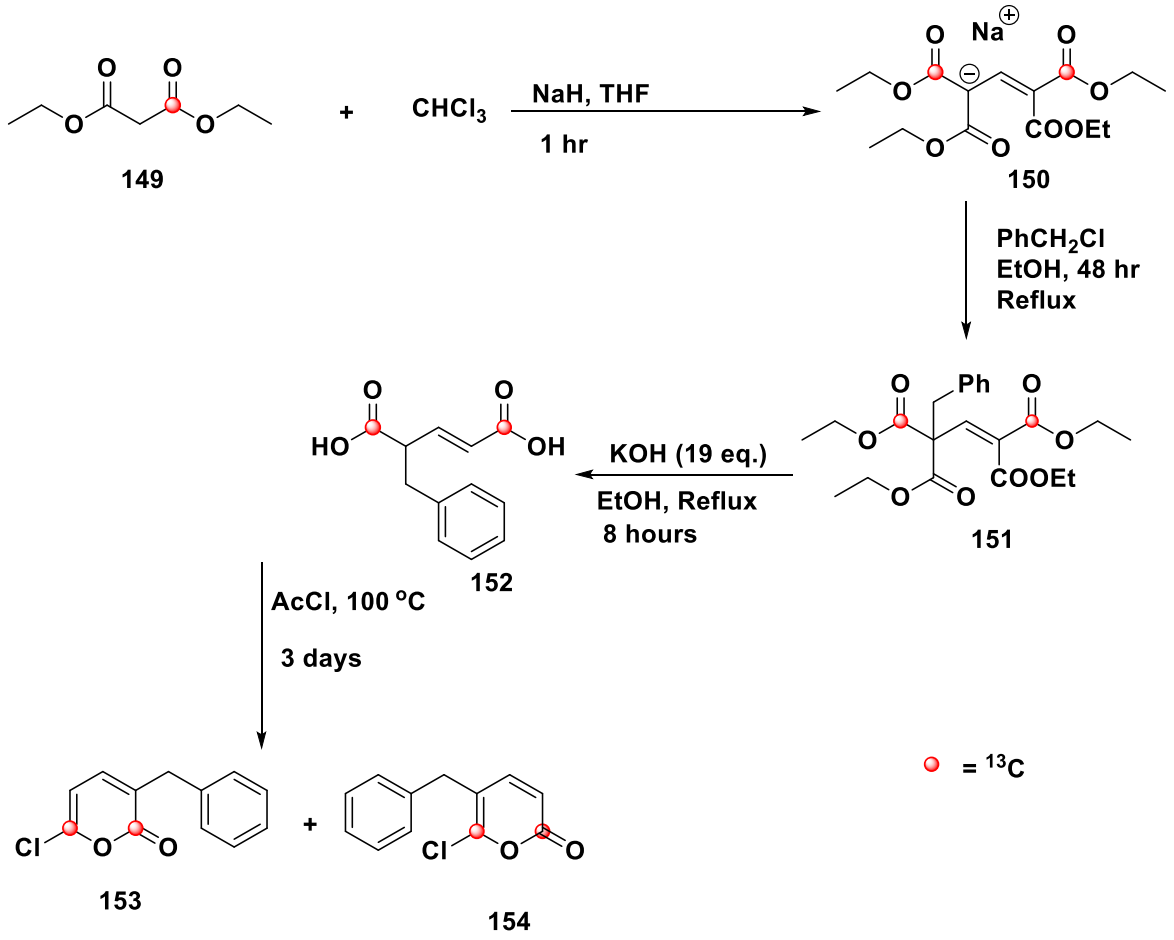

Scheme 17: Synthetic route to ^{13}C-isotopically labelled 3-benzyl-6-chloro-2-pyrones **153** and **154**.[211]

In their synthesis of labelled chloropyrone, enrichment of 75% was reported,[211] but for the purposes of live cell NMR imaging a higher level of isotopic enrichment is required.[218] This high level of isotopic enrichment requires diethyl malonate-[1,3-^{13}C] at a cost of £4500 from Sigma Aldrich United Kingdom. All attempts to optimise this reaction employing the use of non-labelled diethyl malonate led to failure for most of the other alkyl substituents except for the benzyl derivative **128d** which gave 109 mg (14% yield over the four steps) from 1.0 g of diethyl malonate as shown in **Scheme 18**.

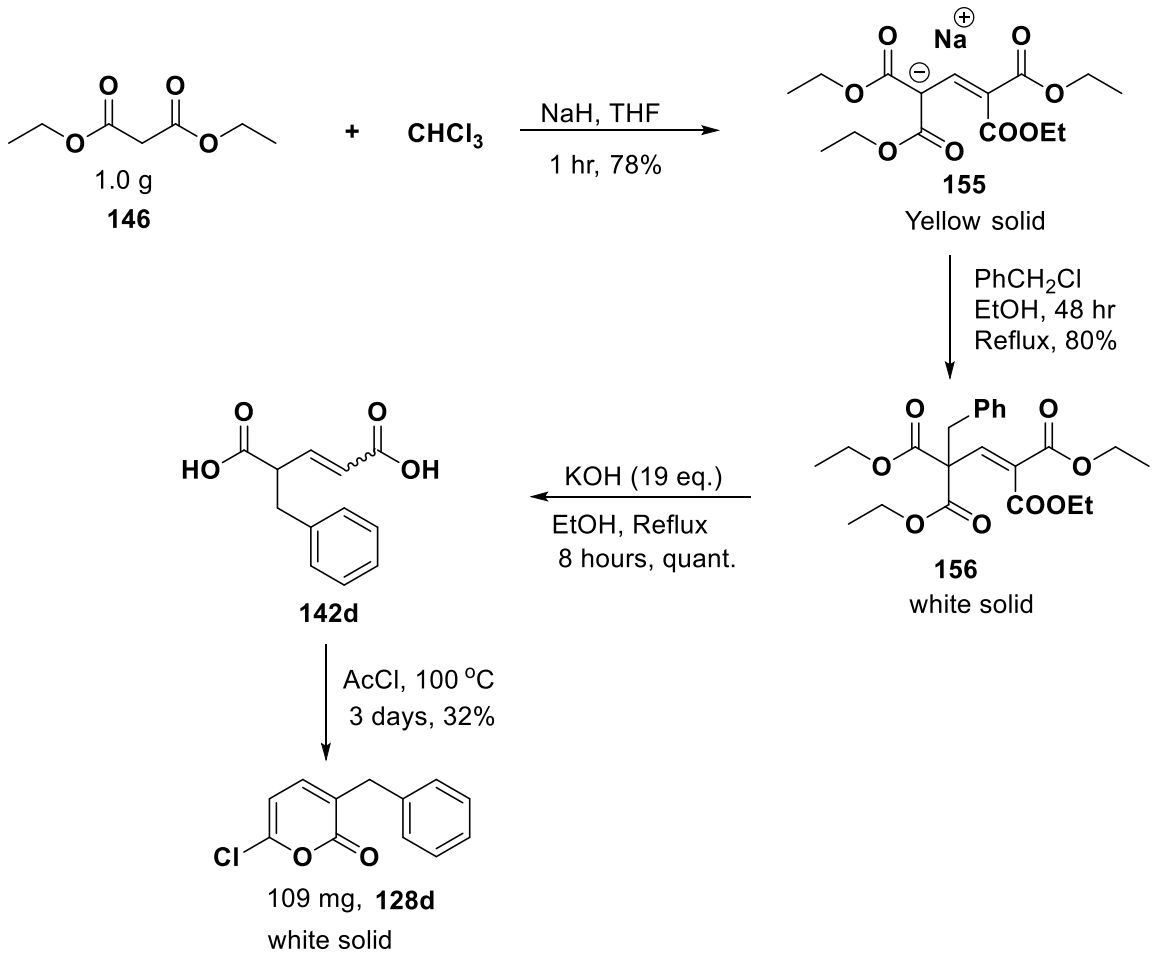

Scheme 18: Synthetic route initially investigated in the synthesis of unlabelled 6-chloro-3-benzyl-2-pyrone **128d**.

The reaction between diethyl malonate and chloroform in the presence of a sodium hydride in tetrahydrofuran afforded compound **155** as a bright yellow salt upon recrystallization from ethanol. The ^{1}H NMR spectrum of **155** indicated the presence of one deshielded olefinic proton at 8.25 ppm. The ^{1}H NMR spectrum for this salt agrees with that reported in the literature.[213, 219-222] The melting point (269-270 °C; lit.[213,219] 270-272 °C) was in close agreement. The mass spectra of both the protiated and sodiated pseudomolecular ions are consistent with those expected.

Treatment of **155** with benzyl chloride in ethanol afforded the tetra-ester **156** as a white solid in 73% yield, observed melting point 71 °C in agreement with the literature value (71 °C).[212-213] The ^{1}H and ^{13}C NMR spectra of **156** in $CDCl_3$ was consistent with the proposed structure.

The base-catalysed hydrolysis and subsequent decarboxylation of **156** afforded 2-benzylglutaconic acid **142d,** following acid hydrolysis as a semi-solid in quantitative yield. Furthermore, the condensation of this acid in excess acetyl chloride at 100 ^{o}C for three days afforded 3-benzyl-6-chloro-2-pyrone **128d** in 22% yield. The spectroscopic data is in agreement with the proposed structures.

The second synthetic procedure, reported by Hatch *et al*.,[223] began with the alkylation of diethyl malonate (**Scheme 19**). The alkylation was optimised using three bases; sodium hydride, sodium methoxide and potassium carbonate the result is presented in **Table 7**. The use of sodium hydride would likely also afford an appreciable amount of the dialkylated product as a direct consequence of the equilibrium that exists between the chemical species involved in this reaction (**Scheme 19**). Since the monoalkylated diethyl malonate is a stronger base and will be deprotonated by the acid and therefore, a further alkylation will lead to dialkylation.[224] The chemical equilibrium in **Scheme 20** lies completely to the right producing the monoalkylated malonate (a stronger conjugate acid to the weak acid diethyl malonate) because of resonance stabilization of the diethyl malonate anion which is initially formed as illustrated in **Scheme 19**. Furthermore, the monoalkylated species being a stronger acid to diethyl malonate; can further be deprotonated by the strong base leading to the dialkylated malonate (**Scheme 19**).

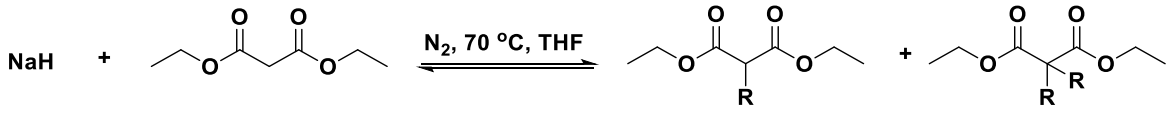

Scheme 19: Formation of monoalkylated and dialkylated diethyl malonate.

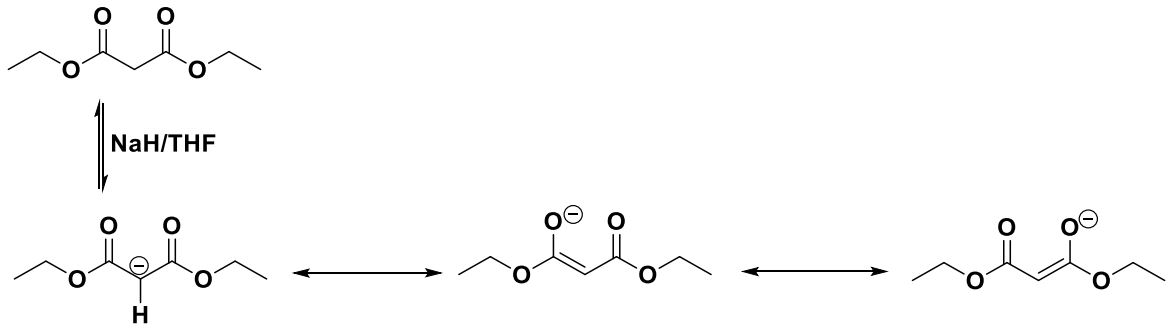

Scheme 20: Resonance stabilization of diethyl malonate.

The carbonate anion (CO_3^{2-}) on the other hand is a very weak base, though it is basic enough to remove a proton from an active methylene compound (pKa = 9~13). However, the equilibrium favours the formation of the weak chemical species (lies far to the left) and therefore leads almost exclusively to monoalkylation as shown in **scheme 21**.[225-226]

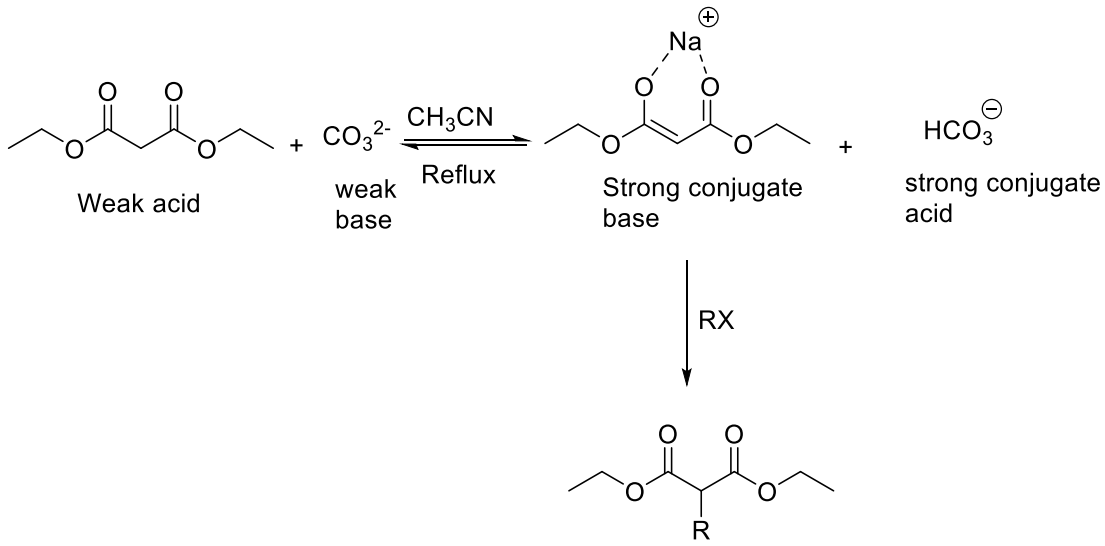

Scheme 21: Illustration of the chemical equilibrium in a weak acid-weak base system.

The solid-liquid phase transfer alkylations of diethyl malonate with various alkyl halides at high temperature (>120 ^oC), employing either potassium carbonate or caesium carbonate, have been reported with the observation of primarily monoalkylation and a trace amount of the dialkylated product <3% as expected from **Scheme 22**.[227-230] It was found in this study that the mild base potassium carbonate in a biphasic reaction with tetrabutylammonium bromide (TBAB) worked well, with no dialkylated product detected, in contrast to a literature report.[227-230]

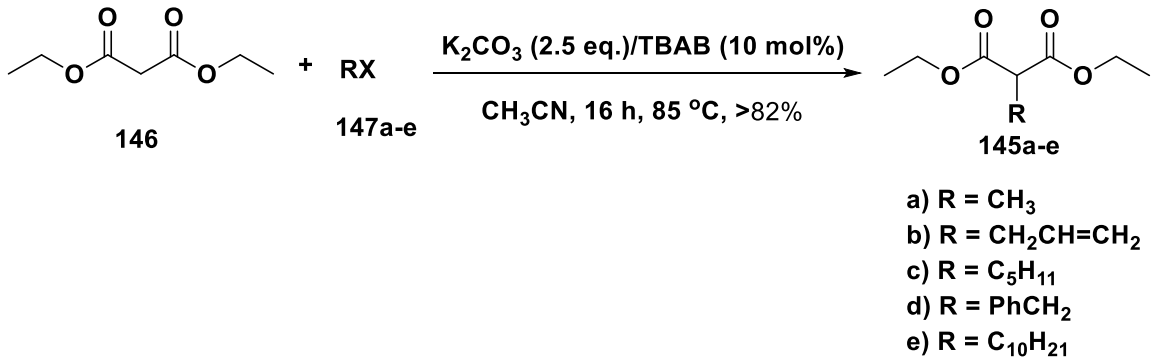

Scheme 22: Biphasic monoalkylation of diethyl malonate.

Table 7: Product yield (%) against the three bases.

R	NaH/ %	K_2CO_3/ TBAB/%	MeONa/%
CH_3CH_2	-	60	-
C_5H_{11}	78	93	-
$PhCH_2$	86	99	-
$C_{10}H_{21}$	68	99	60

The next step was the synthesis of the tri-ester via the reaction of compound **145a-e** with either methyl 3-haloacrylate **143f-g** or methyl propiolate **144** to afford the tri-ester **148a-e** as a mixture of 75% *trans*- and 25% *cis*-isomer (**Scheme 23**).

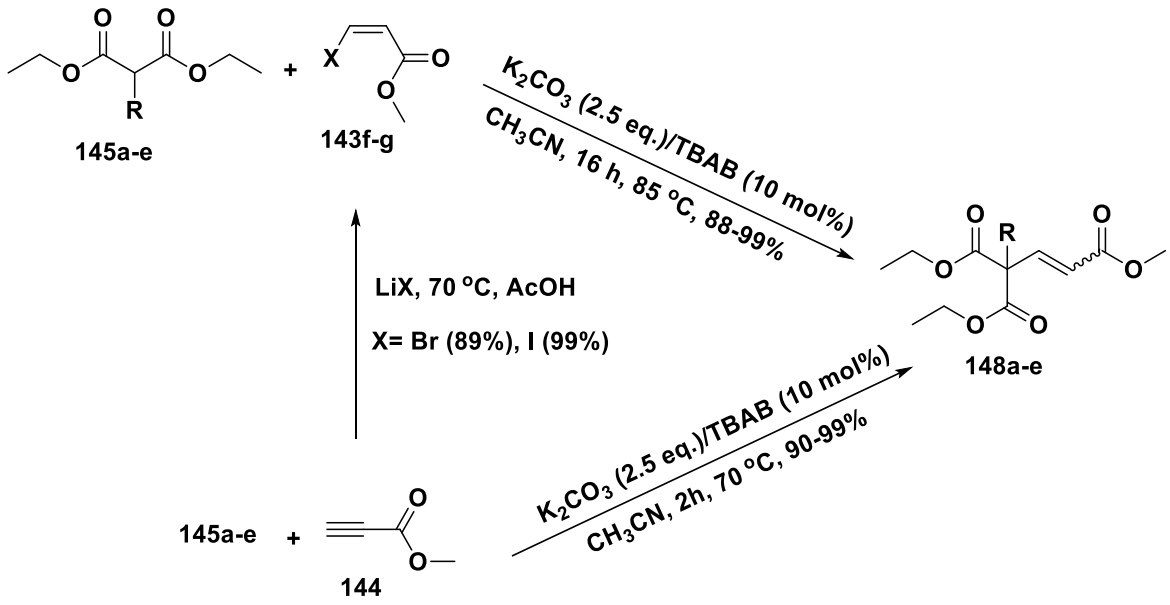

Scheme 23: General approach to tri-ester, **148a-e**.

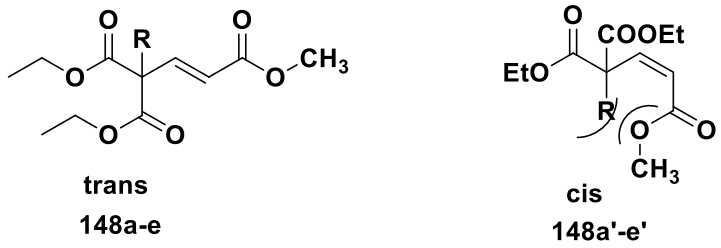

Figure 54: Illustration of the significant steric interactions in the *cis*-isomer (**148a'-e'**).

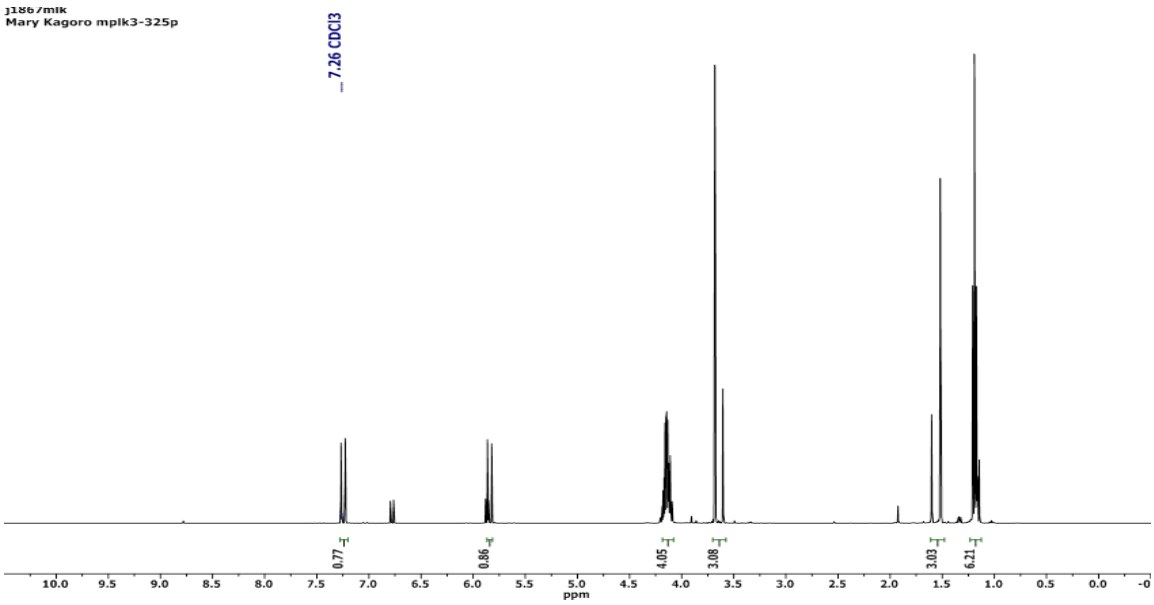

Figure 55: ^{1}H NMR (400 MHz, $CDCl_3$) of a mixture of (*E/Z*)-3,3-diethyl-1-methylbutene-1,3,3-tricarboxylate **(*E*)-148a** and **(*Z*)-148a'.**

The initial optimization was carried out using methyl 3-haloacrylate **143f-g** at 85-100 ^{o}C for 16-24 hours but this was later replaced by reacting the methyl propiolate **144** with the diethyl 2-alkylmalonate employing the same reaction conditions for 2 hours. The ^{1}H NMR shows the presence of both isomers (**Figure 55**).

The formation of methyl 3-haloacrylate **143f-g** amounts to an electrophilic addition of HX to an unsymmetrical alkyne which should in theory afford the Markovnikov addition product (**Scheme 24**), instead the reaction gave the anti-Markovnikov product. This reaction amounts to an electrophilic addition of HX but from two different reagents (acetic acid and lithium bromide/iodide respectively). Several

exhaustive studies have shown that the addition occurs via a concerted 1, 2-addition from the same side leading exclusively to the *cis*-product **143f-g**.[231-235] Meanwhile, further reaction of methyl *cis*-3-haloacrylate **143f-g** with the corresponding diethyl 2-alkylmalonate led to a mixture of two products; the *trans* and *cis*-products in a ratio of 3:1 respectively. Similarly, the reaction of diethyl 2-alkylmalonate with methyl propiolate in acetonitrile with potassium carbonate as base led also to a similar ratio of isomeric products even at room temperature or 70 ^{o}C the latter is known to give exclusively the *cis* isomer of methyl 3-haloacrylate as indicated in **Scheme 2**4

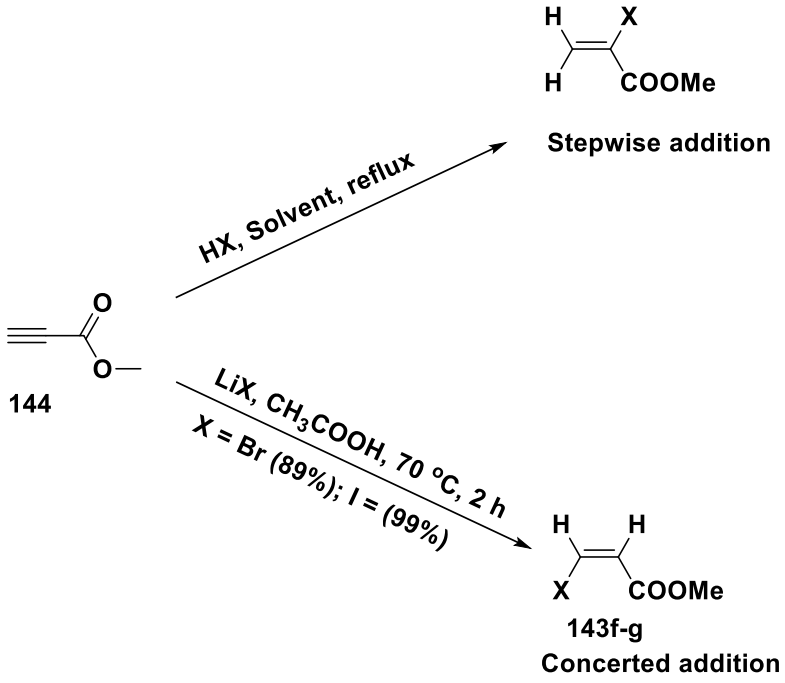

Scheme 24: Stereospecific formation of methyl 3-haloacrylate **143f-g**.

All attempts to isolate the different isomers failed. The photochemical and thermal isomerization of one isomer to the other using iodine crystals failed (**Scheme 25**).[237-238] In addition, attempts to purify the different isomers using silver nitrate impregnated silica gel also failed in my hands.[239-240]

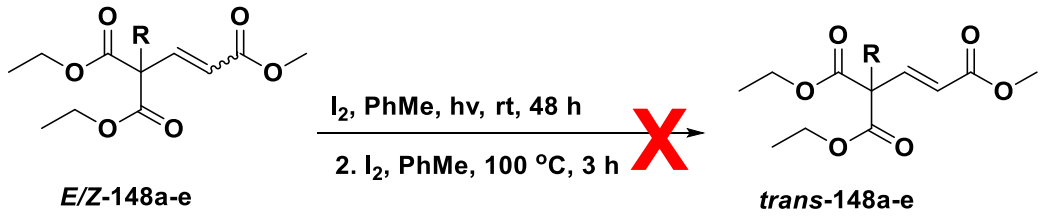

Scheme 25: General procedure for thermal/photochemical induced isomerization of 3-alkylglutaconic tri-ester.

The next step was the base-catalysed hydrolysis of the tri-ester (**Scheme 26**). The reaction was attempted several times with no positive result, until the use of acid-base extraction was employed which afforded the diacid in good to excellent yield. The structure of this class of acid was involved in controversy some years ago until it was resolved by Kagan and Tolentino.[241] This is because of the mobility of the double bond and delocalization between the olefin and the two carbonyl motifs leading to a heptad of stabilised double bonds (**Figure 56**). The structure of the acid synthesized here belong predominantly to the γ-alkyl glutaconic acid (2-alkyl glutaconic acid) series **141a-e** and not the α-alkyl glutaconic acid (4-alkyl glutaconic acid) series' **142a-e** though it was observed that both regioisomers interconvert to each other rapidly at room temperature and due to this rapid interconversion, Thole and Thorpe made the assertion that they are the same compound.[241-243] While the regioisomers are not the same, the energy barrier between the two regioisomers must be small as to allow for facile isomerization. This conclusion was made because on prolonged storage isomerization to the less substituted diacid was observed.

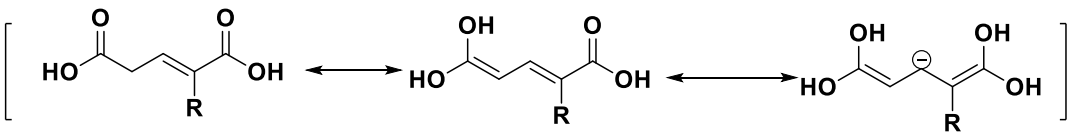

Figure 56: Delocalization and stabilization of 2-alkyl glutaconic acid **141a-e**.

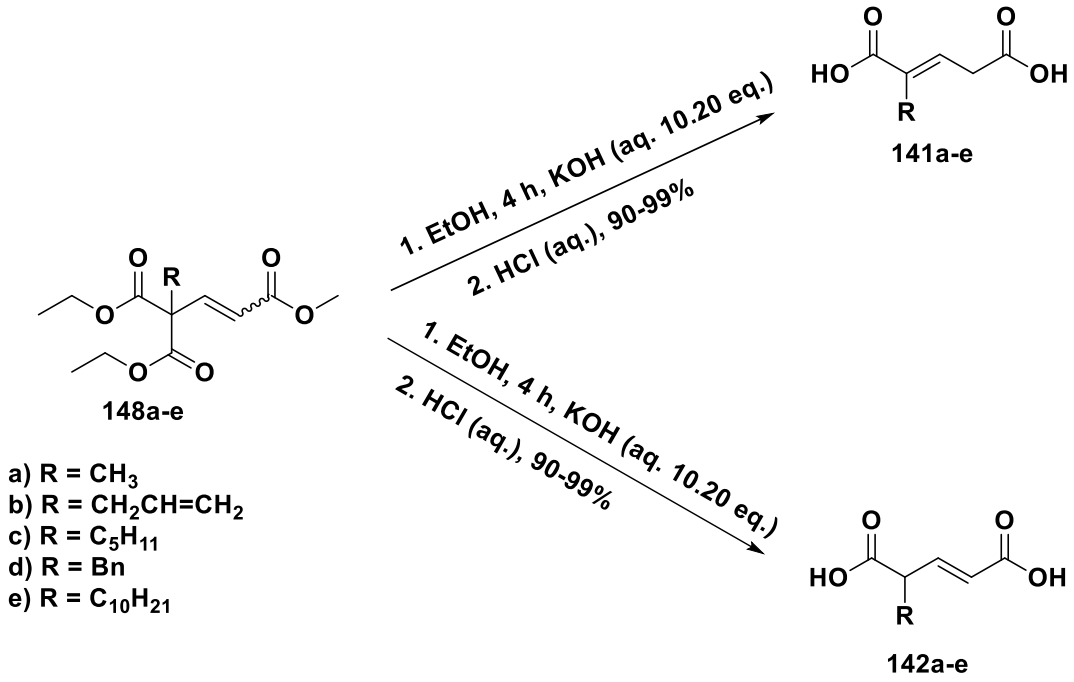

Scheme 26: General procedure for base-catalysed hydrolysis of tri-ester compounds **148a-e**.

The formation of **142a-e** assumes the localization of the double bond during hydrolysis and subsequent *in situ* decarboxylation. However, this was not observed as a migration of the double bond was found to give product, **141a-e.** The structures of **141a-e** were confirmed by the presence of a methylene (CH_2) carbon in the ^{13}C DEPT-135º NMR of **141a** in $(CD_3)_2CO$ (**Figure 57**). The natural abundance ^{13}C NMR spectrum of this diacid showed the presence of three quaternary resonances at δ 171.1, 168.0 and 129.8 ppm. These were assigned to the two carbonyl motifs (δ 171.1 and 168.0 ppm) and C-2 (δ 129.8-132.7 ppm) of the diacid.[211-217] The alkyl region of the ^{13}C NMR spectrum for all the alkyl substituents shows a methylene peak at 33.4 ppm, assigned to the methylene carbon (C-4) based on its negative peak in the ^{13}C DEPT- 135º NMR as is indicated for 2-methyl glutaconic acid **141a** (**Figure 57**). However, the 2-decyl substituted acid **141e** shows a peak at δ 51.3 ppm which is a methine carbon (CH) from the ^{13}C DEPT-135º NMR spectrum and this was assigned to the γ-acid **142e** (4-decyl glutaconic acid). Theoretically this methine peak should appear between δ 50-55 ppm because it is a tertiary carbon, whilst the methylene been a secondary carbon appears between δ 30-35 ppm (**Figure 58**).[217] A difference of δ 18.1 ppm in

chemical shift was observed between these two non-olefinic carbons in 4-alkyl glutaconic acid and 2-alkyl glutaconic acid, which is in close agreement with the report of Gelb and Abeles (1984),[211] noting a difference of δ 21.1 ppm.

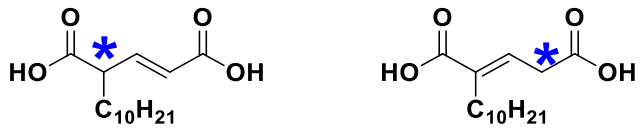

142e **141e**

Figure 57: Regioisomers of n-decyl glutaconic acid.

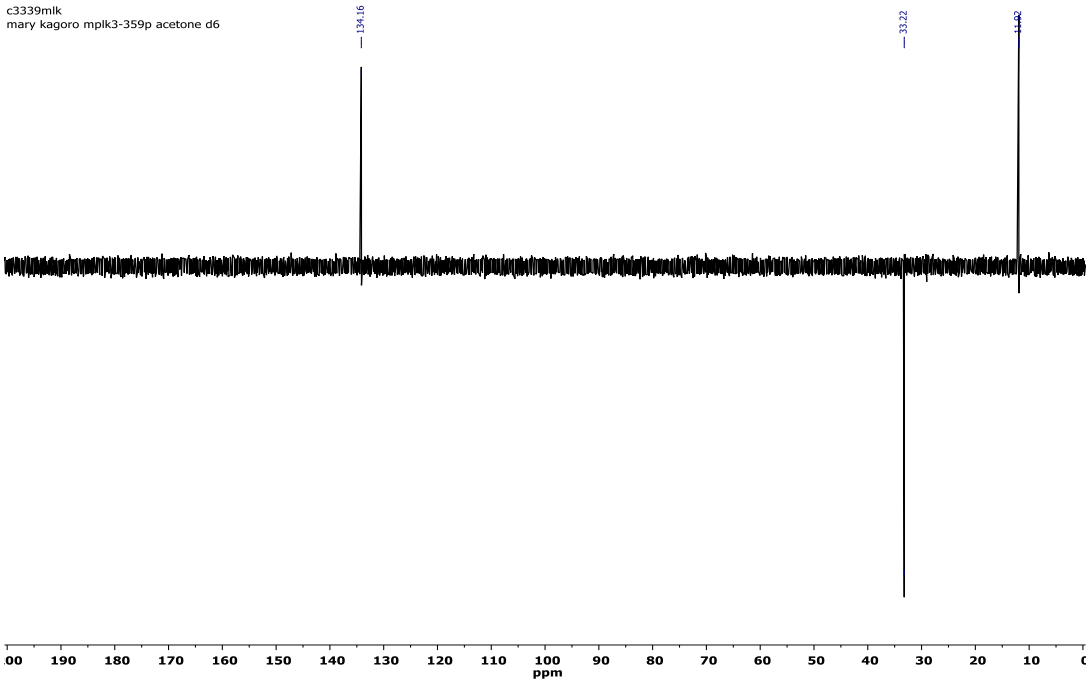

Figure 58: ^{13}C DEPT-135^{o} NMR (400 MHz, $(CD_3)_2CO$) of 2-methyl glutaconic acid, **141a**.

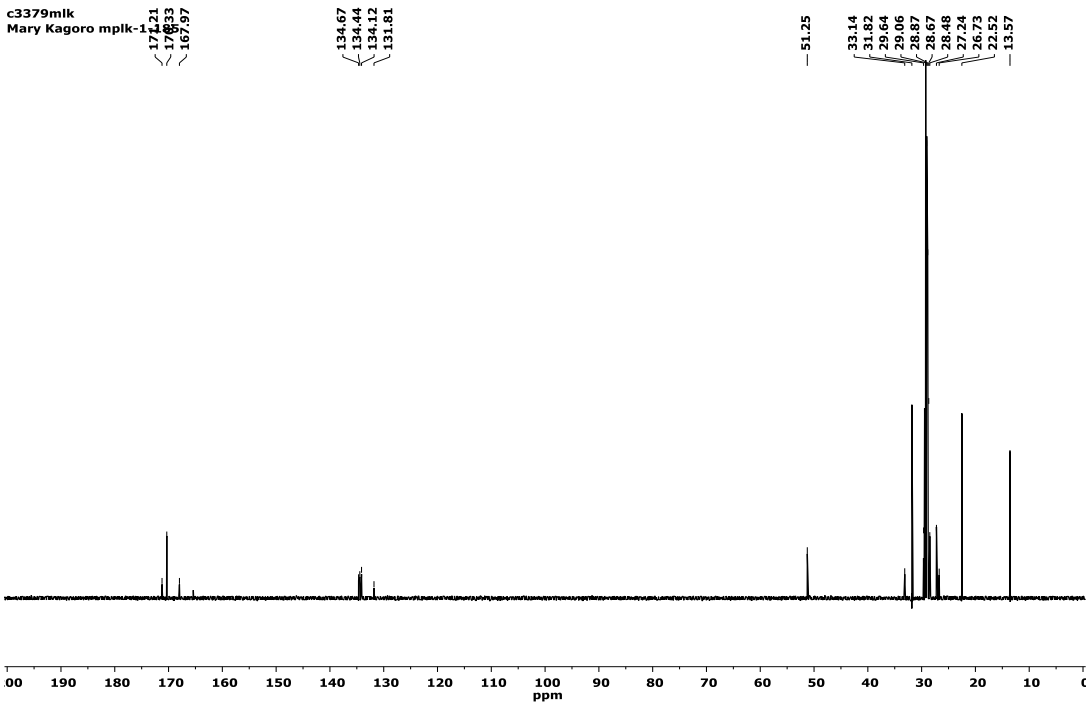

Figure 59: ^{13}C NMR DEPT-135^{o} showing the mixture of **141e** and **142e**.

The next step was the treatment of **141a-e** with excess acetyl chloride at 100 ^{o}C for two days in a sealed tube which afforded fragment **128a-e** in 22-45% yield in addition to the accompanying regioisomer **129a-e** (**Scheme 27**). These regioisomers are differentiated based on coupling constants, of H3 and H4, which are of higher magnitude (9-12 Hz) compared to H4 and H5 (6.3-8 Hz), as shown in Figure 62 for **128e** and **129e**.[243-244] The coupling constants ($^{3}J_{H-H}$) are larger for 5-alkyl-6-chloro-2-pyrone **129a-e** (9-2 Hz) than for 3-alkyl-6-chloro-2-pyrone **128a-e** (6.7-8 Hz).[241,244]

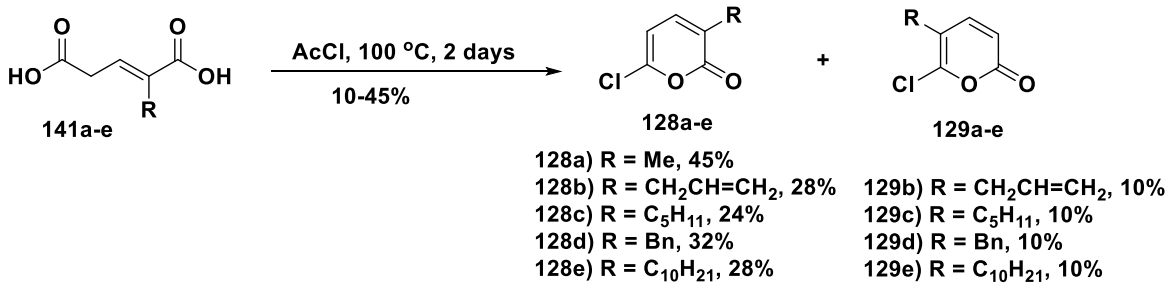

Scheme 27: Generalised procedure towards 3-alkyl-6-chloro-2-pyrone.

The procedure as presented was optimised from the initial point where only the 3-alkyl-2-pyrone **128a-e** was obtained in a yield of 14-22% in three days to a yield of

22-33% over two days; an additional time appears to lead to lower yields. Most of the earlier purification led to one compound though the crude product indicated the presence of two products. It was reported by Kagan and Tolentino,[241] that isomerisation of the 5-alkyl-6-chloro-2-pyrone **129a-e** was occurring on the silica gel column. Repeat reactions consistently led to the isolation two products except for the 6-chloro-3-methyl-2-pyrone **128a** though the presence of the 5-alkyl-6-chloro-2-pyrone **129a** was also seen in the ^{1}H NMR spectrum (in $CDCl_3$, **Figure 60**).

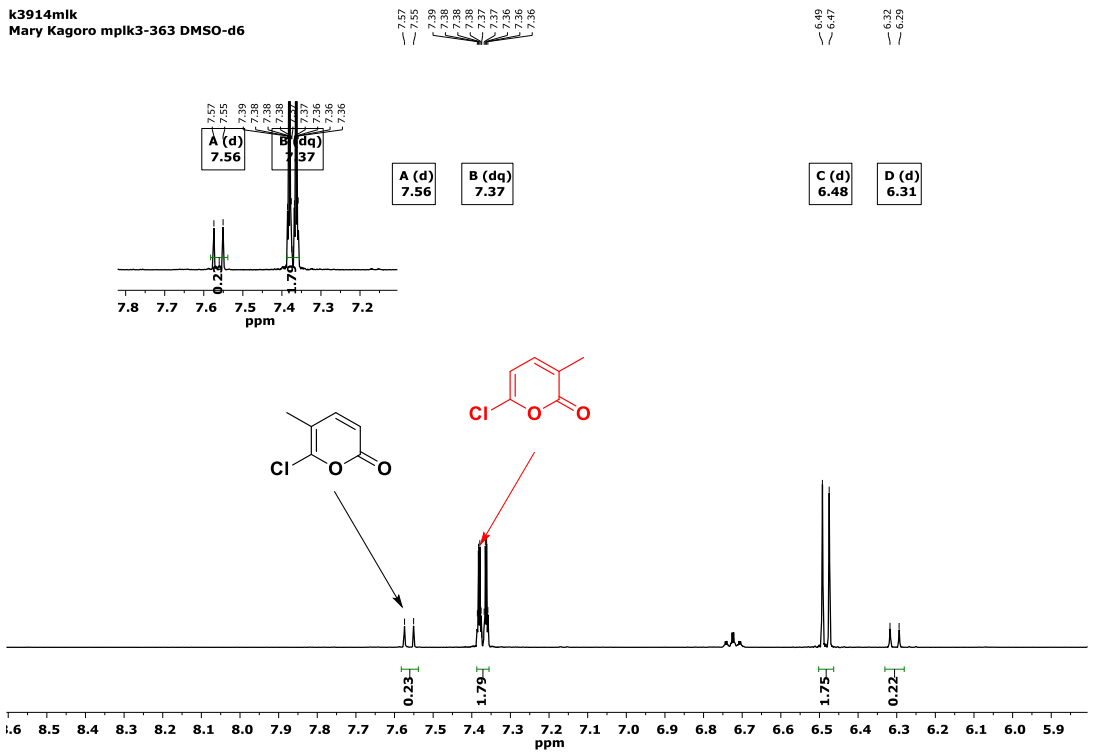

Figure 60: ^{1}H NMR (400 MHz, $CDCl_3$) spectrum of 3-methyl-6-chloro-2-pyrone **128a** showing the presence of both 3-methyl and 5-methyl-6-chloro-2-pyrone (**128a** and **129a,** respectively).

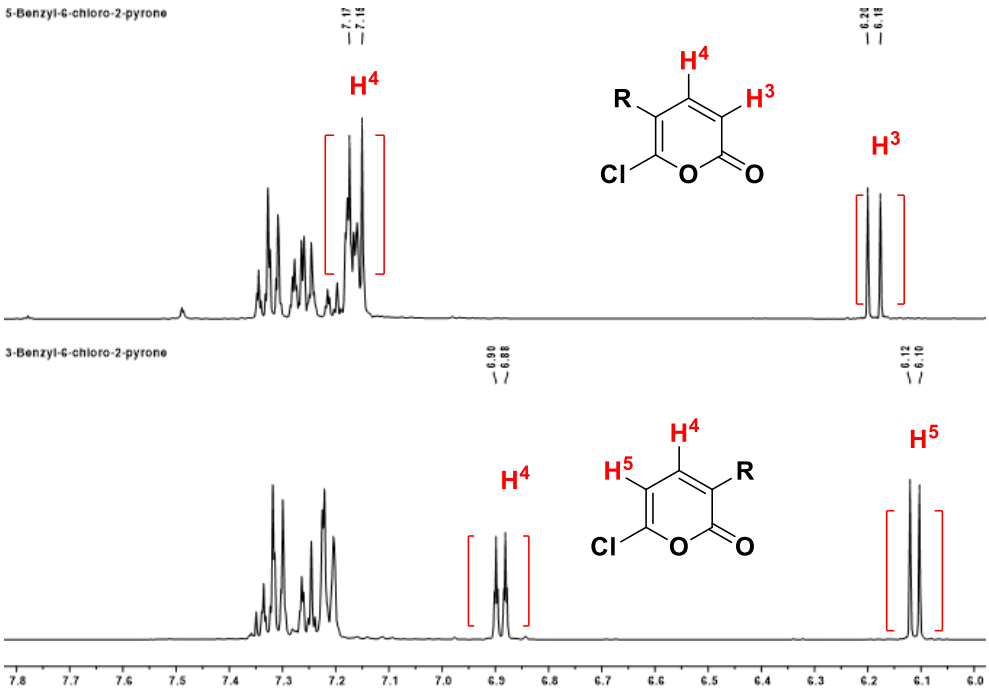

Figure 61: Stacked plot showing the ^{1}H NMR in $CDCl_3$ of the two regioisomers, **128d** and,**129d**.

Table 8: ^{1}H NMR ($CDCl_3$, 298 K, 400 MHz) spectral data of 3-alkyl-6-chloro-2-pyrone **128a-e,** with 2-pyrone protons highlighted in red and the coupling constants given in parentheses.

Nuclei	128a/ ppm	128b/ ppm	128c/ ppm	128d/ ppm	128e/ ppm
δ ArH				7.35	
δ ArH				7.25	
δ H-4	7.09 (7 Hz)	7.08 (7 Hz)	7.03 (7 Hz)	6.88 (7 Hz)	7.04 (7 Hz)
δ H-5	6.11 (7 Hz)	6.16 (7 Hz)	6.14 (7 Hz)	6.11 (7 Hz)	6.13 (7 Hz)
δ HC=		5.84			
δ =CH		5.17			
δ =CH		5.14			
δ CH_2		3.61	2.4	3.73	2.4
δ CH_2			1.53		1.53
δ $(CH_2)n$			1.21		1.25
δ CH_3			0.81		0.85

Table 9: Key ^{1}H NMR ($CDCl_3$, 293 K, 400 MHz) spectral data for 5-alkyl-6-chloro-2-pyrone **129a-e,** with 2-pyrone protons highlighted in red and the coupling constants given in parentheses.

Nuclei	129a/ ppm	129b/ ppm	129c/ ppm	129d/ ppm	129e/ ppm
δ ArH				7.4	
δ ArH				7.25	
δ H-4	7.24 (9 Hz)	7.24 (9 Hz)	7.24 (9 Hz)	7.24 (9 Hz)	7.24 (9 Hz)
δ H-5	6.21 (9 Hz)	6.21 (9 Hz)	6.21 (9 Hz)	6.21 (9 Hz)	6.23 (9 Hz)
δ HC=		5.71			
δ =CH		5.15			
δ =CH		5.05			
δ CH_2		3.61	2.4	3.73	2.4
δ CH_2			1.53		1.53
δ $(CH_2)n$			1.25		1.25
δ CH_3			0.81		0.85

The ^{13}C NMR spectrum of 3-benzyl-2-pyrone **128d** showed a quaternary signal, at δ 161.7 ppm, and another at δ 149.5 ppm. The peak at δ 161.4 ppm was assigned the carbonyl carbon (C-2) and the peak at δ 147.2 ppm assigned to C-6, next to the most deshielded C-2 carbon, which is in close agreement with the data reported.[211-217,244] The ^{13}C NMR spectrum of 6-chloro-3-decyl-2-pyrone **128e** shows three quaternary resonances at (δ 161.7, 146.8, 127.3) whilst **128d** exhibited four quaternary peaks at (δ 127.0, 147.2 and 161.2 ppm in addition to one at δ 137.3 ppm). The additional peak is assigned to the tertiary carbon in the benzyl group involved with **128d**. Based on these chemical shifts, the resonance at δ 126.8 ppm was assigned to the C-3 carbon, with a spin-spin ^{13}C-^{13}C coupling to the enriched carbon (72 Hz). The natural abundance ^{1}H NMR for the synthesized 6-chloro-2-pyrone **128a-e** and **128a-e** were in close agreement with those reported by Fu *et al*.,[245] for similar compounds as those synthesized in this study (**Figure 62**). They gave values of δ 162.8-163.1 ppm for the C-2 carbon, δ 123.1-129.8 ppm for the C-3 carbon, δ 138.0-140.1 ppm for the C-4 carbon, δ 100.8-102.1 ppm for the C-5 carbon and δ 158.8-159.9 ppm for the C-6.

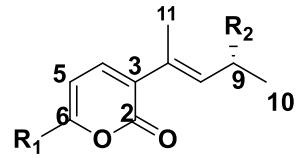

$R_1 = H, R_2 = {}^{12}CH_2{}^{13}CH_3$

$R_1 = H, R_2 = {}^{13}CH_3$

$R_1 = OH, R_2 = {}^{12}CH_2{}^{13}CH_3$

Figure 62: Natural 3-allkenyl-2-pyrone**.**

The spectroscopic data for all known compounds were compared to the literature, agreeing on all counts. Compounds **128a** and **128d** had melting points that agreed with those given of literature.[243-244] The crystal structure of **128d** as determined by single crystal X-ray diffraction confirms the expected regiochemistry of this product; also correlating with the literature data (**Figure 63**).[211-213,241-245]

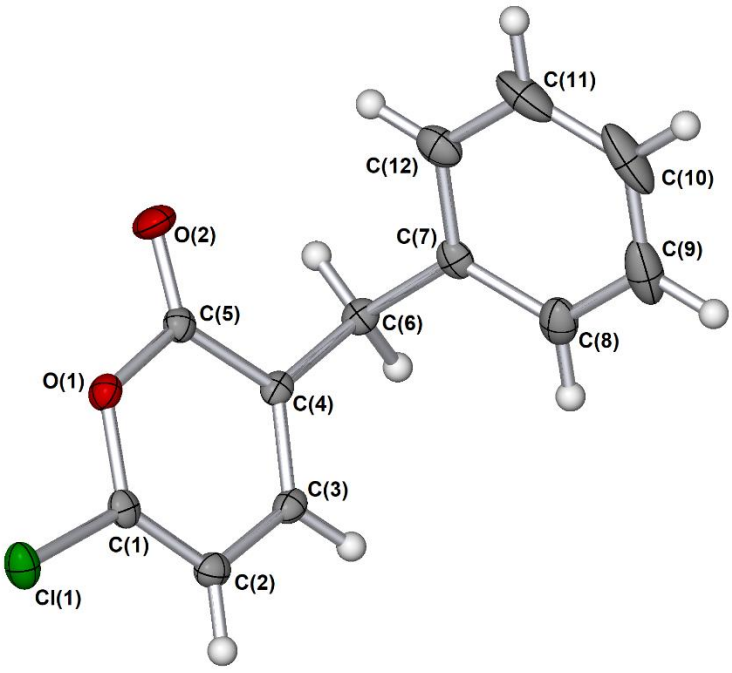

Figure 63: X-ray crystal structure of compound **128d**, shown as a single molecule, (note two molecules were found in the asymmetric unit cell). Arbitrary atom numbering used for the X-ray crystal structure (H atoms not labelled).

The infrared (IR) spectra of the 3-alkyl-6-chloro-2-pyrones **128a-e** give characteristic absorbance frequencies at 1700-1750 cm^{-1} in addition to the peak at

1600 cm^{-1} for the C=C, in agreement with literature on these and related compounds, as exemplified in the IR spectrum of **128a** (**Figure 64**).[241-247] It was found that the IR spectrum for the 5-alkyl-6-chloro-2-pyrone **129b-e** gave lower absorbance frequencies lower at ca. 1689-1698 cm^{-1} (**Figure 65**), whilst 3-alkyl-6-chloro-2-pyrone gave this same absorbance at ca. 1719-1730 cm^{-1}. Practically, IR spectroscopic analysis can therefore be used as a tool for distinguishing between the two regioisomers in compounds **128a-e** and **129b-e**.

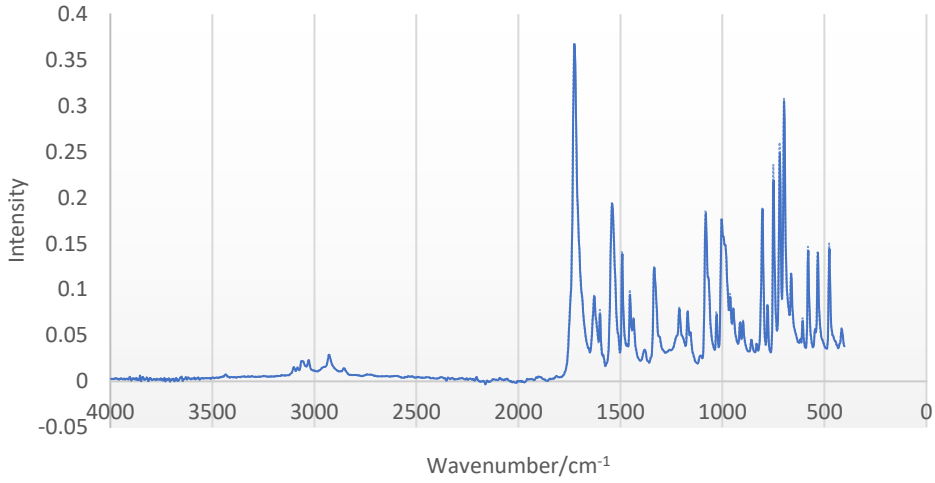

Figure 64: ATIR spectrum of compound **128c** taken neat.

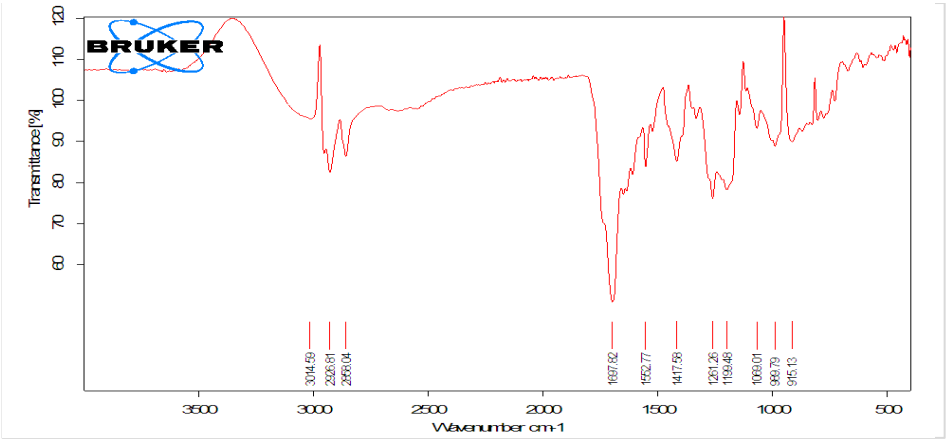

Figure 65: ATIR spectrum of compound 5-alkyl-6-chloro-2-pyrone **129c**

3.4 Palladium-catalysed Alkynylation of 128a-e

Pd-catalysed cross-coupling of 6-chloro-2-pyrone **157** is known.[247-248] However, no report has presented cross-coupling reactions using **128a-e** or **129a-e**. Other Sonogashira cross-couplings involve 4-halogenated-2-pyrone or dihalogenated-2-pyrone **161** (**Scheme 28**).[247-248]

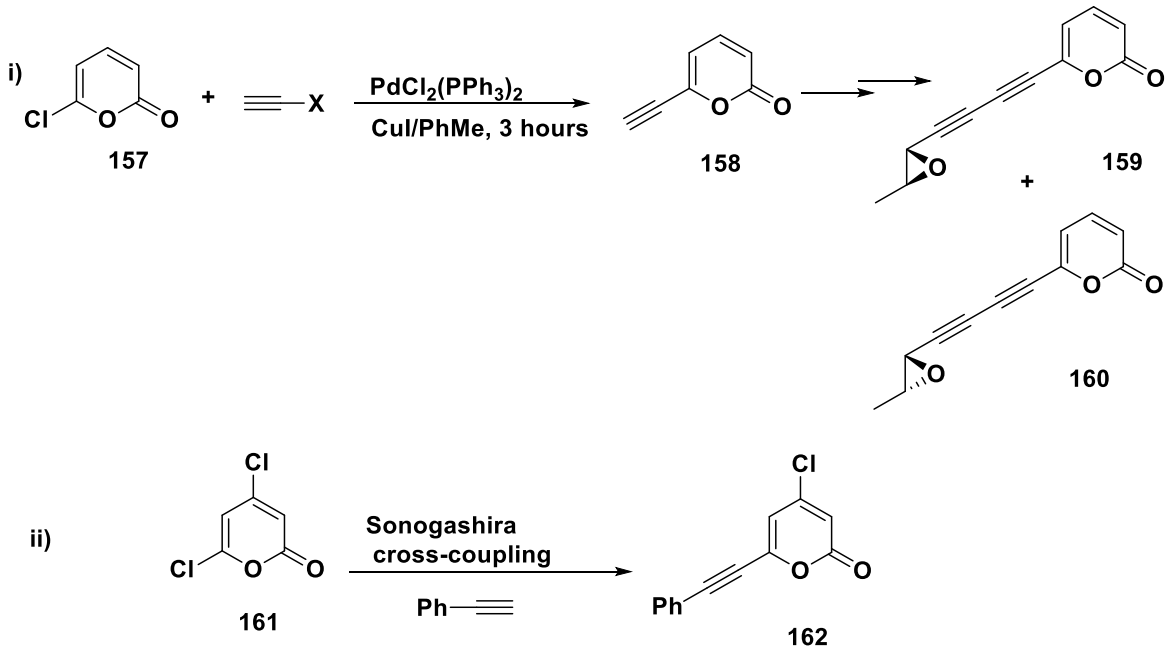

Scheme 28: Pd-catalysed cross-coupling of 6-chloro-2-pyrone with terminal acetylenes.

Initial investigations employing the standard Sonogashira cross-coupling conditions; bis(triphenylphosphine)palladium(II) chloride $PdCl_2(PPh_3)_2$ proved unsuccessful in a variety of solvents and bases (entries 1-4, Table 10). Switching bases and solvents failed to yield positive results (entries 5-6). This was unexpected since this precatalyst works for other 2-pyrone compounds substituted at 2-pyrone positions 3- and 5. Though, the reaction conditions failed to yield good results for aryl acetylenes substituted with electron-withdrawing groups, in this case palladium on carbon ($Pd/C/Et_3N/CuI$) gave better result.[248] The use of a similar catalytic system also failed even when the base was changed (entry 7, Table 10) The failure is reported to be due to the substitution of chlorine with triethyl amine leading to the formation of a salt **157** (**Scheme 29**) as this was observed for the n-pentyl-substituted 6-chloro-2-pyrone **128c**. As a similar reaction was

observed and the product characterised when 6-chloro-2-pyrone **157** was cross-coupled with phenylacetylene in the presence of triethylamine.[248-251]

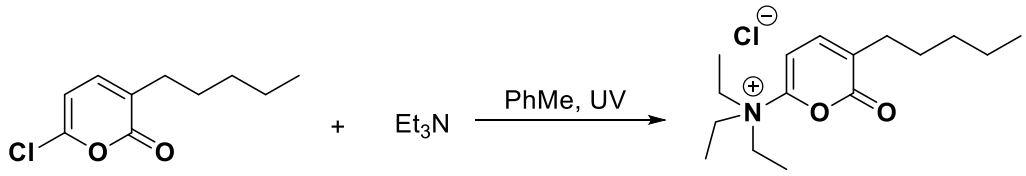

Scheme 29: Deactivation of 3-pentyl-6-chloro-2-pyrone **128c** by triethylamine.

Therefore, returning to the more traditional precatalyst, the effect of change in solvent, base and temperature was investigated (entries 8-16, Table 4) which led to success. From the group's arsenal of knowledge on Pd-catalysed reactions, the conditions that employed the use of a base such as potassium carbonate (K_2CO_3) or 1, 8-diazabicyclo[5.4.0]undec-7-ene (DBU) required heating but not so much those that employ 1,4-diazobicyclo[2.2.2] (DABCO).[252-256] DABCO has also been employed as a ligand in Pd-catalysed cross-coupling reactions.[256-259]

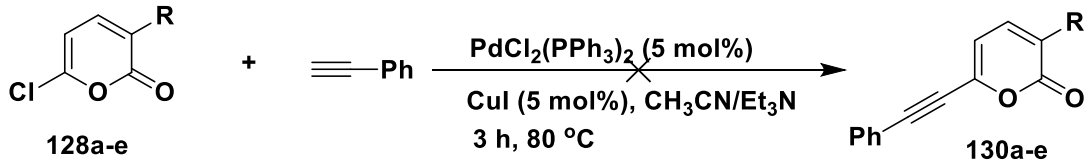

Scheme 30: Initial Sonogashira cross-coupling condition assessed.

Table 10: Optimized Reaction conditions

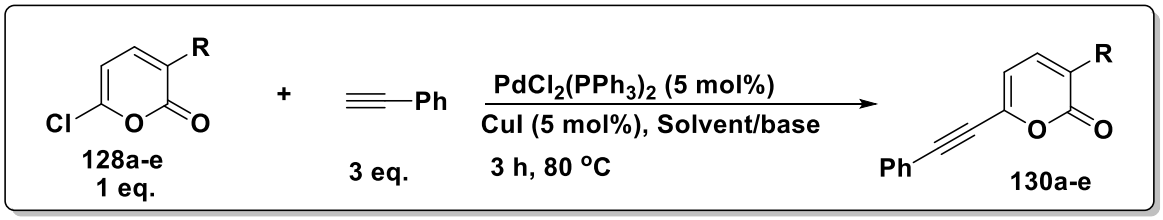

ENTRY	BASE 1	BASE 2	LIGAND	SOLVENT	Pd (CAT)	TEMP/ oC	Yield/ %	TIME/ Hr
1	Et_3N			CH_3CN	$PdCl_2(PPh_2)_2$	80	R	3
2	Et_3N			CH_3CN	$PdCl_2(PPh_2)_2$	80	R	3
3	Et_3N			CH_3CN	$PdCl_2(PPh_2)_2$	80	D	3
4	Et_3N			CH_3CN	$PdCl_2(PPh_2)_2$	80	D	3
5	K_2CO_3			DMF	$PdCl_2(PPh_2)_2$	80	D	3
6	Et_3N			PhMe	$PdCl_2(PPh_2)_2$	70	61[b]	24
7	DBU			PhH	10% Pd/C	100	T	24
8	DABCO	Cs_2CO_3		PhMe	$PdCl_2(PPh_2)_2$	50	100[b]	48
9	DBU	Cs_2CO_3		PhMe	$PdCl_2(PPh_2)_2$	100	D	48
10	DBU	K_2CO_3		PhMe	$PdCl_2(PPh_2)_2$	100	D	20
11	DABCO	Cs_2CO_3		PhMe	$PdCl_2(PPh_2)_2$	35	ND	20
12	DABCO	Cs_2CO_3		THF	$PdCl_2(PPh_2)_2$	60	100[b]	24
13	DABCO	Cs_2CO_3	CombiPhos	THF	$PdCl_2(PPh_2)_2$	35	ND	24
14	DABCO	Cs_2CO_3	XPhos	THF	$PdCl_2(PPh_2)_2$	35	53[c]	24
15	DABCO	Cs_2CO_3	CombiPhos	THF	$PdCl_2(PPh_2)_2$	35	ND	24
16	DABCO	Cs_2CO_3	XPhos	THF	$PdCl_2(PPh_2)_2$	35	80[b]	24

a = unrearranged product, b = ^{1}H NMR conversion (by relative integration of peaks at δ 7.04 and 7.25 ppm), c = yield of isolated product, R = Recovered unreacted starting material, D = decomposition of **128e**, ND = Not determined, T = trace amount of product **133**.

The optimized Sonogashira cross-coupling conditions were carried forward for reactions of phenylacetylene with **128a-e**. Here, an unusual [1,5] rearrangement involving an electrocyclic ring opening (ERO) and, [1,5]-sigmatropic shift of $Ph-C\equiv C$ group occurred, which requires a rotation around C-4 and C-5, and subsequent electrocyclic ring closure (ERC) via the intermediacy of a ketene such as **Ia-e** and **IIa-e** to give the cross coupled products **133a-e** in moderate to good yields (**Scheme 31**). The rearrangement is known for 6-halo-2-pyrone **157** at

temperatures above 500 °C or photochemically induced, neither can be the case here.[260-267]

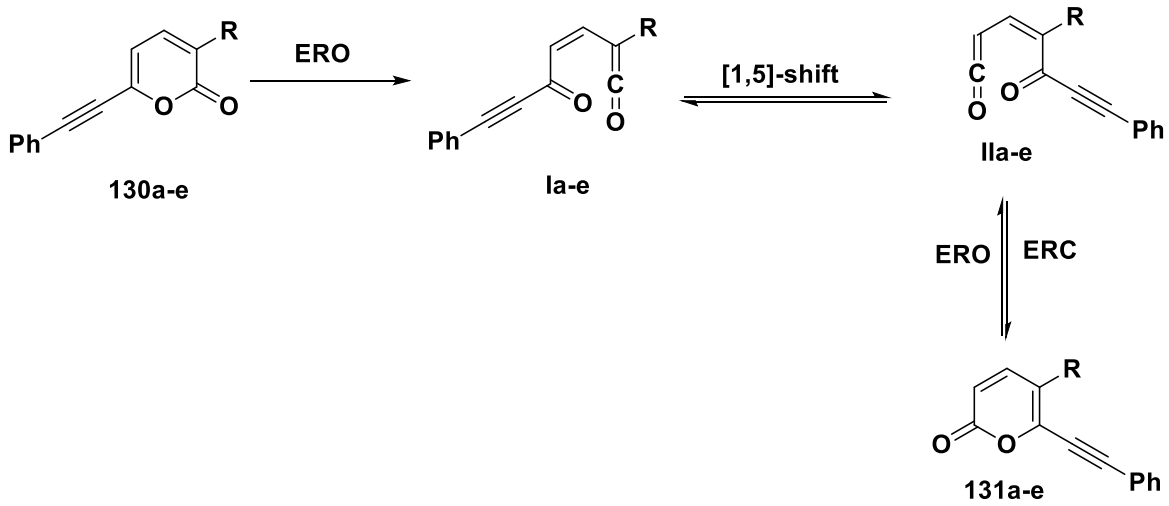

Scheme 31: Unusual [1,5]-rearrangement of 6-substituted-3-alkyl-2-pyrones.

This unusual rearrangement became undisputed only upon the synthesis of the ^{13}C-labelled 5-decyl-6-(phenylethynyl)-2-pyrone **169a-b** which showed an upfield shift from δ 161.5 ppm to δ 141.9 ppm, which could only have happened by rearrangement, moving the isotopic enrichment from a carbonyl motif to the olefinic motif (to ^{13}C=C-6). The ^{1}H NMR spectrum of the rearranged product can be characterised by the coupling constant between the 3-alkyl- and the 5-alkyl-substituted products. The 3-alkyl-product **128a-e** had a spin coupling of 7 Hz, whereas the 5-alkyl product **131a-e** has a spin coupling of 9.5-10 Hz indicative of a 5-alkyl-2-pyrone scaffold; this larger value is characteristic of a $^{3}J_{H4\text{-}H3}$ interaction (Table 9 and **Figure 66**).

To obtain detailed mechanistic insight into this rearrangement, some experiments were performed (**Scheme 32**). When **128a** was treated with the standard conditions in tetrahydrofuran, but in the absence of DABCO and Cs_2CO_3, no rearrangement occurred. The absence of the base implies the activation of the phenyl acetylenic hydrogen for deprotonation did not occur. This process can be visualized as the coordination of copper(I) salt to the triple bond would alter the electronic density over the acetylenic C–H bond, rendering it more acidic (**Scheme 33**). The acetylenic proton could then be deprotonated even by amines. Besides,

copper acetylides can indeed be obtained by the treatment of alkynes with an ammoniacal solution of copper chloride.[259]

Treatment of **128e** with $PdCl_2(PPh_3)_2$ and CuI in THF under standard conditions led to no rearrangement. Again, when **128a** was treated under standard reaction conditions in the absence of phenyl acetylene, no rearrangement occurred.

The rearrangement only takes place when all reactants present as shown in the reaction of **128d** (**Scheme 32**). The control experiments indicate that this rearrangement is not a [1,5]-sigmatropic shift of chlorine, prior to Sonogashira cross-coupling. There is a requirement for phenylacetylene for the rearrangement to occur, which points to the rearrangement of a phenyl acetylide, and therefore the formation of the unrearranged product that exists only transiently. A similar rearrangement process has been reported for 3/5-deuterated-2-pyrone, 6-fluoro and 6-chloro-2-pyrone occurring via a ketene intermediate. In the case of the rearrangement described here, we see a [1,5]-sigmatropic shift of phenyl acetenyl group and not chlorine. This result suggests the possible formation of the unrearranged product **130a-e** (**Scheme 31**) that has a transient existence and is rapidly converted to the rearranged product **131a-e**.[260-267]

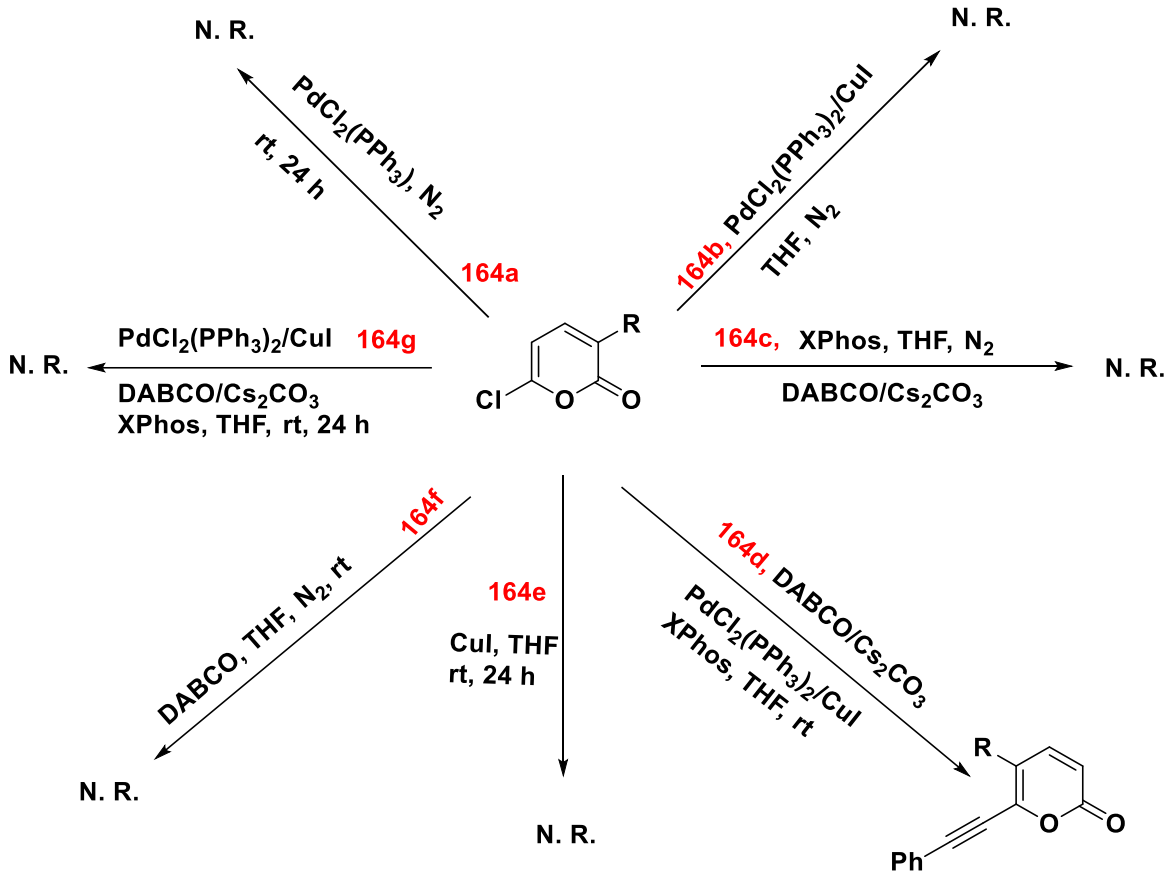

Scheme 32: Control experiments to probe the rearrangement.

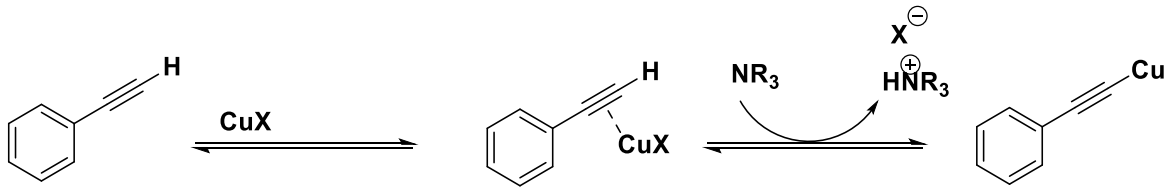

Scheme 33: The copper(I) salt is proposed to act as a Lewis acid and coordination to the triple bond enables the deprotonation by amine.

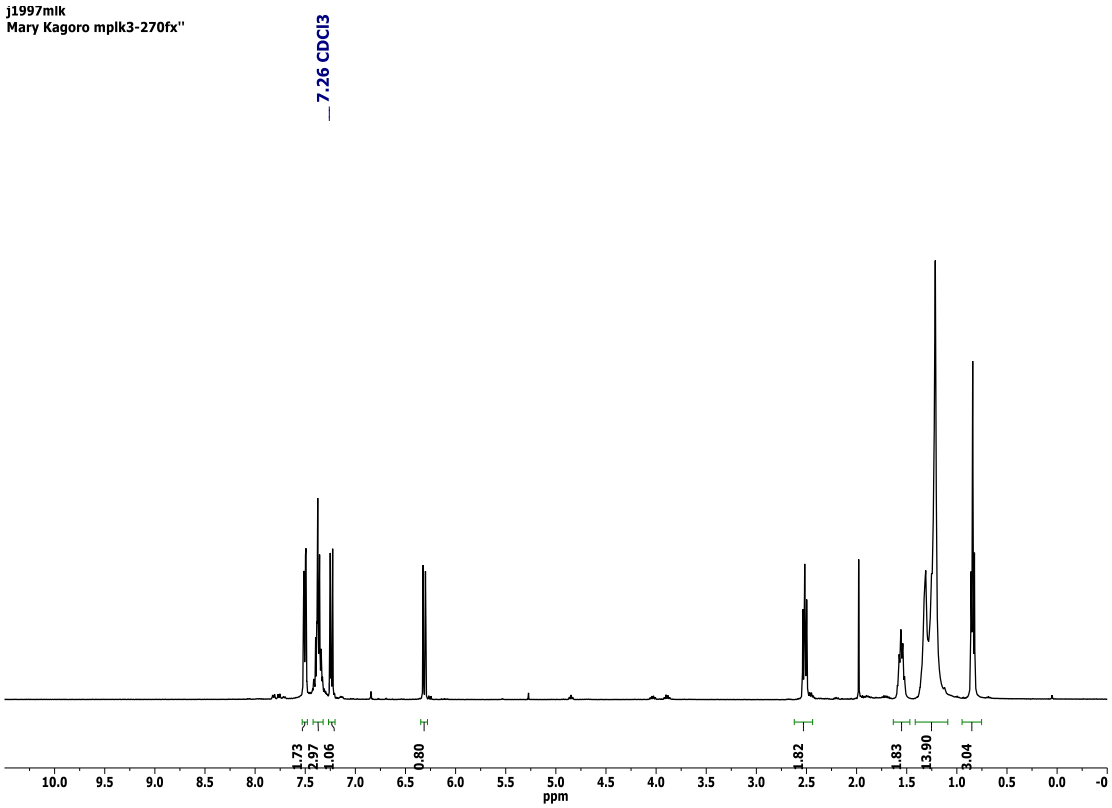

Figure 66: ^{1}H NMR spectrum of compound **131e** ($CDCl_3$, 400 MHz).

The ^{13}C NMR spectrum for this compound indicated that the rearrangement has occurred as the 3-alkyl-2-pyrone always had a peak at 104 ppm, but the 5-alkyl-2-pyrone does not, and the rearranged product had no peak at 104 ppm as seen in **Figure 67**.

The infrared spectrum for the non-labelled probe showed **131a-e** showed the presence of an unsymmetrical internal alkyne (at 2204 cm^{-1}), which is diagnostic for these compounds.

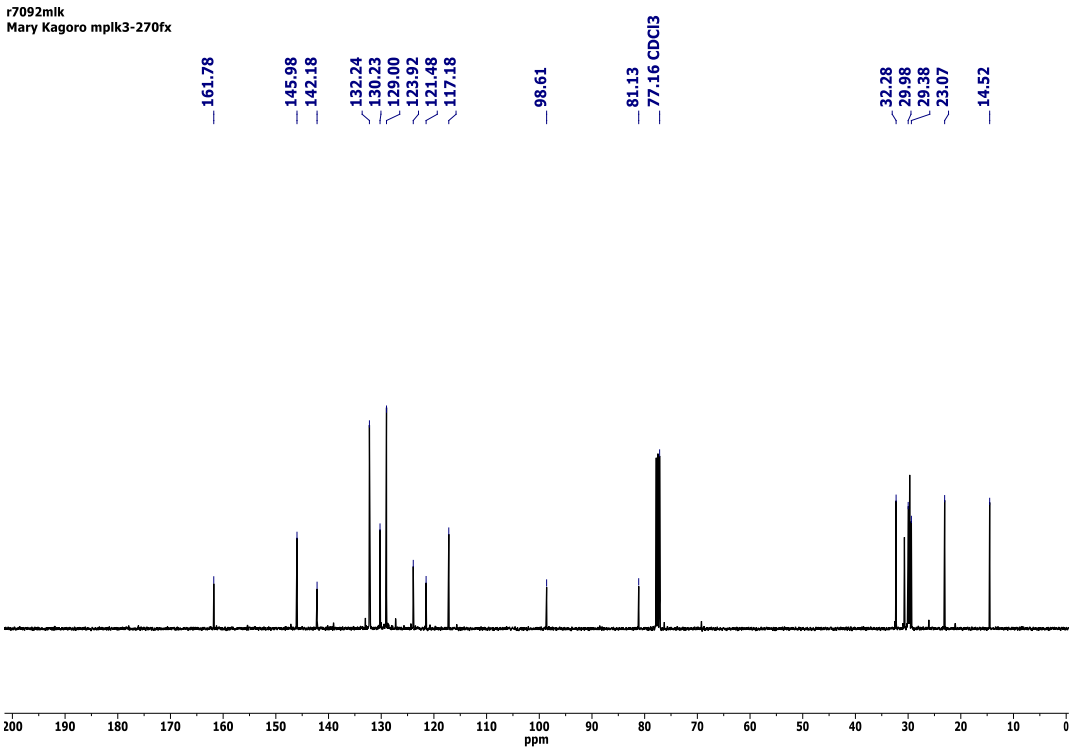

Figure 67: ^{13}C NMR spectrum for 5-alkyl-6-(phenylethynyl)-2-pyrone **131e** ($CDCl_3$, 400 MHz).

A confirmation of this unusual rearrangement was provided by determination of the X-ray diffraction structure of a single crystal of compound **128d** for the benzyl derivative (**Figure 68**). This structure reveals the rearrangement since in the reactant this substituent was on C-10 but now on C-12.

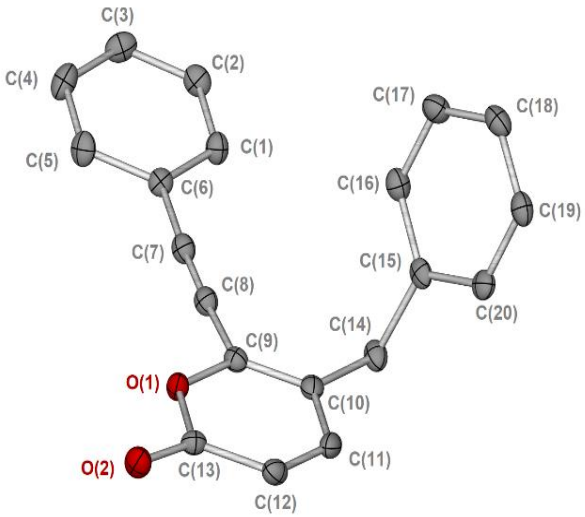

Figure 68: X-ray structure of the rearranged 5-benzyl-6-(phenylethynyl)-2-pyrone **131d**. Arbitrary atom numbering used in the X-ray structure image. H-atoms have been excluded.

3.5 Further analysis of the sigmatropic rearrangements

Rearrangement reactions involve a change in the position of a functional group and involves migration from a position 'a' to a position 'b' denoted as [a,b] shift. Examples include [1,3] or [1,5] hydrogen shift will convert a relatively unstable allene system into a conjugated triene (**Scheme 34**).

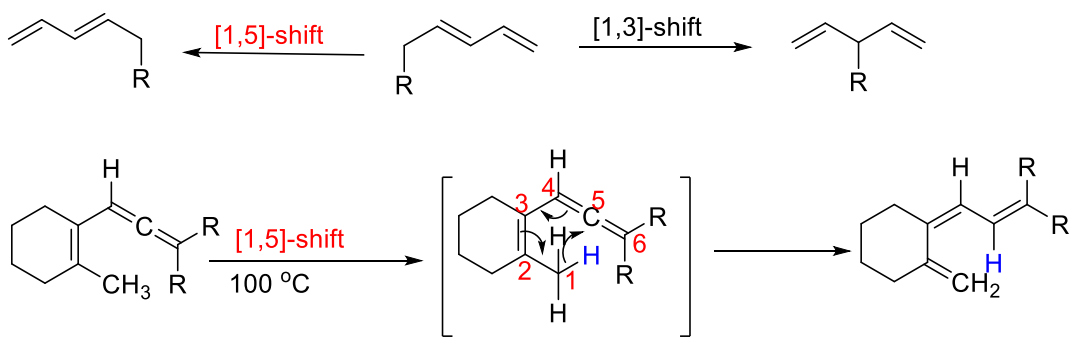

Scheme 34: Illustration of [1, n]-sigmatropic shift

Herein, we report a novel room temperature Pd/Cu mediated [1,5]-sigmatropic shift of phenyl acetylide across a ketene intermediate. This type of reaction is termed pseudopericyclic reaction and does not obey Woodward-Hoffmann rules, as defined by Lemal *and* co-workers.[263] The reactions are facile because they have near zero activation barrier, lack cyclic orbital overlap and have four characteristics, as stated

by Birney, [267] ‘’(1) all are allowed, (2) have nonaromatic transition states, (3) may have very low barriers, and (4) may have planar transition states.’’ The reaction involves the lone pairs of electrons on the carbonyl oxygen atom leading to the product via electrocyclic ring opening (ERO) to ketene **III**, a rotation, a [1,5]-sigmatropic shift leading to ketene **III’** which is in equilibrium with ketene **IV**, then finally a rotation and electrocyclic ring closure (ERC) (**Scheme 35. Scheme 36** shows the proposed [1,5]-sigmatropic shift of methyl ester that was reported not to be observed for this regioisomer. This was observed in our research as the 5-alkyl-6-(phenylethynyl)-2-pyrone gave the expected Sonogashira cross-coupling product whereas the 3-alkyl-6-(phenylethynyl)-2-pyrone rearranged to give the same product as the 5-alkyl-6-(phenylethynyl)-2-pyrone.

A search of the literature indicate that this reaction is known for unsubstituted 2-pyrone, 3/5-deuterium substituted 2-pyrone and their 2-thiopyrone derivatives at high temperatures (>550 ^{o}C) or photochemically induced as shown in Chapter 1. Herein, we report the migration occurring at room temperature, 35 ^{o}C and 60 ^{o}C respectively which were the temperatures the reaction was screened for. Though the rearrangement was observed at these three temperatures and no change in yield was observed, thereafter the reaction was subsequently carried out at room temperature (18-20 ^{o}C). This implies that temperature might not have any effect on this rearrangement.

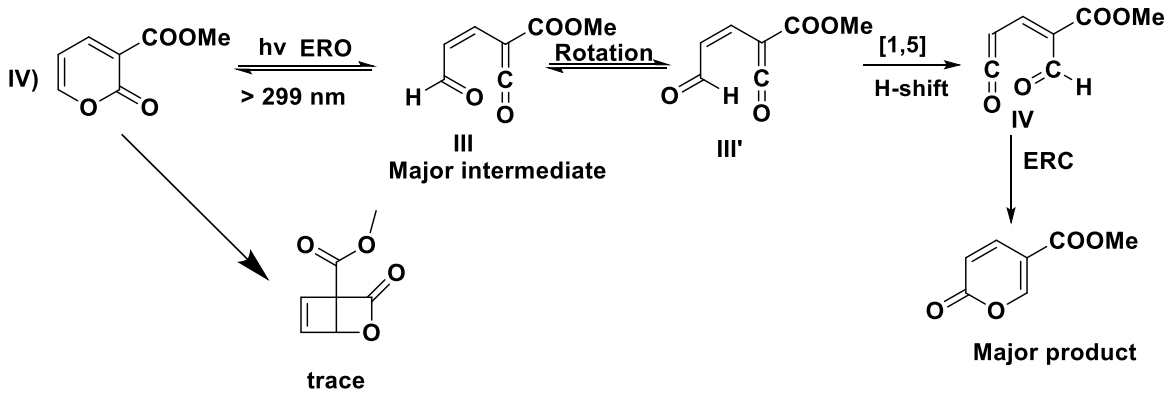

Scheme 35: [1,5]-sigmatropic shift of methyl ester group.

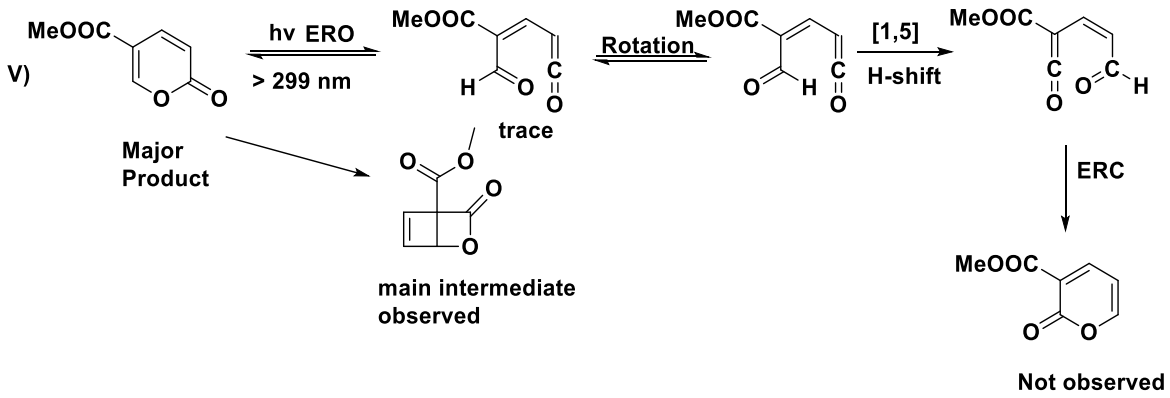

Scheme 36: Proposed [1,5]-shift that was not observed in this substrate.

An electrocyclic reaction is a spontaneous reaction which converts a π-bond to a ring σ-bond. The reverse reaction is called an electrocyclic ring opening (ERO). These reactions are mediated by light or heat. Two examples are shown in **Scheme 37**. The electrocyclic ring closure (ERC) is designated by blue arrows, and the ring opening by red arrows.

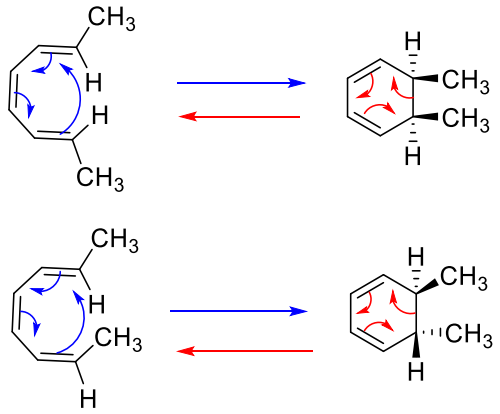

Scheme 37: Examples of electrocyclic ring opening and closure.

Therefore, we observed the first example of a Pd-catalysed [1,5]-sigmatropic rearrangement of phenyl acetenyl moiety.

3.6 Synthesis of antimicrobial imaging agents.

The chemoselective enrichment of the 2-pyrone occurred in four steps to furnish 6-chloro-3-decyl-2-pyrone-^{13}C-2 **167a-b** and 6-chloro-3-decyl-2-pyrone-^{13}C-6 **168a-b** as a mixture of two regioisomers separated by flash column

chromatography with the silica gel wet loaded as (10% w/w deionised water) in yields of 29% and 10% (**Scheme 38**).

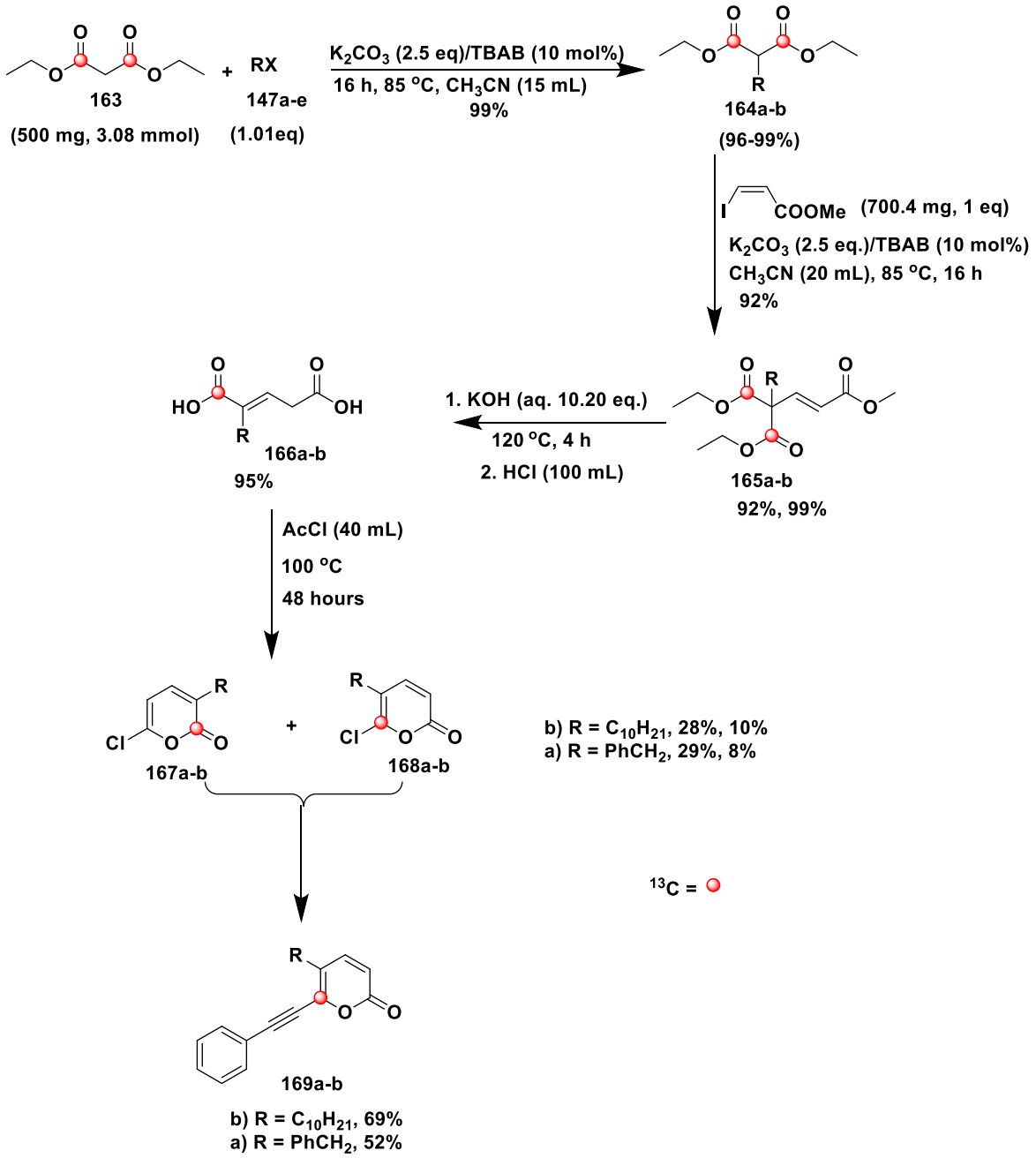

Scheme 38: General procedure towards isotopically labelled 2-pyrone.

The ^{13}C NMR spectrum of the 3-alkyl-2-chloropyrone **128** in deuterated chloroform showed one enriched resonance at δ 161.2 ppm for **128d-e** and at δ 147.2 ppm for **129d-e**. This represents a chemoselective enrichment of these compounds and for analysis of the mass spectrometry data indicate a 99% enrichment for **128e** and **129e** whilst for the benzyl derivative **128d** and **129d** the enrichment was ca. 97%.

Analysis of the mass spectrometry data for synthesized NMR probe (MH^++1) and (MNa^++1) peaks indicate a 99.8% enrichment on the C-6 carbon, so this optimized procedure leads to the synthesis of ^{13}C-isotopically labelled 2-pyrone compounds with an enrichment required for NMR assays

This labelling also provided a tool to differentiate between the two regioisomers based on the respective ^{13}C NMR absorbance peak, **Figure 69** shows the stacked ^{13}C NMR spectra of these two products.

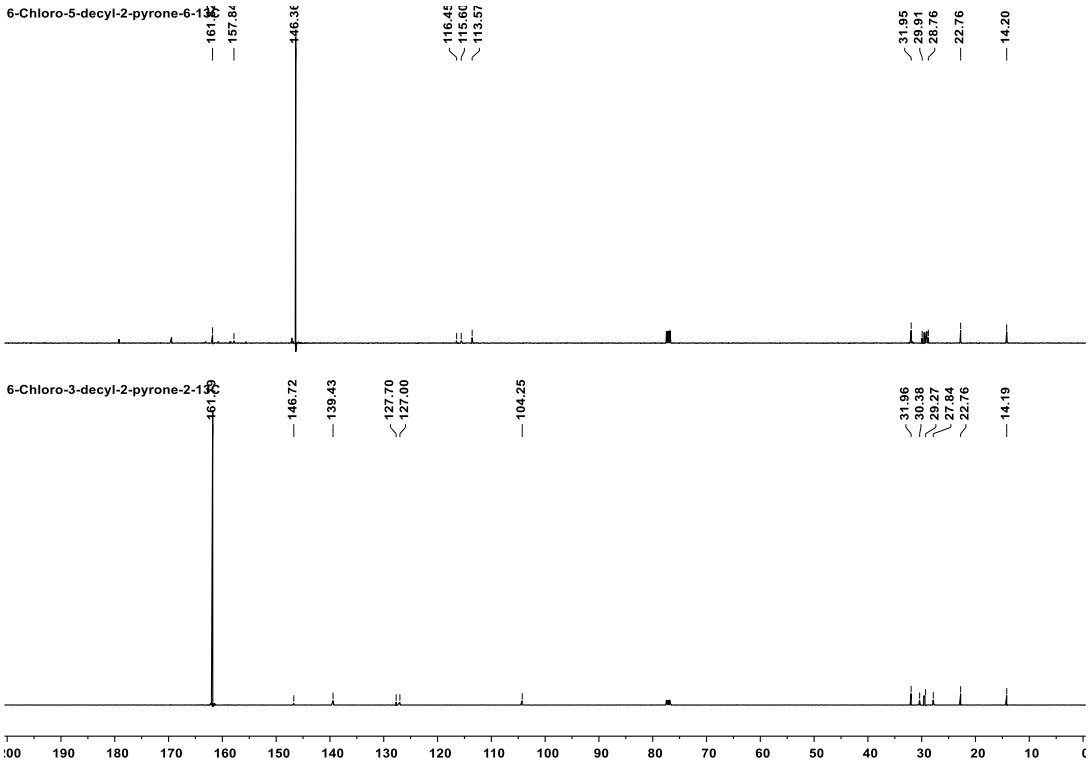

Figure 69: Stacked plot of ^{13}C NMR for the two regioisomers of **167a** and **168a**.

In addition, the results agree with the report of Pirkle *et al.*,[242] which observed that in 3-alkyl-2-pyrone the H4 hydrogen has a long-range interaction with the methine hydrogens attached to C-3 carbon but not for the 5-alkyl-2-pyrone as is the case in **Figure 70** for compound **169a-b**.

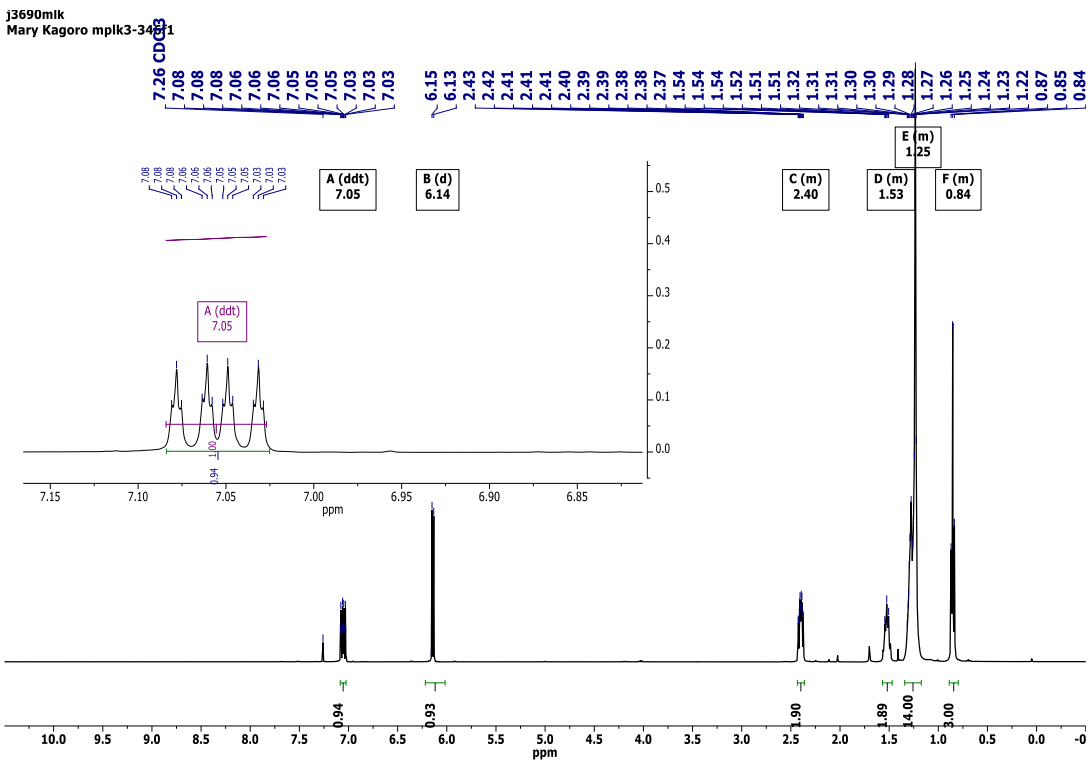

Figure 70: ^{1}H NMR spectrum of 6-chloro-3-decyl-2-pyrone-2-^{13}C **167b** ($CDCl_3$, 400 MHz). Inset shows the multiplicities of H4 within the 2-pyrone.

The synthesis of the imaging agent **169a-b** involved the reaction between phenyl acetylene and **167/168a-b** as shown in **Scheme 35** above. This scheme shows that a [1,5]-shift must have taken place for the 3-alkyl-2-pyrone **167a-b** to give the same compound as the 5-alkyl-2-pyrone **168a-b** and this could only have occurred via the intermediacy of ketene **Va** which is in equilibrium with ketene **VIa** to furnish the same product as shown in **Scheme 39**.

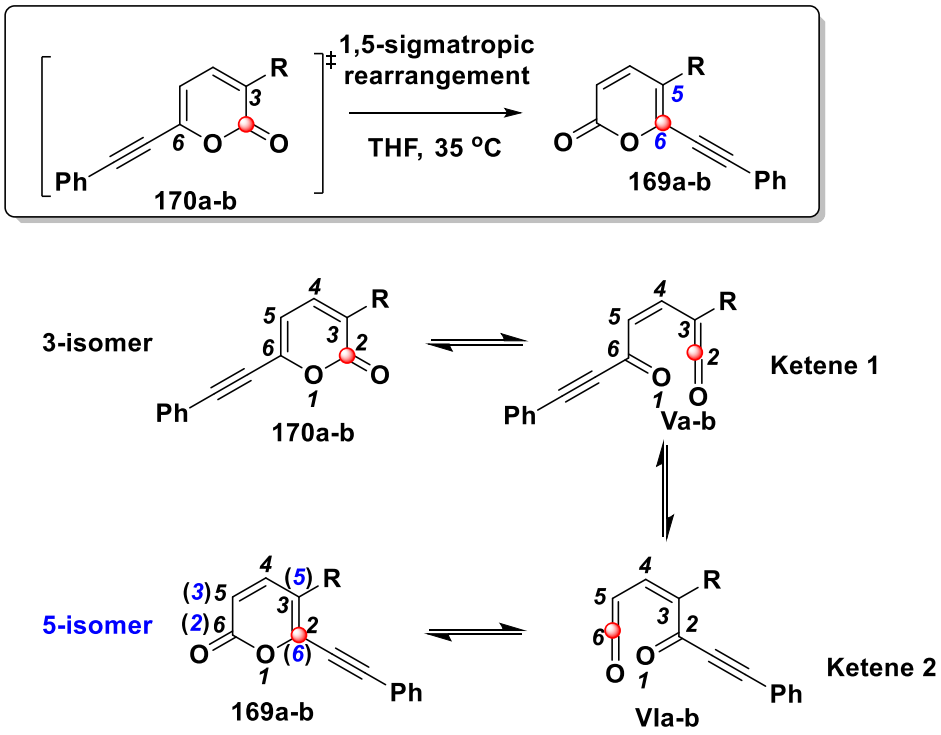

Scheme 39: General scheme illustrating the [1,5]-CC-Ph sigmatropic rearrangement of [^{13}C-6]-3-alkyl-6-(phenylethynyl)-2-pyrone which is proposed to have a transient existence in this reaction as it was never isolated.

3.7 DFT Analysis

Density functional theories (DFT) calculations was done in collaboration with Prof. Zhenyang Lin of the University of Hong Kong, Science and Technology. DFT calculations have emerged as a theoretical chemistry method for studying compounds.[268-271] It allows the prediction of material behaviour based on quantum mechanical considerations. The DFT calculations were performed using ωB97X-D functional and the 6-31G (d, p) basis set to study the relative free energies and relative electronic energies (in parentheses) of the proposed transient compound 3-alkyl-6-(phenylethynyl)-2-pyrone and the ketene intermediates (I and II, **Figure 71**), in addition to the various anionic transition states (sig-TS, sig-IM and sig-TS', **Figure 71**) to explain the observed (1,5)-sigmatropic shift of phenyl acetylide to the observed product 5-alkyl-6-(phenylethynyl)-2-pyrone (**Figure 71**).

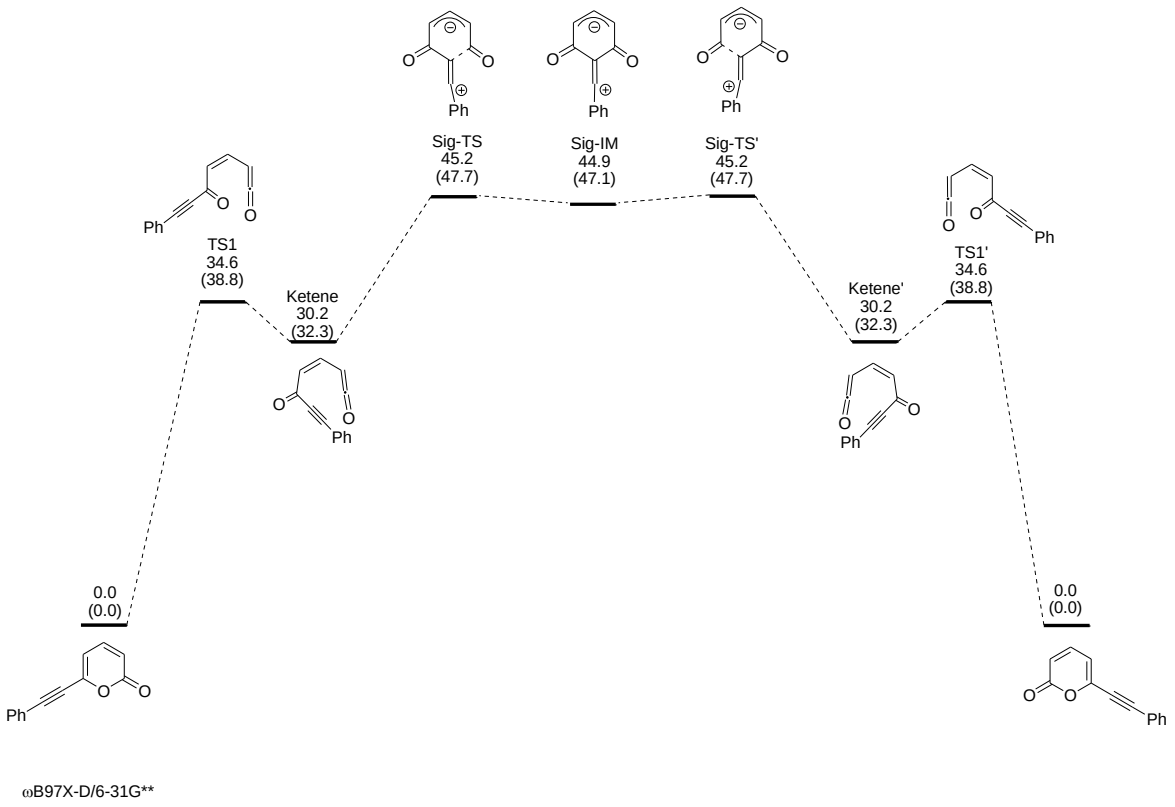

Figure 71: Spontaneous (1,5)-sigmatropic phenyl acetylide shift mediated by Pd. Relative free energies and relative electronic energies (in parentheses) are given in kcal/mol.

The relative free energies of 0.00 Kcal/mol for both the proposed transient product and the rearranged product implies that both products should be isolated however, the unrearranged product was never isolated only observed transiently at low temperature (-25 ^{o}C to -10 ^{o}C). This is also the case for ketene I and ketene II. Experimentally both products were not isolated. This could mean either a new discovery or that the DFT calculation might be inaccurate as experimentally the rearrangement has been proven with ^{13}C labelled compound.

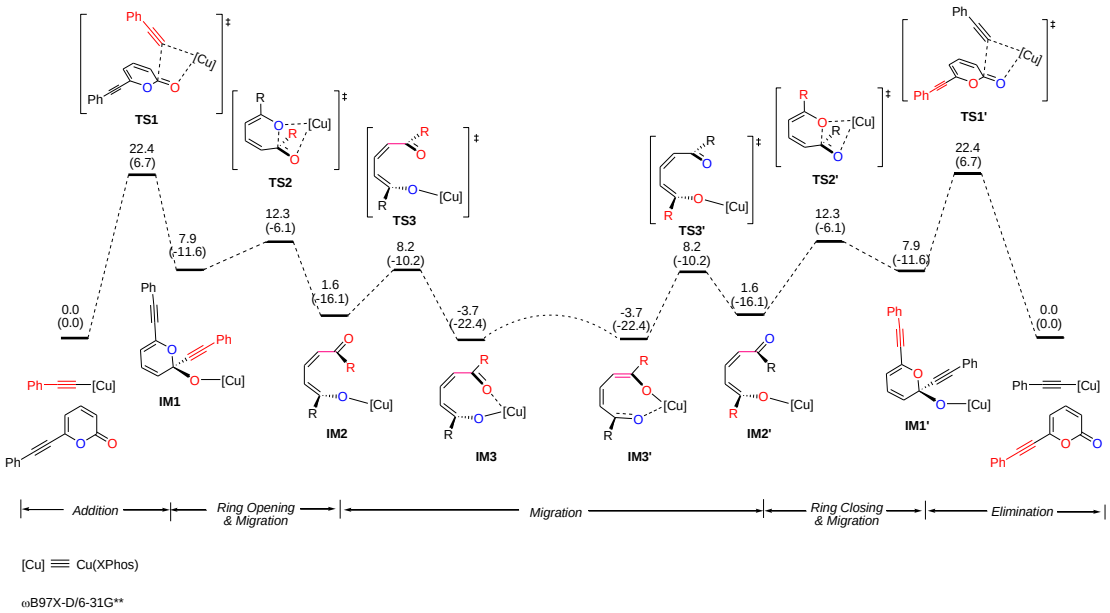

Figure 72: Copper-mediated (1,5)-sigmatropic phenyl acetylide shift. Relative free energies and relative electronic energies (in parentheses) are given in kcal/mol.

The copper-mediated (1,5)-sigmatropic shift of phenyl acetylide goes through a transition state with lower energies (**Figure 72**) relative to the transition state via the ketene intermediate (**Figure 71**). The predicted intermediates **IMI** and **IMI'** as suggested by DFT is unusual in cross-coupling chemistry and might be the first place to start.

3.8 Use of ^{13}C-isotopically labelled 2-pyrone as a mechanistic tool

The evaluation of a set of reactions to elucidate mechanistic findings involves first ensuring that all other parameters do not exert other type of effects on the reaction itself and once this is done then the reaction conditions so designed can be evaluated to provide mechanistic insights. A set of reaction condition was chosen, and change is made one reagent at a time to observe the effect that change would have. The isotopically labelled 3-benzyl-6-chloro-2-pyrone-^{13}C-2 **167b** was employed as an analytical tool. Four control reactions **171a-b** were carried out as shown as **Scheme 40**. When **167b** (Reaction **171a**) was treated with standard conditions but in the absence of Pd catalyst, no 1,5-phenylacetenyl migration was observed. This control experiment corresponds to a reaction carried out in the absence of the palladium catalyst but in the presence of all other reactants. The product obtained here is a trace amount of the oxidative addition/Glaser product as

shown in **Scheme 41** with most of the reactants observed unreacted. The oxidative addition leading to 1,4-diplenylbuta-1,3-diyne **173** is always observed as a by-product and its presence increases with oxygen.[247-249]

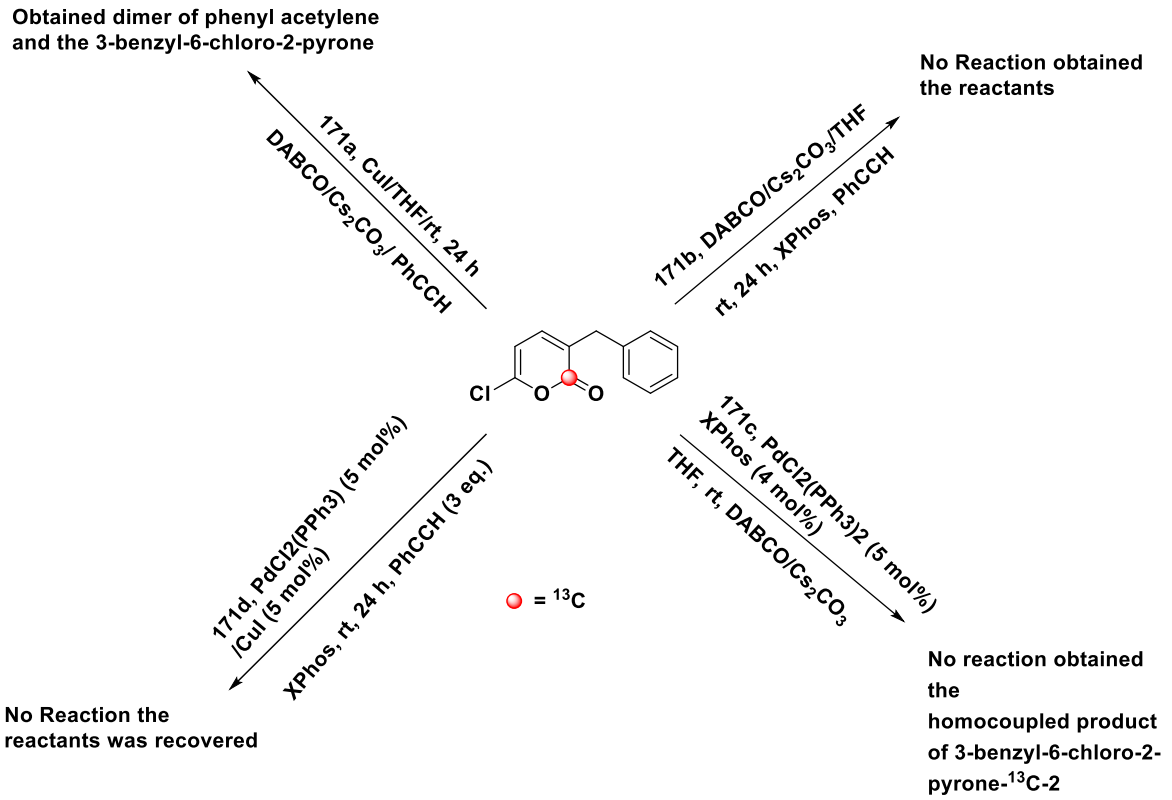

Scheme 40: The second controlled reactions illustrating that the rearrangement is palladium/copper mediated.

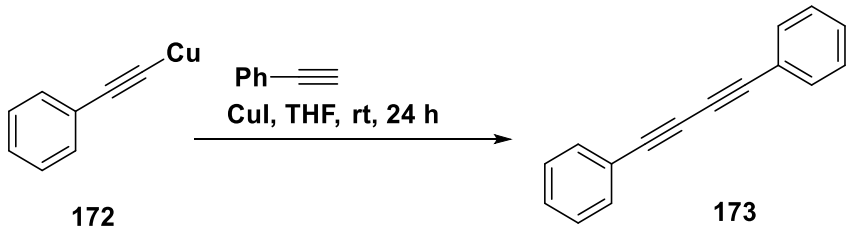

Scheme 41: Glaser reaction catalysed by copper.

Control reaction **171b** corresponds to an uncatalyzed Sonogashira cross-coupling reaction between phenylacetylene and 3-benzyl-6-chloro-2-pyrone. In this case both reactants were observed with no reaction having taken place as shown in **Scheme 39**. In the same light, the control reaction **171c** corresponds to a copper-free Sonogashira cross-coupling reaction with palladium catalyst $PdCl_2(PPh_3)_3$, base, and ligand present. No observed rearrangement took place. The weak base

(DABCO) was unable to deprotonate phenyl acetylene (pKa 25 relative to 33) as is theoretically expected. Control reaction **171d** corresponds to a Sonogashira cross-coupling reaction carried in the absence of base. No rearrangement nor product were formed. These results demonstrate the requirement of all reactants together before the [1,5]-rearrangement can occur as was observed with the unlabelled compound.

3.9 Conclusion

In this research, hyperpolarizable NMR imaging agents **169a-b** were designed and synthesized by six consecutive steps, in 20% overall yield. Their structures were confirmed by spectroscopic data. The synthesis led to the development of an efficient procedure for monoalkylation of diethyl malonate via a biphasic reaction employing potassium carbonate as base and TBAB as phase transfer catalyst. A novel room temperature Pd/Cu mediated (1,5)-sigmatropic rearrangement of the 3-alkyl-6-(phenylethynyl)-2-pyrones **128a-e** to the 5-alkyl-6-(phenylethynyl)-2-pyrones **131a-e** was observed and confirmed employing the isotopically labelled compounds and X-ray crystallographic data.

Chapter Four: Protein Binding Assay Using Saturation Transfer Difference (STD) NMR; Preliminary Signal Enhancement Studies.

4.1 Introduction

In the light of our interest in designing antituberculosis drugs and the success in the synthesis of ^{13}C-labelled 2-pyrone compounds in addition to their good AD MET properties and behaviour of the 3-alkyl-6-chloro-2-pyrone **128a-e** synthesized here it became imperative to study their binding interactions with known receptors sites. These have previously been predicted by *in-silico* modelling as reported by Katzenellenbogen and co-workers.[267]

Proteases form one of the largest and most important groups of enzymes. They selectively catalyse the hydrolysis of peptide bonds and can be subdivided into four groups; aspartic,[268-269] serine,[270] cysteine,[271] and metalloproteases.[272] Proteases play a vital role in a range of diseases such as hepatitis C,[273] cardiovascular,[274] malaria,[275] herpes,[276] inflammatory, and immunological, and respiratory.[277] A large array of protease inhibitors have therefore been evaluated such lactones,[278-279] lactams,[280] α-ketoheterocycles,[281-283] carbamates,[284-285] other activated carbonyl-containing compounds;[286] which act through covalent modification of the serine nucleophile.[287] Recently, significant progress has been made in the design of irreversible inhibitors of serine proteases. These include haloenol lactones,[288] substituted 6-chloro-2-pyrones,[217] β-nitroso lactams,[289] halomethyl coumarins,[290-291] and 2-bromomethyl-3,1-benzoxazin-4-one.[292] 6-Chloro-2-pyrones **128/129a-e** react with serine proteases to give an acyl enzyme and release an extremely reactive acyl chloride or ketene which is capable of acylating another active site residue.

Protein receptors are vital for cellular integrity and function and a number are involved in pathological conditions. The binding events between receptors and their ligands are important in drug discovery and biology. This knowledge should therefore lead to more efficient drug discovery.

NMR spectroscopic techniques have emerged as a powerful method for screening receptor-ligand interactions. These techniques involve saturation transfer difference

(STD), WaterLOGSY, NOE pumping and relaxation-edited processes. In fact, many are fast to complete and can now screen pure drug compounds or mixtures of them. Here, we focus primarily on the applications of saturation transfer difference (STD) NMR and its variant WaterLOGSY.[293] These techniques have matured and are now employed widely to unravel the receptor–ligand interactions. To achieve this, highly resolved proton NMR spectra, and in some cases ^{13}C- and ^{15}N-edited NMR spectra, are employed. There are however a few sensitivity issues that surround the use of heteronuclear STD NMR methods but working with isotope-labelled compounds is only applicable to a small subset of receptor–ligand systems. The large chemical shift dispersions of ^{13}C and ^{15}N nuclei are though helpful in probing the STD effects arising from attached protons. The STD-NMR experiment is based on the nuclear Overhauser effect. It can be used as a screening technique for the identification of lead structures or as a tool useful for identifying ligand moieties that are important for binding. Basically, an STD experiment involves subtracting a spectrum in which the receptor is pulsed and saturated (in a region where ligand protons do not absorb, on-resonance) such as 0 ppm to -1 ppm. As protons of the receptors are excited, they relax by exchanging energy with protons of the ligands that are near (10^{-5} Å) via the nuclear overhauser effect. The protons close to the receptors therefore yield reduced intensity signals in the off-resonance spectrum. A subtraction of the on-resonance and off-resonance spectra gives what is known as the STD difference spectrum as shown in **Figure 73**.[294] The difference in intensities because of saturation transfer can be quantified and linked to a binding event.

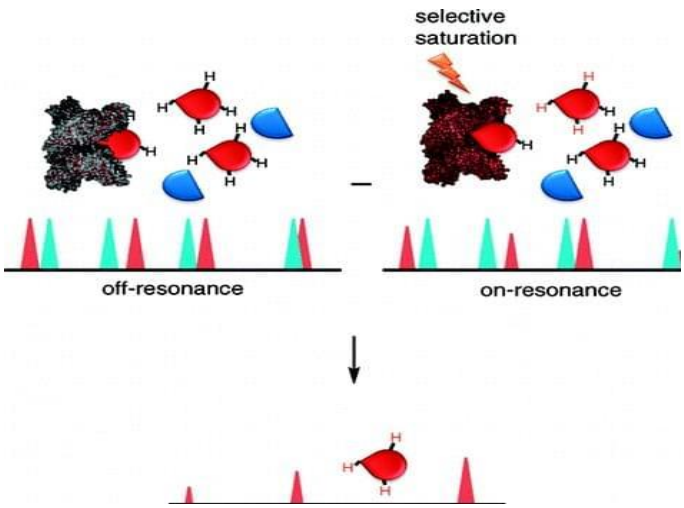

Figure 73: Generic depiction of STD NMR.

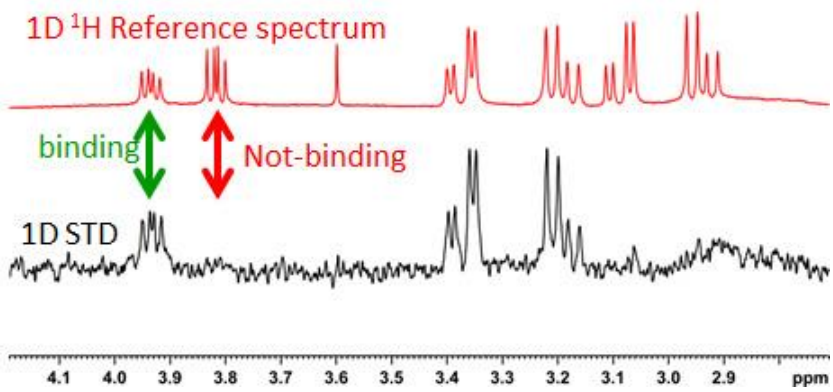

Figure 74: STD effect due to binding, and non-binding effect on STD NMR.[271]

Experimental parameters that employ long saturation times, see more extensive saturation to all hydrogens in the ligand and vice versa.[295] Ligand binding with high affinity are not be detected in the STD experiment. Ligands with K_d values >10 µM and in fast exchange on the NMR time scale are low affinity binders.[296]

4.2 Results and data analysis.

4.2.1 STD results and data analysis.

Analysis of the STD difference spectra revealed negative results for all the compounds tested. This is unexpected as a binding interaction between either of 3/5-benzyl-6-chloro-2-pyrone and chymotrypsin has been reported by Ringe *et al*., 1983,[297] and Katzenellenbogen and Westkaemper, 1983.[298]

The data found here is contrary to the docking result of **Figures 75-76**. The figures show the interaction between bovine pancreatic protein, trypsin (PDB ID: 1AUJ),[263] 3-benzyl-6-chloro-2-pyrone **128d** and 6-chloro-3-decyl-2-pyrone **128e** indicate the presence of favourable interactions (hydrogen bonding, π-alkyl, hydrophobic interaction, and halogen bond) and some unfavourable bumps. The bovine pancreatic protein is known to have four other binding sites. Figures 75 and 76 shows the numerous favourable interactions between chloropyrone and trypsin showing a lot of unfavourable bumps that possibly indicate non-bonding interactions. However, the PyRx docking studies show that the decyl derivative **128e** was a better binder. Thus, the choice of the decyl derivative to move forward for contrast agent synthesis.

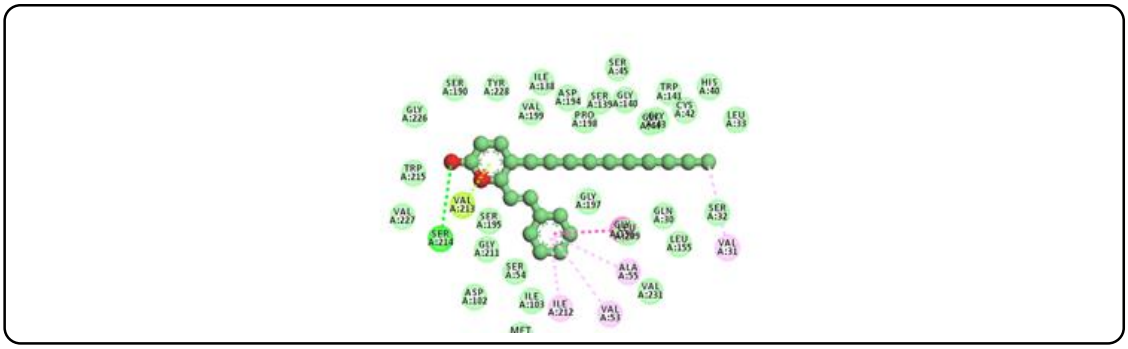

Figure 75: This interaction is showing the possible orientation that could possibly lead to binding as other researchers have observed binding involving the following amino acids at the binding site Ser195, Gly35 and His57.

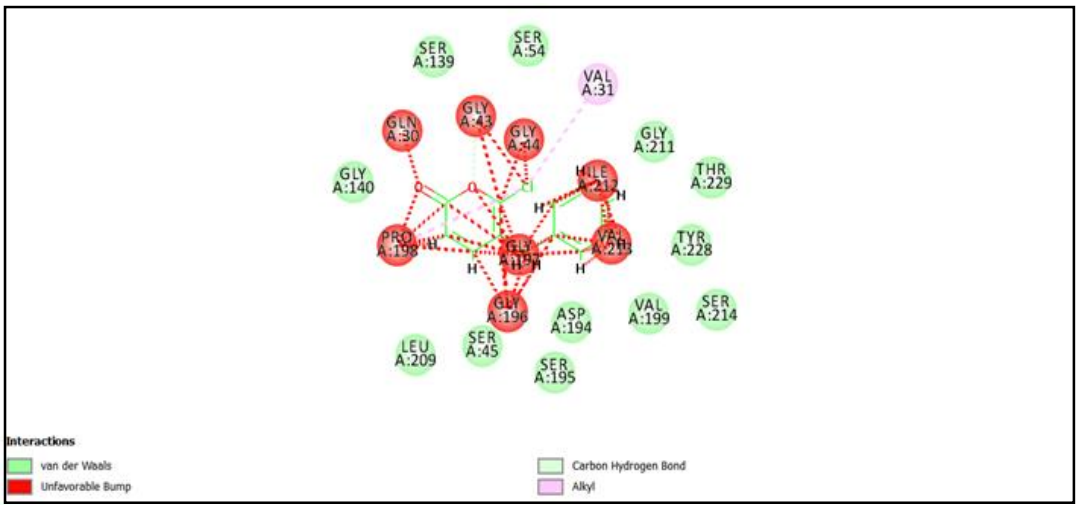

Figure 76: Illustrating the molecular interaction between 3-benzyl-6-chloro-2-pyrone **128d** and bovine pancreatic trypsin treated using BioSolve.

4.2.2 WaterLOGSY results and data analysis

A variant of STD NMR spectroscopy utilizes bound water at protein–ligand interfaces. Negative peaks are now thought to result from the presence of water between the receptor and the ligand **Figure 77**.[298-303] This method is termed water-LOGSY (Water-Ligand Observation with Gradient Spectroscopy).

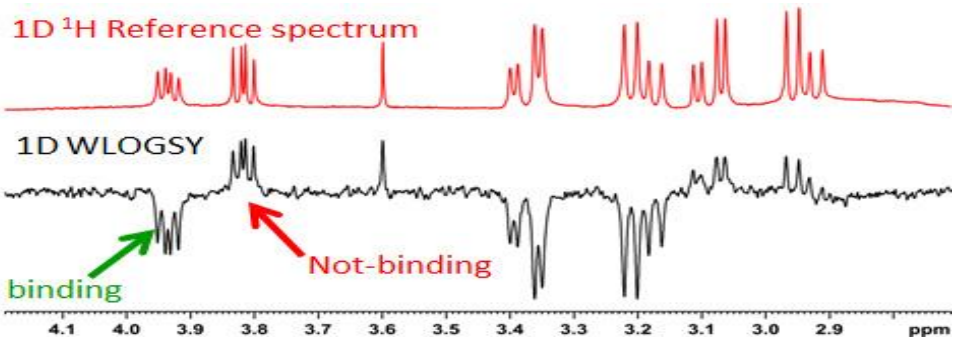

Figure 77: A typical waterLOGSY 1D ^{1}H NMR spectrum.

The WaterLOGSY experiment on 6-chloro-3-benzyl-2-pyrone and trypsin also shown no binding. It has been reported that this approach is useful for complexes that are strongly hydrated. For large proteins, even transiently interacting water molecules should give an effect on the ligand. Admittedly, this process is less effective for a relatively small protein like trypsin.

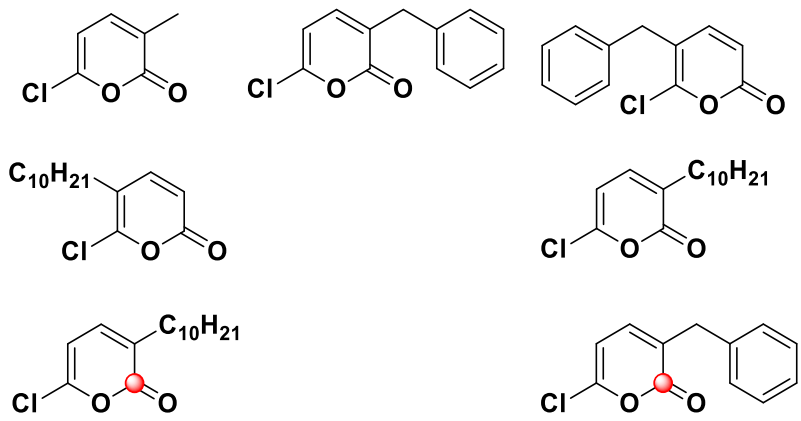

Figure 78: The structures of the 7 compounds tested in STD experiments with a WaterLOGSY experiment for the 3-benzy-6-chloro-2-pyrone **128d**.

The ^{1}H STD-NMR spectra for the chloropyrones tested here gave negative results indicating that they might interact with trypsin possibly forming a covalent linkage which STD NMR might not be the right technique to determine such interaction. Other researchers have shown the interaction between chymotrypsin and 6-chloro-2-pyrone using UV-Visible spectroscopic methods, enzyme binding assay and chemical shift perturbation.[217,267]

4.3 Preliminary Signal Enhancement Studies.

Nuclear magnetic resonance (NMR) spectroscopy measures the magnetic properties of nuclei on application of an external field of strength (B_0). This field lifts the degeneracy of the spin energy levels. The intensity of the signals depends on the field strength B_0, temperature, T in kelvin and the gyromagnetic ratio (γ) peculiar to the nuclei under evaluation. NMR suffers from low sensitivity due to the small difference in population between these energy levels and this can be improved by using a higher magnetic field. There is a technique that enhances the sensitivity of NMR by selectively populating one level and this non-equilibrium process is called hyperpolarization. There are four techniques that can presently enhance the sensitivity of NMR as shown in Figure 79. Optical pumping of ^{3}He or spin-exchange optical pumping of ^{3}He and ^{129}Xe.[304-306] Others are parahydrogen-induced polarization (PHIP),[307-308] and dynamic nuclear polarization (DNP) (**figure 79**).[309-310] Both methods can be used to polarize molecules containing ^{13}C, an important advance because of the very large chemical shift range of ^{13}C in organic molecules and the opportunity for direct tracing of drugs or key metabolic intermediates. DNP has been employed to increase the sensitivity of pyruvate,[311-312] bicarbonate,[313-315] fumarate,[316] lactate,[317] glutamine,[318] and others by more than four orders of magnitude.[319] This has led to applications in medicine and clinical studies.

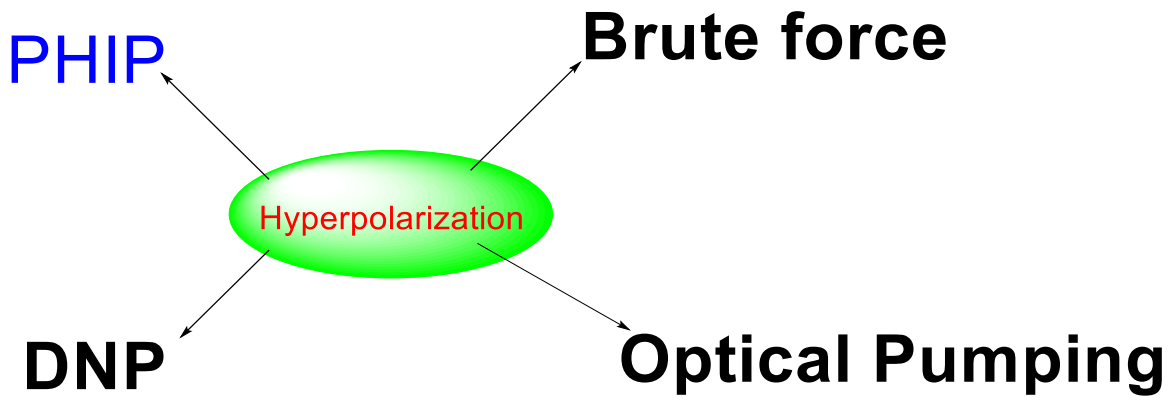

Figure 79: Four methods for hyperpolarized-MR imaging and spectroscopy.

Nevertheless, our interest in this project lies with the less expensive procedure of PHIP which occurs as para hydrogen molecules adds to a new molecule. This

implies unsaturated organic molecules are involved and is termed hydrogenative PHIP (h-PHIP). It occurs via two protocols termed ALTADENA (Adiabatic

Longitudinal Transport After Dissociation Engenders Nuclear Alignment),[320] and PASADENA (Parahydrogen and Synthesis Allow Dramatically Enhanced Nuclear Alignment).[321]

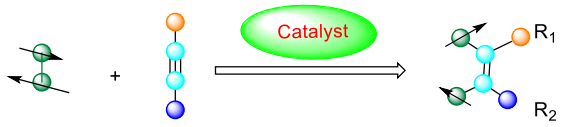

Scheme 42: General procedure for catalytic hydrogenation with para-H_2 leading to PHIP.

In the PASADENA experiment the molecules are polarized inside the NMR spectrometer and the NMR spectrum is detected immediately. Under these conditions the initial singlet state of para-H_2 evolves into αβ and βα product states. These two states are equally populated and associated with four NMR transitions, two absorptive and two emissive, of the spin system. The PHIP spectrum therefore consists of two anti-phase doublets. The corresponding population pattern and PHIP spectrum are shown in **Figure 80a**.

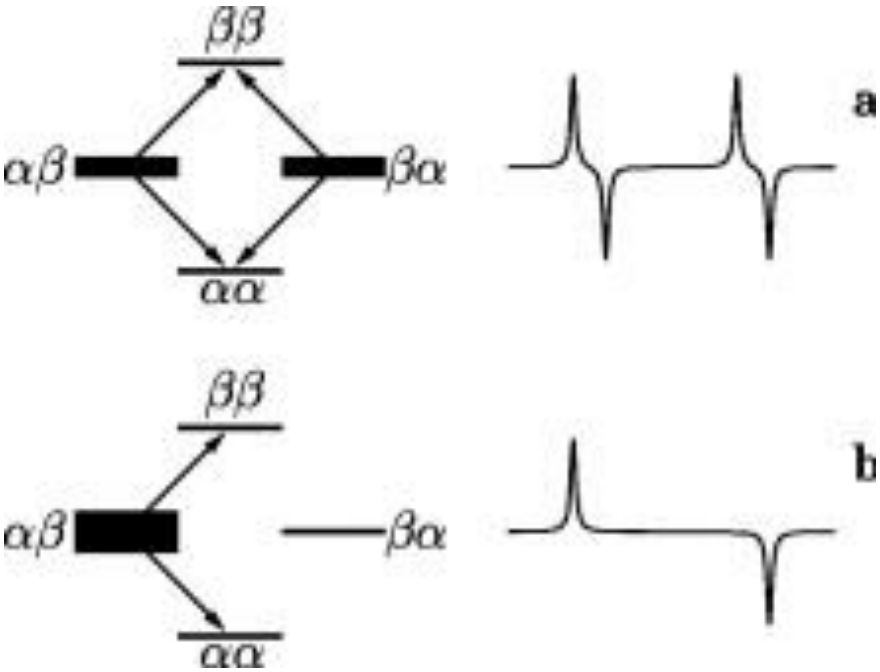

Figure 80: PASADENA (a) and ALTADENA (b) population patterns and the corresponding NMR spectra. The widths of the energy levels reflect their

populations; NMR transitions are shown by arrows. State populations are shown on the left, NMR spectra on the right-hand side.

In the ALTADENA experiment, non-thermal polarization is first created at low field (often the Earth's magnetic field) in the reaction products. The polarized sample is then transported to high field where the final NMR spectrum is recorded. Now only the low energy αβ or βα product state is selectively populated. Hence in the spectrum there are only two lines, one absorptive and one emissive, the other two disappear. The ALTADENA population pattern and NMR spectrum are shown in **Figure 80b**. Several reviews have dealt with PHIP and the role of polarization transfer in PHIP. Kuhn and Bargon,[322] gave several examples of PHIP transfer to various nuclei. PHIP also has another technique which does not involve a chemical reaction instead exchange occurs between the catalyst and the substrate termed SABRE (signal amplification by reversible exchange) as shown in **Scheme 43**. SABRE enhancement has been observed for with various iridium catalysts.[323-329]

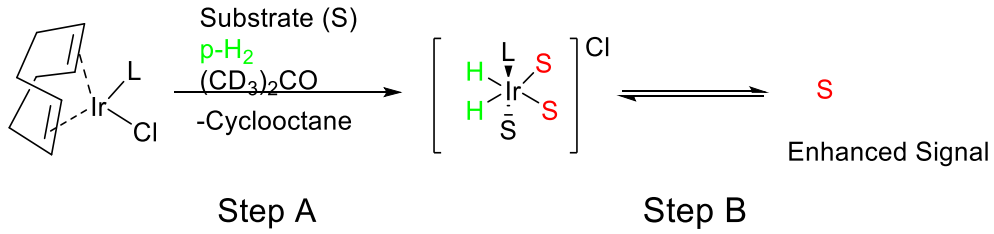

Scheme 43: Illustration of the SABRE experiment.

The application of hyperpolarized MRI and magnetic resonance spectroscopic imaging (MRSI) is promising because it employs natural abundant non-radioactive isotopes that are ideal for repeated monitoring of *in vivo* events.

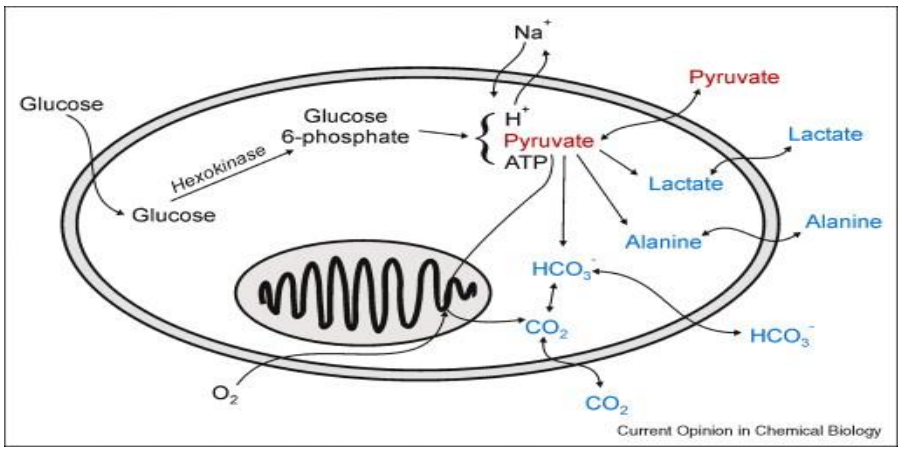

Figure 81: Metabolic products of pyruvate in mammalian cells. Ref.[330]

In a recent paper, Duwel *et al*.,[331] synthesized and demonstrated that hyperpolarized [1,5- $^{13}C_2$]zymonic acid (ZA) **178** is a new probe for imaging cellular pH. They demonstrated that ZA enabled the non-invasive imaging of extracellular pH both *in vitro* and *in vivo* in the bladder, the kidneys and a tumour model.

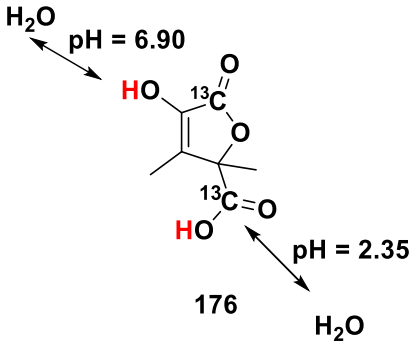

Figure 82: pH sensitive hyperpolarized MRS agent.

Diffusion-weighted magnetic resonance spectroscopy (MRS) of hyperpolarized ^{13}C-labelled pyruvic acid, fumaric acid, lactate and malate is useful to provide information about lactate efflux, about the viability and the state of necrosis of tumour cells. This provides another diagnostic tool to characterise tumour cells beyond morphological characterization.[332-333] Gutte *et. al.,* reported the introduction of a multimodal imaging modality they termed hyperPET which they employed to directly and indirectly image the Warburg effect with hyperpolarized ^{13}C-pyruvate and ^{18}F-FDG PET imaging.[334-335]

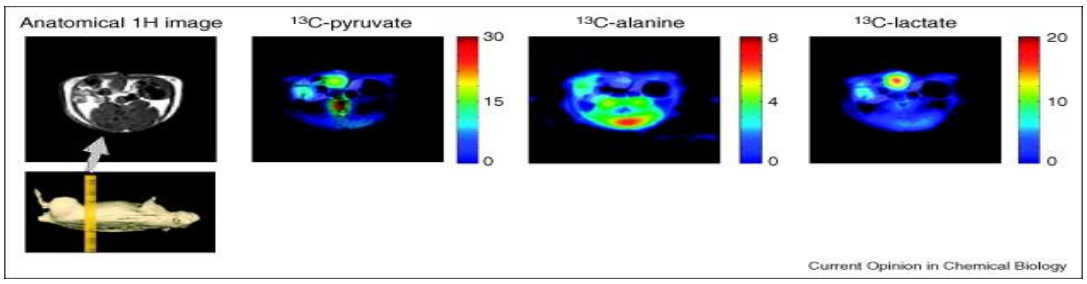

Figure 83: ^{1}H image of the distribution of $^{13}C_1$-pyruvate and its metabolites $^{13}C_1$-alanine and $^{13}C_1$-lactate. Reprinted with permission from Ref. 330.

A recent paper has shown that [1,1-^{13}C] acetic anhydride can be polarized and that the hyperpolarized ^{13}C can be chemically transferred to other molecules because of the preferential reaction of acetic anhydride with amine nucleophiles; this was demonstrated with several hyperpolarized [1-^{13}C]N-acetylated amino acids.[336] This provides a procedure for introduction of isotopic labelling to other molecules.

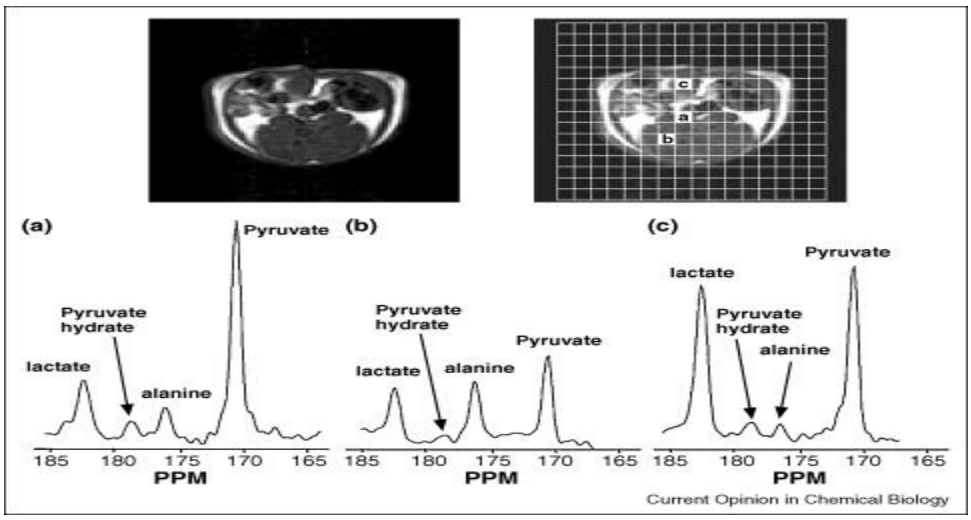

Figure 84: Change of metabolic pattern as visualized by ^{13}C-MR spectra. Reprinted with permission from Ref. 330.

Besides hyperpolarized pyruvate, lactate, urea, acetate and other molecules are currently under testing for molecular/metabolic imaging. Hyperpolarized ^{13}C imaging is possible at polarization level of 10–30% with relaxation times of 60 seconds (T_1) and T_2 of 5 seconds for imaging pathological and therapeutic responses. The feasibility of hyperpolarized ^{13}C NMR imaging has recently been investigated.[337] MRI using ^{13}C hyperpolarized agents are in their infancy but has shown a great deal of potential in model animals.

4.4 Results and discussion

PHIP in hydrogenation reactions. For polarization to occur, hydrogen enriched in the para form is required. According to Weitekamp,[338] polarization can arise if para-H_2 is transferred pairwise to a substrate to yield a product in which the two transferred protons are magnetically distinct. Typical NMR experiments were performed in CD_2Cl_2 containing the catalyst and a 4-fold excess of unlabelled substrate. About four atmospheres of para-H_2 was then introduced over the solution at 295 K, and the ensuing reaction was monitored by multinuclear NMR spectroscopy between 261.5, 262.5 and 272.5 K. During these studies, the utilization of para-H_2 resulted in the observation of enhanced proton resonances for the products of **Scheme 44** containing two hydrogen atoms that were originally present in a single para-H_2 molecule (**Scheme 43**).

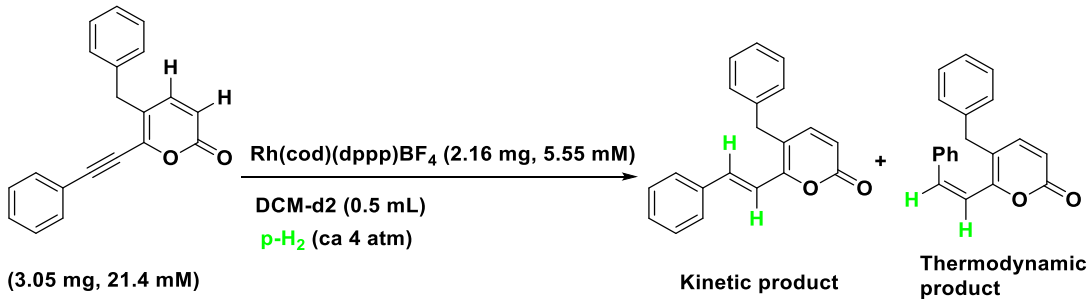

Scheme 44: In situ catalytic para-hydrogenation reaction.

This contrasts the situation under normal conditions, **Figure 85**, which show an ^1H NMR of the spectrum that indicates the formation of only one hydrogenation product, with coupling constant of 14 Hz indicating it is the trans isomer. The olefinic hydrogens of this species appear at 6.93 ppm and 6.32 ppm. For the system given here, the signal enhancement (SE) can be derived from the S/N by comparing the S/N value of the largest signal of the quartet at 6.93 ppm observed during the reaction to that corresponding to the equivalent product concentration as determined after the addition reaction.[339]

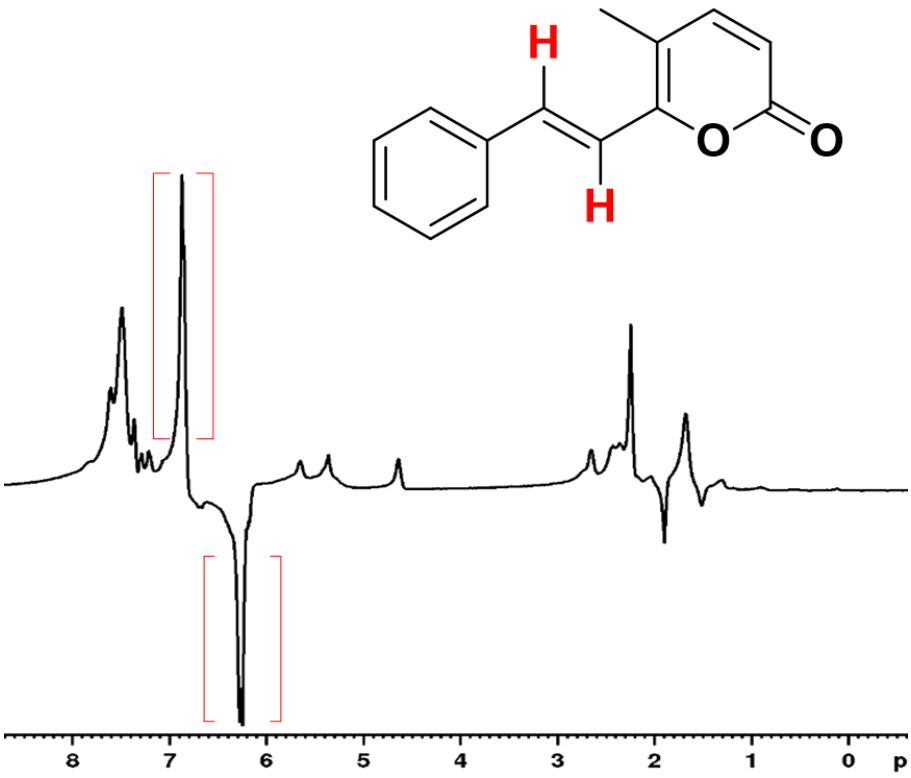

Figure 85: A single scan of compound **133a** at 261.5 K after 45º pulse.

The polarization pattern remains the same during the entire reaction. In **Figure 85**: Product signals seen during the addition of para-H_2 to **131a** at 262.5 K. This shows 100% enhancement at 262.5 K after 45º pulse with the initial E/A pattern as explained by Eisenberg 1991.[340]

A flow reactor was then employed to follow the change in product signal intensity as a function of reaction time for substrate **131a** and Product **133a** decays with a time constant of 140 seconds as shown in **Figure 86** which suggests a slow reaction. Hence in situ hydrogenation of the unlabelled substrate in DCM-d_2, with this rhodium catalyst led to strong polarization signals of the hydrogenation product indicating a pairwise transfer of dihydrogen.

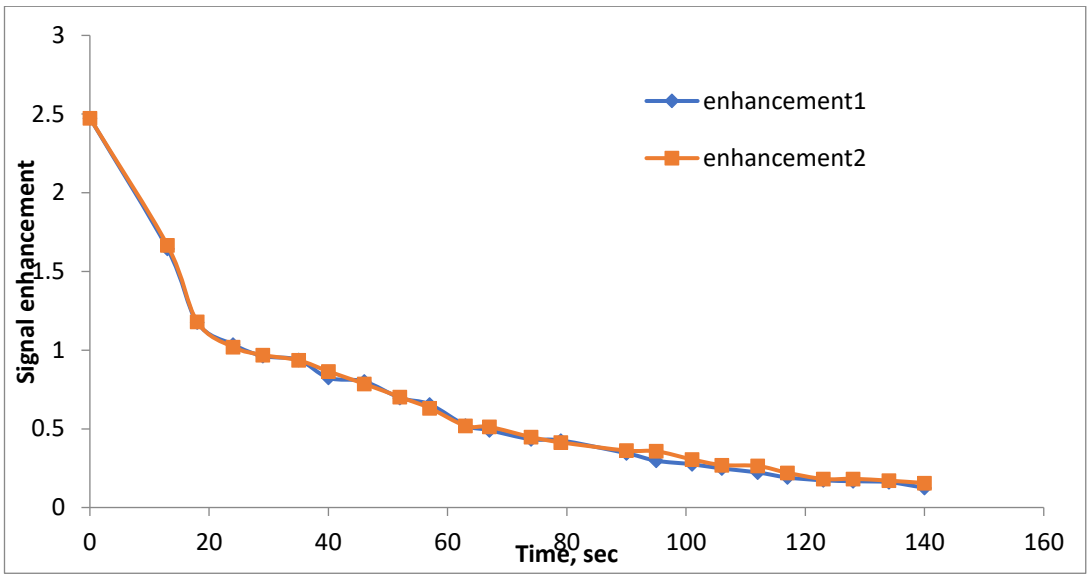

Figure 86: Graph of PHIP enhancement of 5-methyl-6-(phenylethynyl)-2-pyrone **131a**-**133a** using Flow probe reactor. The signal enhancements are for the two added hydrogens of the styryl motif in **133a**.

Similar results were obtained during the catalytic hydrogenation of the other substrates using the same catalyst in DCM-d_2 except for the 5-benzyl-6-(phenylethynyl)-2-pyrone which shown little enhancement at 261.5 K (**figure 87**) but on warming observed a 92% enhancement of the same peaks.

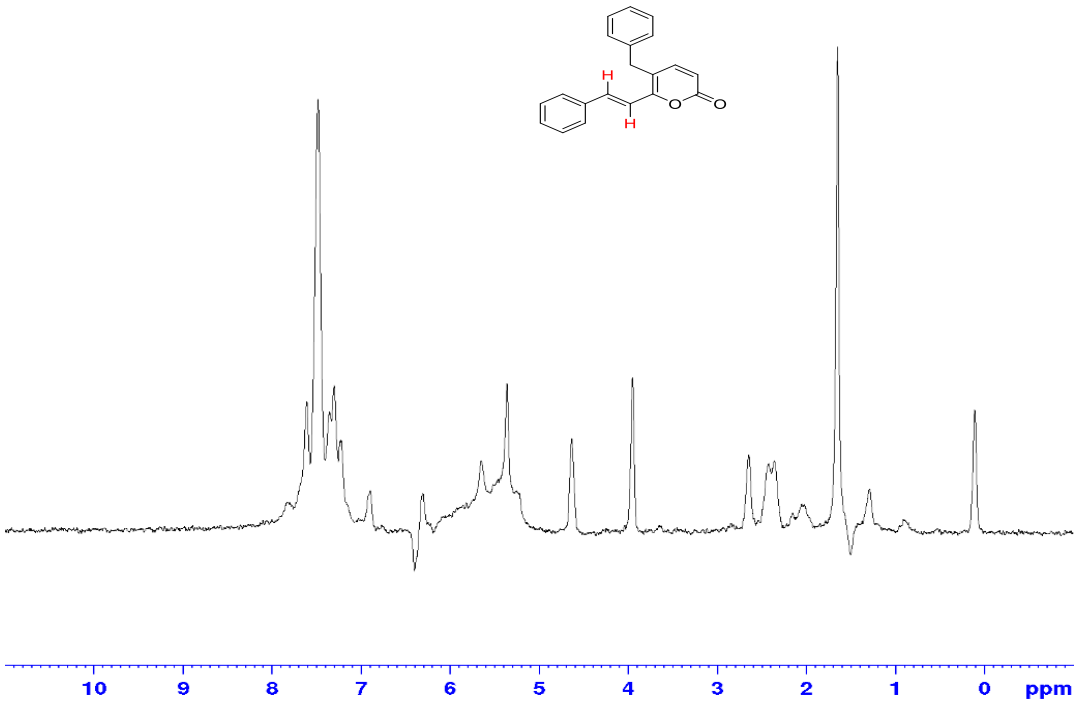

Figure 87: Enhanced ^{1}H NMR for **133d** at 261.5 K at 90°

In summary, the ^{1}H NMR spectra show strongly enhanced signals a second after the addition of para-hydrogen with the formation of the trans -product with peaks at δ 6.93 ppm and δ 6.32 ppm. Since the two alkene protons of the trans isomer are not chemically nor magnetically equivalent, the observation of a para-H_2 enhanced emission signal at δ 6.37 and δ 6.93 ppm is consistent with the involvement of an intermediate where two hydrogen atoms of the para-H_2 molecule have become inequivalent and this is formed stereoselectively. Furthermore, this indicates the trans product is the kinetic product. The thermodynamic product yields signal at 7.14 and 6.38 ppm and forms later, presumably by alkene isomerisation. Further confirmation of this hypothesis is revealed in the stacked NMR spectrum of **Figure 88** which shows the thermal ^{1}H NMR trace of the compound before hydrogenation and after hydrogenation.

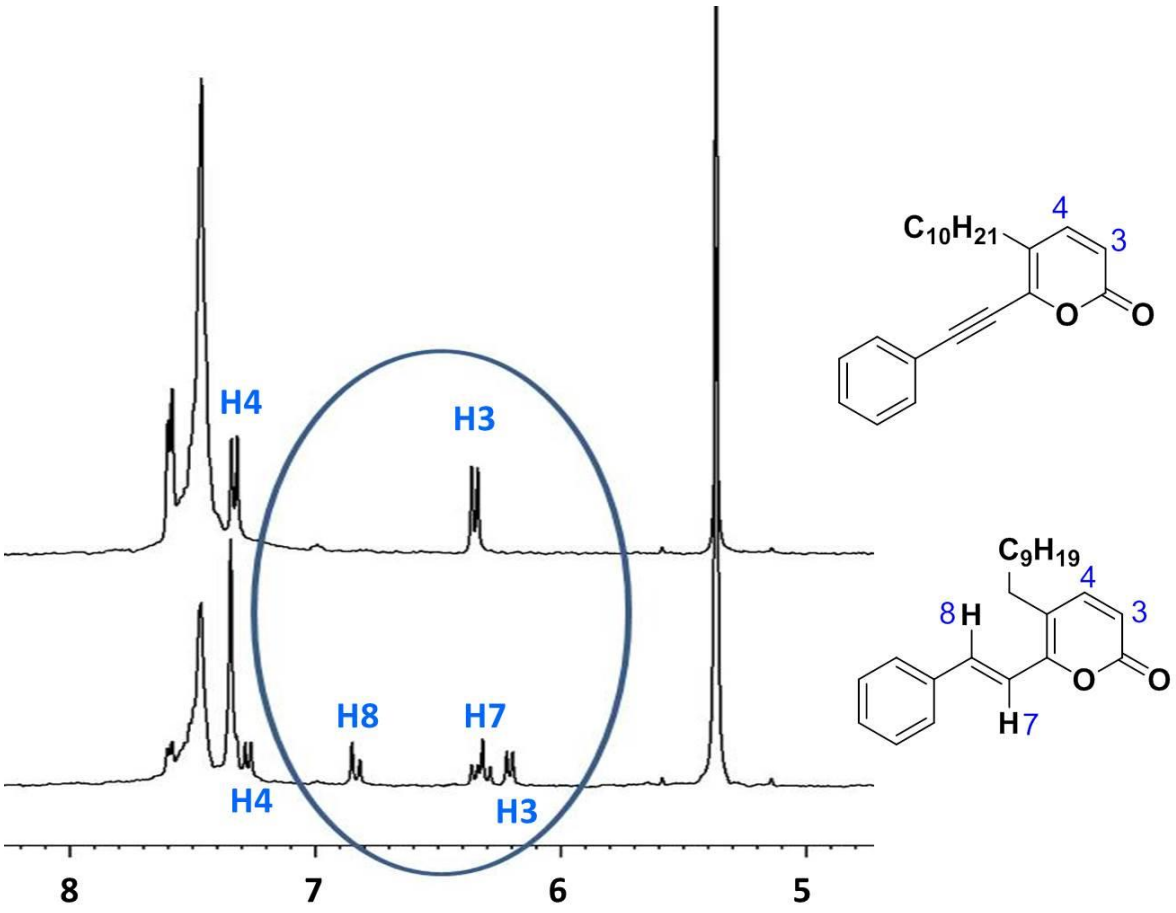

Figure 88: Thermal ^{1}H NMR spectra before adding H_2 to the system and after 10 minutes after adding.

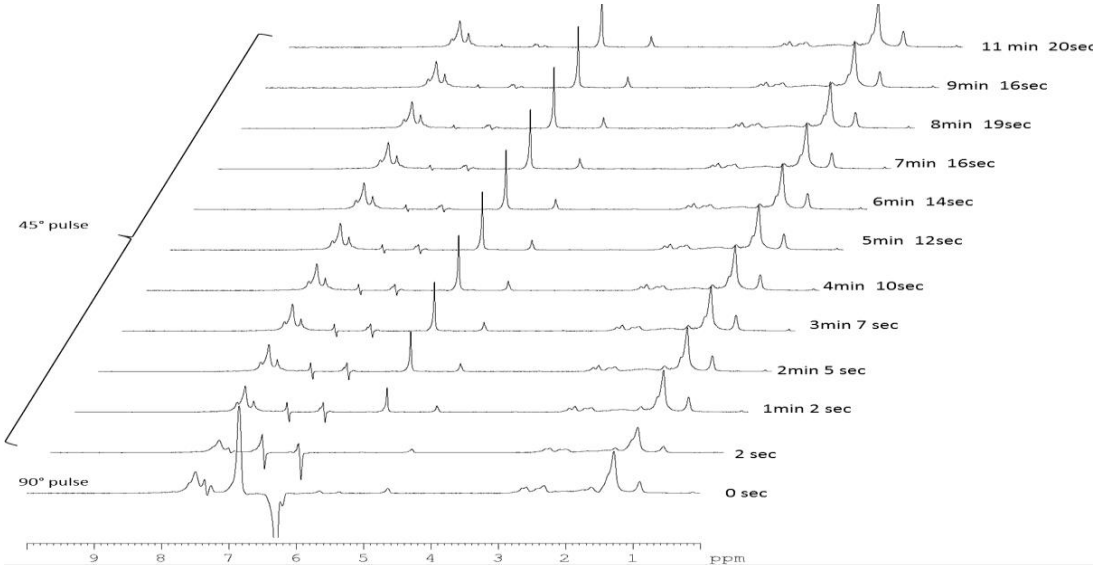

Figure 89: Depletion of polarization (PHIP) on the ^{1}H NMR signals of the product of hydrogenation (-CH=CH-) for **133e** in DCM-d_2.

The series of NMR measurements used to obtain the kinetic profile are illustrated in **figure 89** above.

4.5 Result and discussion of ^{13}C-PHIP

Most organic chemists are aware of the low sensitivity of carbon-13 as it is only 1.1% that of its other isotope (carbon-12) in addition to being much less sensitive to detect in comparison to proton.[341]

Proton-based hyperpolarized MR signals are limited by short relaxation times T_1^H and the transfer of the polarization from hydrogen to carbon either through bond or by nuclear overhauser effects.[342] Another solution depends on polarization transfer to a slowly relaxing, low-γ nucleus using a suitable pulse sequence such as INEPT.[343] Recently, spontaneous enhancements in solution-phase ^{1}H NMR of hydrogens covalently bound to HP ^{13}C spins have been reported.[344] Heteronuclear cross-relaxation effects arising in rapidly tumbling small molecules were identified as the mechanism responsible for this $^{13}C \rightarrow ^{1}H$ polarization transfer. The ^{13}C NMR of the unlabelled h-NMR

contrast agent did not show any absorbance as is expected from theory due to low natural abundance of ^{13}C isotope **Figure 90**.

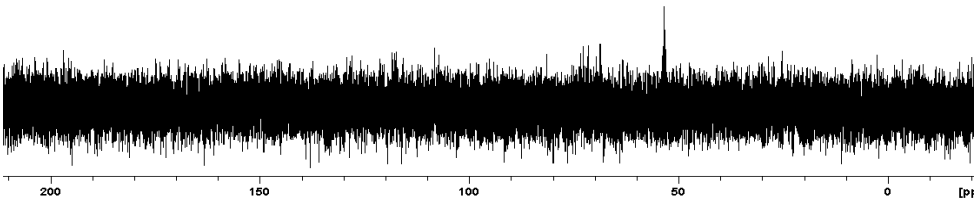

Figure 90: ^{13}C NMR of substrates showing no peaks aside that of DCM-d_2. The ^{13}C-H polarization transfer of [^{13}C-6]-5-decyl-6-(phenylethynyl)-2-pyrone **169b** on addition of para-H_2 shown a single peak at 141 ppm whilst those of the addition product which also showed a single scan occurred at 154 ppm after INEPT experiment using a 45º pulse and a single scan (**Figure 91-93**).

A field screening was carried out and this led to the result as shown in **Figure 91**. Before the addition of para-H_2 the thermal one scan ^{13}C NMR indicated the presence of only the enriched ^{13}C peak at 141 ppm of **169b** (**Figure 91**). After the addition of para-H_2 , the ^{13}C signals of the product of hydrogenation appear at 154 ppm (^{13}C-DE=). The best intensity was obtained at 0, 100 and 120 G (using the shield). At 30 G, there were no signals, while at 50 G both peaks of the starting compound and the hydrogenated product appeared. The transfer of polarization would best be carried out at lower field strength of either 0, 100 or 120 G before the ^{13}C imaging experiments is performed.

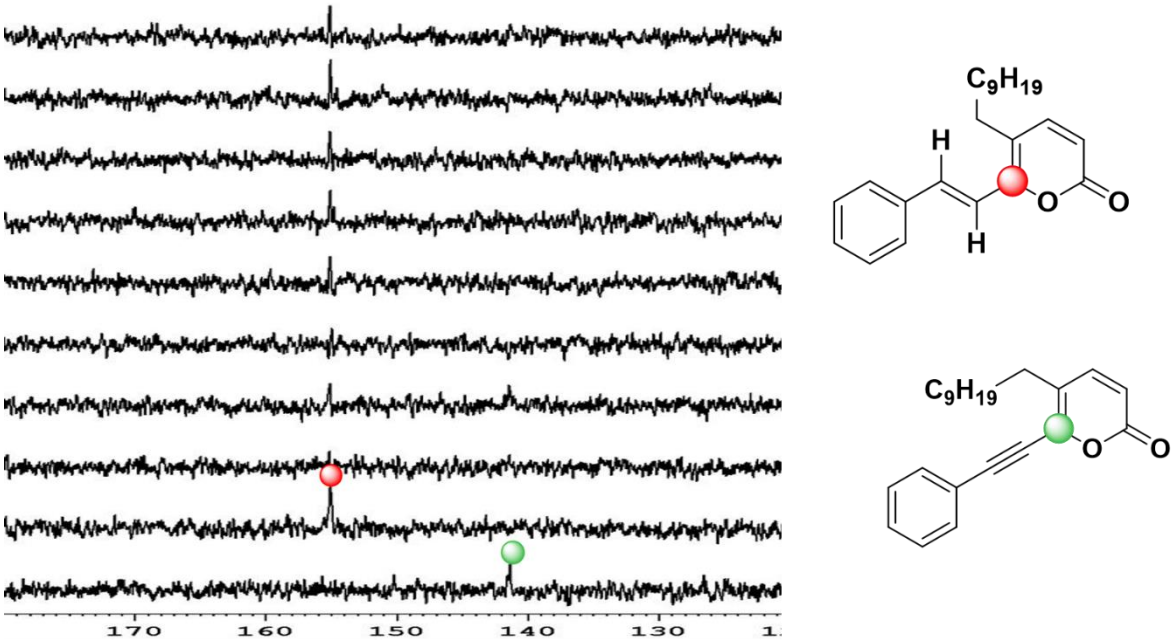

Figure 91: Polarization transfer into ^{13}C atoms of the DE substrate at different magnetic field.

The AA'X system (two protons–one ^{13}C spin system) resulting from the hydrogenation of the molecules, its interactions and the proton spin order produced using para-hydrogenation. Here the use of field-cycling method was employed to transfer the polarization of proton to the ^{13}C enriched carbon.

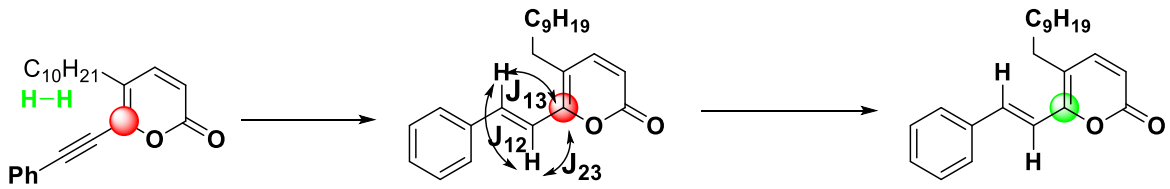

Scheme 45: Generic depiction of pulse transfer in an AAX spin system for [1-^{13}C-6]-5-decyl-6-styryl-2-pyrone **169b**. (a) para-H_2 (H-H) is added to [1-^{13}C-6]-5-decyl-6-(phenylethynyl)-2-pyrone catalysed by rhodium complex. (b) A pulse sequence is applied transferring the spin order via J-couplings in a typical AAX spin system as described by Goldman et al.[344]

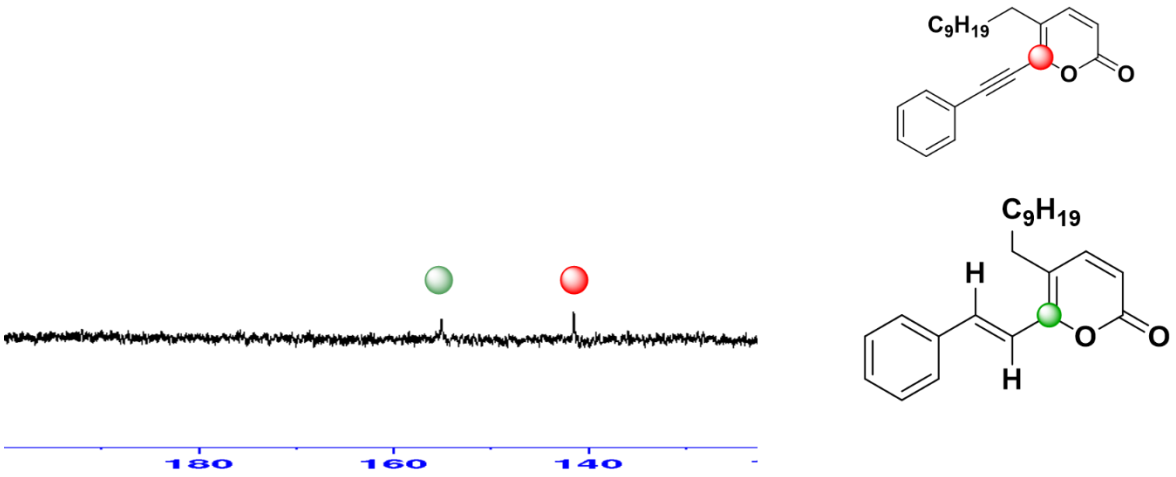

Figure 92: A single scan ^{13}C NMR of HP [^{13}C-6]-5-decyl-6-(phenylethynyl)-2-pyrone **169b** (3.75 mg, 11.12 µmol, 22.24 mM) with signal at 141 ppm whilst the signal at 154 ppm is indicative of the product of the catalytic para H_2 addition reaction ([^{13}C-6]-5-styryl-2-pyrone) **169b**.

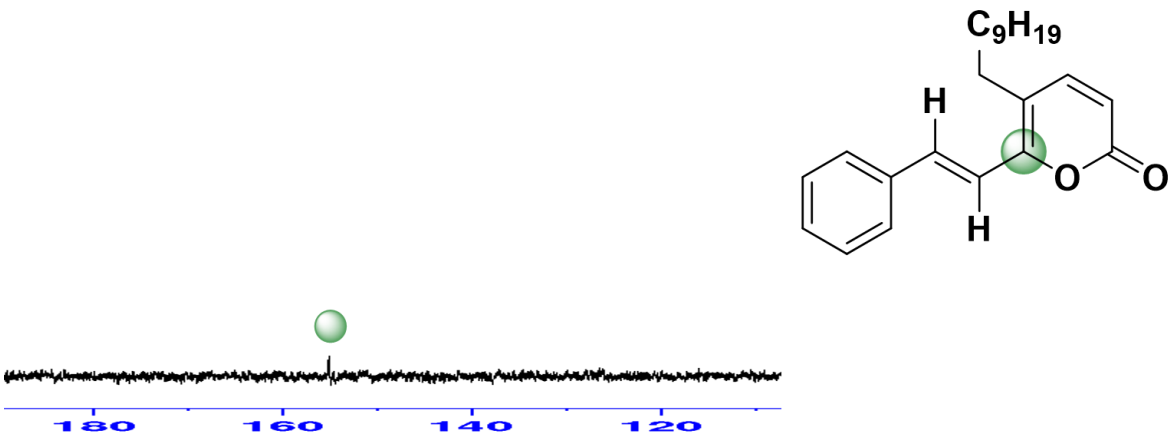

Figure 93: A single scan showing the presence of the product only using field-cycling at some low field only the product was observed at others both and yet other indicated none.

Only PHIP Spectroscopy (OPSY) is a technique that shows the peaks that are enhanced on application of para-H_2 as shown in **Figure 94**.[345-347]

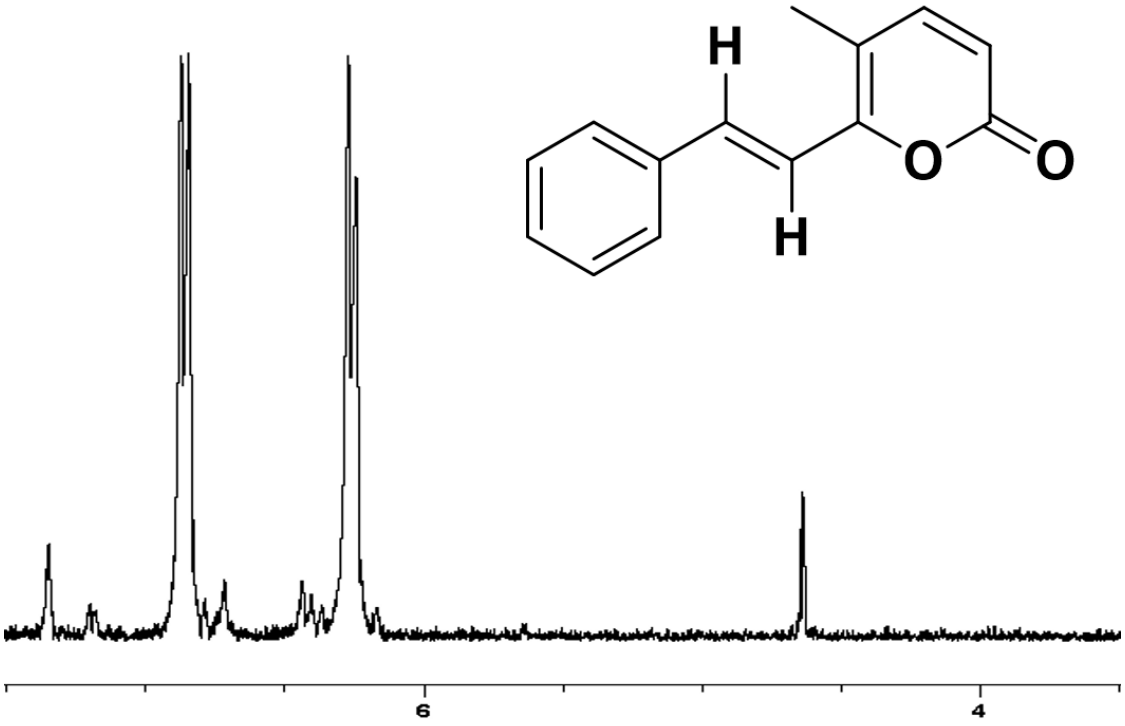

Figure 94: OPSY.dq ^{1}H NMR spectrum that shows only signals that are derived from para-H_2 for compound **133a**.

4.6 CONCLUSION

Binding affinity measurements can made employing either spectroscopic techniques or non-spectroscopic techniques. In this research we employed the use STD NMR technique which is ultrafast and versatile in providing information either using chemical shift mapping, peak broadening or chemical perturbations. However, the use of STD NMR technique to probe the interaction between bovine serine protease (trypsin) and 3/5-alkyl-6-chloro-2-pyrone **128a**, **128d** and 1**28e** led to failure in all experiments it was employed for. The use of the labelled **167a-b** employing both 1D and 2D STD experiments led to failure in my hand.

The signal enhancement was evaluated and found to be over a 100% in **133a**, **133c**, **133d** and **133e**. The use of low field cycling method was employed to carry out the polarization transfer from hydrogen to ^{13}C-isotopically labelled carbon and the results showed that low fields of 0, 100 and 120 G showed better signal enhancement than 50, 60, 70 and 80 G showed lower signal enhancement whilst

low field strength of 30 G showed no signal at all. The low field strength of 50 G showed the signal for both the starting compound **169b** and the para-hydrogenated product. It is this chemical information that should be extracted and use to carry out the cell-based imaging in live cells.

Chapter Five: Conclusion and Recommendation for Future Studies

5.1 Conclusion

The aim of designing and synthesising (^{13}C)-isotopically labelled hydrogenative PHIP imaging agents (**169a-b**) was achieved using ^{13}C-isotopically labelled diethyl malonate and methyl propiolate (methyl 3-haloacrylate) in a biphasic reaction employing tetrabutylammonium bromide as phase transfer agent and potassium carbonate as base. The Sonogashira cross-coupling between [^{13}C-3]-3-alkyl-6-chloro-2-pyrone using the optimized procedure, led to the discovery of an unprecedented (1,5)-sigmatropic rearrangement to afford the same product as the [^{13}C-6]-5-alkyl-6-chloro-2-pyrone via the intermediacy of a ketene (as discussed in Chapter Three). This rearrangement is novel because what we observe is a carbon shift contrary to literature assertion that the presence of even a methyl group on position 6 of the 2-pyrone ring prevents this rearrangement from taking place.

The preliminary enhancement studies showed a significant enhancement on addition of parahydrogen using a rhodium catalyst. The para-hydrogenation reaction took place very rapidly and observed a great level of enhancement with a good T1 (>140 seconds) to warrant further studies. The molecular docking studies using predicted targets for **133d-e** led to quantifying the binding affinity between human tyrosyl-DNA phosphodiesterase (PDB ID: 1qzq), and the designed bioactive ligands (**133d-e**). Free energy of binding of -48.87±0.99 KJ.mol^{-1} and 34.87±0.87 KJ.mol^{-1} respectively was obtained for **133e** and **133d** with a resolution of 2.21 and 2.41 Å respectively. This receptor target is predicted to be the best match for both compounds in addition, to muscleblind-like 1 and 2 for **133d** and thromboxane A and chymotrypsin-C for **133e.**

The *in silico*-based ADMET properties of the bioactive hNMR agents showed good physicochemical properties as well as ADMET properties particularly for **133e** but **133d** was a close alternative. Their toxicity profile was relatively good; however, further studies need to be carried out on their *in vivo* interaction with metabolizing enzymes (e.g. CYP 450 isoforms). The antibacterial activity of the precursor to the unlabelled contrast agent viz: 6-chloro-3-benzyl-2-pyrone **128d**, 6-chloro-3-decyl-2-pyrone **128e** and 6-chloro-3-methyl-2-pyrone **128a** was tested against *E. coli* and

found to be active in a dose-dependent manner with an MIC of 2.21 µg/mL for 6-chloro-3-benzyl-2-pyrone **128d** derivative.

5.2 Recommendation for Future Studies

The fact that we achieved the aim of designing a 2-pyrone-based ^{13}C-NMR imaging agent with good relaxation profile to serve as contrast agents in cell-based imaging there is a need to further investigate their contrast property in cell-based assays to characterise the binding interaction with their molecular targets.

Apart from the use of this compound **169b** to characterise its binding with its target protein, it can be used as an imaging agent to characterise the metabolic flux to study downstream metabolites to provide better understanding of its *in vivo* effect and rule out toxic intermediates. The metabolic flux study could also provide an intermediate that could lead to a better drug or prodrug as the case with benzamide.[349-351] The synthesis of a such an imaging agent **169a-b** could lead to the characterization of not only its binding with its target but also the characterization of potential hitherto unknown off-target enzyme.[352] Besides, since our designed and synthesized hNMR agents have a high structural similarity to Iophendylate, the next logical step is to test these compounds for imaging disc herniations and spinal tumours hopefully it would not have the toxicity related to Iophendylate.

The premise on which these imaging agents were designed is on the basis that they possess antimicrobial properties, with the potential target been a DNA gyrase topoisomerase. Therefore, it would be important to fully investigate the antibacterial activity, in addition to exploring the inhibitory effects against DNA gyrase using appropriate biophysical methods/assays. These imaging agents can also be used to investigate off-targets effects of this potential drug, in addition to characterising its binding to cellular targets.

Besides, the discovery of a novel (1,5)-sigmatropic shift of phenyl acetenyl group requires further investigation. First there is a need to experimentally validate or refute the presence of the diphenylacetylide intermediate IM1 and IM1' as suggested by the DFT study.

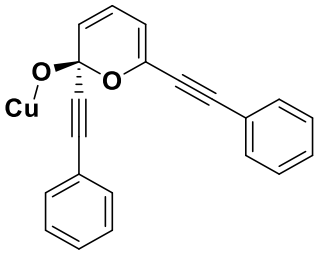

Figure 95: A DFT proposed intermediate.

Secondly, to study the effect of electron-withdrawing groups by using a benzyl-substituted derivative, *e.g.* chemical structures **174** and **175** (**Figure 96**), with a view to assessing the substituent and reaction constants (σ and ρ) respectively.

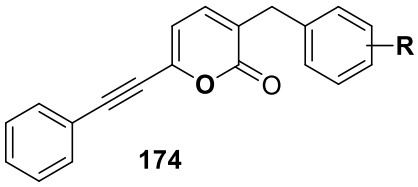

174

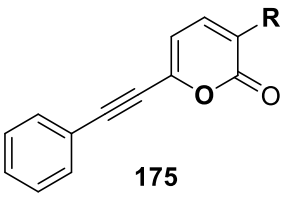

175

R = CF_3
R = CO_2R
R = X, Br or Cl
R = NO_2
R = CHO
R = OR

Figure 96: Possible structures to correlate the effect of aryl substituents on this unusual rearrangement.

When our present understanding of drug design and molecular imaging is combined a better starting point is to design an imaging agent employing a known approved drug. Ethambutol (ETH) is an antituberculosis drug that targets arabinosyl transferases via arabinogalactan (AG) and lipoarabinomannan (LAM). ETH is anti-TB used in the treatment of both drug susceptible and drug resistant *M. tuberculosis* and *M. avium*.[348] More so, ETH is water soluble and its incorporation into our already optimized (^{13}C)-hNMR contrast agent will possibly modify the aqueous solubility of this contrast agent, in addition to making it target specific. Here the design of a target specific contrast agent **177-181** is proposed for study (**Figure 96**), by incorporating the 5-methyl-6-(phenylethynyl)-2-pyrone with ethambutol (a known antiTB drug). This drug/imaging agent can then be employed to characterise its target organ,

ADMET parameters and compare it with the predicted ADMET properties as already analysed in this project as well as to characterise the metabolic products and its cellular target in live organism (mouse, rat, bacterial cell).

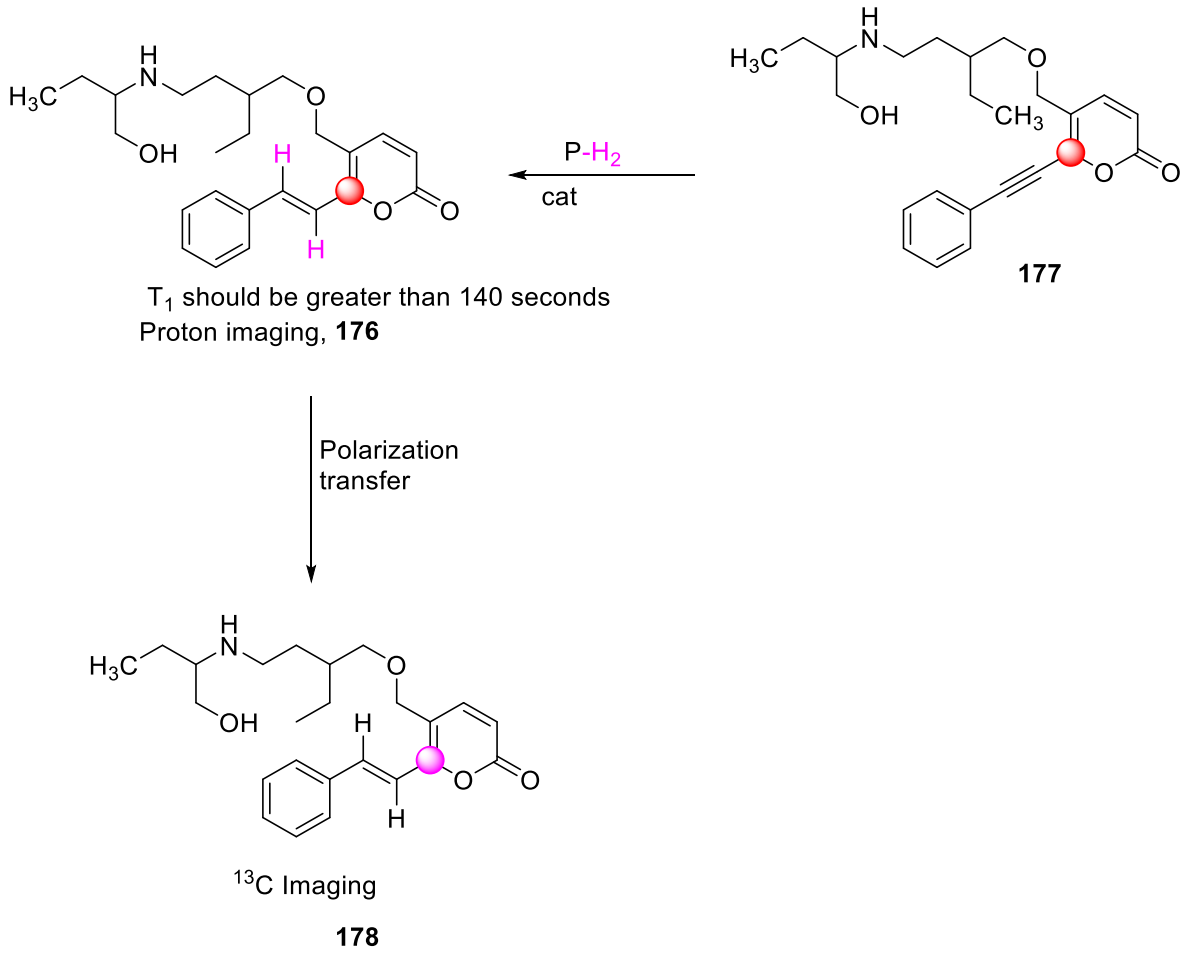

Figure 97: Anti-tuberculosis hNMR imaging agent.

Chapter Six: Experimental Section

6.1 Experimental Section

6.1.1 Predicted ADMET Parameters Procedure

The designed compounds were drawn in the Java script window of the SwissADME website. The site converts that to the sdf format and predict the absorption, distribution, metabolism, excretion and toxicity (ADMET). The results are presented in Tables 1 and 2 (Chapter Two).

6.1.2 Target Prediction procedure

The target prediction was carried out using SwissTarget where the compounds are drawn, and the software compares these compounds with those of similar compounds and then ranks the prediction on the fifteen most likely targets as shown in table 3 and 4 (Chapter Two). This free web-based tool predicts the targets of bioactive molecules based on a combination of 2D and 3D similarity with known ligand of the targets and compares the results to five different species.

6.1.3 Similarity Score Data

Determination of molecular similarity is gaining increasing relevance in drug discovery and is important in analysing large compound databases in medicinal chemistry and pharmaceutical research. When molecules are described by binary vectors with bits corresponding to the presence or absence of structural features, the Tanimoto association coefficient is the most commonly used measure of similarity or chemical distance between two compounds. Tanimoto coefficient attributes binary bit which represents the absence of ('0') or presence of ('1') of a fragment. Simply put, the Tanimoto coefficient uses the ratio of the intersecting set to the union set as the measure of similarity. Represented mathematically as:

$$T(a,b) = \frac{N_c}{N_a + N_b - N_c}$$

Where N represents the number of attributes in each object (a,b). C bits in common in the two fingerprints of a and b.

Python Implementation

```
# Inputs: two lists

# Output: the Tanimoto Coefficient

def tanimoto (list1, list2):

  intersection = [common_item for common_item in list1 if common_item in
list2]

  return float(len(c))/(len(a) + len(b) - len(c))
```

The structure of the compounds was drawn in the SwissSimilarity window and the

Software compares the sdf format of each compounds to the library of compounds it has based on electroshape similarity and scores each compound to how similar it is to the available compounds where a similarity score of >0.70 is enough to purpose your compound to the target the receptor of the known chemical structure. This web-based tool screen compounds that are drugs, bioactive and commercial molecules as well as 205 million virtual compounds that can be synthesized from commercially available reagents. The result is displayed Figures 37-38, 40 and 42 (Chapter Two).

6.1.4 Procedure for Molecular Docking and docking score

The structures of receptors were downloaded from RSCB PDB and identity of each receptor identified and saved in a folder. After Downloading the pdb format of each protein, bound water molecules were removed by editing the text of the protein. The protein structures were then optimized, and the binding site identified by the PyRx software. The ligand structure was then drawn using ChemDraw and copied as the sdf format and this was converted to the pdbqt format by OpenBabel software. All ligands were made to dock against the receptor using the PyRx software. The docking results were represented in the form of binding energies negative values (Tables 5 and 6, Chapter Two).

6.2.1 General Synthetic Details

The reagents and solvents reported here were purchased from Sigma Aldrich, Alfa Aesar or Fluorochem. TLC was carried out using Merck 5554 aluminium- backed silica plates and visualised using UV light (254 nm or 340 nm). Stains from either basic aqueous solution of potassium permangate, anisaldehyde, iodine crystals were employed to aid compound characterization. ^{1}H and ^{13}C NMR were recorded on a Jeol ECX400 or Jeol ECS400 spectrometer at 400 and 100 MHz respectively. Mass Spectrometry was recorded by electrospray (ESI) on a Bruker daltronics micrOTOF spectrometer and electron impact (EI) performed on a Waters GCT Premier mass spectrometer. The mass to charge ratio (m/z) are reported in Daltons. Infrared spectra were recorded using a PerkinElmer spectrum Two spectrometer using an UATR attachment. Melting point were determined using a Stuart SMP3 melting point apparatus using a temperature ramp of 3 ^{o}C/min. UV-Visible spectroscopy was performed on a JASCO V-560 spectrometer, using a cell with a path length of 1 cm. The wavelength of maximum absorption (λmax) is reported in nm with the extinction coefficient (Ɛ) in moldm^{-3}cm^{-1}. Elemental analysis was carried out using an Exeter Analytical CE-440 Elemental Analyser, with the percentages reported as an average of over two runs.

6.2.2 Solvents and Reagents

Commercially sourced solvents and reagents were purchased from Acros Organics, Alfa Aesar, Fisher Scientific, Fluorochem, Sigma-Aldrich or VWR and used as received unless otherwise noted. Petrol refers to the fraction of petroleum ether boiling in the range of 40-60 ^{o}C. Dry acetonitrile, THF and toluene were obtained from a PureSolv MD-7 solvent machine and stored under nitrogen. The acetonitrile and THF were also degassed by bubbling nitrogen gas through the solvent with sonication. Dry triethylamine (Et_3N) was obtained by distillation over KOH and stored under nitrogen.

6.2.3 Typical conditions

Room temperature (RT) refers to reactions where no thermostatic control was applied and recorded as 16-23 ^{o}C. Reactions requiring anhydrous or air-free

conditions were performed in dry and degassed solvent under an argon or nitrogen atmosphere using oven-dried glassware. Nitrogen gas was oxygen-free and dried immediately prior to use by passing through a column of potassium hydroxide pellets and silica.

6.3 Synthetic Procedures and Compound Data

Throughout this section, laboratory notebook references are given for the experiment from which the synthetic procedure is quoted. For experiment references for specific data, see the relevant NMR spectra in Appendix. Known compounds are prepared using literature procedures are indicated with a literature reference next to the compound name. Known compounds prepared using modified procedures are compared to literature analytical data and referenced accordingly.

6.4 Alkylation of Diethyl Malonate

6.4.1 Diethyl 2-pentylmalonate (145c)[353-355]

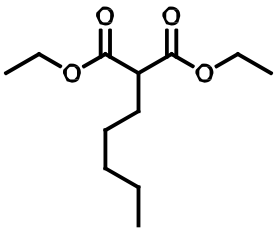

Into a round bottomed flask was added potassium carbonate (6.04 g, 43.71 mmol, 1.0 eq.), acetonitrile (30ml), diethyl malonate (7.0g, 43.70 mmol, 1.0 eq.), 1-bromopentane (8.52 g, 56.4 mmol, 1.21 eq.), and tetrabutylammonium bromide (TBAB) (10 mol%) as phase transfer agent and stirred at reflux for 5 hours. Allowed to cool and quenched with water (100 mL) and extracted with ether (2 x 100 mL). The combined ether phase was washed with I M hydrochloric acid (100 mL), decanted, dried over magnesium sulphate, filtered and concentrated in vacuo. The crude product was further distilled under reduced pressure (ca 15 mmHg) to obtain colourless oil (8.71 g, 33.53 mmol, 87 %). **IR** (ATR)/cm: 2960 (CH), 2934 (CH), 1752 (C=O), 1465 (CH_3),1369 (CH_3), 1329 (C-O).^{1}**H NMR** [400 MHz, $CDCl_3$] δ: 4.13 (q, 4H, 7 Hz, -($CO_2C\underline{H}_2CH_3)_2$), 3.23 (t, 1H, 7 Hz, -$CH_2C\underline{H}(CO_2CH_2CH_3)_2$), 1.80 (m, 2H, -$C_3H_6\underline{CH}_2CH(CO_2Et)_2$-), 1.30-1.18 (m, 12H, -$C_3\underline{H}_6$-, and -($CO_2CH_2C\underline{H}_3)_2$)

and 0.80(t, 3H,7Hz, $C\underline{H_3}(CH_2)_3CH_2$). **^{13}C NMR** (100MHz,$CDCl_3$)δ: 166.7 (C=O, $CH(\underline{C}O_2Et)_2$), 61.4 ($CO_2\underline{C}H_2CH_3)_2$), 41.6 ($-CH_2\underline{C}H(CO_2CH_2CH_3)_2$), 36.6 ($CH_2$,-$C_3H_6\underline{C}H_2CH(CO_2Et)_2$), 25.2 ($CH_2$, of C_5H_{11}), 24.9 (CH_2, of C_5H_{11}), 14.3 ($CO_2CH_2C\underline{H_3})_2$, $C\underline{H_3}C_3H_6CH_2$). **HRMS-ESI**, m/z 253.1418 (MNa^+, 100%) theoretical (253.1496); 231.1594 (MH^+, 10%), theoretical 231.1596.

6.4.2 Diethyl 2-benzylmalonate (145d)[354-357]

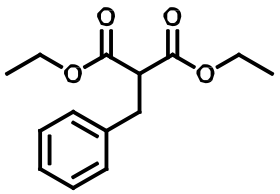

Into potassium carbonate (6.45 g, 46.88 mmol, 1.0 eq.) was added acetonitrile (30 mL), diethyl malonate (3.0 g, 20.63 mmol, 1.1 eq.) and TBAB (454.3 mg, 1.875 mmol, 10 mol %) as a phase transfer catalyst in 100 ^oC for 5 hours. The reaction mixture was left to cool; water (100 mL) was added and extracted with diethyl ether (2 x 50 mL). The combined ether phase was washed with 1Mhydrochloric acid, decanted and dried over magnesium sulphate, filtered and concentrated in vacuo. The crude product was distilled under reduced pressure (ca 15 mmHg) to give the title compound as pale-yellow oil (6.82g, 27.30 mmol, 99%). **IR** [neat]/cm:2939 (CH), 2859 (CH), 1755 (C=O), 1369-1329 [C-O]. **^{1}H NMR** (400 MHz, $CDCl_3$) δ: 7.30 (tdd, 2H, 7.7 Hz, 1.5 Hz, 1.0 Hz), 7.26-7.11(tt,3H, 7.7 Hz, 1.5 Hz, PhH),4.16(q,4H,7Hz, $CH(COOC\underline{H_2}CH_3)_2$),3.64(t,1H,8Hz, $C\underline{H}(COOCH_2CH_3)_2$),3.22(d,2H,J=8Hz, benzylic C$\underline{H2}$Ph), 1.18 (t, 7Hz, 6H, $COOCH_2C\underline{H_3}$). **^{13}C NMR** (100 MHz, $CDCl_3$) δ: 168.8 ($CH(\underline{CO}OCH_2CH_3)_2$), 137.7 (CH, PhH), 136.3 (CH, PhH), 129.4 (CH, PhH), 128.1 (CH, PhH), 126.3 (CH, PhH), 128.1 (CH, PhH), 61.3 ($COO\underline{C}H_2CH_3)_2$), 53.1 ($\underline{C}H(COOCH_2CH_3)_2$), 34.2 ($\underline{C}H_2Ph$),14.1 ($CH(COOCH_2\underline{C}H_3)_2$). **HRMS-ESI**: m/z 273.1086 (MNa^+, 100%),theoretical 273.1103; 251.1267 (MH^+, 3%) theoretical 251.1283.

6.4.3 Diethyl 2-decylmalonate (145e)[355,357]

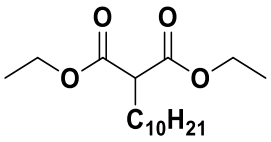

Into a round-bottomed flask was added potassium carbonate (2.16 g, 15.63 mmol, 2.5 eq.), acetonitrile (30 mL), diethyl malonate (1.0 g, 6.25 mmol, 1.0 eq.), 1-bromodecane (1.38 g, 6.25 mmol, 1.0 eq.) and TBAB (10 mol%) to and refluxed at 85 ^{o}C for 16 hours. The reaction mixture was left to cool; deionised water (100 mL) was added, extracted with ether (2 x 50 mL) and combined. The combined ether phase was washed with hydrochloric acid (100 mL), decanted, dried over magnesium sulphate and filtered. The filtrate was then concentrated in vacuo and further purified by filtering through silica gel with 35/5 petroleum ether/ethyl acetate to afford the product as a yellow oil (1.86 g, 99%). **IR (neat)/**cm^{-1}: 2939 (CH), 2859 (CH), 1755/1737 (C=O),1369-1329 [CH_3]. **^{1}H-NMR** (400MHz, $CDCl_3$) δ: 3.77(s,6H, $COOCH_2C\underline{H_3}$), 3.25 (t, 1H, 7Hz, $C\underline{H}(CO_2Et)_2$), 2.28 (m, 2H, $C\underline{H_2}(CH_2)_8CH_3$), 1.73 (m, 2H, $CH_2C\underline{H_2}(CH_2)_7CH_3$), 1.12 (m, 14H, -($C\underline{H_2}$)$_7$-), 0.74 (t, 3H, 7 Hz, $C\underline{H_3}$). **^{13}C NMR** (400 MHz, $CDCl_3$)δ: 169.9 (C=O), 61.5 (CH_3, $COOCH_2\underline{CH_3}$), 40.9 (CH, malonate) 33.5 ($\underline{CH_2}$), 31.8 ($\underline{CH_2}$), 29.1 (CH_2), 28.7 (CH_2), 27.2 (CH_2), 22.6 ($\underline{CH_2}$), 13.9 ($\underline{C}H_3$). **HRMS-EI-** m/z, 272 (MH^+-Et) theoretical (272), 227 (M-CO_2Et), 160 (M-$C_{10}H_{21}$).

6.5 Stereospecific Synthesis of Methyl 3-haloacrylate

6.5.1 Methyl (*Z*)-3-bromoacrylate (143f)[231]

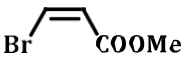

Into a round-bottomed flask was added lithium bromide (4.56 g, 55.65 mmol, 1.1 eq.), acetic acid (10 ml) and methyl propiolate (4.25 g, 50.59 mmol, 1.0 eq.) which was refluxed for 2 hours 70 ^{o}C. Left to cool to room temperature and deionised water (100 mL) was added and solid K_2CO_3 was added in small amounts until effervescence stopped. The mixture was then extracted with ether (2x 100 mL), dried over magnesium sulphate, filtered and concentrated in vacuo to give colourless oil [7.42 g, 45.20 mmol, 89 %]. **IR (Neat**)Vmax/cm^{-1}: 3080 (HC=C), 2952

(CH), 2852 (CH_3), 1731 (C=O), 1613 (C=C). **^{1}H NMR** (400MHz, $CDCl_3$) δ: 3.72 (s, 3H, COOC$\underline{H}_3$), 6.98 (1 H, d, J_{12} = 8Hz, d, $\underline{H}$C=CH), 6.62 (1 H, d, J_{12} = 8 Hz, $\underline{H}$C=CH). **^{13}C NMR** (100 MHz, $CDCl_3$) δ: 164.3 (C=O, COOMe), 124.2 (C=C, HC=$\underline{C}$H), 121.7 (C=C, H$\underline{C}$=CH), 51.7 (CH_3 of HC=CHCOOC$\underline{H}_3$). **HRMS-ESI:** m/z 186.9373 (MNa^+, 50%) theoretical 186.9371.

6.5.2 Methyl (Z)-3-iodoacrylate (143g)[231, 359]

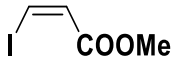

Into a round bottomed flask was added lithium iodide (5.78 g, 43.18 mmol, 1.1 eq.), acetic acid (15 mL) and methyl propiolate (3.3 g, 39.25 mmol, 1.0 eq.), and refluxed at 70 ^oC for 2 hours. The mixture was left to cool to ambient temperature and deionised water (100 mL) was added and solid K_2CO_3 was added in small amounts until effervescence stopped. The mixture was then extracted with ether (2 x 100 mL), dried over magnesium sulphate, filtered and concentrated in vacuo to afford the product as tan coloured oil (8.25g, 38.92mmol, 99%). R_f 0.53 (ethyl acetate/petroleum ether (40-60 ^oC)1:1.14, v/v). IR (Neat)Vmax/cm^{-1}: 3075, 3000 (HC=C), 2952-2852 (CH_2), 1731 (C=O), 1608 (C=C). ^{1}H NMR (400 MHz, $CDCl_3$) δ: 3.72(3 H, s, COOC$\underline{H}_3$), 7.42(1 H, d, J_{12} = 8.0 Hz, HC=C$\underline{H}$), 6.48(1 H, d, J_{12} = 8.0 Hz, $\underline{H}$C=CH). ^{13}C NMR (100 MHz, $CDCl_3$) δ: 164.8 (C=O, HC=CH$\underline{C}$OOCH_3), 129.5 (IHC=$\underline{C}$HCOOCH_3), 95.5 (H$\underline{C}$=CH), 51.7 (COO$\underline{C}H_3$). HRMS-EI m/z: 212 [M^+, 100%).

6.6 Synthesis of Ethyl Glutaconate Analogues

6.6.1 Synthesis of 3,3-Diethyl-1-methylbutene-1,3,3-tricarboxylate (148a)

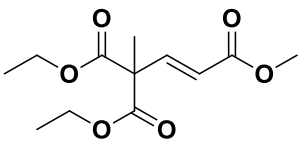

Into a round bottomed flask was added diethyl 2-methylmalonate (2.00 g, 11.48 mmol, 1.0 eq.), methyl propiolate (965.0 mg, 10.79 mmol, 1.0 eq.), potassium

carbonate (3.96 g, 28.70 mmol, 2.5 eq.), CH_3CN (40 mL) and tetrabutylammonium bromide (1.15 mmol, 10 mol%) and refluxed at 70 ^{O}C for 16 hours. The reaction mixture was left to cool; deionised water (100 mL) was added and extracted with ether (3 x 100 mL). The ether extracts were combined and washed with hydrochloric acid (150 mL), the mixture was decanted, the ether phase was dried over magnesium sulphate, filtered and then concentrated in vacuo to give the crude product. The crude product was further purified via filtering through a Buchner funnel loaded with silica gel using EtOAc/n-hexane in a ratio 5:35 to obtain colourless oil (2.50 g, 84%). **IR (ATR)/**cm^{-1}: 2984 (w, CH), 2953 (w, CH), 1724 (s, C=O), 1655 (w, C=C), 1437 (w, CH), 1377 (w, CH), 1244 (w, C-O). **^{1}H NMR** (400 MHz, $CDCl_3$) δ: 7.19 (d, 16 Hz, 1H, HC=C<u>H</u>COOCH_3, major product), 6.82(d, 12Hz, 1H,HC=C<u>H</u>COOCH_3, minor product), 6.01 (d, 12 Hz, 1H, <u>H</u>C=CHCOOCH_3, minor product), 5.82(d,16Hz,1H,<u>H</u>C=CHCOOCH_3,major product), 3.89 (s, 3H, CH_3, HC=CHCOOC<u>H_3</u>), 4.09 (q, 7 Hz, 4H, $2CH_2$, (<u>H</u>C=CHCOOCH_3), 1.11 (m, 6H, $2CH_3$, ($COOCH_2C$<u>H_3</u>$)_2$)). **^{13}C NMR** (100 MHz, $CDCl_3$) δ: 166.5 (HC=CH<u>CO</u>OCH_3), 169.2 <u>CO</u>O$CH_2CH_3)_2$)), 146.1 (HC=<u>CH</u>COOCH_3), 122.9 (<u>HC</u>=CHCOOCH_3), 61.7 (<u>C</u>H_2, COO<u>C</u>$H_2CH_3)_2$). **HRESI-MS**: m/z (relative abundance); 281.0985 (MNa^+, 100%), $C_{12}H_{18}NaO_6$.

6.6.2 Synthesis of 3,3-Diethyl-1-methylhexan-1,5-dienyl-1,3,3-tricarboxy-late (148b)

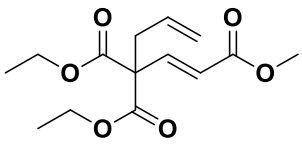

Into a round bottomed flask was added diethyl 2-methylmalonate (2.00 g, 9.95 mmol, 1.0 eq.), methyl 3-iodoacrylate (2.11 g, 9.95 mmol, 1.0 eq.), potassium carbonate (3.43 g, 24.88 mmol, 2.5 eq.), CH3CN (40mL) and tetrabutylammonium bromide (10 mol%) and refluxed at 85 ^{O}C for 16 hours. The reaction mixture was allowed to cool; water (100 mL) was added and extracted with ether (3 x 100 mL). The ether extracts were combined and washed with hydrochloric acid (150 mL), the aqueous phase was decanted, dried over magnesium sulphate, filtered and then concentrated in vacuo. The tan oil was further purified via filtering through a Buchner

funnel loaded with silica gel using EtOAc/n-hexane, in a ratio 5:35 to obtain a brown coloured oil (2.36 g, 87%). **IR(Neat**)/cm^{-1}:3087 (C=C),3063 (C=C),2983 (CH),2954 (CH), 1731 (C=O), 1646 (C=C), 1604 (C=C). **^{1}H NMR** (400 MHz, $CDCl_3$) δ: 7.25 (d, 1H, 17 Hz, HC=C<u>H</u>COOCH3, major product), 6.79(d, 1H, 13Hz,HC=C<u>H</u>COOCH3, minor product), 5.95 (d, 1H, 13 Hz, <u>H</u>C=CHCOOCH3, minor product), 5.88 (d,1H,17 Hz, <u>H</u>C=CHCOOCH3, major product), 5.77-5.54 (m, 1H, CH), 5.03 (m, 2H, =CH_2), 4.15 (q, 4H, 7 Hz, 2CH_2, (<u>H</u>C=CHCOOCH3), 3.69 (s, 3H, CH_3, HC=CHCOOC<u>H3</u>), 2.77 (d, 1H, 2 Hz) 2.58 (t, 1H, 7 Hz), 1.19 (m, 6H, 2CH_3, ($COOCH_2C\underline{H_3})_2$)). **^{13}C NMR** (100 MHz, $CDCl_3$) δ: 168.9 (HC=CH<u>CO</u>OCH3), 166.1 <u>CO</u>$OCH_2CH_3)_2$)), 143.7 (HC=<u>CH</u>COOCH3), 129.5 (<u>HC</u>=CHCOOCH3), 122.8 (=CH), 119.7 (=CH_2), 62.0 (<u>C</u>H_2, COO<u>C</u>$H_2CH_3)_2$), 51.6 ($COOCH_3$), 50.7 (C), 32.8 (CH_2), 14.0 (CH_3). **^{13}C NMR-DEPT-135º** (100 MHz, $CDCl_3$) δ: 143.7 (HC=<u>CH</u>COOCH3), 129.5 (<u>HC</u>=CHCOOCH3), 122.8 (CH=), -119.3 (=CH_2), -61.4 (COO<u>CH_2</u>CH_3), 51.4 ($COOCH_3$), -32.8 (CH2) **HRESI-MS**: m/z (relative abundance); 307.1052 (MNa, 100%), $C_{14}H_{21}NaO_6$, theoretical 307.1152.

6.6.3 (E/Z)-1-Carbomethoxy-3,3-dicarbethoxyoctene (148c)

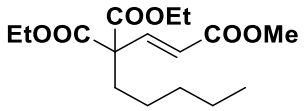

Into a round bottomed flask was added diethyl 2-pentylmalonate (7.21 g, 31.83 mmol, 1.0 eq.), potassium carbonate (4.21 g, 30.46mmol, 1.0 eq.), CH_3CN (30 ml) and tetrabutylammonium bromide (10 mol%) and stirred at 85 ^{O}C for 16 hours. The reaction mixture was left to cool to ambient temperature, deionised water (100 mL) and extracted with ether (3 x 30 mL), combined and dried over magnesium sulphate, filtered and concentrated in vacuo. The dark brown liquid was purified over silica gel using EtOAc/Petroleum ether (40-60 ^{o}C), in a ratio 5:10 to obtain a yellow oil [3.58 g, 10.92 mmol, 75%]. **IR [neat]**/cm^{-1}: 3081 (C=C), 3063 (C=C), 2955 (CH), 2846 (CH), 1731 (C=O),1645 (C=C),1437 (CH_3).**^{1}H NMR** (400 MHz,$CDCl_3$) δ ppm: 7.32 (d, 1H, J = 16 Hz, (HC=C<u>H</u>COOCH3, major product), 6.86 (d, 1H, J=16 Hz, (-HC=C<u>H</u>COOCH3, major product), 5.92 (d, 1H, 12 Hz, (-<u>H</u>C=CHCOOCH3, minor product), 5.87 (d, 1H, 16 Hz, (<u>H</u>C=CHCOOCH3, major product), 4.16 (q, 4H, 7Hz,

(2COOC$\underline{H_2}$CH$_3$)$_2$), 3.66 (s, 3H, (COOC$\underline{H_3}$), 2.18 [m, 2H, (-C(C$\underline{H_2}$ CH$_2$CH$_2$CH$_2$CH$_3$)), 1.99 (m, 2H, (-C(CH$_2$ C$\underline{H_2}$CH$_2$CH$_2$CH$_3$), 1.75-1.35 (m, 10H, (-C(CH$_2$ CH$_2$$\underline{CH_2}$$\underline{CH_2}CH_3$), 2(COOCH$_2$$\underline{CH_3}$), 0.83 (t, 3H, 7Hz, (C(CH$_2$ CH$_2$CH$_2$CH$_2$C$\underline{H_3}$). **^{13}C NMR** (100 MHz, CDCl$_3$) δ: 169.4 (COOCH$_2$CH$_3$), 166.3 (HC=CHCOOCH$_3$), 144.4 (HC=$\underline{CH}$COOCH$_3$), 122.4 (HC=$\underline{CH}$COOCH$_3$), 120.6 (HC=CHCOOCH$_3$), 124.6 (HC=CHCOOCH$_3$), 61.9 (COO$\underline{CH_2}$CH$_3$)$_2$), 59.7(COO$\underline{CH_3}$), 51.8 ($\underline{C}$(CH$_2$CH$_2$CH$_2$CH$_2$CH$_3$)), 35.3 (C($\underline{C}$H$_2$CH$_2$CH$_2$CH$_2$CH$_3$)), 23.8 (-C(CH$_2$$\underline{CH_2}CH_2CH_2CH_3$), 22.2 (-C(CH$_2CH_2$$\underline{CH_2}$$\underline{CH_2}CH_3$), 14.0 (-C(CH$_2CH_2CH_2CH_2$$\underline{CH_3}$)). **HRMS-ESI**– m/z 337.1601 (MNa$^+$, 100%), $C_{16}H_{26}NaO_6$, theoretical 337.1622, 315.1750 (MH$^+$, 18%), $C_{16}H_{27}O_6$, theoretical 315.1802.

6.6.4 (E/Z)-4-Phenyl-1-Carbomethoxy-3,3-dicarbethoxybutene (148d)

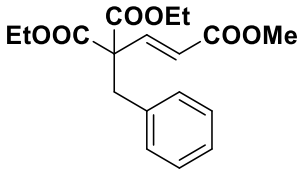

Into a round bottomed flask was added diethyl 2-benzylmalonate (7.62g, 30.46 mmol, 1.0 eq.), potassium carbonate (4.21 g, 30.46 mmol, 1.0 eq.), CH$_3$CN (30 mL), methyl 3-bromoacrylate (5.0 g, 30.48 mmol, 1 eq.), tetrabutylammonium bromide (10 mol %) and refluxed at 85 ^{O}C for16 hours. The reaction mixture was left to cool, water (30 mL) was added and extracted with diethyl ether (3 x 20 mL) and washed with hydrochloric acid (1 M). The yellow coloured oil was dried over magnesium sulphate, filtered and concentrated in vacuo. The oil was further purified by filtering through a Buchner funnel loaded with silica gel with ethyl acetate/petroleum ether as mobile phase in a ratio of 7:8 to obtain a colourless oil (9.16 g, 27.43 mmol, 90%]. **IR (Neat)/**cm^{-1}-3087 (C=C), 3063 (C=C), 2983 (CH), 2954 (CH),1731 (C=O),1646 (C=C),1604 (C=C). **^{1}H NMR** (400MHz, CDCl$_3$), 7.26-7.22 (m, 5H, (CH$_2$$\underline{Ph}$), 7.17 (d, 1H, 16 Hz, (HC=C$\underline{H}$COOCH$_3$), major product), 6.95 (d,1H, 12 Hz, (HC=C$\underline{H}$COOCH$_3$), minor product), 5.98 (d, 1H 12 Hz, ($\underline{H}$C=CHCOOCH$_3$), minor product), 5.89 (d, 1H, 16 Hz, ($\underline{H}$C=CHCOOCH$_3$), major product), 4.15 (q, 4H, 7 Hz, (COOC$\underline{H_2}$CH$_3$)$_2$), 3,74 (s, 3H, (COOC$\underline{H_3}$)), 3.38 (s, 2H, CH$_2$, benzylic, (C$\underline{H_2}$Ph), 1.20 (t, 6H,7 Hz, (COOCH$_2$C$\underline{H_3}$)$_2$). **^{13}C NMR** (400MHz, CDCl$_3$) δ: 168.9

(HC=CHCOOCH$_3$), 166.1 (COOCH$_2$CH$_3$)$_2$), 144.4 (HC=CHCOOCH$_3$), 138.9 (HC=CHCOOCH$_3$), 134.7 (HC=CHCOOCH$_3$), 129.5 ((CH$_2$Ph), 128.1 (CH$_2$Ph), 127.0 (CH$_2$Ph), 122.6 (CH$_2$Ph), 62.1 (COOCH$_2$CH$_3$)$_2$), 51.7 (COOCH$_3$), 42.0 (-C(CH$_2$Ph), 39.2((CH$_2$Ph), 13.9 (COOCH$_2$CH$_3$)$_2$). **HRMS-ESI**: m/z (relative abundance), 357.1307 (MNa, 100%), $C_{18}H_{22}NaO_6$, theoretical 357.1314, 335.1492 (MH, 3%), $C_{18}H_{23}O_6$, theoretical 335.1492.

6.6.5 (E/Z)-Dimethyl-1-methyltridec-1-ene-1,3,3-tricarboxylate (148e')

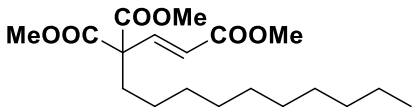

Into a round bottomed flask was added dimethyl 2-decylmalonate (3.50 g, 12.87 mmol, 1.0 eq.), methyl 3-bromoacrylate (2.00g, 12.18 mmol, 1.0 eq.), potassium carbonate (2.02 g, 14.62 mmol, 1.2 eq.), CH_3CN (30 ml) and tetrabutylammonium bromide (10 mol%) and refluxed at 85 ^{O}C for 16 hours. The reaction mixture was allowed to cool; water (20 ml) was added and extracted with ether (2 x 25ml), dried over magnesium sulphate, filtered and concentrated in vacuo. The yellow coloured oil was filtered over a Buchner funnel loaded with silica gel and eluted using; EtOAc/Petroleum ether (40-60^{O}C), in a ratio 7:8 to obtain a pale-yellow oil [2.91 g, 10.92 mmol, 69%]. **IR (Neat)/**cm-3087 (C=C), 3063 (C=C), 2983 (CH), 2954 (CH), 1731 (C=O),1646 (C=C), 1604 (C=C). **^{1}H NMR** (400 MHz, $CDCl_3$) δ: 7.28 (d, 1H, 16 Hz, (HC=CHCOOCH$_3$), major product), 6.84 (d, 1H, 12 Hz, (HC=CHCOOCH$_3$), minor product), 5.92 (d, 1H, 12 Hz, (HC=CHCOOCH$_3$), minor product), 5.83 (d, 1H, 16 Hz, (HC=CHCOOCH$_3$), major product), 3.67 (s, 9H, (COOCH$_3$)$_2$, HC=CHCOOCH$_3$), 2.38 (apt. 2H, (-C(CH$_3$(CH$_2$)$_7$CH$_2$CH$_2$), 1.54 (m, 2H, (-C(CH$_3$(CH$_2$)$_7$CH$_2$CH$_2$)), 1.29-1.12, (br, m, 14H, (-C(CH$_3$(CH$_2$)$_7$CH$_2$CH$_2$)), 0.87 (t, 3H, 7Hz, (-C(CH$_3$(CH$_2$)$_7$CH$_2$CH$_2$). **^{13}C NMR** (100MHz, $CDCl_3$) δ: 169.9 (HC=CHCOOCH$_3$), 165.3 (COOCH$_3$)$_2$), 144.1 (HC=CHCOOCH$_3$), 134.5 (HC=CHCOOCH$_3$), 131.2 (HC=CHCOOCH$_3$), 122.5 (CH=CHCOOCH$_3$), 60.1 (COOCH$_3$)$_2$), 51.7 (C(CH$_3$(CH$_2$)$_7$CH$_2$CH$_2$)), 33.9 (CH$_3$(CH$_2$)$_7$CH$_2$CH$_2$)), 29.6 (CH$_3$(CH$_2$)$_7$CH$_2$CH$_2$)), 28.2 (CH$_3$(CH$_2$)$_7$CH$_2$CH$_2$), 27.4 (CH$_3$(CH$_2$)$_7$CH$_2$CH$_2$), 22.7

($CH_3(\underline{C}H_2)_7CH_2CH_2$), 14.1 ($\underline{C}H_3(CH_2)_7CH_2CH_2$). **HRMS-ESI**: m/z (relative abundance), 379.2095 (MNa, 100%), $C_{19}H_{32}NaO_6$, theoretical 379.2097.

6.6.6 (E/Z)-Diethyl-1-methyltridec-1-ene-1,3,3-tricarboxylate (148e)

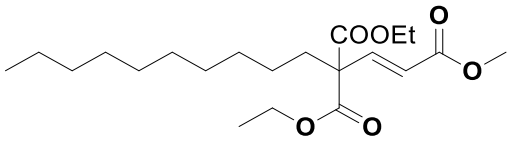

Into a round bottomed flask was added diethyl 2-decylmalonate (1.14 g, 3.70 mmol, 1.0 eq.), methyl propiolate (280.0 mg, 3.33 mmol, 1.0 eq.), potassium carbonate (1.29 g, 9.35 mmol, 2.46 eq.), CH_3CN (20 ml) and tetrabutylammonium bromide (10 mol%) and refluxed at 70 ^{O}C for 16 hours. The reaction mixture was allowed to cool, water (100 ml) was added and extracted with ether (2 x 100 mL), and the ether phase was washed with hydrochloric acid (100 mL), decanted and dried over magnesium sulphate, filtered and concentrated in vacuo. The yellow coloured oil was filtered through a Buchner funnel loaded with silica gel and eluted using; EtOAc/Petroleum ether (40-60^{O}C), in a ratio 5:35 to obtain a pale-yellow oil [1.14 g, 3.20 mmol, 96 %]. **IR (Neat)**/cm^{-1}: 3087 (C=C), 3063 (C=C), 2983 (CH), 2954 (CH), 1731 (C=O),1646 (C=C), 1604 (C=C). **^{1}H NMR** (400 MHz, $CDCl_3$) δ: 7.28 (d, 1H, 16 Hz, ($HC=C\underline{H}COOCH_3$), major product), 6.84 (d, 1H, 12 Hz, ($HC=C\underline{H}COOCH_3$), minor product), 5.92 (d, 1H, 12 Hz, ($\underline{H}C=CHCOOCH_3$), minor product), 5.83 (d, 1H, 16 Hz, ($\underline{H}C=CHCOOCH_3$), major product), 4.14 (q, 4H, $2COO\underline{CH_2}CH_3$), 3.67 (s, 3H, $CH=CHCOOC\underline{H_3}$), 2.38 (apt. 2H, ($-C(CH_3(CH_2)_7CH_2C\underline{H_2}$), 1.54 (m, 2H, ($-C(CH_3(CH_2)_7C\underline{H_2}CH_2)$), 1.29-1.12, (br, m, 14H, ($-C(CH_3(C\underline{H_2})_7CH_2CH_2)$), 0.87 (t, 3H, 7Hz, ($-C(C\underline{H_3}(CH_2)_7CH_2CH_2$). **^{13}C NMR** (100MHz, $CDCl_3$) δ: 169.9 ($HC=CH\underline{C}OOCH_3$), 165.3 ($(\underline{C}OOCH_3)_2$), 144.1 ($HC=\underline{C}HCOOCH_3$), 134.5 ($HC=\underline{CH}COOCH_3$), 131.2 ($\underline{HC}=CHCOOCH_3$), 122.5 ($\underline{CH}=CHCOOCH_3$), 60.1 ($COO\underline{C}H_2CH_3)_2$), 58.8 ($CH=CHCOO\underline{C}H_3$), 51.7 ($\underline{C}(CH_3(CH_2)_7CH_2CH_2)$), 33.9 ($CH_3(CH_2)_7CH_2\underline{C}H_2)$), 29.6 ($CH_3(CH_2)_7\underline{C}H_2CH_2)$), 28.2 ($CH_3(\underline{C}H_2)_7CH_2CH_2$), 27.4 ($CH_3(\underline{C}H_2)_7CH_2CH_2$), 22.7 ($CH_3(\underline{C}H_2)_7CH_2CH_2$), 14.1 ($\underline{C}H_3(CH_2)_7CH_2CH_2$). **HRMS-ESI**: m/z (relative abundance) $C_{19}H_{32}NaO_6$, 379.2095 (MNa-Et, 100%), theoretical 378.2018.

6.7 Sodium Alkyl Glutaconate Salt

6.7.1 Sodium 1,5-Diethoxy-2,4-bis[ethoxycarbonyl]-1,5-dioxopent-3-en-2-ide (155i)[211, 213]

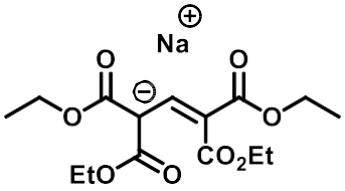

Into an oven-dried Schlenk tube was added sodium hydride (4.50 g, 187.3 mmol, 3.0 eq.) was attached to a vacuum line and evacuated thrice and the NaH was washed with pentane (2x 20ml). Diethylmalonate(10.0g, 62.43mmol, 2.0 eq.), chloroform (3.73 g,31.21 mmol,1.0 eq.), and ethanol (80 mL) was added and refluxed for 1 hour and filtered while hot to obtain a red solution that was concentrated in vacuum and recrystallized from ethanol to obtain bright yellow powder [6.50 g, 18.45 mmol, 59%], the yield is based on chloroform. Melting point 269-270^{o}C**.** **^{1}H NMR** (400 MHz DMSO-d_6) δ: 7.98 (s, 1H, ($(COOCH_2CH_3)_2CNaCH=C(COOCH_2CH_3)_2$), 3.91 (q, 8H, 7Hz, ($(COOCH_2CH_3)_2CNaCH=C(COOCH_2CH_3)_2$), $4CH_2$), 1.08 (t,12H,7Hz, $4CH_3$ ($(COOCH_2CH_3)_2CNaCH=C(COOCH_2CH_3)_2$)).**^{13}C NMR** (DMSO-$d_6$,100MHz)δ:170.2 (d,-CH=C($COOCH_2CH_3)_2$), 168.4 ($COOCH_2CH_3)_2$), 146.1 (-CNaCH=C($COOCH_2CH_3)_2$), 94.3 (-CNaCH=C($COOCH_2CH_3)_2$), 60.0 (d, ($COOCH_2CH_3)_2$),14.6(d,(($COOCH_2CH_3)_2$). **HRMS-ESI**- m/z (relative abundance): 353.1206 (MH, 100%), $C_{15}H_{22}NaO_8$, theoretical 353.1207.

6.7.2 Sodium 1,1,3,3-tetracarbomethoxypropene-1,1,3,3-tricarboxylate (155j)

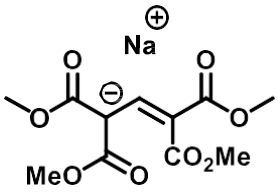

In an oven dried Schlenk tube was added sodium hydride (4.50g, 187.29 mmol, 3.0 eq.) and attached to a vacuum line and evacuated thrice with nitrogen. Then

washed with pentane (2 x 20 mL), and diethyl malonate (10.0g, 62.43 mmol, 2.0 eq.), chloroform (3.73 g, 31.21mmol, 1.0 eq.) and methanol (30 ml) were added via syringe and the mixture was refluxed for 1 hour. The mixture was filtered while still hot to remove sodium chloride a by-product of the reaction. The reddish solution was concentrated in vacuum and recrystallized from ethanol to obtain bright yellow powder (6.50 g, 18.45 mmol, 59%), the yield is based on chloroform. Melting point: 250-252 ^{o}C. **^{1}H NMR** (400 MHz, DMSO-d_6) δ: 7.98(s,1H, $(COOCH_3)_2C(Na)C\underline{H}=C(CO_2CH_3)_2$), 3.91(s, 12H, 7Hz, $(COOC\underline{H_3})_2C(Na)CH=C(CO_2C\underline{H_3})_2$). **^{13}C NMR** (100 MHz, DMSO-d_6,) δ: 170.2 $(\underline{C}OOCH_3)_2C(Na)CH=C(CO_2CH_3)_2$), 168.4 $(\underline{C}OOCH_3)_2$,) 147.1 (-$\underline{C}H=\underline{C}(CO_2CH_3)_2$), 94.3 (-$\underline{C}$(Na)CH=C$(CO_2CH_3)_2$), 60.0 (COO$\underline{C}H_3$), 58.2 ($(COO\underline{C}H_3)_2C(Na)CH=C(CO_2C\underline{H_3})_2$). **HRMS-ESI**- 297.0583 (MH, 100%), $C_{11}H_{14}NaO_8$, theoretical 297.0581.

6.7.3 4-phenylbut-1-ene-1,1,3,3-tetracarbethoxybutene (156)[211-213]

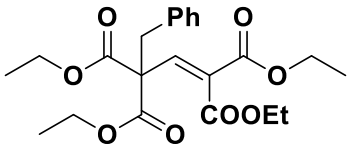

Into a round bottomed flask was added 1,1,3,3-tetracarbethoxypropene (3.0 g, 8.52 mmol, 1.0 eq.), benzyl chloride(1.40 g,11.05 mmol,1.3 eq.) and ethanol (20 mL) and refluxed at 83 ^{o}C for 48 hours to obtain whitish suspension which was concentrated on vacuo to remove ethanol and recrystallized from ethanol to give colourless solid(2.15g, 5.12 mmol, 60 %). Melting point: 78 ^{o}C (Literature, [191-193] 78 ^{o}C). **^{1}H NMR** (400 MHz, DMSO-d_6) δ: 7.39 (d, 1H,^{4}J = 2Hz, olefinic proton, *H*-2), 7.21-7.08 (m, 5H, $\underline{PhH}$), 4.21(m,8H, $(COOC\underline{H_2}CH_3)_2C(PhCH_2)CH=C(COOC\underline{H_2}CH_3)_2$), 3.52(d,2H,2Hz, CH_2, $((COOEt)_2C(PhC\underline{H_2})CH=C(COOEt)_2)$,), 1.27 (m,12H, $4CH_3(2(COOCH_2C\underline{H_3})_2)$,). **^{13}C NMR** (100 MHz, DMSO-d_6), 168.2 $(\underline{CO_2}Et)_2$), 164.6 $((\underline{CO_2}Et)_2)$, 163.5 $(CH=\underline{C}(CO_2Et)_2)$,143.1 $(\underline{C}H=C(CO_2Et)_2)$, 134.9 $((\underline{Ph}CH_2))$, 130.0 $(\underline{Ph}CH_2)$, 128.3 $(\underline{Ph}CH_2)$, 127.3 $(\underline{Ph}CH_2)$, 62.2 $(COO\underline{C}H_2CH_3)_2$), 61.7 $(COOEt)_2\underline{C}(PhCH_2)$), 41.4 $(Ph\underline{C}H_2)$, 13.9 $(COOCH_2\underline{C}H_3)_2$). **HRMS-ESI**: (MNa,

100%), $C_{22}H_{28}NaO_8$, theoretical 443.1676. 421.1867 (MH, 3%), $C_{22}H_{29}O_8$, theoretical 421.1857.

6.8 Synthesis of Substituted Glutaconic acid

6.8.1 2-Methylglutaconic acid (141a)[238]

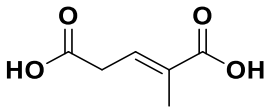

Into a round bottomed flask was added 3,3-diethyl-1-methylbutene-1,3,3-tricarboxylate (2.50 g, 9.69 mmol, 1.0 eq.) in ethanol (20 mL), aqueous potassium hydroxide (50%) and refluxed at 110 ^oC for four hours while monitoring the reaction progress by TLC. The reaction mixture was allowed to cool to room temperature and deionised water (100 mL) was added then extracted with ethyl acetate (2 x 100 mL) to remove all non-acidic organic components. The aqueous phase was acidified to pH 1 with 1 M hydrochloric acid (100 mL) and re-extracted with ethyl acetate (2 x 100 mL), dried over $MgSO_4$, filtered and concentrated in vacuo to obtain an oily solid (1.28 g, 8.86 mmol, 91%). **IR (ATR)/cm^{-1}**3100-2888, 1703, 1665, 1643, 1432, 1397, 1371, 1301, 1273, 1217, 1141, 1094, 1048. **^{1}H NMR** (400 MHz, CD_3OD) δ: 6.93 (tq, 7 Hz, 1 Hz, 1H), 3.26 (dq, 7 Hz, 1 Hz, 1H), 1.97 (s, 3H, CH_3). **^{13}C NMR** (100 MHz, CD_3OD) δ: 174.0 ($HO\underline{OC}CH_2CH=CH(CH_3)$), 169.7 ($HOOCCH_2CH=CH(CH_3)\underline{CO}OH$), 147.3 ($HOOCCH_2CH=\underline{CH}(CH_3)$), 133.9 ($HOOCCH_2\underline{CH}=CH(CH_3)COOH$), 130.1 ($HOOCCH_2\underline{C}H=CH(CH_3)$), 121.9 ($HOOCCH_2\underline{C}H=CH(CH_3)COOH$), 33.3 ($HOOC\underline{C}H_2CH=CH$), 19.4 ($HOOCCH_2CH=CH(\underline{C}H_3)COOH$). **^{13}C NMR DEPT-135^o:** (100 MHz, CD_3OD) δ: 147.3 ($HOOCCH_2CH=\underline{C}H(CH_3)$), 134.0 ($HOOCCH_2CH=\underline{C}H(CH_3)COOH$), 121.9 ($HOOCCH_2\underline{C}H=CH(CH_3)$), -33.3 ($HOOC\underline{C}H_2CH=CH(CH_3)$), 19.4 ($HOOCCH2CH=CH(\underline{C}H_3)$). **HRMS-ESI**: m/z (relative abundance); 167.0136 (MNa^+, 100%), $C_6H_8NaO_4$, theoretical 167.0320.

6.8.2 2-(2'-Propenyl) glutaconic acid (141b)

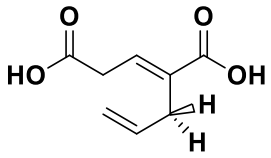

Into a round bottomed flask was added 1-carbomethoxy-3,3-dicarbethoxypentene (2.20 g,8.03 mmol, 1.0 eq.) in ethanol (20 mL), aqueous potassium hydroxide (50%) and refluxed at 110 ^{o}C for four hours while monitoring the reaction progress by TLC. The reaction mixture was allowed to cool to room temperature and deionised water (100 mL) was added then extracted with ethyl acetate (2 x 100 mL) to remove all non-acidic organic components. The aqueous phase was acidified to pH1 with 1 M hydrochloric acid (100 mL) and re-extracted with ethyl acetate (2 x 100 mL), dried with $MgSO_4$, filtered and concentrated in vacuo to obtain an oily solid (1.35 g, 99%). **ATIR (neat)/**cm^{-1} 3100-2876, 2628, 1713, 1676, 1638, 1428, 1381, 1309, 1269, 1206, 1122, 1060. **^{1}H NMR** (400 MHz, $(CD_3)_2CO$) δ: 7.05 (t, 1H, 7 Hz), 5.80 (dddd, 1H, 17 Hz, 12 Hz, 6 Hz, 2 Hz, CH=CH2), 5.02 (dd, 1H, 17 Hz, 2 Hz, CH=CH_2), 4.94 (dd, 12 Hz, 2 Hz, CH=CH_2), 3.29 (d, 2H, 7 Hz, 2 Hz, CH_2), 3.08 (d, 1H, 6 Hz, CH_2). **^{13}C NMR** (100 MHz, $(CD_3)_2CO$) δ: 171.7, 168.2, 136.3, 135.9, 132.7, 115.5, 33.8, and 31.4. **HRMS-ESI**: m/z (relative abundance): 193.0435 (MNa, 100%), $C_8H_{10}NaO_4$, theoretical 193.0477, 171.0652 (MH, 15%), $C_8H_{11}O_4$, theoretical 171.0657.

6.8.3 2-Pentylglutaconic acid (141c)

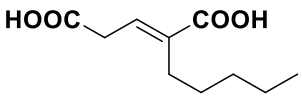

Into a round bottomed flask was added 1-carbomethoxy-3,3-dicarbethoxyoctene (2.75 g, 8.75 mmol, 1.0 eq.), KOH (5g, 89.29 mmol 10.20 eq.) in 10ml of water and ethanol (20 ml) and refluxed for 8 hours then acidified with hydrochloric acid until a pH of 1 then refluxed for a further 1 hour to obtain a dark oil. Quenched with water and extracted with diethyl ether (2 x20 ml), dried over $MgSO_4$, filtered and concentrated to obtain dark oil. A Buchner flask was loaded with silica gel and the dark oil was added and eluted using ethyl acetate-petroleum ether (40-60 ^{o}C), 6/9

oily solid [1.75 g, 8.49mmol, 97%]. **ATIR/neat**/cm^{-1}: 3100-2917 {br, OH}, 2616 (CH), 1683 [C=O], 1638 (C=C), 1409 (CH bending), 1354, 1316 [C-O bending]. **^{1}H NMR** (400MHz, CD_3OD) δ: 7.45 (t, 17 Hz, 1H, C<u>H</u>=C), 6.91(d, 17Hz, 1H, CH=C<u>H</u>, minor product), 2.38 (m, 2H, C<u>H_2</u>(C_4H_9)), 1.83 (m,2H, CH_2 C<u>H_2</u>(C_3H_7)), 1.26 (m, 4H, $(CH_2)_2C\underline{H_2}C\underline{H_2}CH_3$), 0.85 (t, 3H, $(CH_2)_2CH_2CH_2C\underline{H_3}$). **^{13}C NMR** (100MHz, CD_3OD) δ: 172 (COOH), 160.6 (<u>CO</u>OH), 134.9 ($COOHCH_2CH=\underline{C}(C_5H_{11})COOH$), 132.2 ($COOHCH_2\underline{C}H=C(C_5H_{11})COOH$), 51.8 ($(COOH\underline{C}H(C_5H_{11})CH=CCOOH$), 32.0 ($\underline{C}H_2(C_4H_9)$), 29.4 ($CH_2$ $\underline{C}H_2(C_3H_7)$), 27.4 ($(CH_2)_2\underline{C}H_2\underline{C}H_2CH_3$)), 22.9 ($(CH_2)_2\underline{C}H_2\underline{C}H_2CH_3$)), 13.9 ($(CH_2)_2CH_2CH_2\underline{C}H_3$)). **HRMS-ESI**- m/z (relative abundance): 223.0941 (MNa, 100%), $C_{10}H_{16}NaO_4$, theoretical 223.0946, 195.0711(MNa^+-Et, 22%).

6.8.4. 2-Benzylglutaconicacid (141d)[214-215, 211]

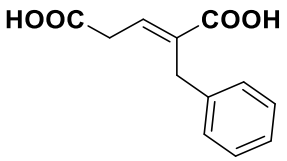

Into a round bottomed flask was added 4-phenyl-1-carbomethoxy-3,3-dicarbethoxybutene (2.75 g, 8.75mmol, 1.0 mmol), KOH (5 g, 89.29 mmol 10.20 eq.) in 10 ml of water and ethanol (20 ml) and refluxed for 4 hours then acidified with hydrochloric acid until a pH of 1 then refluxed for a further 1 hour to obtain a dark oil. Quenched with water and extracted with diethyl ether (2 x 30 ml), dried over magnesium sulphate, filtered and concentrated to obtain dark oil. A Buchner flask was loaded with silica gel and the dark oil was added and eluted using ethyl acetate-petroleum ether (40-60 ^{o}C), 6/9 (1.75g, 8.49 mmol, 97 %). Melting point-142-144 ^{o}C (Literature melting point 139 ^{o}C, 151-153 ^{o}C[192-193]). **IR (neat)** cm^{-1}: 3391.07-2500 {br, OH}, 1716.75 [C=O], 1375.33 [C-O]. **^{1}H NMR** (400 MHz, CD_3OD) δ: 7.35-7.24 (m, 5H, PhH). 7.03 (t, 1H, 7Hz, *H*-3), 3.65 (s, 2H, $PhCH_2$), 3.53 (d, 2H, 7Hz, <u>CH_2</u>COOH). **^{13}C NMR** (100 MHz, CD_3OD) δ: 171.1 ($CH_2C=C(CH_2Ph)\underline{C}OOH$), 167.7 ($HOO\underline{C}CH_2C=C(CH_2Ph)$, 139.5 ($CH_2\underline{C}=C(CH_2Ph)COOH$)), 135.7 ($CH_2\underline{C}=C(CH_2Ph)COOH$), 133.3 ($CH_2C=C(CH_2\underline{Ph})$), 130.2 ($CH_2C=C(CH_2\underline{Ph})$), 128.4 ($CH_2C=C(CH_2\underline{Ph})$), 126.0 ($CH_2C=C(CH_2\underline{Ph})$), 33.4 ($HOOC\underline{C}H_2C=C(CH_2Ph)$,

32.1 (CH_2, ($CH_2C=C(\underline{C}H_2Ph)$). **HRMS-ESI**- 243.0619 (MNa, 100%), $C_{12}H_{12}NaO_4$, theoretical 243.0623.

6.8.5 2-Decylglutaconicacid (141e)

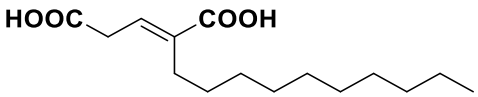

Into a round bottomed flask was added 3,3-dimethyl-1-methyltridec-1-ene-1,3,3-tricarboxylate (1.92 g, 5.01 mmol, 1.0 eq.) in ethanol (20 mL), aqueous potassium hydroxide (50%) and refluxed for 100 ^oC for four hours while monitoring by TLC. The reaction mixture was kept cooling to ambient temperature and deionised water (50 mL) was added and subsequently extracted first with ethyl acetate (2x 30 mL) to remove all non-acidic organic impurities. The aqueous phase which contains the desired compound as the sodium salt was acidified to pH1 with 1M hydrochloric acid (50 mL) and re-extracted with ethyl acetate (2x 50 mL), dried with MgSO4, filtered and concentrated in vacuo to obtain off-white solid (947.7 mg,3.51mmol,70%). Melting point: 80-82 ^oC. **IR (ATR)/**cm^1: 3100-2859, 1680, 1606, 1405, 1268, 1207, 1106. **^{1}H NMR** (400 MHz, CD_3OD, δ): 6.89 (apt. 14Hz,1H, $CH_2C\underline{H}=C(CH_2CH_2(CH_2)_7CH_3)$, major product), 5.85 (d, 1H,14Hz, $CH(CH_2CH_2(CH_2)_7CH_3)CH=C\underline{H}$, trace product), 3.22(m,2H, $C\underline{H_2}CH=C(CH_2CH_2(CH_2)_7CH_3)$), 2.28 (m,2H, $CH_2CH=C(C\underline{H_2}CH_2(CH_2)_7CH_3)$, 1.80 (m, 2H, $CH_2CH=C(CH_2C\underline{H_2}(CH_2)_7CH_3)$, 1.26(m, 14H, $CH_2CH=C(CH_2CH_2(C\underline{H_2})_7CH_3)$, 0.88 (t, 3H, 7Hz, $CH_2CH=C(CH_2CH_2(CH_2)_7C\underline{H_3})$. **^{13}C NMR** (100MHz, CD_3OD) δ: 169.5(C=O), 161.7 (C=O), 144.4 (C=C), 129.2 (C=C), 45.5 (CH_2), 33.6 (CH_2), 32.5 (CH_2),30.2 (CH_2), 29.5 (C=O), 28.8 (CH_2), 27.5 (CH_2), 25.3 (CH_2), 22.5 (CH_2), 14.2 (CH_3). **HRMS-ESI**: m/z (relative abundance), 293.1726 (MNa, 21%, $C_{15}H_{26}NaO_4$), theoretical 293.1729. UV(EtOH) (λmax, ε) 284nm, 246 $Lmol^{-1}cm^{-1}$. Elemental Calculated for $C_{15}H_{26}O_4.CH_3OH$, C 63.550, H 10.000; Found C 64.008, H9.471.

6.9 Synthesis of 3-Alkyl-6-chloro-2-pyrone

6.9.1 6-Chloro-2-pyrone (128')[211]

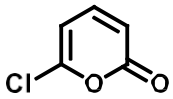

To a thick-walled flask was added glutaconic acid (739 g, 2.74 mmol, 1.0 eq.), phosphorus trichloride (10 mL) at 0 ^{o}C then heated to 100 ^{O}C for 15 minutes in a sealed tube. The reaction mixture was left to cool, tried using cold finger since the compound sublimes on heating but failed. **^{1}H NMR** (400 MHz, $CDCl_3$) δ ppm: 7.30 (dd, 1H, 9Hz, 8Hz), 6.22 (dd, 1H, 8Hz,1H), 6.33 (dd,1H,9Hz,1Hz).**^{13}C NMR**(100.6 MHz) δ ppm: 160.5 (C-2 of 2-pyrone), 150.3 (C-6 of 2-pyrone), 144.1 (C-4 of 2-pyrone), 113.0 (C-3 of 2-pyrone), 104.0 (C-5 of 2-pyrone). **HRMS-ESI**, (M-Cl),95.

6.9.2 6-Chloro-3-methyl-2-pyrone (128a/129a)[238]

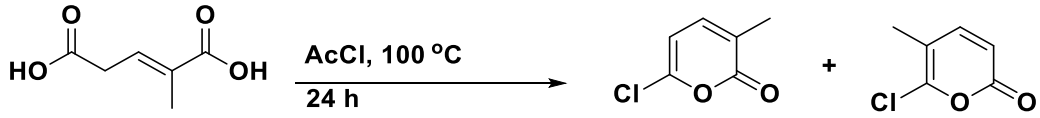

In a thick-walled tube was added 3-methylglutaconicacid (1.20 g, 8.34 mmol, 1 equiv.) and acetyl chloride (15 mL) was heated at 100 ^{o} C for two days. Allowed to cool, then evaporated to remove the excess acetyl chloride, added ether and washed with saturated sodium bicarbonate until alkaline to litmus, decanted and concentrated the ether phase to obtain the product as a mixture of the 6-chloro-3-methyl-2-pyrone (**128a**) and 6-chloro-5-methyl-2-pyrone (**129a**) as a brown powder (738.3 mg, 62%).

Characterization for 129a

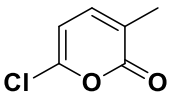

Melting Point: 37-39 ^{o}C. **ATIR (neat)/**cm: 3115, 2955, 2926, 1714, 1635, 1538, 1438, 1376, 1328, 1280, 1224, 1085.**^{1}H NMR** (400MHz, $CDCl_3$) δ: 7.09 (dq, 7 Hz, 1 Hz, 1H), 6.11 (d, 7 Hz, 1H), 2.08 (s, 3H, CH_3). **^{13}C NMR** (100 MHz, $CDCl_3$) δ:

162.2 (C-2 of 2-pyrone), 147.9 (C-6 of 2-pyrone), 140.2 (C-4 of 2-pyrone), 123.2 (C-3 of 2-pyrone), 104.3 (C-5 of pyrone), 16.4 (CH_3).

Characterization for mixture of 129a

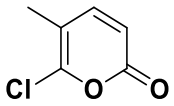

^{1}H NMR (400 MHz, $CDCl_3$) δ: 7.24 (d, 10 Hz, 1H), 6.21 (d, 10 Hz, 1H, minor product, 33f), 2.08 (s, 3H, CH_3).**^{13}C NMR** (100 MHz, $CDCl_3$) δ: 162.2 (C-2 of 2-pyrone), 147.7 (C-6 of 2pyrone), 140.2 (C-4 of 2-pyrone), 113.4 (C-3 of 2-pyrone), 16.8 (CH_3). **ATIR (neat)/**cm: 3005, 2953, 2852, 1698, 1632, 1553, 1465, 1414, 1377, 1334, 1260, 1191, 1083.

6.9.3 6-Chloro-3-(2'-propenyl)-2-pyrone (128b/129b)

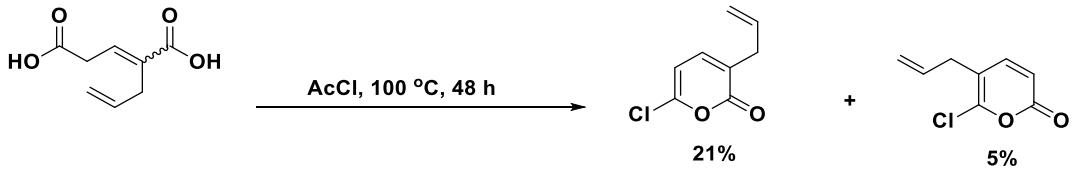

Into a thick-walled tube was added 3-methyl glutaconic acid (1.30 g, 7.65 mmol, 1 eq.) and acetyl chloride (30 mL) and heated at 100 ^{o} C for two days. Allowed to cool, then evaporated to remove excess acetyl chloride, added ether and added saturated sodium bicarbonate until alkaline to litmus, decanted, dried over magnesium sulphate, filtered and concentrated the ether phase to obtain tan oil. Purified using flash CC over silica gel wet loaded as 10% water (w/w) with 5% ether/n-hexane to obtain two products 6-chloro-3-propylidene-2-pyrone (**128b**) as a pale-yellow oil (268.0 mg, 21%) and 6-chloro-5-methyl-2-pyrone (**129b**) as orange oil (66.10 mg, 5%).

Characterization for 128b

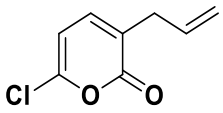

IR (Neat)/cm:3038, 2956, 2928, 1730, 1633, 1548, 1415, 1336, 1200, 1070. **^{1}H NMR** (400 MHz, $CDCl_3$) δ: 7.08 (dt, 7 Hz, 1 Hz, 1H), 6.16 (d, 7 Hz, 1H), 5.84 (m, 1H), 5.17 (br, s, 1H), 5.14 (d, 6 Hz, 1H), 3.16 (d, 7 Hz, 2H, CH_2). **^{13}C NMR** (100 MHz, $CDCl_3$) δ: 161.5 (C-2 of 2-pyrone), 147.3 (C-6 of 2-pyrone), 140.0 (C-4 of 2-pyrone), 133.4 (C-3 of 2-pyrone), 125.4 (HC=$\underline{CH_2}$), 118.4 ($\underline{HC}$=CH_2), 104.4 (C-5 of 2-pyrone), 34.1 (CH_2).

Characterization for 129b

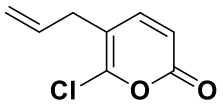

IR (Neat)/cm^{-1}:3080, 3038, 2980, 2909, 1698, 1650,1553, 1458, 1415, 1281, 1200. **^{1}H NMR** (400 MHz, $CDCl_3$) δ: 7.24 (d, 9 Hz, 1H), 6.21 (d, 9 Hz, 1H), 5.82-5.71 (m, 1H), 5.15-5.05 (m, 2H, =CH_2), 3.16 (s, 3H, CH_3). **^{13}C NMR** (100 MHz, $CDCl_3$) δ: 160.6 (C-2 of 2-pyrone), 147.0 (C-6 of 2-pyrone), 136.5 (C-4 of 2-pyrone), 133.2 (C-3 of 2-pyrone), 117.9 (HC=$\underline{CH_2}$), 115.8 ($\underline{HC}$=CH_2), 113.7 (C-5 of 2-pyrone), 34.0 (CH_2).

6.9.4 6-Chloro-3-n-pentyl-2-pyrone (128c/129c)

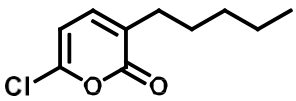

Into a thick-walled glass tube was added 4-pentylglutaconic acid (3.35 g, 16.73 mmol, 1 eq.) and acetyl chloride (15 mL) and refluxed at 100 ^{o}C for 72 hours. Allowed to cool to ambient temperature and concentrated in vacuo. To the dark coloured oil was added ether and the lower aqueous phase was made alkaline to litmus paper on addition of saturated sodium bicarbonate (50 mL) and decanted, dried over magnesium sulphate, filtered and concentrated in vacuo. Purification of the crude by flash column chromatography (CC) gave the titled product as orange

oil (770.3 mg, 3.84 mmol, 22%). The silica gel for the CC was wet loaded as 10% water (w/w) and eluted with 5% ether/n-hexane. R_f: 0.41(5% diethyl ether/n-hexane). This compound fluorescence under ultraviolet light at long wavelength.

Characterization for 128c

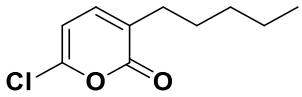

IR (Neat)/cm: 2955, 2927, 2858, 1732, 1634, 1552, 1466, 1378, 1336, 1194, 1115. **^{1}H NMR** (400 MHz, $CDCl_3$) δ: 7.03 (dt, 1H, 7 Hz, 1 Hz, Pyrone H4), 6.14 (d, 1H, 7 Hz, Pyrone H5), 2.40 (m, 2H, $CH_2CH_2CH_2CH_2CH_3$), 1.21 (m, 6H, $CH_2CH_2CH_2CH_2CH_3$) and 0.81 (t, 3H,7 Hz, $CH_2CH_2CH_2CH_2CH_3$). **^{13}C NMR** (100 MHz, $CDCl_3$) δ: 161.8 (C=O, C-2, pyrone), 146.7 (C-6 of 2-pyrone), 139.4 (C-3 of 2-pyrone), 127.3 (C-4 of 2-pyrone), 104.2 (C-5 of 2-pyrone), 31.4 ($CH_2CH_2CH_2CH_2CH_3$), 30.3 ($CH_2CH_2CH_2CH_2CH_3$), 27.5 ($CH_2CH_2CH_2CH_2CH_3$),22.4 ($CH_2CH_2CH_2CH_2CH_3$),14.0 ($CH_2CH_2CH_2CH_2CH_3$). **HRMS-EI**: m/z (relative abundance) 201.0604 (MH^+, 100%), $C_{10}H_{13}ClO_2$, theoretical 201.0682, 202.0577 (M+2, 35%) theoretical 202.0575. UV (λmax) 302 nm, (ε 5400 $Lmol^{-1}cm^{-1}$) in PhH. Elemental Anal. Calc. for $C_{10}H_{13}ClO_2$, Found C 62.670, H7.856.

Characterization for 129c

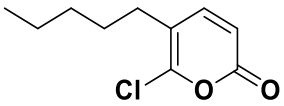

IR (Neat)/cm: 2956, 2927, 2858, 1698, 1633, 1608, 1552, 1457, 1417, 1379, 1336, 1168, 1116, 1068. **^{1}H NMR** (400 MHz, $CDCl_3$) δ: 7.03 (dt, 1H, 7 Hz, 1 Hz, Pyrone H4), 6.14 (d, 1H, 7 Hz, Pyrone H5), 2.40 (m, 2H, $CH_2CH_2CH_2CH_2CH_3$), 1.21 (m, 6H, $CH_2CH_2CH_2CH_2CH_3$) and 0.81 (t, 3H,7 Hz, $CH_2CH_2CH_2CH_2CH_3$). **^{13}C NMR** (100 MHz, $CDCl_3$) δ: 161.8 (C=O, C-2, pyrone), 146.7 (C-6 of 2-pyrone), 139.4 (C-3 of 2-pyrone), 127.3 (C-4 of 2-pyrone),104.2 (C-5 of 2-pyrone), 31.4 ($CH_2CH_2CH_2CH_2CH_3$), 30.3 ($CH_2CH_2CH_2CH_2CH_3$), 27.5 ($CH_2CH_2CH_2CH_2CH_3$), 22.4 ($CH_2CH_2CH_2CH_2CH_3$),14.0 ($CH_2CH_2CH_2CH_2CH_3$). **HRMS-EI**: 200.0604 (MH,

100%), $C_{10}H_{13}ClO_2$, 202.0577 (M+2, 35) theoretical 202.0575. UV (λmax) 302 nm, (ε 5400 $Lmol^{-1}cm^{-1}$) in PhH. Elemental Anal. Calc. for $C_{10}H_{13}ClO_2$, Found C 62.670, H7.856.

6.9.5 3-Benzyl-6-chloro-2-pyrone (128d/129d)[212-215]

Into a thick-walled flask was added 4-benzylpent-2-enedioic acid (1.26 g, 5.72 mmol, 1.0 eq.) was added acetyl chloride (30 ml) and refluxed at 100 ^{O}C for 2 days in a sealed tube. Allowed to cool to ambient temperature and concentrated in vacuo. To the dark coloured oil was added ether and the aqueous phase was made alkaline to litmus paper on addition of saturated sodium bicarbonate (50 mL) and decanted, dried over magnesium sulphate, filtered and concentrated in vacuo. Purification of the crude by flash column chromatography (CC) gave the titled product as a white powder (348.1mg,28%) and a pale-yellow powder (53.7 mg, 4%) of the 5-benzyl-6-chloro-2-pyrone with melting point 50-51 ^{o}C (literature 50-51 ^{o}C,[193]).The silica gel for the CC was wet loaded as 10% water (w/w) and eluted with 5% ether/n-hexane. This compound fluorescence under ultraviolet light at long wavelength.

Characterization data for 128d

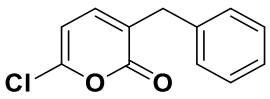

Rf 0.45 in EtOAc/Petroleum ether 7/8. Melting Point- 71-72^{o}C (literature 71-72 ^{o}C). **IR (ATR)**/cm^{-1}: 3084, 3061, 2982, 2952, 1730,1637, 1602, 1546, 1494, 1453, 1431, 1169, 1075, 992, 809. **^{1}H NMR** (400 MHz, $CDCl_3$) δ: 7.40- 7.25 (m, 5H, PhH), 6.87 (dt, 1H, 7.0 Hz, 1.0 Hz, H-4 of pyrone), 6.11 (d, 1H, 7.0 Hz, H-5 of pyrone), 3.73 (s, 2H). **^{13}C NMR** (100 MHz, $CDCl_3$) δ: 161.6 (C-2 of 2-pyrone), 147.3 (C-6 of 2-pyrone), 140.2 (C-4 of 2-pyrone), 137.3 (C-3 of 2-pyrone), 130.2 (Ph),129.3 (Ph),128.6

(Ph),128.8 (Ph),127.0 (Ph),126.8(Ph),104.3(C-5 of 2-pyrone),36.1(PhCH$_2$ of benzylic group). **HRMS-ESI**: 243.0179 (MNa, 100%), $C_{12}H_9ClNaO_2$, theoretical 243.0189.

Characterization data for 129d

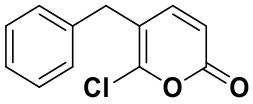

Rf [0.45 in EtOAc/Petroleum ether 7/8]. Melting Point- 50-51 ^oC (literature 50-51 ^oC). **IR (ATR)/**cm^{-1}: 3027,2934, 2918, 1698 (very intense),1602, 1583, 1550, 1494, 1454, 1438, 1420,1327, 1272, 1246, 1193, 1079, 1029, 930. **^{1}H NMR** (400 MHz, $CDCl_3$) δ: 7.40- 7.25 (m, 5H, PhH), 6.87 (dt, 1H, 7.0 Hz, 1.0 Hz, H-4 of pyrone), 6.11 (d, 1H, 7.0 Hz, H-5 of pyrone), 3.73 (s, 2H). **^{13}C NMR** (100 MHz, $CDCl_3$) δ: 161.6 (C-2 of 2-pyrone), 147.3 (C-6 of 2-pyrone), 140.2 (C-4 of 2-pyrone), 137.3 (C-3 of 2-pyrone), 130.2 (Ph),129.3 (Ph),128.6 (Ph),128.8 (Ph),127.0 (Ph),126.8(Ph),104.3(C-5 of 2-pyrone),36.1(PhCH$_2$ of benzylic group). **HRMS-ESI**: 243.0179 (MNa, 100%), $C_{12}H_9ClNaO_2$, theoretical 243.0189.

6.9.6 6-Chloro-3-decyl-2-pyrone (128e/129e)

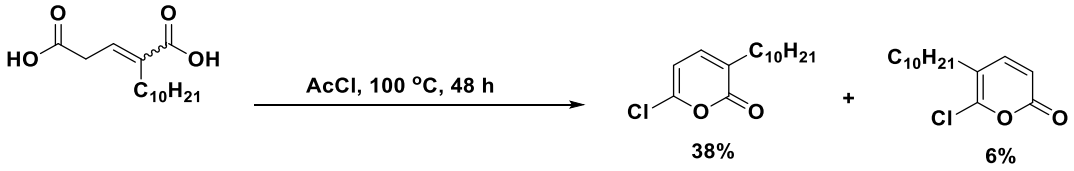

Into a thick-walled tube was added 4-decylglutaconic acid (739 g, 2.74 mmol, 1.0 eq.) was added acetyl chloride (10 mL) and refluxed at 100 ^oC for three days. The reaction mixture was allowed to cool; water (20 mL) was added and extracted with diethyl ether (2 x 20 mL), dried over magnesium sulphate, filtered and concentrated in vacuum to obtain tan oil. The tan oil was column chromatographed using 5% diethyl ether/n-hexane over silica gel loaded with 10 % water to obtain a white solid (244 mg, 33%) for **128e** and pale-yellow solid (44.3 mg, 6%) for **129e**.

Characterization for 128e

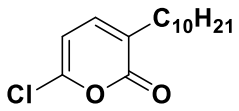

Rf: 0.28 in 5% diethyl ether/n-hexane. Melting point 37-39 ^{o}C and this compound fluorescence at long wavelength. **IR (Neat)/cm^{-1}**: 2953, 2916, 2852, 1720, 1632, 1554, 1471, 1422, 1329, 1191, 1085, 1062, 1046, 1026.**^{1}H NMR** [400 MHz, $CDCl_3$] ∂: 7.04 (dt, 1H, 8Hz, 1Hz), 6.13 (d, 1H, 8Hz), 2.40 (apt, 2H, 7 Hz), 1.53 (m, 2H), 1.25 (m, 14H), 0.85 (t, 3H, 7Hz).**^{13}C NMR** (100 MHz, CDCl3) δ: 161.7 (C-2 of 2-pyrone), 146.8 (C-6 of 2-pyrone), 139.3 (C-4 of 2-pyrone), 132.2(C-3 of 2-pyrone), 104.1 (C-5 of 2-pyrone), 31.9 (CH_2), 30.4 (CH_2), 29.2 (CH_2), 27.8 (CH_2), 22.7 (CH_2), 14.2 (CH_2). **HRMS-ESI**: m/z (relative abundance): 293.1280 (MNa, 100%)$^{+}$, $C_{15}H_{23}ClNaO_2$, theoretical 293.1284. UV λmax ^{PhH}, ε): 304 nm, 6540 Lmol^{-1}cm^{-1}. Elemental Anal Calc. for $C_{15}H_{23}ClO_2.C_6H_{14}$, C 70.66, H 10.45; Found C 70.20, H 9.75.

Characterization for 129e

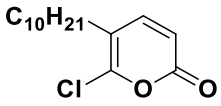

IR (Neat)/cm^{-1}: 2916, 2850, 1720 (shoulder, weak), 1632 (more intense), 1468, 1430, 1385, 1267, 1212, 1151, 1212, 1151, 1110, 891. **^{1}H NMR** [400 MHz, $CDCl_3$] ∂: 7.24 (d, 1H, 9 Hz, 1H), 6.21 (d, 1H, 9Hz), 2.40 (apt, 2H, 7 Hz), 1.53 (m, 2H), 1.25 (m, 14H), 0.85 (t, 3H, 7Hz).**^{13}C NMR** (100MHz, $CDCl_3$) δ: 161.7 (C-2 of 2-pyrone), 146.8 (C-6 of 2-pyrone), 139.3 (C-4 of 2-pyrone), 132.2(C-3 of 2-pyrone), 104.1 (C-5 of 2-pyrone), 31.9 (CH_2), 30.4 (CH_2), 29.2 (CH_2), 27.8 (CH_2), 22.7 (CH_2), 14.2 (CH_2). **HRMS-ESI**: m/z (relative abundance), 293.1280 (MNa, $C_{15}H_{23}ClNaO_2$), theoretical 293.1284. UV λmax ^{PhH}, ε): 304 nm, 6540 Lmol^{-1}cm^{-1}. **Elemental Anal**: Calc. for $C_{15}H_{23}ClO_2.C_6H_{14}$, C 70.66, H 10.45; Found C 70.196, H 9.754.

6.10 Syntheses of 6-(Phenylethynyl)-5-alkyl-2-Pyrone

6.10.1 5-Methyl-6-(phenylethynyl)-2-pyrone (131a)

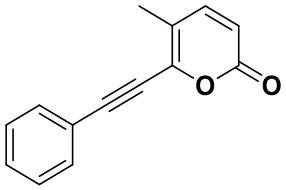

Into an oven-dried Schlenk tube was added 6-chloro-3-decyl-2-pyrone (144 mg, 1.0 mmol, 1 eq.), DABCO (286.6 mg, 2.5 eq.), Cs_2CO_3 (162.9 mg, 0.5 eq.), $PdCl_2(PPh_3)_2$ (35.05 mg, 5 mol%), CuI (9.5 mg, 5 mol%) and XPhos (19.07 mg, 4 mol%) was attached to a vacuum line and evacuated thrice. Degassed and dried THF (15 ml) was added and Phenyl acetylene (306.0 mg, 3.0 mmol, 3.0 eq.) was added slowly and stirred under nitrogen at 60 ^{o} C for 24 hours. Allowed to cool and filtered through celite and washed with DCM, concentrated in vacuum and purified using 10% DCM/ether; 1:9 to obtain tan oil (101.7 mg) and on preparative TLC with 5%DCM/ether obtained a yellow solid (84.8 mg, 40%). **MP:** 118-121 ^{o}C. **IR (ATR)/**cm^{-1}:3056, 2916, 2204, 1710, 1624, 1530, 1442, 1420, 1383, 1332, 1266, 1211, 1181, 1091. **^{1}H NMR** (400 MHz, $CDCl_3$) δ: 7.52 (dd, 2H, 8 Hz, 2 Hz, ArH), 7.43-7.34 (m, 3H, ArH), 7.23 (d, 1H, 9.50 Hz), 6.26 (d, 1H, 9.50 Hz), 2.19 (s, 3H, CH_3). **^{13}C NMR** (100 MHz, $CDCl_3$) δ: 161.4, 146.4, 141.8, 131.9, 129.9, 128.6, 121.1, 118.1, 116.7, 98.8, 80.8, 16.3. **HRMS-ESI**: m/z (relative abundance): 236.0832 (MH^+, 25%) $C_{16}H_{12}O_2$, theoretical 236.0837; 259.0732 (MNa^+, 100%) $C_{16}H_{12}NaO_2$, theoretical 259.0735.

6.10.2 5-Allyl-6-(phenylethynyl)-2-pyrone (131b)

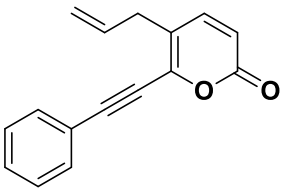

Into an oven-dried Schlenk tube was added 6-chloro-3-(2$^{'}$-propenyl)-2-pyrone (165.4 mg, 0.97 mmol, 1eq.), DABCO (317 mg, 2eq.), Cs_2CO_3 (207.0 mg, 1eq.), $PdCl_2(PPh_3)_2$ (36.30 mg, 5 mol%) and CuI (9.50 mg, 5 mol%) and XPhos (19.07 mg, 4 mol%) was attached to a vacuum line and evacuated thrice. Degassed and

dried THF (15 mL) was added and phenyl acetylene (306 mg, 3.0 mmol, 2 eq.) was added slowly and stirred under nitrogen at 60 ^{o} C for 24 hours. Allowed to cool and filtered through celite and washed with DCM, concentrated in vacuum and purified using 10% EtOAc/n-hexane: 2 ml acetic acid to obtain tan oil (80.60 mg, 36%). Rf 0.33 (10% EtOAc/n-hexane: 2 ml acetic acid). MP 84-86 ^{o}C. **IR (neat)/**cm: 3079, 2906, 2207, 1716, 1639, 1613, 1523, 1444, 1430, 1416, 1334, 1260, 1215, 1100, 1059, 997, 924, 896. **^{1}H NMR** (400 MHz, $CDCl_3$) δ: 7.54-7.30 (m, 5H, ArH), 7.24 (d, 1H), 6.30 (d, 1H, 9 Hz), 5.84 (br, m, 1H), 5.18-5.14 (br, s, 2H), 3.30 (d, 2H, CH_2). **^{13}C NMR** (100 MHz, $CDCl_3$) δ: 161.2, 145.5, 142.2, 134.1, 132.0, 128.7, 120.9, 117.9, 116.9, 98.7, 80.5, 34.7. **^{13}C DEPT-135^{o}C NMR** (100 MHz, $CDCl_3$) δ: 145.50, 134.1, 132.0, 130, 128.7, -118.1, 120.9, 116.9, +34.6 **HRMS-ESI**- m/z (relative abundance): 211.0747 (MH^+, 48%) theoretical 211.0754, 233.0566 (MNa^+, 100%) theoretical 233.0566.

6.10.3 6-[Phenylethynyl]-5-n-pentyl-2-pyrone (131c)

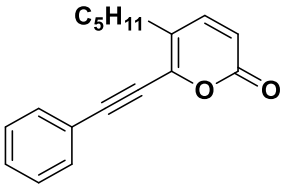

Into an oven-dried Schlenk tube was added $PdCl_2(PPh_3)_2$ (40.10 mg, 5.72 mol %), CuI (43.90 mg, 5 mol %), DABCO (285.5 mg, 2.5 eq.), Cs_2CO_3 (165.8 mg, 0.5 eq.) XPhos (19.07 mg, 4 mol %) and attached to a vacuum line and evacuated thrice with nitrogen.6-Chloro-3-pentyl-2-pyrone (183.6 mg, 0.92 mmol, 1.0 eq.), was poured into a round bottomed flask and dried and degassed THF (10 mL) was added and degassed for 1 hour. The degassed pyrone mixture was added via a syringe and phenylacetylene (306 mg, 3.0 mmol, 3.3 eq.) was added via a syringe and stirred under nitrogen at 60 ^{o}C for 24 hours. There action was monitored by TLC at 3 hours and after 24 hours and it indicated the formation of a product. The reaction mixture was left to cool and filtered through celite, washed with dichloromethane and concentrated in vacuum. Preparative TLC of the crude using 2% DCM/ether gave the product as tan oil (120.5 mg, 45%). **IR (neat)**/cm^{-1}: 3057, 2955, 2926, 2857, 2204, 1720, 1618, 1528, 1489, 1441, 1419, 1377, 1332, 1261, 1185, 1100, 904, 808. **^{l}H NMR** (400 MHz, $CDCl_3$) δ: 7.61-7.27 (m, 5H, ArH), 7.22

(d, 9 Hz, 1H), 6.35 (d, 9 Hz, 1H), 2.48 (t, CH_2, 2H), 1.47-1.13 (br, 6H, $3CH_2$), 0.95 (t, 7 Hz, 3H, CH_3). **^{13}C NMR** (100 MHz, $CDCl_3$) δ: 161.0, 147.6, 141.9, 137.9, 135.9, 132.0, 126.5, 121.9, 116.2, 81.8, 92.5, 31.3, 30.4, 29.2, 22.6, 14.2. **^{13}C DEPT-135 ^{o}C NMR** (100 MHz, $CDCl_3$) δ: 141.9, 135.9, 132.0, 128.6, 121.9, 116.2, -31.3, -30.4, -29.2, -22.6, +14.2. **HRMS-ESI**; m/z (relative abundance): 289.1196 (MNa^+, 80%) theoretical 289.1199 $C_{18}H_{18}NaO_2$.

6.10.4 6-[Phenylethynyl]-2-pyrone (131d)

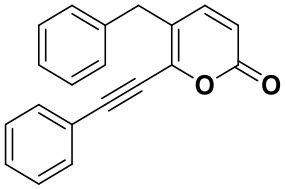

Into an oven-dried Schlenk tube was added $PdCl_2(PPh_3)_2$ (23.5 mg, 5 mol%), CuI (30.5 mg, 5 mol%), XPhos (44.6 mg, 4 mol%), 6-chloro-3-benzyl-2-pyrone (153.7 mg, 0.68 mmol,1.0 eq.), DABCO (153.0 mg, 2.0 eq.) and Cs_2CO_3 (0.5 eq.) and attached to the vacuum manifold. Dried and degassed THF (40 mL) and phenylacetylene (208.6 mg, 2.05 mmol, 3 eq.) was added via a syringe and stirred under nitrogen for 24 hours at 35 ^{o}C. Allowed to cool and filtered through celite, washed with dichloromethane. It was then concentrated in vacuum. Purification was by flashy column chromatography using 14% EtOAc/n-hexane to obtain the product as a tan solid (142.1 mg, 61%). MP 108-110 ^{o}C**. IR (ATR)/cm^{-1}**: 3057 (w, C=CH), 3057, 3023, 2961, 2923 (w, CH), 2851 (w, CH), 2202 (w, C≡C), 1722 (s, C=O), 1619 (m, C=C), 1527 (m, C=C), 1491 (w, CH), 1439 (w, CH), 1331, 1260 (w, CH), 1151 (w, C-O), 1095, 1080, 1019**. ^{1}H NMR** (400 MHz, $CDCl_3$) δ: 7.53-7.49 (m, 2H, ArH), 7.43-7.29 (m, 5H, ArH), 7.28-7.20 (m, 3H, ArH), 6.87 (dt, 1H, 7 Hz, 1 Hz, 2-pyrone H), 6.37 (d, 1H, 7Hz), 3.81 (br, s, 2H, benzylic CH_2). **^{13}C NMR** (400 MHz, $CDCl_3$) δ: 161.3 (C=O), 145.4 (C=C), 142.4 (C=C), 138.1 (C=C), 132.0 (C=C), 130.0 (C=C), 128.8 (C=C), 127.1 (C=C), 123.3 (C=C), 122.4 (C=C), 120.9 (C=C), 116.9 (C=C), 98.7 (C≡C), 82.6 (C≡C), 36.12 (CH_2, Benzylic CH_2). **^{13}C DEPT NMR** (400 MHz, $CDCl_3$) δ: 145.4 (C=C), 132.0 (C=C), 128.8 (C=C), 127.1 (C=C), 116.9 (C=C), -36.1

(CH_2, Benzylic CH_2). **HRMS-ESI**: m/z (relative abundance) 309.0884 (MNa, 100%), $C_{20}H_{14}NaO_2$, 287.0992 (MH, 100%), $C_{20}H_{15}O_2$, theoretical 287.0992.

6.10.5 5-Decyl-6-(phenylethynyl)-2-pyrone (131e)

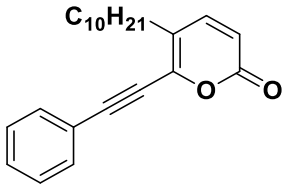

Into an oven-dried Schlenk tube was added 6-chloro-3-decyl-2-pyrone (270 mg, 1.0mmol, 1eq.), DABCO (225.4 mg, 2eq.), Cs_2CO_3 (325.8 mg, 1eq.), $PdCl_2(PPh_3)_2$ (35.05 mg, 5 mol%) and CuI (9.5 mg, 5 mol%) was attached to a vacuum line and evacuated thrice. Degassed and dried THF (15 mL) was added and Phenyl acetylene (204 mg, 2.0 mmol, 2eq.) was added slowly and stirred under nitrogen for 3 hours and then at 60 ^{o} C for 24 hours. Allowed to cool and filtered through celite and washed with DCM, concentrated in vacuum and purified using 10% EtOAc/n-hexane: 2 mL acetic acid to obtain tan oil (176.1 mg, 0.5 mmol, 53%). Rf of 0.13. **IR (ATR,** Neat)/cm: 3057 (C=C), 2923, 2852, 2205 ($C\equiv C$), 1731 (C=O), 1620, 1529 (C=C), 1489 (C-C), 1444, 1102 (C-O), 902, 826. **^{1}H NMR** (400 MHz, $CDCl_3$) δ: 7.50 (m, 2H, ArH), 7.37 (m, 3H, ArH), 7.24 (d, 1H, 7Hz, 2-Pyrone H), 6.32 (d, 1H, 7Hz, 2-Pyrone H), 2.51 (apt, 2H, CH_2), 1.56 (br, 2H, CH_2), 1.19 (br, 14H, $7CH_2$), 0.85 (t, CH_3, 7 Hz). **^{13}C NMR** (100 MHz, $CDCl_3$) δ: 161.5 (C=O), 145.6 (C=C), 141.9 (C=C), 132.0 (C=C), 129.9 (C=C), 128.4 (C=C), 123.6 (C=C), 121.1 (C=C), 116.9 (C=C), 98.3 ($C\equiv C$), 80.8 ($C\equiv C$), 32.0 (CH_2), 30.4 (CH_2), 29.7 (CH_2), 29.4 (CH_2), 29.1 (CH_2), 22.7 (CH_2), 14.2 (CH_3). **^{13}C NMR DEPT-135^{o}**: 145.7 (C=C), 131.9 (C=C), 129.9 (C=C), 128.7 (C=C), 116.9 (C=C), -32.0 (CH_2), -30.4 (CH_2), -29.7 (CH_2), -29.6 (CH_2), -29.4 (CH_2), -29.4 (CH_2), -29.1 (CH_2), -22.7 (CH_2), 14.2 (CH_3). **HRMS-EI**: 336.2085 (MH, 100%, $C_{23}H_{28}O_2$). **Elemental analysis**: calculated C 82.10, H 8.39, and Found: C 81.72, H 8.19.

6.10.7 5-Benzyl-6-(pyridin-3'-ylethynyl)-2-pyrone (131d')

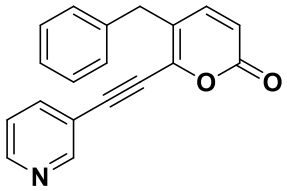

Into an oven-dried Schlenk was added $PdCl_2(PPh_3)_2$ (31.90 mg, 5 mol%), DABCO (204.1 mg, 2eq), CombiPhos (28.51mg, 4 mol%), CuI (8.65 mg, 5mol%) was attached to a vacuum manifold and evacuated thrice. Degassed and dried THF was added to 3-benzyl-6-chloro-2-pyrone (208 mg, 0.95 mmol, 1eq.) and further degassed for 30 minutes. The 2-pyrone solution was added to the Schlenk tube via a syringe and stirred at room temperature for 2 hours and at 35 ^oC for 22 hours. Filtered through celite and concentrated in vacuo. Purified through silica gel using 50% EtOAc/n-hexane: 2 mL acetic acid to obtain brown solid (70.5 mg, 0.24 mmol, 27%). Melting point: 129-132 ^oC. **IR (ATR**, Neat)/cm: 3052, 3008 (C=C), 2930, 2206 ($C\equiv C$), 1724 (C=O), 1615, 1528 (C=C), 1490 (C-C), 1450, 1403, 1336, 1274, 1184, 1152, 1105 (C-O), 1081, 1021, 955. **^{1}H NMR** (400 MHz, $CDCl_3$) δ: 7.81 (d, 1H, 8Hz), 7.65 (dd, 1H, 8.0 Hz, 2.0 Hz), 7.54 (apt, 1H, 8.0 Hz), 7.45 (dd, 1H, 8.0 Hz, 2.0 Hz), 7.36-7.30 (2H, m, ArH), 7.26-7.19 (m, 3H, ArH), 7.16 (d, 1H, 7.0 Hz, 2-pyrone H), 6.32 (d, 1H, 7.0 Hz, 2-pyrone H), 3.87 (s, 2H, CH_2, $PhCH_2$). **^{13}C NMR** (100 MHz, $CDCl_3$) δ: 160.8 (C=O), 152.2 (HC=N), 149.9 (C=C), 145.3 (C=C), 141.4 (C=C), 139.2 (C=C), 137.7 (C=C), 132.3 (C=C), 129.1 (PhH), 128.7/128.6 (PhH), 127.3 (PhH), 123.0 (PhH), 117.9 (C=C), 94.7 ($C\equiv C$), 83.9 ($C\equiv C$), 36.3 (CH_2).**^{13}C NMR DEPT-135^o**: (100 MHz, $CDCl_3$): 152.2 (C=N), 149.6 (C=C), 145.2 (C=C), 139.2 (C=C), 132.2 (C=C), 129.1 (C=C), 128.7 (C=C), 127.3 (C=C), 117.9 (C=C), -36.31 (Ph$\underline{CH_2}$). **HRMS-ESI**: m/z 288.1019 (MH^+, 36%) $C_{19}H_{14}NO_2$, theoretical 288.1025, 310.0838 (MNa^+, 100%) $C_{19}H_{13}NNaO_2$, theoretical 310.0844. UV-vis (λmax, $CHCl_3$): 344 nm (ε_{max}, 12,000 L/mol/cm), 266 nm (ε_{max}, 16,000 L/mol/dm^3).

6.10.8 5-Decyl-6-(pyridine-3-ethynyl)-2-pyrone (131e')

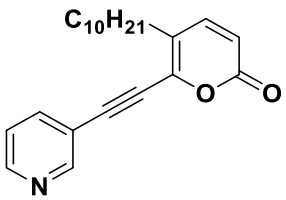

Into an oven dried Schlenk tube was added 6-chloro-3-decyl-2-pyrone (179.5 mg, 0.66mmol, 1eq.), DABCO (168.4 mg, 2eq.), Cs_2CO_3 (286.7.8 mg, 0.5 eq.), $PdCl_2(PPh_3)_2$ (38.05 mg, 5 mol%) and CuI (28.5 mg, 15 mol%) was attached to a vacuum line and evacuated thrice. Degassed and dried THF (15 mL) was added and 3-ethynylpyridine (137.0 mg, 2.0 mmol, 2eq.) was added slowly and stirred under nitrogen for 3 hours and then at 35 ^{o} C for 24 hours. Allowed to cool and filtered through celite and washed with DCM, concentrated in vacuum. Purified using silica gel using 29% EtOAc/n-hexane: 0.02 mL acetic acid to obtain tan oil (79.4 mg, 36%). **IR (ATR**, Neat)/cm: 3081 (C=C), 2923, 2853, 2209 ($C\equiv C$), 1733 (C=O), 1622, 1530 (C=C), 1464 (C-C), 1408, 1260, 1189, 1160, 1102, 1021, 902. **^{1}H NMR** (400 MHz, $CDCl_3$) δ: 8.72 (br, 1H), 8.59 (dd, 5 Hz, 2 Hz, 1H), 7.79 (dt, 8 Hz, 2 Hz, 1H), 7.31 (dd, 8 Hz, 5 Hz, 1 Hz), 7.24 (d, 8 Hz, 1H, 2-pyrone), 6.34 (d, 8 Hz, 1H, 2-pyrone), 2.51 (t, 7 Hz, 2H, CH_2 of $C_{10}H_{21}$), 1.55 (m, br, 2H), 1.35-1.15 (br, 14H, 7CH_2 of $C_{10}H_{21}$), 0.82 (t, 7 Hz, CH_3 of $C_{10}H_{21}$).**^{13}C NMR** (400 MHz, $CDCl_3$) δ:161.03 (C=O), 152.33, 149.91, 140.93 124.29, 123.36, 118.53, 117.58, 94.45, 83.74, 31.92, 30.39, 29.63, 29.35, 29.04, 22.72, 14.17. **^{13}C NMR DEPT-135^{o}** (100 MHz, $CDCl_3$) δ: 152.33, 149.91, 123.36, 117.58, -31.92, -30.39, -29.63, -29.35, -29.04, -22.72, 14.17. **HRMS-EI**: m/z (relative abundance): 360.1930 (MNa+, 100%) $C_{22}H_{27}NaNO_2$, theoretical 360.1938; 338.2100 (MH+, 26%), $C_{22}H_{28}NO_2$, theoretical 338.2120.

^{13}C-LABELLED SYNTHESIS

6.11 Synthesis of ^{13}C-Labelled 2-Alkylmalonate

6.11.1 Diethyl 2-benzylmalonate-^{13}C-1,3 (164a)

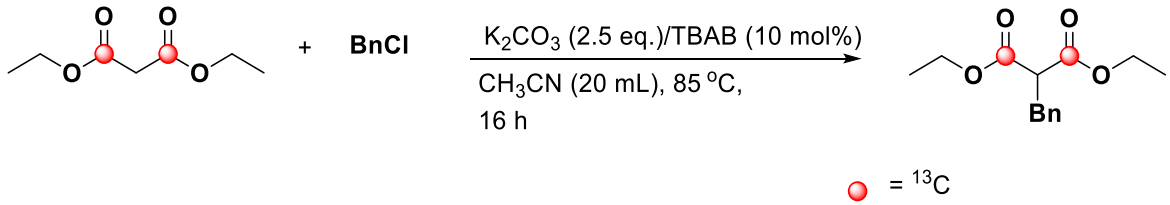

Into a round-bottomed flask was added potassium carbonate (1.06 g, 7.7 mmol, 2.5 eq.), acetonitrile (20 mL), [^{13}C-1,3]diethyl malonate (500 g, 3.08 mmol, 1.0 eq.), and benzyl chloride (491.1 mg, 3.39 mmol, 1.1 eq.), TBAB (102.9 mg, 0.308 mmol, 10 mol%) to afford pale yellow oil(768.8 mg, 99%).**^{1}H NMR** (400 MHz, $CDCl_3$) δ: 7.16-7.00 (m, 5H, PhH), 4.41(q, 4H, 7Hz, $CH(COOC\underline{H}_2CH_3)_2$), 3.51(t, 1H, 8Hz, $C\underline{H}(COOCH_2CH_3)_2$), 3.10 (d, 2H, J = 8Hz, benzylic $C\underline{H}2Ph$), 1.21 (t, 7Hz, 6H, $COOCH_2C\underline{H}_3$). **^{13}C NMR** (100 MHz, $CDCl_3$) δ: 170.7,168.7 ($(^{13}\underline{CO}OCH_2CH_3)_2$), 138.1, 136.5 (Ph), 130.2 (Ph), 128.8 (Ph), 128.4 (Ph), 128.2 (Ph), 126.9/126.7 (Ph), 61.3 ($COO\underline{C}H_2CH_3)_2$), 53.5 (p, 55 Hz, 27 Hz), 38.9 ($\underline{C}H_2Ph$),13.7 ($\underline{C}H_3$). **HRMS-ESI**: m/z 275.1163 (MNa^+, 44%)$C_{14}H_{18}NaO_4$, theoretical 274.1136.

6.11.2 Diethyl2-decylmalonate-^{13}C-1,3 (164b)

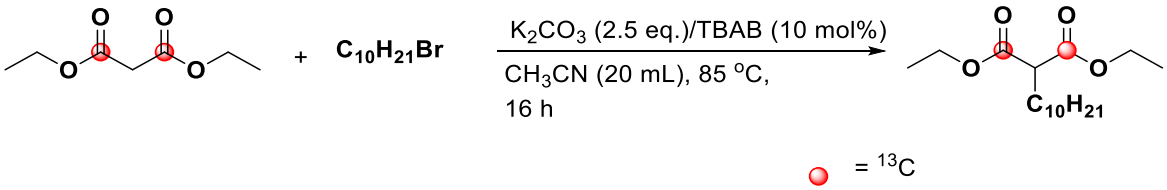

Same procedure as the unlabelled analogue. Into a round-bottomed flask was added potassium carbonate (1.08 g, 7.82 mmol, 2.5 eq.), acetonitrile (15 mL), [^{13}C-1,3]diethyl malonate (500 mg, 3.08 mmol, 1.0 eq.), 1-bromodecane (690 mg, 3.12 mmol, 1.0 eq.) and TBAB (102.9 mg, 10 mol%) to afford the product as a yellow oil (936 mg, 99%). ^{1}H-NMR (400MHz, $CDCl_3$)δ: 4.15 (4 H, dq, 7 Hz), 3.27(1 H, p, 8 HZ),3.25), 1.84 (2 H, br), 1.73 (m, 2H, $CH_2C\underline{H_2}(CH_2)_7CH_3$), 1.12 (m, 14H, -($C\underline{H_2})_7$-), 0.74 (t, 3H,$CH_2)_9C\underline{H_3}$), 1.23 (br, m, 22H, $8CH_2$+2($COOCH_2C\underline{H_3}$), 0.84 (3 H, t, 7 Hz). ^{13}C NMR (100 MHz, $CDCl_3$) δ: 172.1, 169.9 (^{13}C=O), 166.6, 61.2 (p, 3 Hz, 1 .40 Hz, $COO\underline{CH_2}CH_3$), 52.1 (CH), 31.9 ($\underline{CH_2}$), 29.2 (CH_2), 27.3 (CH_2), 22.7 (CH_2), 14.1 ($\underline{C}H_3$). HRMS-EI: m/z (relative abundance); 273.2007 (MH^+-Et) theoretical 273.2021, 228 (M-CO_2Et), 162 (M-$C_{10}H_{21}$).

6.12 Synthesis of ^{13}C-Labelled Glutaconate Ester

6.12.1 *(E/Z)*-4-Phenyl-1-carbomethoxy-3,3-dicarbethoxybutene-^{13}C-3,3 (165a)

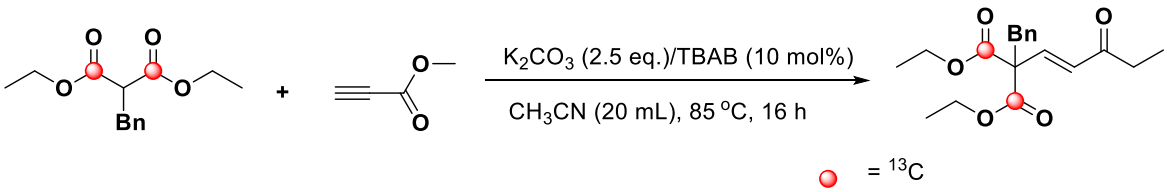

Into a round bottomed flask was added Diethyl 2-benzylmalonate (726.8 mg, 2.88 mmol, 1.0 eq.), potassium carbonate (993.6 mg, 7.20 mmol, 2.5 eq.), CH_3CN (20 mL), methyl propiolate (242 mg, 3.17 mmol, 0.91 eq.), TBAB (96.19 mg, 0.288 mmol, 10 mol %). The crude oil was purified by filtering through a Buchner funnel loaded with silica gel and eluted with ethyl acetate/petroleum ether 5/35 to obtain a colourless oil (841.8 mg, 96 %]. **^{1}H NMR** [400MHz, $CDCl_3$], 7.20-7.10 (m, 5H, (CH_2**Ph**), 7.20 (d, 1H, 16 Hz, (HC=C**H**$COOCH_3$), major product), 6.66 (d,1H, 12Hz,

(HC=C**H**COOCH$_3$), minor product), 5.98 (d, 1H 12Hz, (**H**C=CHCOOCH$_3$), minor product), 5.89 (d, 1H, 16Hz, (**H**C=CHCOOCH$_3$), major product), 4.15 (q, 4H, 7 Hz, (COOC**H$_2$**CH$_3$)$_2$), 3,74 (s, 3H, (COOC**H$_3$**)), 3.38 (s, 2H, CH$_2$, benzylic, (C**H$_2$**Ph), 1.20 (t, 6H,7 Hz, (COOCH$_2$C**H$_3$**)$_2$). **^{13}C NMR** (100MHz, CDCl$_3$) δ: 168.9 (HC=CH**CO**OCH$_3$), 166.1 (**C**OOCH$_2$CH$_3$)$_2$),144.4 (HC=**CH**COOCH$_3$), 135.0 (HC=**CH**COOCH$_3$), 134.7 (**HC**=CHCOOCH$_3$), 129.5 ((CH$_2$**Ph**), 128.1 (CH$_2$**Ph**), 127.0 (CH$_2$**Ph**), 122.6 (CH$_2$**Ph**), 62.1 (COO**CH$_2$**CH$_3$)$_2$), 51.7 (COO**CH$_3$**), 42.0 (-**C**(CH$_2$Ph), 39.2((**CH$_2$**Ph), 13.9 (COOCH$_2$**CH$_3$**)$_2$). **HRMS-ESI**: m/z 359.1380 (MNa$^+$, 100%) C$_{16}$^{13}C$_2$H$_{22}$NaO$_6$, theoretical 359.1381; 337.1561 (MH$^+$, 38%) C$_{16}$^{13}C$_2$H$_{23}$O$_6$, theoretical 337.1562.

6.12.2 (*E/Z*)-Diethyl-1-methyltridec-1-ene-1,3,3-tricarboxylate-^{13}C-3,3 (165b)

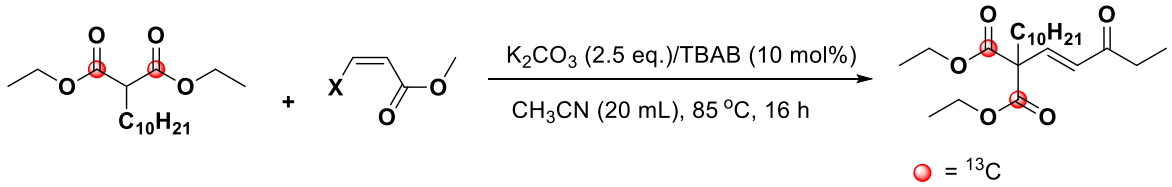

Diethyl 2-decylmalonate (997.7 mg, 3.30 mmol, 1.0 eq.), methyl 3-iodoacrylate (700.4 mg, 3.30 mmol, 1.0 eq.), potassium carbonate (1.53 g, 11.09 mmol, 3.36 eq.), CH$_3$CN (20 mL) and TBAB (119.1 mg, 0.37 mmol,10mol%) and refluxed at 85 ^{o}C for 24 hours. The yellow coloured oil was filtered through a Buchner funnel loaded with silica gel and eluted using; EtOAc/Petroleum ether (40-60 ^{O}C), in a ratio 5:35 to obtain a pale-yellow oil [1.11 g, 2.88 mmol, 92%]. **^{1}H NMR** (400 MHz, CDCl$_3$) δ: 7.32 (1 H, dt, J$_{12}$ = 16 Hz, H-1, (*E*)-major product), 6.87 (d, 1H, J$_{12}$ = 12 Hz, H-1, (*z*)-minor product), 5.93 (1 H, d, 1H, J$_{12}$ = 12 Hz, H-2, (z)-minor product), 5.86 (1 H, d, J$_{12}$ = 16 Hz, H-2, (*E*)-major product), 4.10-4.16 (4 H, q, J$_{12}$ = 7 Hz, 2COO<u>CH$_2$</u>CH$_3$), 3.70 (3 H, s, COOC<u>H$_3$</u>), 2.38 (apt. 2H, CH$_3$(CH$_2$)$_7$CH$_2$C<u>H$_2$</u>), 1.54 (2 H, p, CH$_3$(CH$_2$)$_7$C<u>H$_2$</u>CH$_2$), 1.29-1.12, (22 H, br s, CH$_3$(C<u>H$_2$</u>)$_8$CH$_2$+2(COOCH$_2$C<u>H$_3$</u>)), 0.84 (3 H, t, 7Hz, (-C<u>H$_3$</u>(CH$_2$)$_7$CH$_2$CH$_2$). **^{13}C NMR** (100MHz, CDCl$_3$) δ: 172.0, 169.6 (d, 8 Hz, <u>C</u>OOCH$_3$), 169.3 (^{13}<u>C</u>OOCH$_2$CH$_3$)$_2$), 145 (t, 2 Hz), 144.4 (t, 2 Hz, C=C), 122.4 (t, 3 Hz, <u>HC</u>=CH), 120.6 (t, 3 Hz, <u>CH</u>=CH), 60.1 (COO<u>C</u>H$_2$CH$_3$)$_2$), 58.8 (COO<u>C</u>H$_3$),

51.7 (C^{t}) 33.9 ($CH_3(CH_2)_7CH_2CH_2$)), 29.6 ($CH_3(CH_2)_7CH_2CH_2$)), 28.2 ($CH_3(CH_2)_7CH_2CH_2$), 27.4 ($CH_3(CH_2)_7CH_2CH_2$), 22.7 ($CH_3(CH_2)_7CH_2CH_2$), 14.1 ($CH_3(CH_2)_7CH_2CH_2$). **HRMS-ESI**: m/z 409.2470 (MNa^+, 100%) $C_{19}{}^{13}C_2H_{32}O_6$ theoretical 409.2477.

6.13 Synthesis of ^{13}C-Enriched Glutaconic acid

6.13.1 2-Benzylglutaconic acid-^{13}C-1(166a)

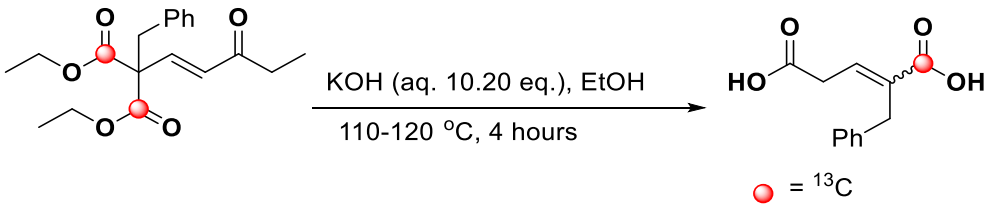

4-Phenyl-1-carbomethoxy-3,3-dicarbethoxybutene [841.8 mg, 2.51mmol, 1.0 mmol], KOH (1.71 g, 30.50 mmol 10.20eq.) in 5 ml of water and ethanol (20 mL) and refluxed at 120 °C for 4 hours. Work up and concentration afforded the product as a white solid (415.0 mg,75%).^{1}**H NMR** (400 MHz, CD_3OD) δ: 7.35-7.24 (m, 5H, PhH). 7.03 (t, 1H, 7Hz, *H*-3), 3.65 (s, 2H, $PhCH_2$), 3.53 (d, 2H, 7Hz, CH_2COOH). ^{13}**C NMR** (100 MHz, CD_3OD) δ: 168.1 (**C**OOH), 164.2 (HOO**C**), 146.2 (**C**=C), 139.4 (**C**=C), 128.46 (**Ph**), 127.4 (**Ph**)), 125.1 (**Ph**), 122.1 (**Ph**), 46.2 (**C**H_2C=C), 38.2 (CH_2, ((**C**H_2Ph). **HRMS-ESI**- m/z 244.0658 (MNa+, 43%) $C_{11}{}^{13}CH_{12}NaO_4$, theoretical 244.0667.

6.13.2 4-Decylglutaconic acid-^{13}C-1 (166b)

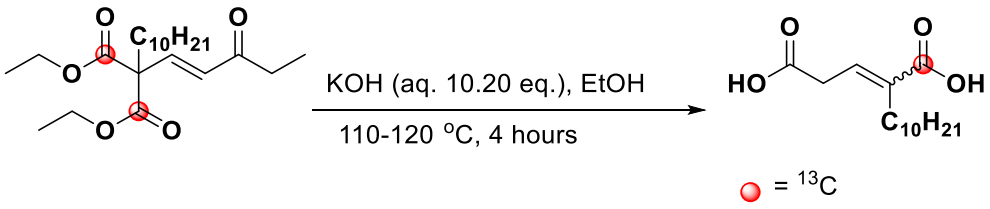

3,3-Dimethyl-1-methyltridec-1-ene-1,3,3-tricarboxylate (1.02 g, 2.64 mmol, 1.0 eq.) in ethanol (20 mL), potassium hydroxide (1.51 g, 26.93 mmol, 10.20 eq.) and refluxed for 100 °C for four hours. The reaction mixture was left to cool and extracted into aqueous phase and the acidified with hydrochloric acid (100 mL, 1M)

to afford the product as an off-white solid (712.4 mg, quant). **^{1}H NMR** (400 MHz, CD_3OD, δ): 6.88 (1 H, m, 14Hz,C**H**=C, major product), 5.85(1 H, d, 13 Hz, CH=C**H**, trace product),3.23(1 H, 7 Hz, C**H$_2$**CH=C),1.45-1.09(19 H, br, m, CH=C(C**H$_2$**$CH_2(CH_2)_7CH_3$),0.81(3 H, t, J_{12} = 7Hz, $CH_2CH_2(CH_2)_7C$**H$_3$**). **^{13}C NMR** (100 MHz, CD_3OD) δ: 169.5 (C=O), 161.7 (C=O), 144.4 (C=C), 129.2 (C=C), 45.5 (CH_2), 33.6 (CH_2), 32.5 (CH_2),30.2 (CH_2),29.5 (C=O),28.8 (CH_2),27.5 (CH_2),25.3 (CH_2),22.5 (CH_2),14.2 (CH_3).**H R MS-ESI**, m/z 293.1726 (MNa^+, 21%) $C_{14}{}^{13}CH_{26}NaO_4$, theoretical 294.1762.

6.14 Synthesis of ^{13}C 6-Chloro-2-pyrone

6.14.1 3-Benzyl-6-chloro-2-pyrone-^{13}C-2/^{13}C-6 (167a/168a)

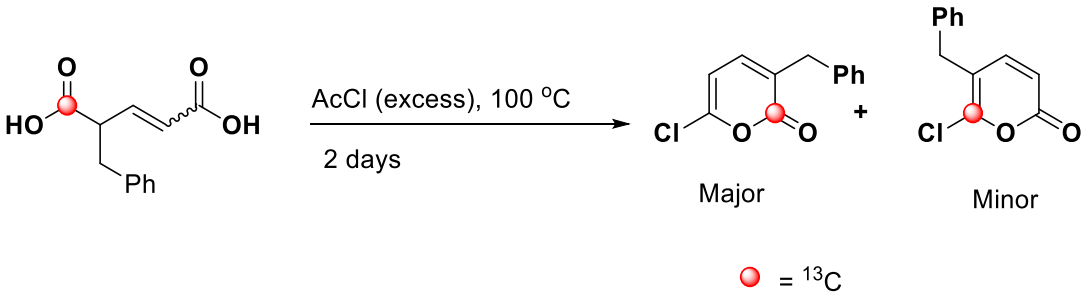

In a thick-walled flask was added 2-benzylpent-2-enedioic acid (1.26 g, 5.72 mmol, 1.0 eq.) and acetyl chloride (30 mL) and refluxed at 100 °C for 2 days in a sealed tube. Purification of the crude by flash column chromatography (CC) gave the titled product as a white powder (348.1mg,28%) and a pale-yellow powder (53.7 mg, 4%) of the 5-benzyl-6-chloro-2-pyrone with melting point 50-51 °C (literature 50-51 °C,[174]). **3-Benzyl-6-chloro-2-pyrone-^{13}C-2**-Rf 0.45 in EtOAc/Petroleum ether 7/8. ^{1}H NMR(400 MHz, $CDCl_3$) δ: 7.31 (t, 2H, 8 Hz, Ph), 7.21 (m, 2H, Ph**H**), 6.87 (ddt, 1 H, J_{H-H} = 7.0 Hz, J^{13}_{C-H} = 11.6 Hz, J_{H-H} =1.0 Hz, H-4), 6.14 (d, 1 H, J_{H-H} = 7.0 Hz, H-5), 3.73 (d, 2 H, J^{13}_{C-H} = 4 Hz, CH_2Ph**).** ^{13}C NMR (100 MHz, $CDCl_3$) δ: 161.8 (s, J^{13}_{C-H} = 71.34 Hz, **C-2** of 2-pyrone), 147.5 (d, Jc-c = 4 Hz, **C-6** of 2-pyrone), 140.9 (d, 4 Hz, **C-4** of 2-pyrone), 138.1 (d, 2 Hz, **Ph**), 130.5 (**Ph**),129.6 (**Ph**),129.2 (**Ph**), 128.7 (**Ph**),127.3 (**Ph**),127.1 (d, J^{13}_{C-H} 72.07 Hz, **C-3** of 2-pyrone),104.8(d, Jc-c = 6 Hz, **C-5** of 2-pyrone),36.6(d, J_{C-H} = 4 Hz, Ph**C**H_2 of benzylic group). MS-ESI: m/z (% relative intensity), 244.0218 (MNa^+, 100%), theoretical 244.0222; 222.0400

(MH$^+$, 33%) theoretical 222.0403. **5-benzyl-6-chloro-2-pyrone^{13}C-6-^{1}H NMR** (400 MHz, $CDCl_3$) δ: 7.40- 7.25 (5 H, m, Ph**H**), 7.16 (1 H, d, J_{12} = 9 Hz, H-4), 6.21 (1 H, d, J_{12} = 9 Hz, H-5), 3.79 (2 H, s, CH_2Ph**). ^{13}C NMR** (100 MHz, $CDCl_3$) δ: 161.2 (d, **C-2** of 2-pyrone), 147.30 (d, $J_{C\text{-}C}$ = 2 Hz, **C-4** of 2-pyrone),146.8 (s, $J_{C\text{-}C}$ = 86.76 Hz, **C-6** of 2-pyrone), 139.2 (**Ph**), 137.8 (**Ph**), 132.3 (**Ph**), 129.1 (d, $J_{C\text{-}C}$ = 5 Hz), 128.7 (d, $J_{C\text{-}C}$ = 12 Hz), 127.2 (**Ph**),126.1 (**Ph**),128 (**Ph**),127.2 (**Ph**), 115.2 (d, $J_{C\text{-}C}$ = 86.61 Hz, **C-5** of 2-pyrone), 113.9 (d, $J_{C\text{-}C}$ = 2 Hz, **C-3** of 2-pyrone), 38.1 (d, $J^{13}_{C\text{-}H}$ = 2 Hz, Ph**C**H_2 of benzylic group). **HRMS-ESI**- m/z (relative intensity), 244.0223 (MNa$^+$, 47%) theoretical 244.0222; 222.0402 (MH$^+$, 27%) theoretical 222.0403.

6.14.2 6-Chloro-3-decyl-2-pyrone-^{13}C-2/^{13}C-6 (167b/168b)

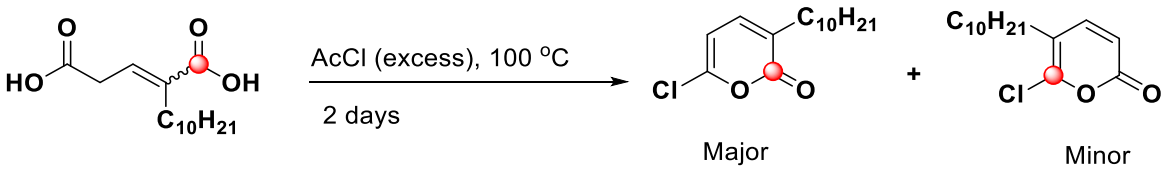

Into a thick-walled flask was added 4-decylglutaconic acid (739 g, 2.74 mmol, 1.0 eq.), and excess acetyl chloride (10 mL) and the mixture was refluxedat100 oC for two days. The reaction mixture was concentrated and water (20 mL) was added and neutralized with 10% NaOH and extracted with ether (2x50 mL), dried over magnesium sulphate, filtered and concentrated in vacuo. The tan oil was column chromatographed using 5% diethyl ether/n-hexane over silica gel loaded with 10 % water to obtain a white solid (244 mg, 33%) and pale-yellow solid (44.3 mg, 6%). **6-Chloro-3-decyl-2-pyrone^{13}C-2**-Rf 0.28 in 5% diethyl ether/n-hexane. **^{1}H NMR** [400MHz, $CDCl_3$] *∂*: 7.04 (1H, ddt, 7 Hz, 5 Hz, 1Hz), 6.13 (1H, d, 1H, J_{13} = 7Hz, H-5), 2.40 (2 H, m), 1.53 (2 H, p, J_{12} = 15 Hz, J_{12} = 7 Hz), 1.25 (14 H, br m, 7CH_2), 0.85 (3 H, t, 7Hz).**^{13}C NMR** (100MHz, $CDCl_3$) δ: 161.7 (s, J^{13}C-H = 70.5 Hz C-2 of 2-pyrone), 146.7(d, 4 Hz, C-6 of 2-pyrone), 139.4 (d, 2 Hz, C-4 of 2-pyrone), 127.3(d, J^{13}C-H = 70.5 Hz, C-3 of 2-pyrone), 104.2 (d, j = 5 Hz, C-5 of 2-pyrone), 31.97 (CH_2), 30.41 (CH_2), 29.28 (CH_2), 27.85 (CH_2), 22.76 (CH_2), 14.22 (CH_2). **6-Cloro-5-decyl-2-pyrone-^{13}C-6-^{1}HNMR** [400 MHz, $CDCl_3$] *∂*: 7.24 (dd, 1 H, 9 Hz, 4 Hz), 6.21 (1 H, dd, 9 Hz, 2 Hz), 2.40 (2 H, q, 7 Hz), 1.53 (2 H, br, CH_2), 1.25 (14

H, br s, 7CH_2), 0.85 (3H, t, J_{12} = 7Hz,).**^{13}C NMR** (100 MHz, $CDCl_3$) δ: 161.9 (s, JC-C = 86.26 Hz, C-2 of 2-pyrone), 147.1 (d, 2Hz, C-4 of 2-pyrone), 146.0 (s, J^{13}C-H = 86.2 Hz, C-6 of 2-pyrone), 116.0 (d, J^{13}C-H = 86.2 Hz, C-5 2-pyrone), 113.5 (d, 4 Hz, C-3 of 2-pyrone), 31.9 (CH2), 30.4 (CH_2), 29.2 (CH_2), 27.8 (CH_2), 22.7 (CH_2), 14.2 (CH2). HRMS-ESI: m/z (% relative intensity), 272.1491 (MH+, 100%) theoretical 272.1498, 294.1306 (MNa+,21%) theoretical 294.1318. The protiated peak due to ^{37}Cl, is 24% of the protiated molecular ion peak.

6.15 5-Decyl-6-(phenylethynyl)-2-pyrone-^{13}C-6

6.15.1 (^{13}C-6)-5-Benzyl-6-(phenylethynyl)-2-pyrone (169a)

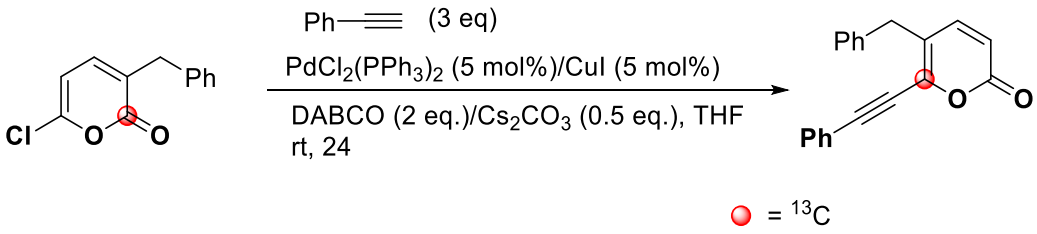

Into an oven-dried Schlenk tube was added $PdCl_2(PPh_3)_2$ (46.8mg,5 mol%), CuI [30.5mg,5mol%], XPhos (44.6 mg, 4mol%), 6-chloro-3-benzyl-2-pyrone(153.7mg,0.68 mmol,1.0eq.), and DABCO (153.0 mg, 2.0 eq.) and Cs_2CO_3 (0.5 eq.), degassed/dried THF (3 mL) and phenyl acetylene (38.6 mg, 2.05 mmol, 3 eq.) and stirred at room temperature. The reaction mixture was filtered through celite and washed with DCM and concentrated in vacuum. The crude product was purified was by flashy column chromatography using dichloromethane to obtain the product as a tan solid (142.1 mg, 61%). **IR(ATR)/**cm^{-1}: 3056 (w, C=CH), 2922 (w, CH), 2851 (w, CH), 2201 (w, C≡C), 1719 (s, C=O), 1600 (m, C=C), 1527 (m, C=C), 1490 (w, CH), 1438 (w, CH), 1330 (w, CH), 1271 (w, C-O). **^{1}H NMR** (400 MHz, CD_2Cl_2) δ: 7.58 (dd, 2 H, 8 Hz, 2 Hz, ArH), 7.43 (m, 3H, ArH), 7.33 (m, 2H, ArH), 7.27 (br, d, 3 H, ArH, 7.6 Hz), 7.19 (dd, 1H, 9.80 Hz, 2 Hz, H-4), 6.27 (d, 1H, 9.80 Hz, 2 Hz, H-3), 3.92 (d, 2H, 7.40 Hz, $PhCH_2$). **^{13}C NMR** (100 MHz, $CDCl_3$) δ: 161.3 (C=O), 154.2 (C=C), 145.3 (C=C), 142.8 (s, J^{13}C-^{13}C = 79.07 Hz, C=C, C-6, enriched carbon), 138.8 (d, 3.0 Hz, C=C), 131.9 (d, 1.40 Hz, C=C), 130.0 (C=C), 128.8 (C=C), 128.6 (C=C), 126.9 (C=C), 122.3 (d, J^{13}C-^{13}C = 79.7 Hz, C-5, C=C), 120.8 (d, 2.5 Hz,

C=C), 117.5 (d, 5.4 Hz, C=C), 98.6 (d, 19.40Hz, C≡C), 80.78 (d, 116.4 Hz, C≡C), 36.7 (CH_2, Benzylic CH_2). **^{13}C DEPT 135^o NMR** (100 MHz, $CDCl_3$) δ: 145.4 (C=C), 132.0 (C=C), 128.8 (C=C), 127.1 (C=C), 116.9 (C=C), -36.1 (CH_2, Benzylic CH_2). **HRMS-ESI**: m/z 309.0884 (MNa^+, 100%) theoretical 309.0891.

6.15.2 5-Decyl-6-(phenylethynyl)-2-pyrone-^{13}C-6 (169b)

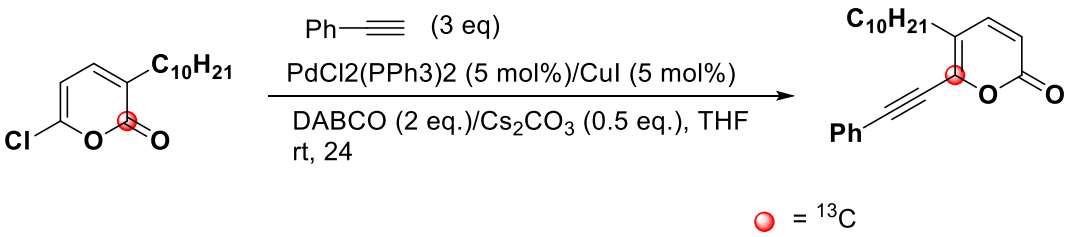

Into an oven-dried Schlenk tube was added 6-chloro-3-decyl-2-pyrone (50.40 mg, 0.1845 mmol, 1eq.), DABCO (109 mg, 2eq.), Cs_2CO_3 (60.11 mg, 0.5eq.), $PdCl_2(PPh_3)_2$ (20 mg, 5 mol%), XPhos (3.52 mg, 4 mol%), and CuI (10 mg, 5 mol%) was attached to a vacuum line and evacuated thrice. Degassed and dried THF (10 mL) was added and phenyl acetylene (56.60 mg, 3.0 mmol, 2eq.) was added slowly and stirred under nitrogen for 24 hours. The crude product was purified by flash CC using 10% EtOAc/n-hexane: 2 ml acetic acid to obtain tan oil (43.30 mg, 69%). **^{1}H NMR** (400 MHz, $CDCl_3$) δ: 7.53 (2 H, dt, 8.0 Hz, 2 Hz, ArH), 7.42-7.35 (3 H, m, ArH), 7.25 (1 H, dd, 9.50 Hz, 7.5 Hz, H-4), 6.27 (1 H, d, 9.50 Hz, 1.0 Hz, H-3), 2.52 (2 H, t, 7Hz, CH_2), 1.53 (2 H, br, CH_2), 1.36-1.17 (14 H, br s, 7CH_2), 0.84 (3 H, t, 7 Hz, CH_3). **^{13}C NMR** (100 MHz, $CDCl_3$) δ: 161.5 (d, 2 Hz, C=O), 155 (s), 154.1 (d, 28.59Hz), 145 (s), 141.8 (s, ^{13}C-C-H = 77.94 Hz, ^{13}C-6), 131.9 (C=C), 129.9 (C=C), 128.6 (C=C), 123.5 (d, J^{13}C-C-H = 77.63 Hz, C-5), 121.1 (d, 2 Hz), 116.8 (d, 5.50 z), 98.2 (s, —C≡**C**—Ph), 81.3 (d, J = 50 Hz, Ph—C≡**C**—), 31.9 (CH_2), 30.3 (CH_2), 29.6 (CH_2), 29.4 (CH_2), 29.0 (CH_2), 22.7 (CH_2), 14.2 (CH_3)**. ^{13}C DEPT-135^o**: 145.7 (C=C), 131.9 (C=C), 129.9 (C=C), 128.7 (C=C), 116.9 (C=C), -32.0 (CH_2), -30.4 (CH_2), -29.7 (CH_2), -29.6 (CH_2), -29.4 (CH_2), -29.4 (CH_2), -29.1 (CH_2), -22.7 (CH_2), 14.2 (CH_3)**. HRMS-EI**, m/z 338.2187 (MH^+, 73%) theoretical 338.2201, 360.2033 (MNa^+, 100%) theoretical 360.2021. (MH^+ + 1) and (MNa^++1) peaks indicate a 99.8% enrichment on the C-6 carbon, so this optimized procedure leads to the

synthesis of ^{13}C-isotopically labelled 2-pyrone compounds with an enrichment required for NMR assays.

6.16 Experimental Procedure for Protein binding Studies

6.16.1 Binding specificity by STD experiment

STD experiments were carried out on a series of samples over 5 minutes. These samples reflected solutions that contained 10 µM trypsin, a serine protease, 10% D 2 O. A total volume of 750 µl was used for each sample and phosphate buffer, 50mM pH 6.4, added such that there was a final DMSO concentration of 2% v/v. STD measurements were then made on a Bruker 700 MHz Avance spectrometer with 5 mm triple resonance cryoprobe. These ^{1}H NMR spectra were acquired at 25 ºC with a delay time of 10 µs using the Bruker STDDFFESGP.3 pulse program. In the on-resonance experiment, irradiation was applied to protein resonances (-0.6 ppm), whereas in the off-resonance experiment, the irradiation point is shifted to 30 ppm, such that no NMR resonances are perturbed. A total saturation time of 2 seconds and a suppression of water signal for 20 ms was employed. The contrasting WaterLOGSY experiment was completed on one sample for comparison purposes. It involves the selective perturbation of the bulk water magnetization (between 4.6 and 4.7 ppm) for time 1.5 seconds.

6.16.2 STD experiment of 3-methyl-6-chloro-2-pyrone, 128a.

A simple STD binding experiment was conducted by adding trypsin, from bovine pancreas, purchased from Sigma Aldrich UK. Each sample contained 10 µM of the protein, 3-methyl-6-chloro-2-pyrone at a 115 µM concentration and 11.07% D_2O. A total volume of 542 µL was used for each sample that was made up with phosphate buffer 60 µL pH 6.4, containing DMSO at a level 2.21 %.

6.16.3 STD experiment of 3/5-benzyl-6-chloro-2-pyrone, 128/129d.

An analogous sample of 3-benzyl-6-chloro-2-pyrone at a 116 µM final concentration was prepared in H_2O/D_2O as solvent.

6.16.4 STD experiment of 3/5-decyl-6-chloro-2-pyrone, 128/129e.

An analogous sample of 3-decyl-6-chloro-2-pyrone at 115 µM final concentration was prepared in H_2O/D_2O as solvent.

6.16.5 STD experiment of 3/5-decyl-6-chloro-2-pyrone-^{13}C-2, 167/168b.

An analogous sample of 3-methyl-6-chloro-2-pyrone at a 115 µM final concentration was prepared in H_2O/D_2O as solvent.

6.16.6 STD experiment of 3-benzyl-6-chloro-2-pyrone-^{13}C-2, 167/168a.

An analogous sample of 3-methyl-6-chloro-2-pyrone at a 115 µM final concentration was prepared in H_2O/D_2O as solvent.

6.17 Experimental Procedure for Signal Enhancement studies

6.17.1 General procedures: The hydrogenation catalyst used here is $[Rh(COD)(PPh_2)_2C_3H_6]BF_4$. Solutions of the rhodium catalyst (ca. 5.55 mM; ca. 2.5 mg of catalyst in 500 µL of deuterated solvent) in a Young's tap topped NMR tubes were added to a ca. 4-fold excess of the test compounds (ca. 3 mg; ca. 0.31 M) and then reacted with para-H_2 (3-3.5 atm.) at room temperature.

6.17.2 NMR spectroscopy: All standard NMR spectra were recorded on Jeol 400 spectrometers, unless otherwise stated, in NMR tubes fitted with Young's tap. All ^{1}H and ^{13}C chemical shifts are reported in ppm (δ) relative to tetramethylsilane and referenced using the chemical shifts of residual protio solvent resonances ($CDCl_3$, δ 5.30). Using the shake and drop method. NMR spectra were recorded on a Bruker WH-400 spectrometer operating at 400 MHz for ^{1}H and 100 MHz for ^{13}C.

Appendix 1: X-ray crystallographic data for compounds **128d** and **169d**.

Table 11: Summary of X-ray structure for **128d** and **169d**

Identification code	**169d**(ijsf1707)	**128d**(ijsf1702)
Empirical Formula	$C_{20}H_{14}O_2$	$C_{12}H_9ClO_2$
Formula weight	286.31	220.64
Temperature/K	109.95(10)	110.05(10)
Crystal System	monoclinic	orthorhombic
Space group	$P2_1/c$	$Pca2_1$
a/Å	10.2099(4)	13.27321(11)
b/Å	10.9983(4)	6.11486(5)
c/Å	13.5108(5)	25.2027(2)
α/°	90	90
β/°	106.713(4)	90
γ/°	90	90
Volume/Å^3	1453.06(10)	2045.55(3)
Z	4	8
P_{calc} mg/mm^2	1.309	1.433
Mm/mm^{-1}	0.665	3.102
F (000)	600.0	912.0
Crystal Size/mm^3	0.217 × 0.143 × 0.08	0.352 × 0.18 × 0.123
Radiation	CuKα (λ = 1.54184)	CuKα (λ = 1.54184)

2^{θ}range for data collection	9.044 to 134.142	7.014 to 142.352
Index Ranges	-9 ≤ h ≤ 12, -9 ≤ k ≤ 13, -16 ≤ l ≤ 15	-16 ≤ h ≤ 15, -7 ≤ k ≤ 7, -30 ≤ l ≤ 25
Reflections collected	4900	9992
Independent Reflections	2584 [R_{int} = 0.0174, R_{sigma} = 0.0266]	3227 [R_{int} = 0.0142, R_{sigma} = 0.0125]
Data/restraints/parameters	2584/0/199	3227/1/271
Goodness-of-fit on F^2	1.035	1.074
Final R indexes [I≥2δ (I)]	R_1 = 0.0354, wR_2 = 0.0865	R_1 = 0.0218, wR_2 = 0.0595
Final R indexes [all data]	R_1 = 0.0435, wR_2 = 0.0921	R_1 = 0.0218, wR_2 = 0.0596

Appendix 2: ^{1}H and ^{13}C NMR data

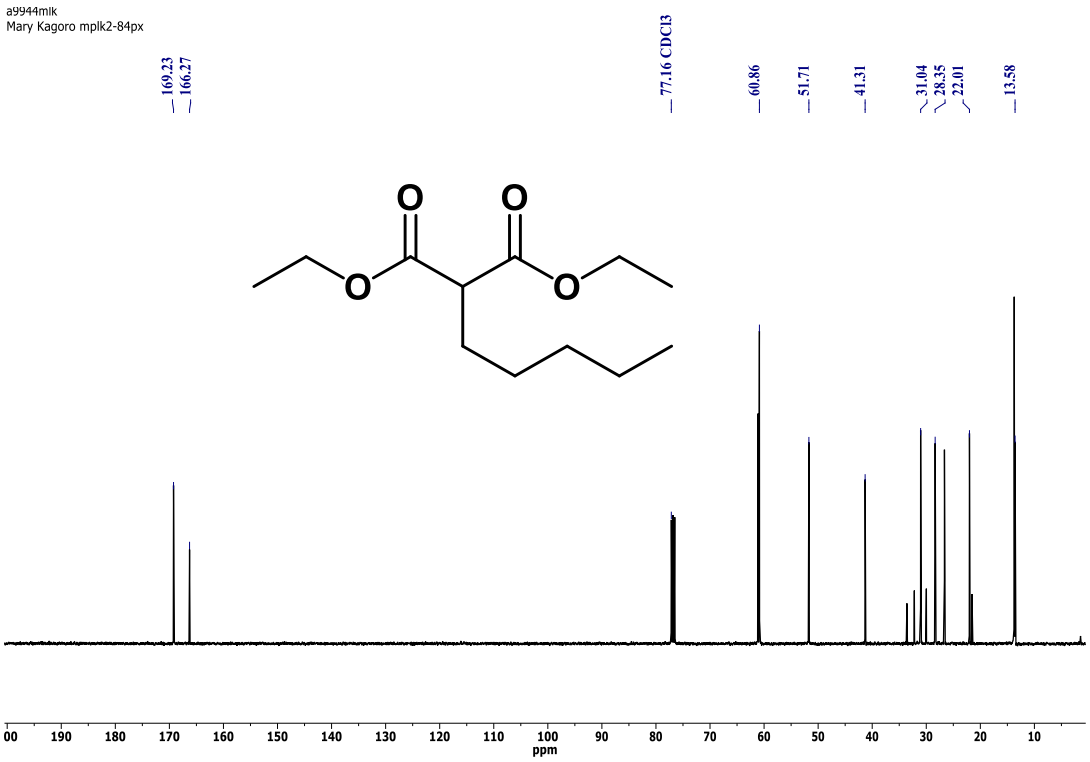

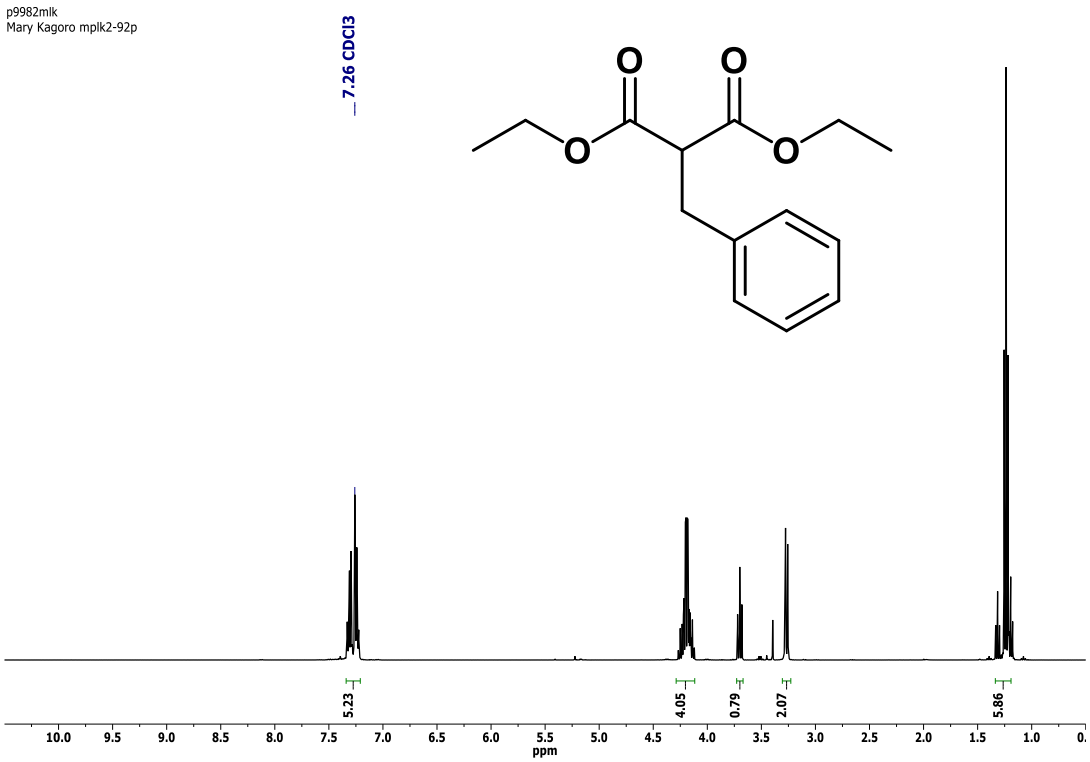

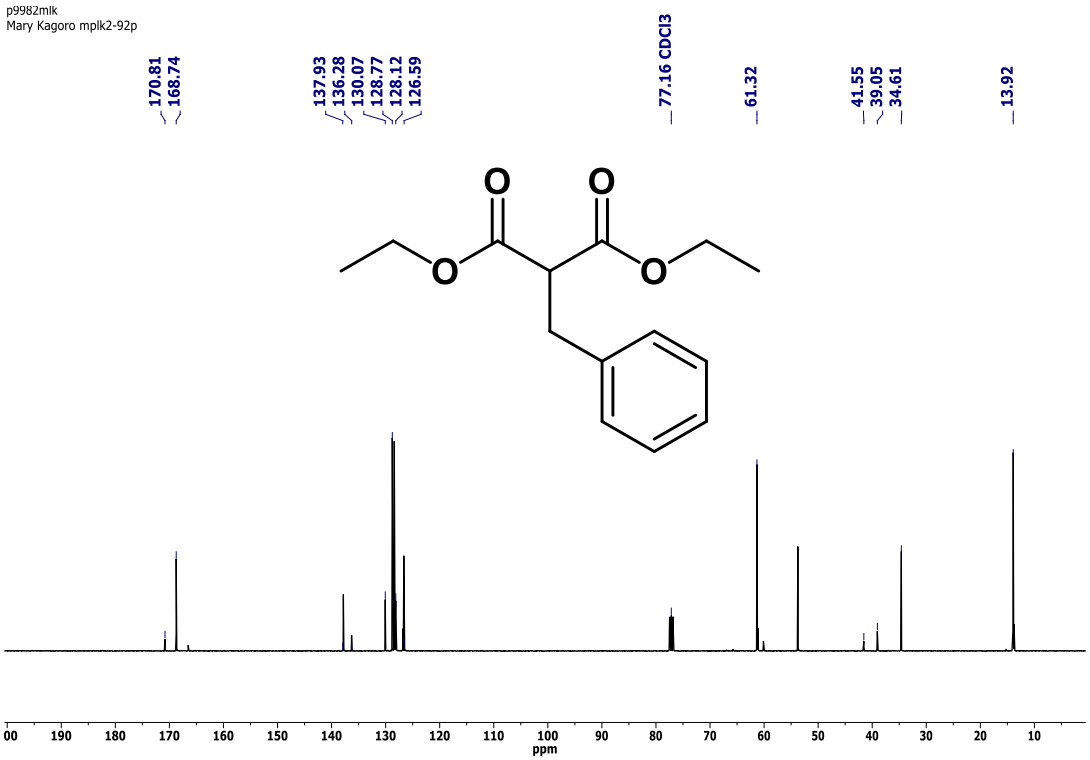
p9982mlk
Mary Kagoro mplk2-92p
170.81
168.74
137.93
136.28
130.07
128.77
128.12
126.59
77.16 CDCl3
61.32
41.55
39.05
34.61
13.92
O
O
O
O
ppm

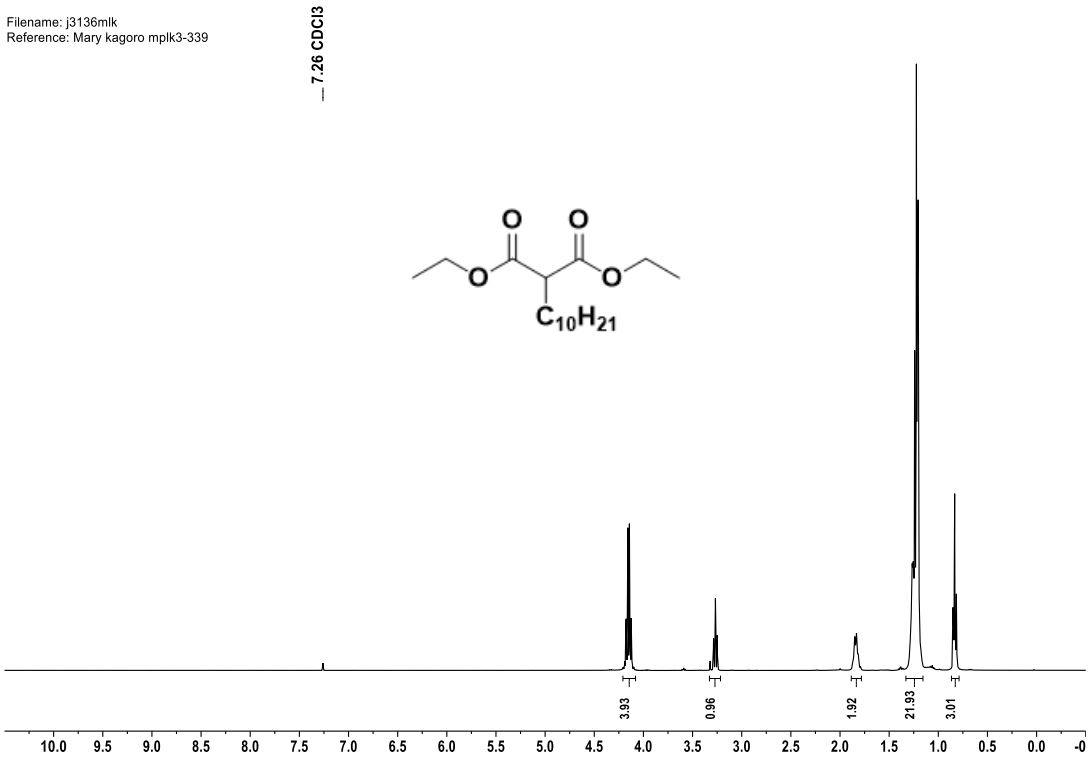
Filename: j3136mlk
Reference: Mary kagoro mplk3-339
7.26 CDCl3
O
O
O
O
C10H21
3.93
0.96
1.92
21.93
3.01

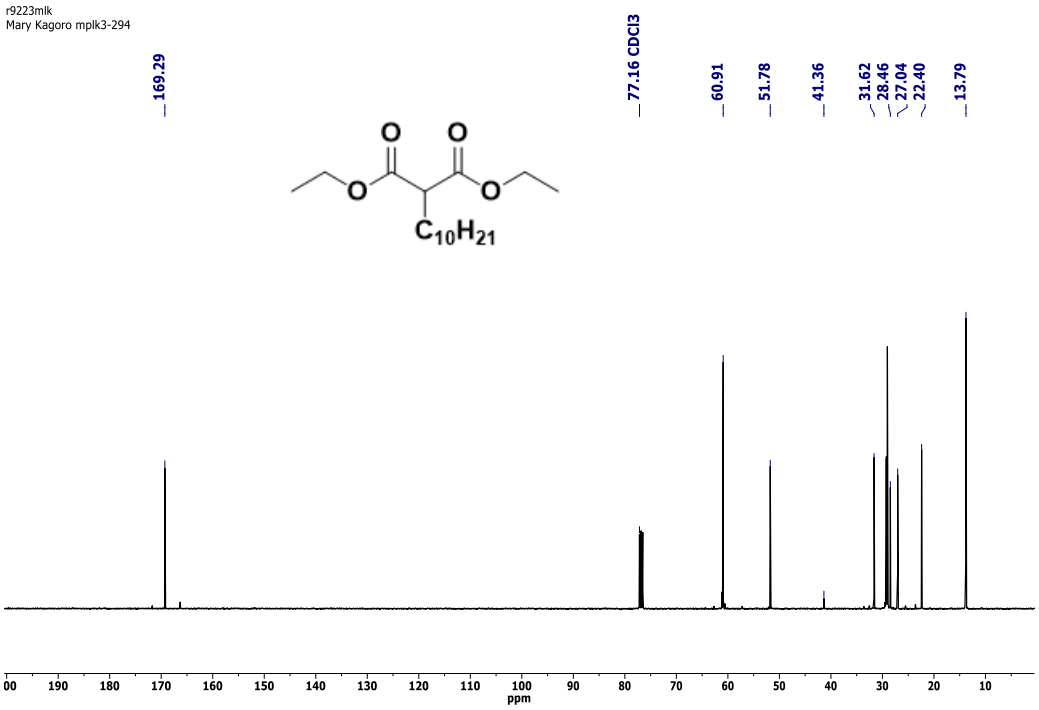
r9223mlk
Mary Kagoro mplk3-294
169.29
77.16 CDCl3
60.91
51.78
41.36
31.62
28.46
27.04
22.40
13.79
O
O
O
O
C10H21
ppm

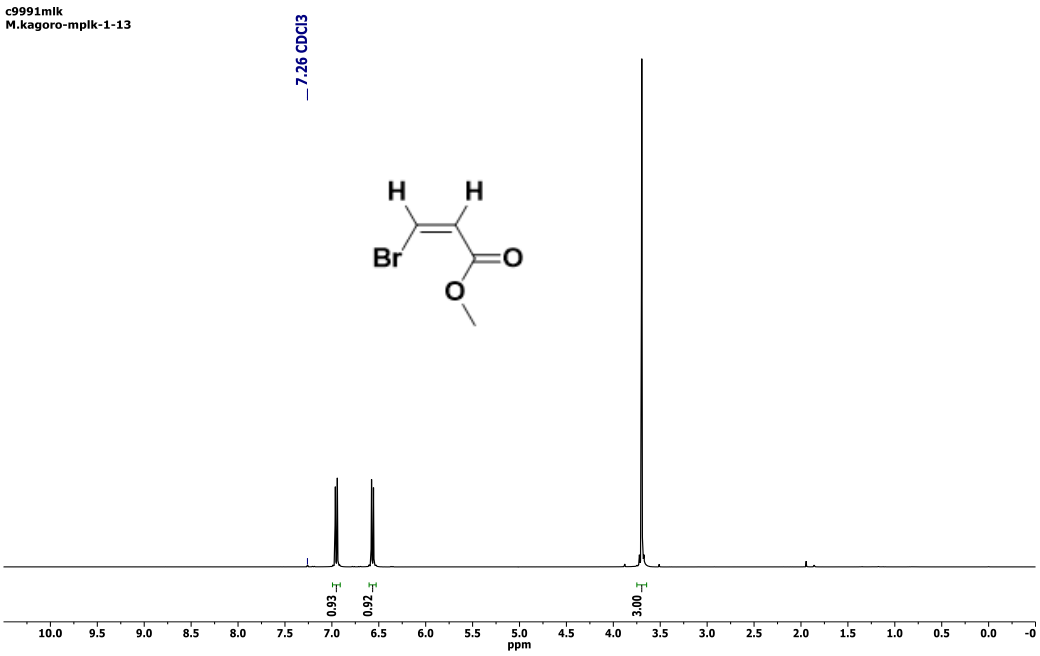
c9991mlk
M.kagoro-mplk-1-13
7.26 CDCl3
H
H
Br
O
O
0.93
0.92
3.00
ppm

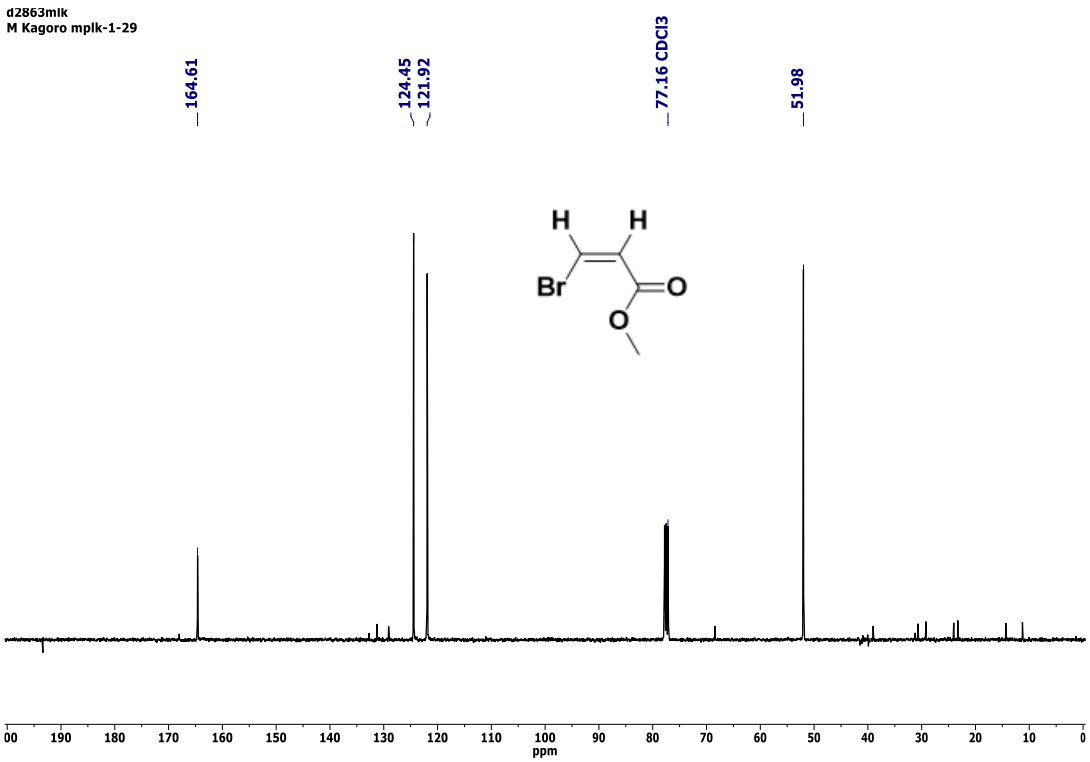
d2863mlk
M Kagoro mplk-1-29
164.61
124.45
121.92
77.16 CDCl3
51.98
H
H
Br
O
O
00 190 180 170 160 150 140 130 120 110 100 90 80 70 60 50 40 30 20 10 0
ppm

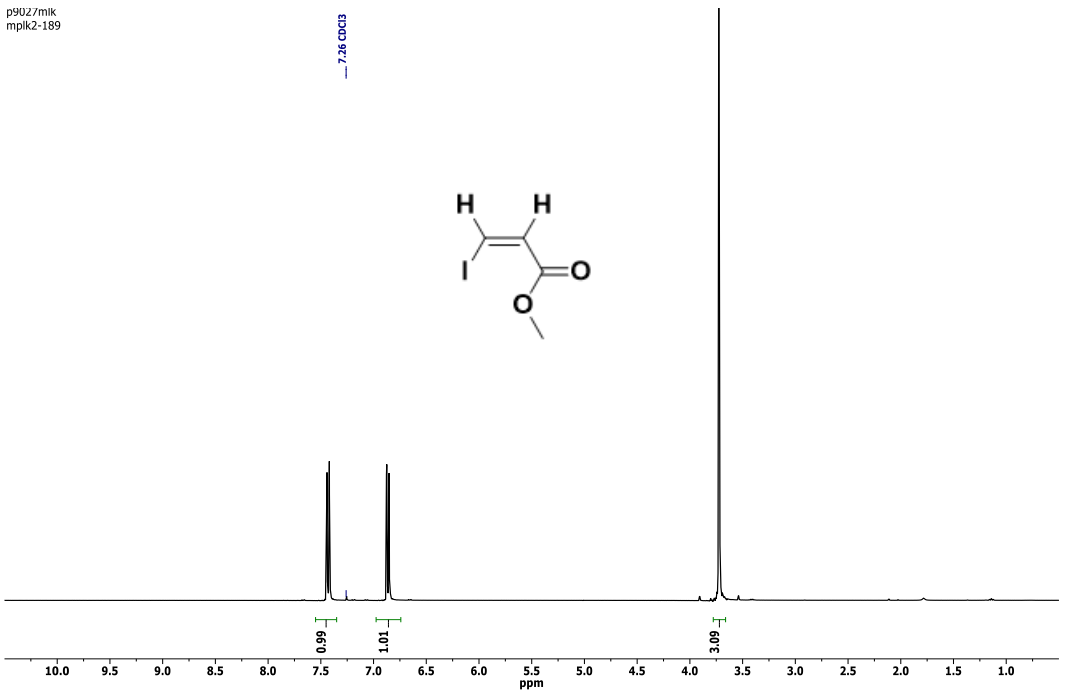
p9027mlk
mplk2-189
7.26 CDCl3
H
H
I
O
O
0.99
1.01
3.09
10.0 9.5 9.0 8.5 8.0 7.5 7.0 6.5 6.0 5.5 5.0 4.5 4.0 3.5 3.0 2.5 2.0 1.5 1.0
ppm

r3949mlk
Mary Kagoro mplk2-232

164.88
129.52
95.59
51.76

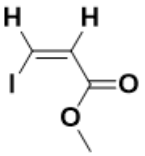

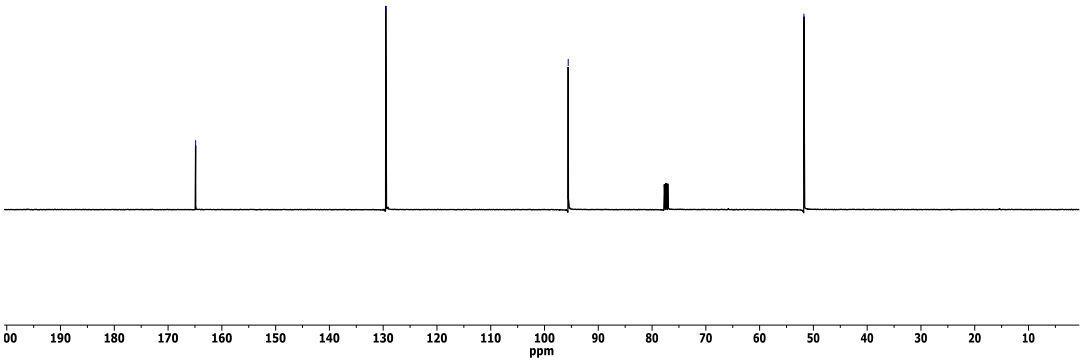

p0786mlk
Mary Kagoro mplk2-98f1

169.89
166.63
144.81
122.75
120.95
77.16 CDCl3
62.23
60.11
52.13
35.71
32.25
24.21
22.65
14.26

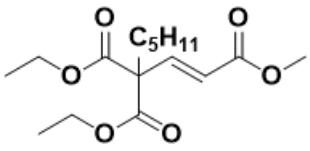

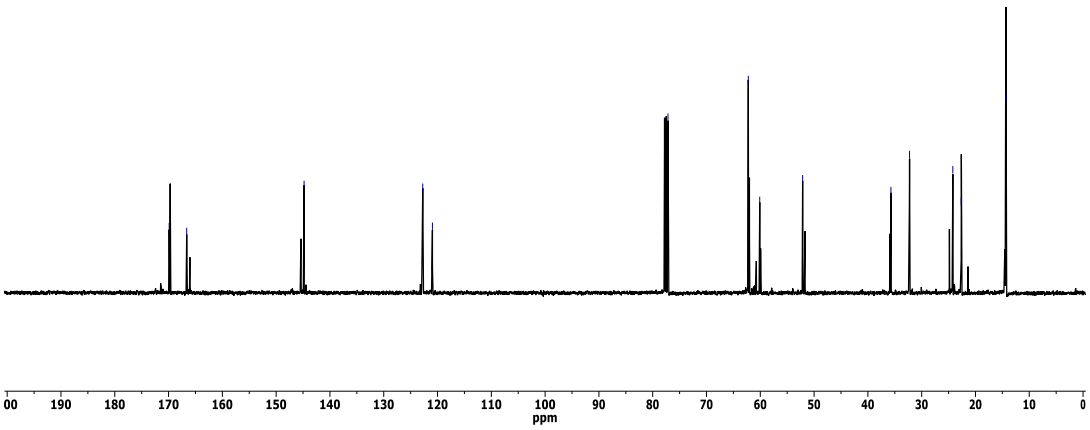

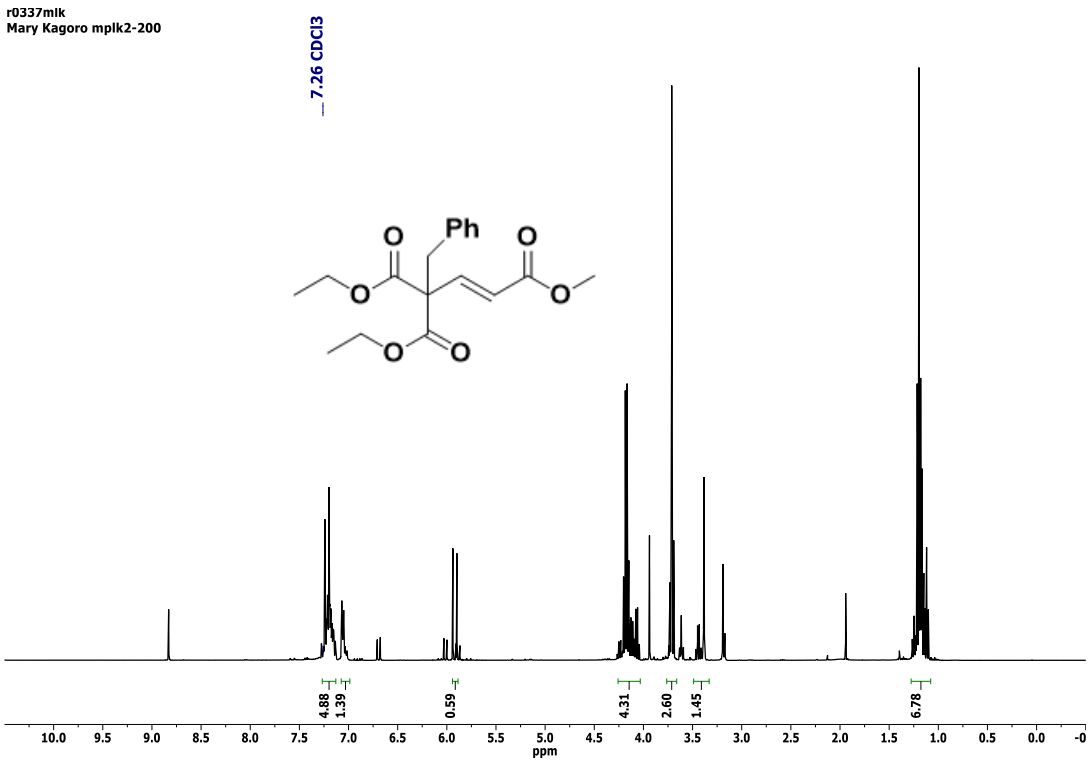
r0337mlk
Mary Kagoro mplk2-200
7.26 CDCl3
Ph
O
O
O
O
O
O
4.88
1.39
0.59
4.31
2.60
1.45
6.78
10.0 9.5 9.0 8.5 8.0 7.5 7.0 6.5 6.0 5.5 5.0 4.5 4.0 3.5 3.0 2.5 2.0 1.5 1.0 0.5 0.0 -0
ppm

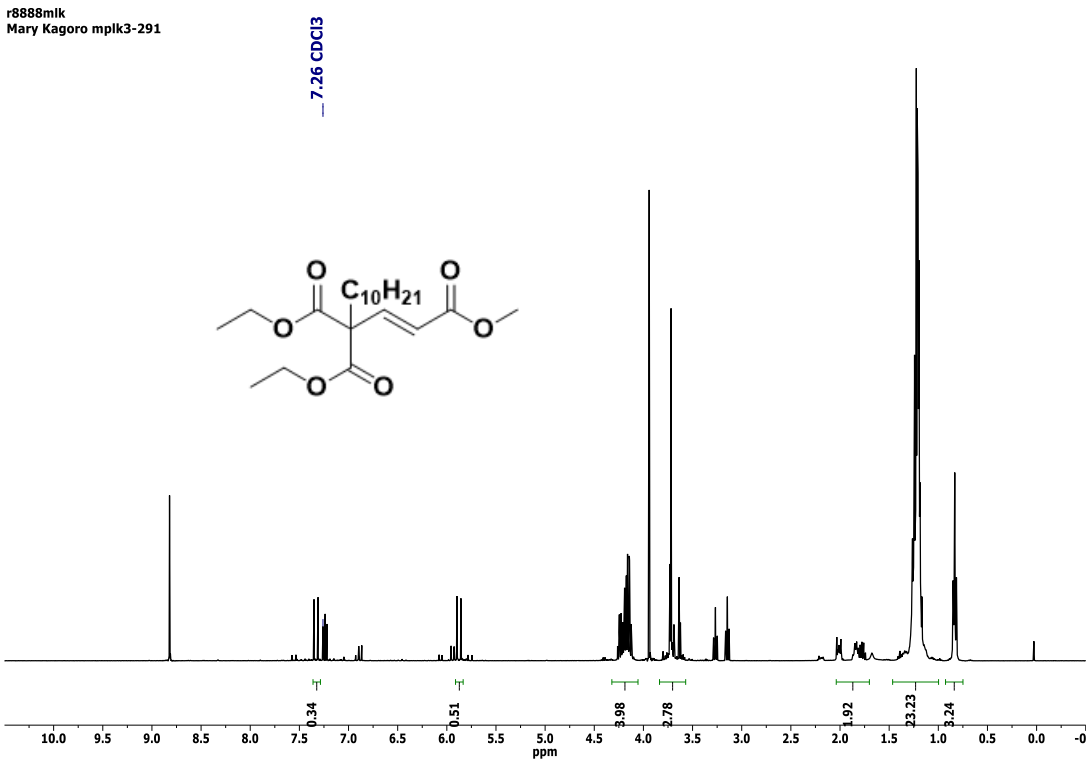
r8888mlk
Mary Kagoro mplk3-291
7.26 CDCl3
C10H21
O
O
O
O
O
O
0.34
0.51
3.98
2.78
1.92
23.23
3.24
10.0 9.5 9.0 8.5 8.0 7.5 7.0 6.5 6.0 5.5 5.0 4.5 4.0 3.5 3.0 2.5 2.0 1.5 1.0 0.5 0.0 -0
ppm

r8888mlk
Mary Kagoro mplk3-291

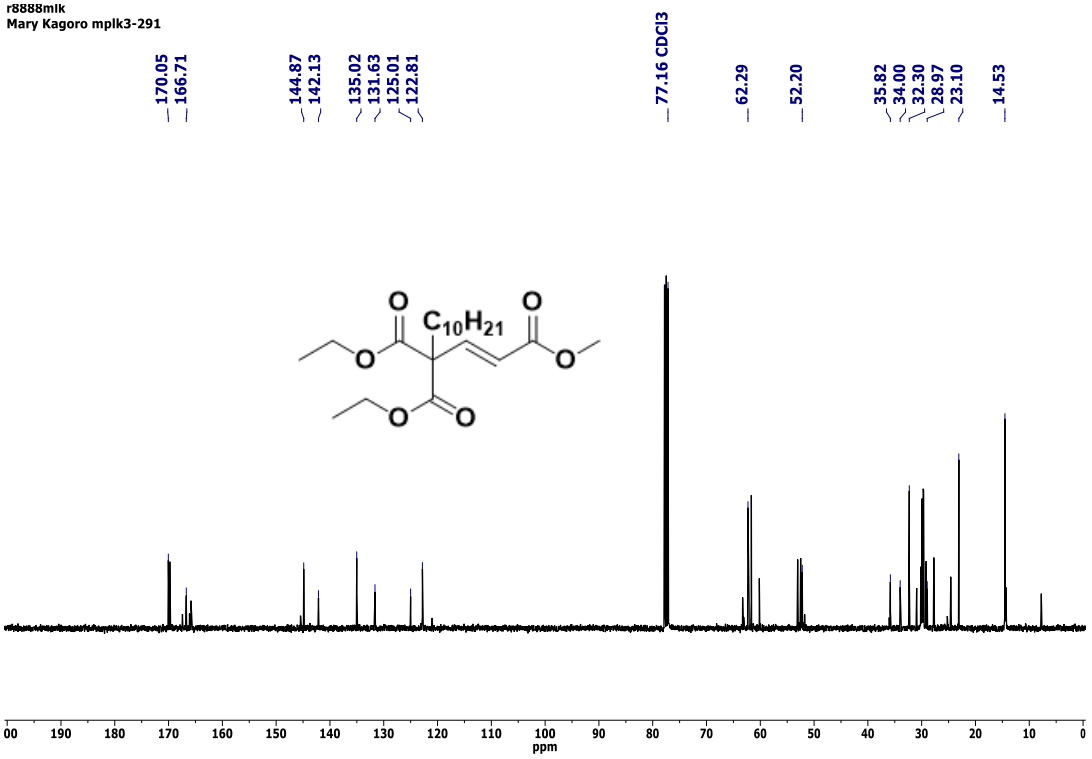

j1867mlk
Mary Kagoro mplk3-325p

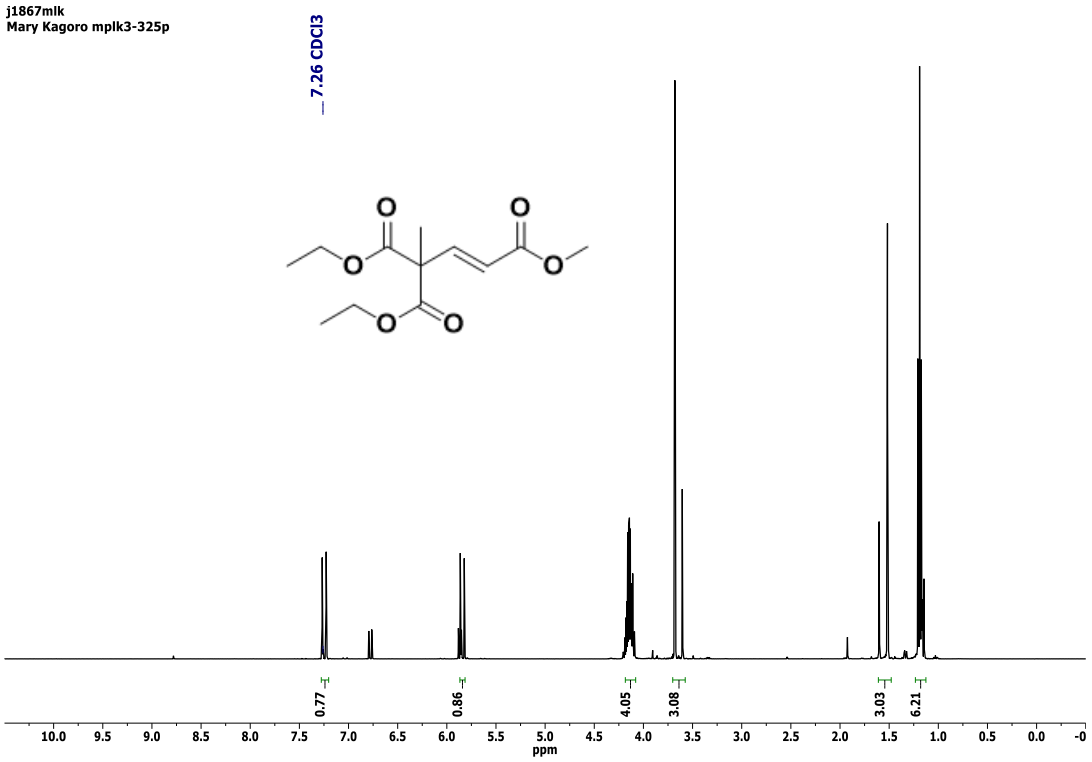

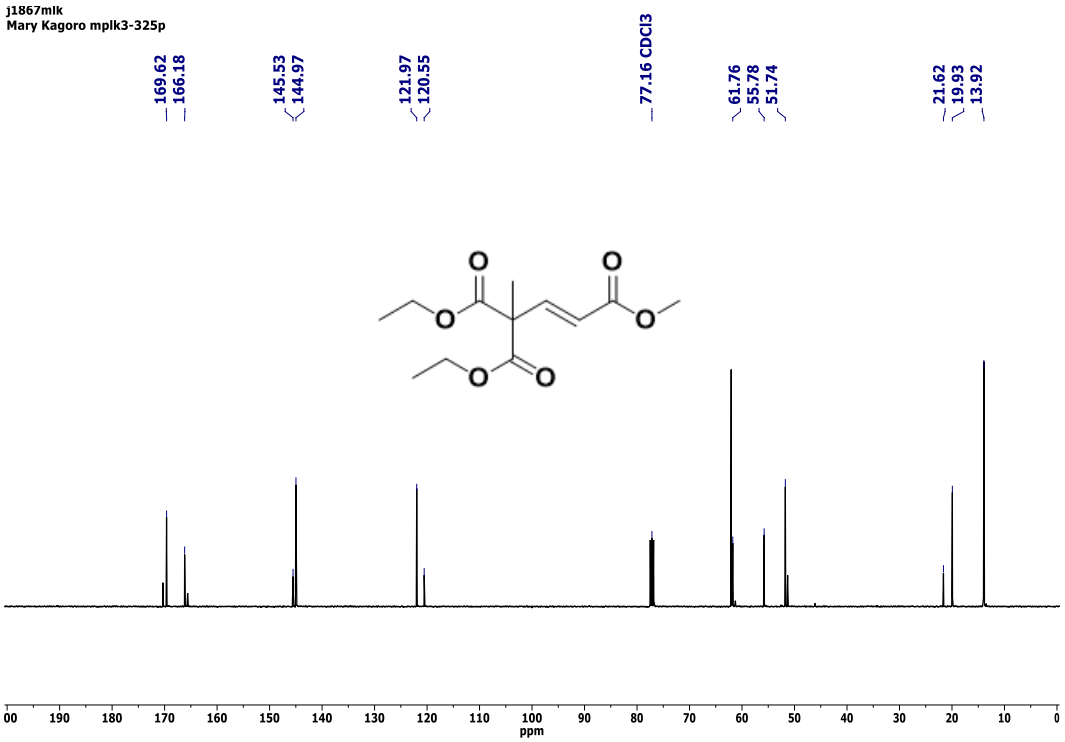
j1867mlk
Mary Kagoro mplk3-325p
169.62
166.18
145.53
144.97
121.97
120.55
77.16 CDCl3
61.76
55.78
51.74
21.62
19.93
13.92
O
O
O
O
O
O
ppm

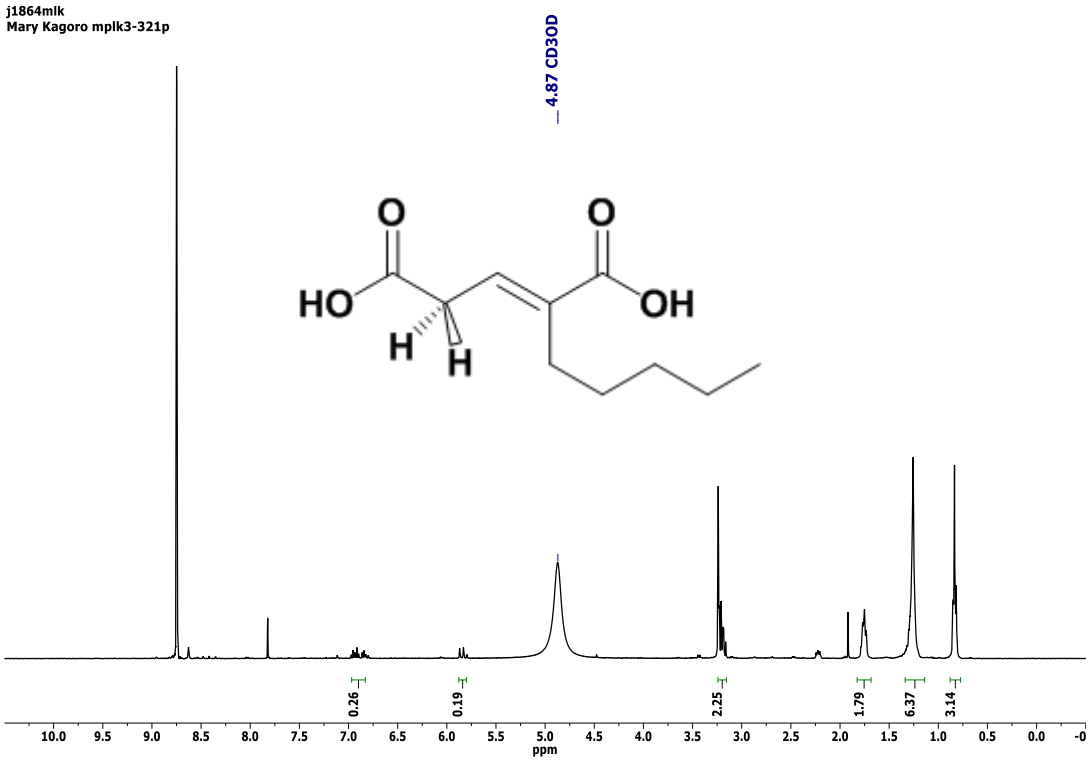
j1864mlk
Mary Kagoro mplk3-321p
4.87 CD3OD
O
O
HO
OH
H
H
0.26
0.19
2.25
1.79
6.37
3.14
ppm

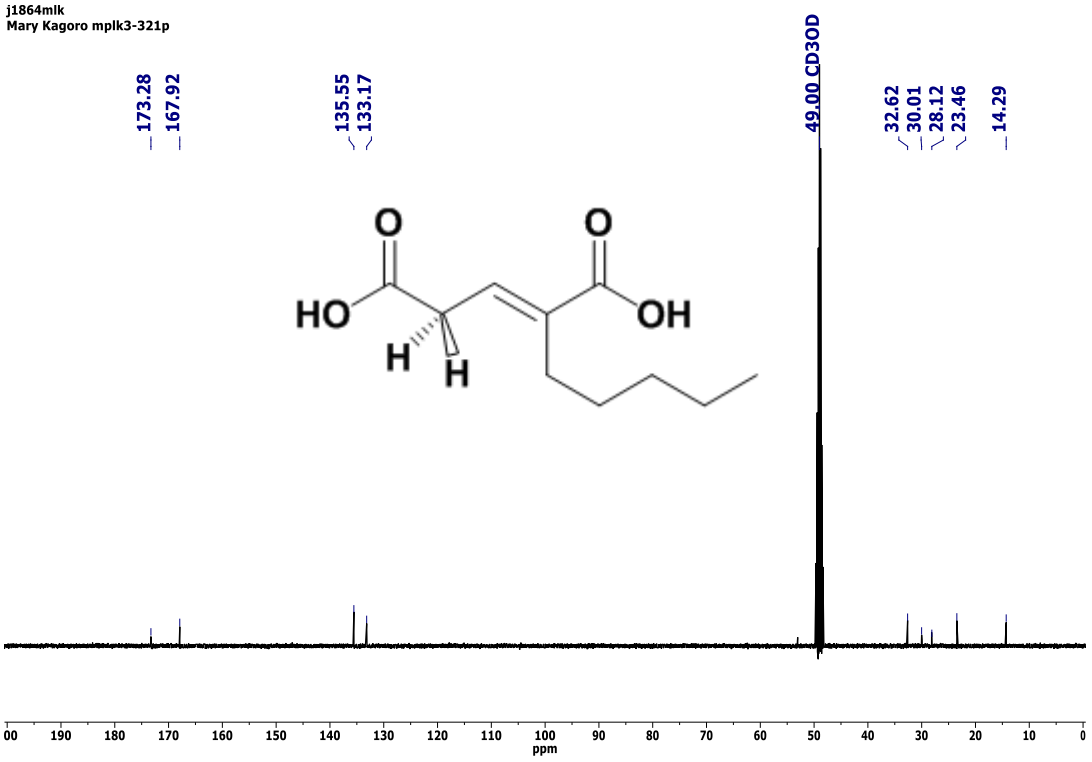
j1864mlk
Mary Kagoro mplk3-321p
173.28
167.92
135.55
133.17
49.00 CD3OD
32.62
30.01
28.12
23.46
14.29
HO
O
O
OH
H
H
ppm

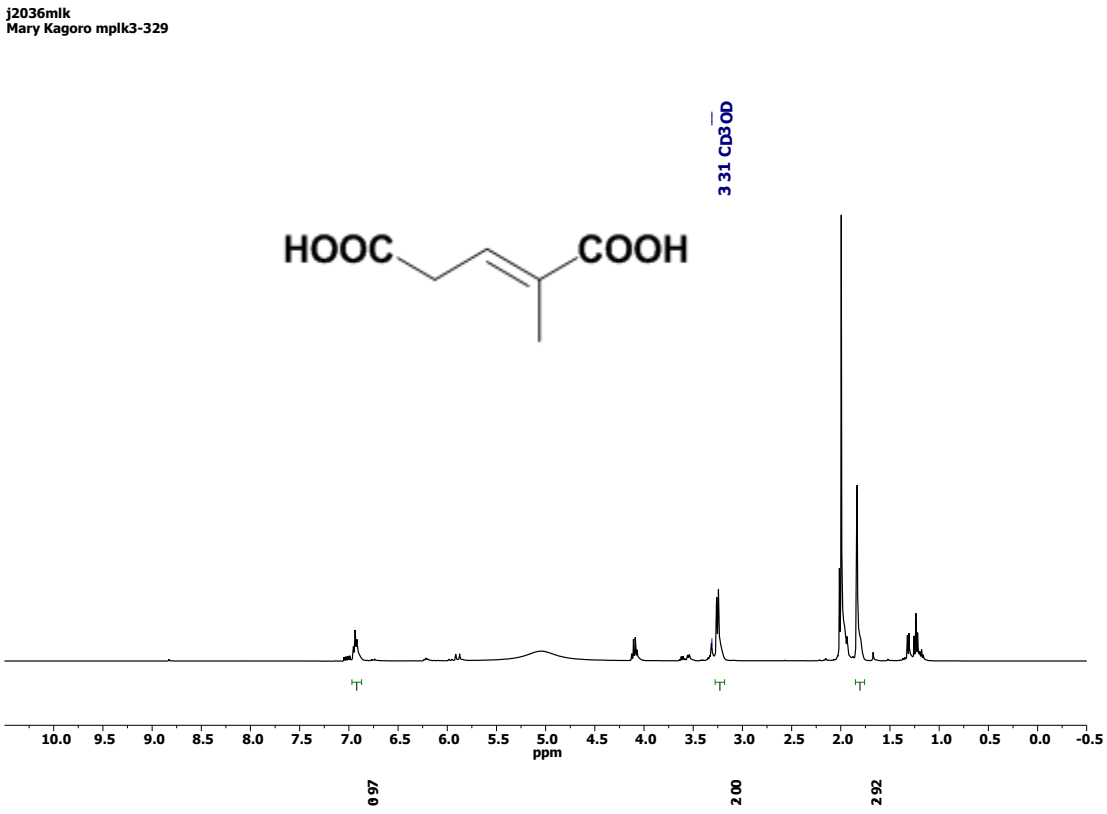
j2036mlk
Mary Kagoro mplk3-329
3.31 CD3OD
HOOC
COOH
ppm
0.97
2.00
2.92

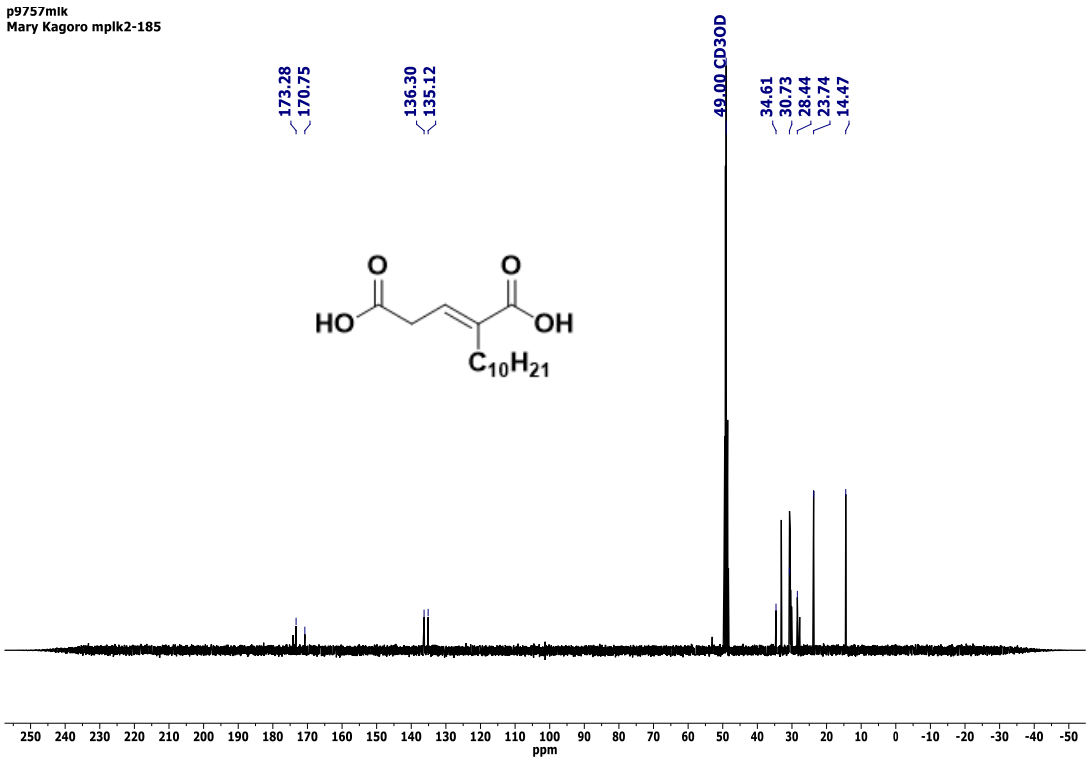
p9757mlk
Mary Kagoro mplk2-185
173.28
170.75
136.30
135.12
49.00 CD3OD
34.61
30.73
28.44
23.74
14.47
HO
O
O
OH
C10H21
250 240 230 220 210 200 190 180 170 160 150 140 130 120 110 100 90 80 70 60 50 40 30 20 10 0 -10 -20 -30 -40 -50
ppm

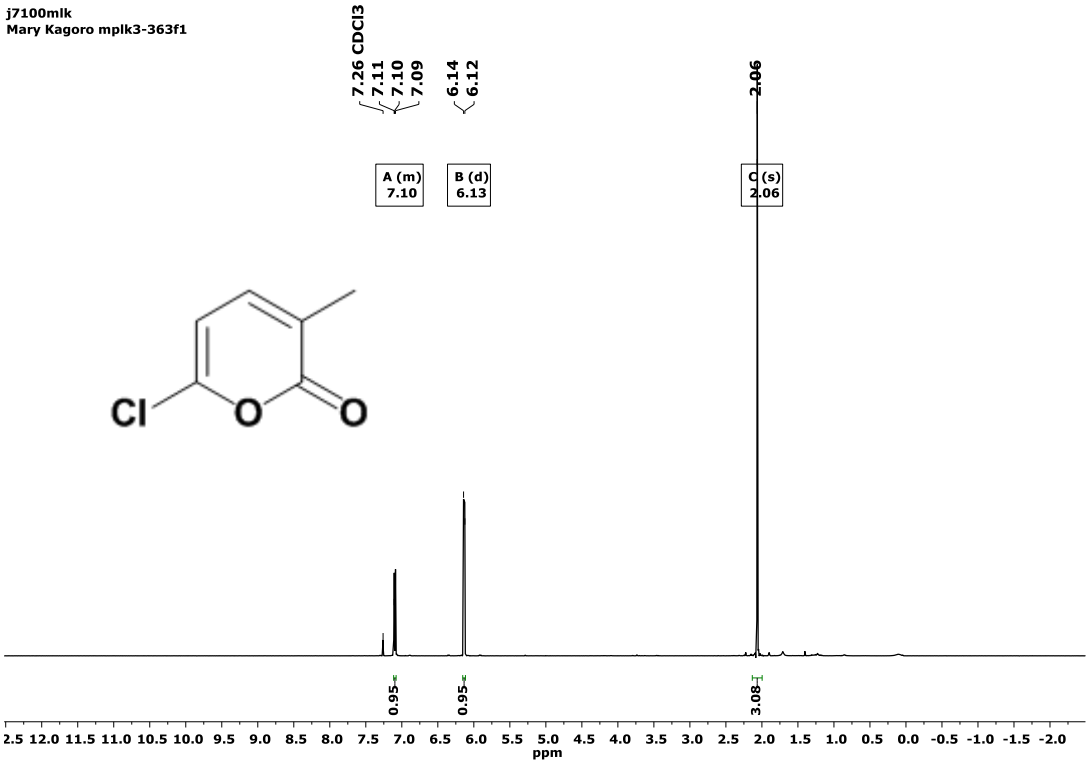
j7100mlk
Mary Kagoro mplk3-363f1
7.26 CDCl3
7.11
7.10
7.09
6.14
6.12
2.06
A (m)
7.10
B (d)
6.13
C (s)
2.06
Cl
O
O
0.95
0.95
3.08
2.5 12.0 11.5 11.0 10.5 10.0 9.5 9.0 8.5 8.0 7.5 7.0 6.5 6.0 5.5 5.0 4.5 4.0 3.5 3.0 2.5 2.0 1.5 1.0 0.5 0.0 -0.5 -1.0 -1.5 -2.0
ppm

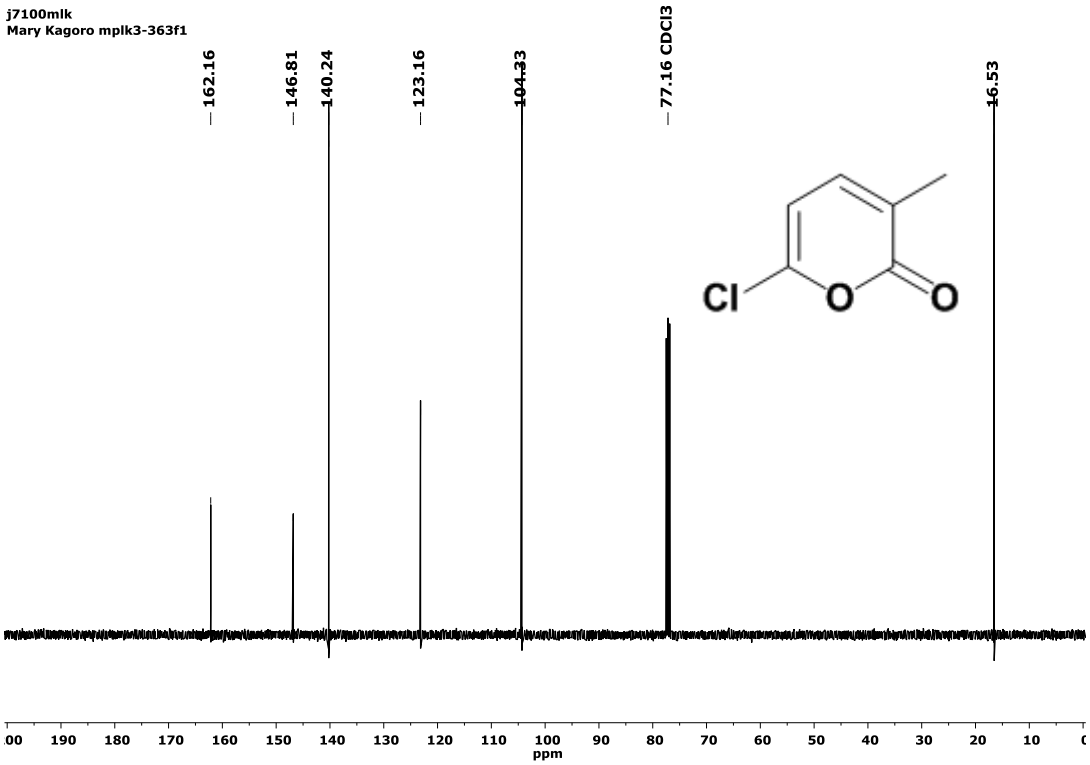
j7100mlk
Mary Kagoro mplk3-363f1
162.16
146.81
140.24
123.16
104.33
77.16 CDCl3
16.53
Cl
O
O
ppm

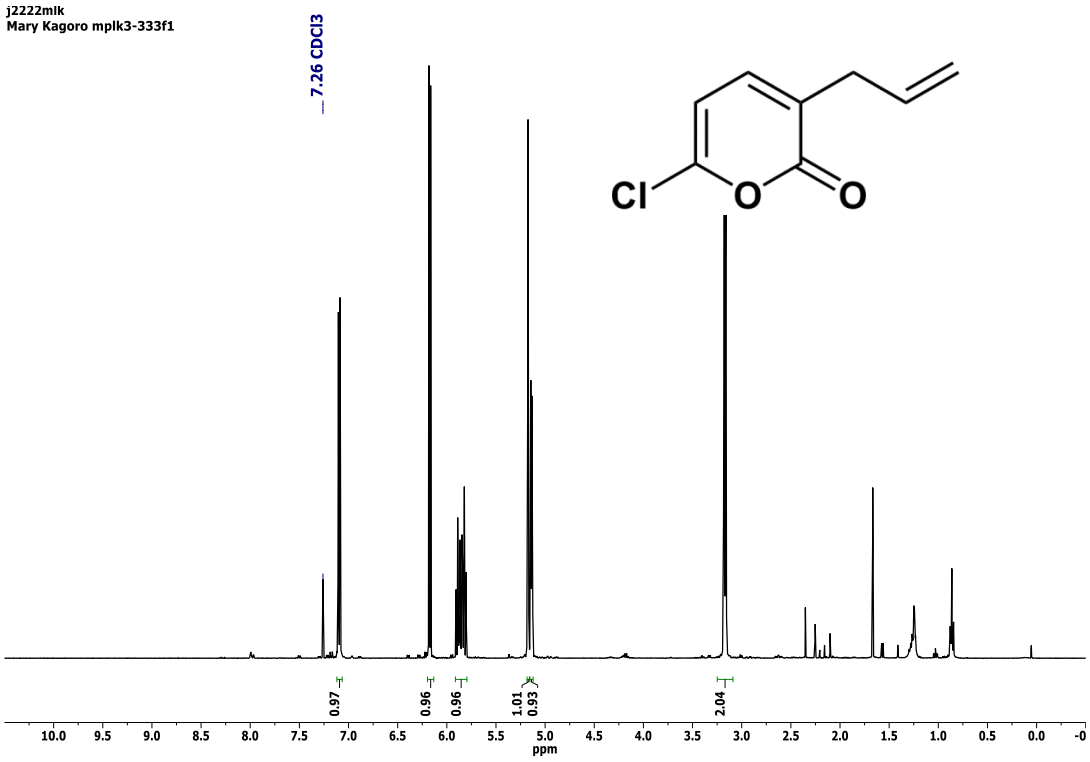
j2222mlk
Mary Kagoro mplk3-333f1
7.26 CDCl3
Cl
O
O
0.97
0.96
0.96
1.01
0.93
2.04
ppm

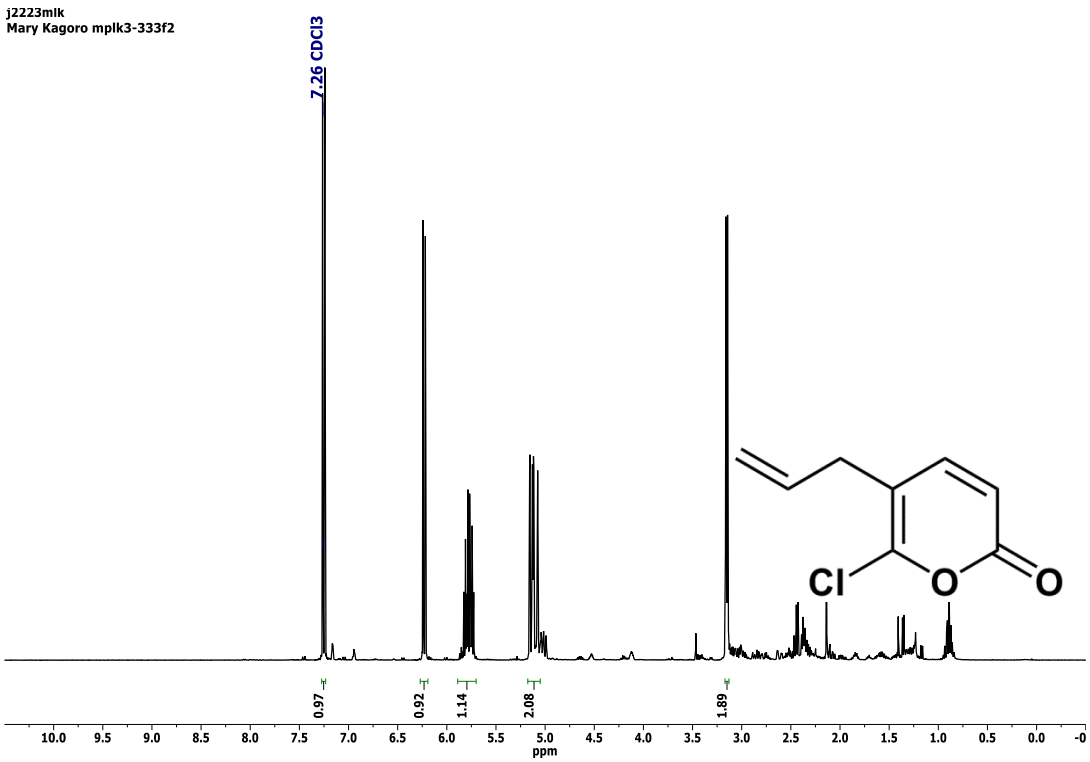
j2223mlk
Mary Kagoro mplk3-333f2
7.26 CDCl3
Cl
O
O
0.97
0.92
1.14
2.08
1.89
10.0 9.5 9.0 8.5 8.0 7.5 7.0 6.5 6.0 5.5 5.0 4.5 4.0 3.5 3.0 2.5 2.0 1.5 1.0 0.5 0.0 -0
ppm

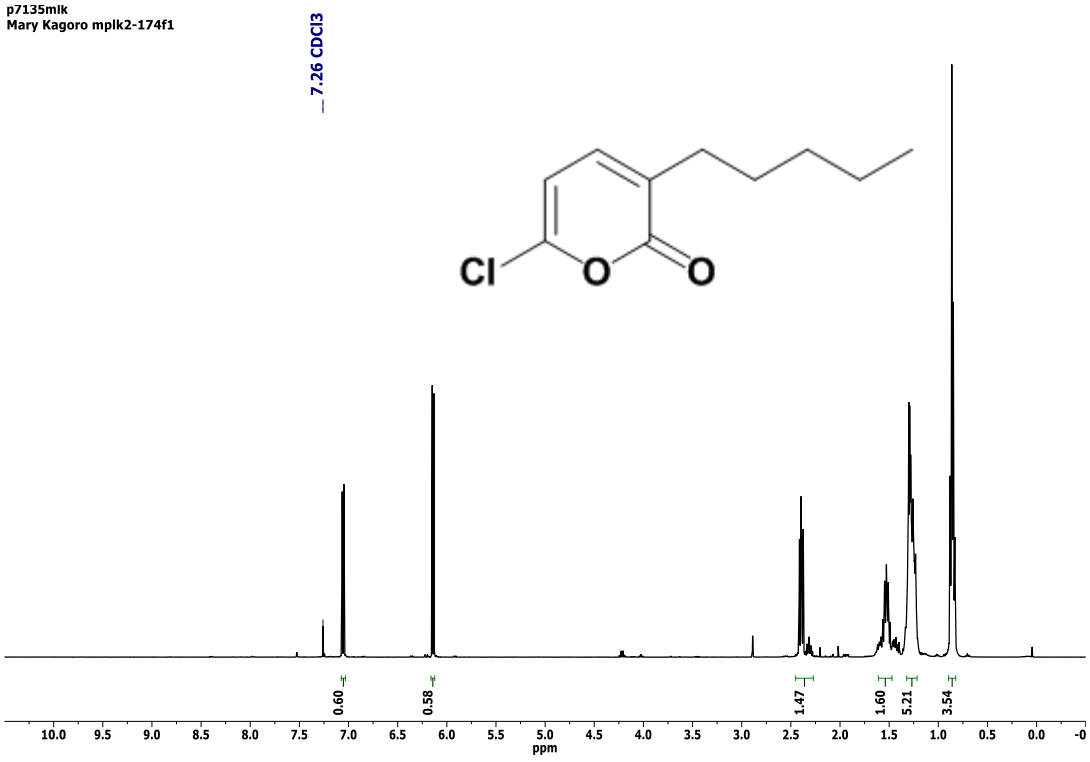
p7135mlk
Mary Kagoro mplk2-174f1
7.26 CDCl3
Cl
O
O
0.60
0.58
1.47
1.60
5.21
3.54
10.0 9.5 9.0 8.5 8.0 7.5 7.0 6.5 6.0 5.5 5.0 4.5 4.0 3.5 3.0 2.5 2.0 1.5 1.0 0.5 0.0 -0
ppm

p7135mlk
Mary Kagoro mplk2-174f1

161.80
146.75
139.46
127.33
104.29
31.40
30.34
27.10
22.71
14.02

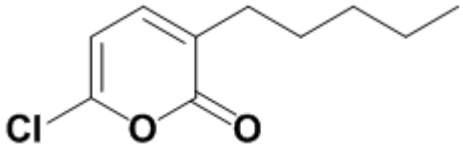

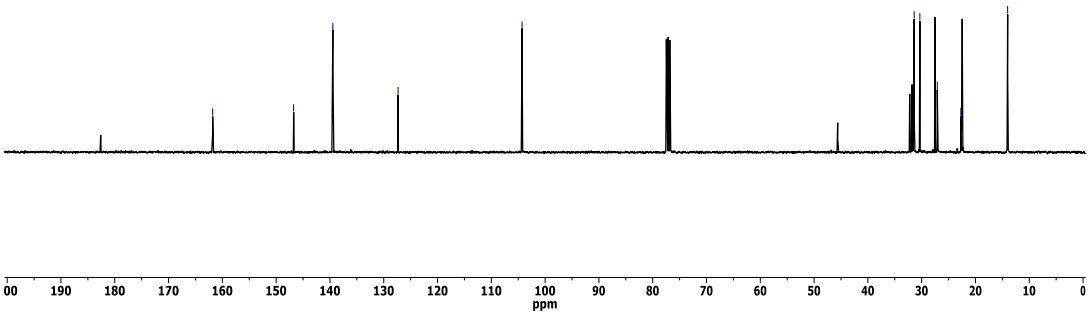

j7101mlk
Mary Kagoro mplk3-361f2

7.26 CDCl3

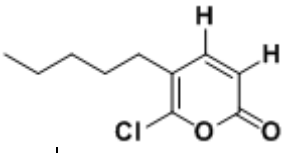

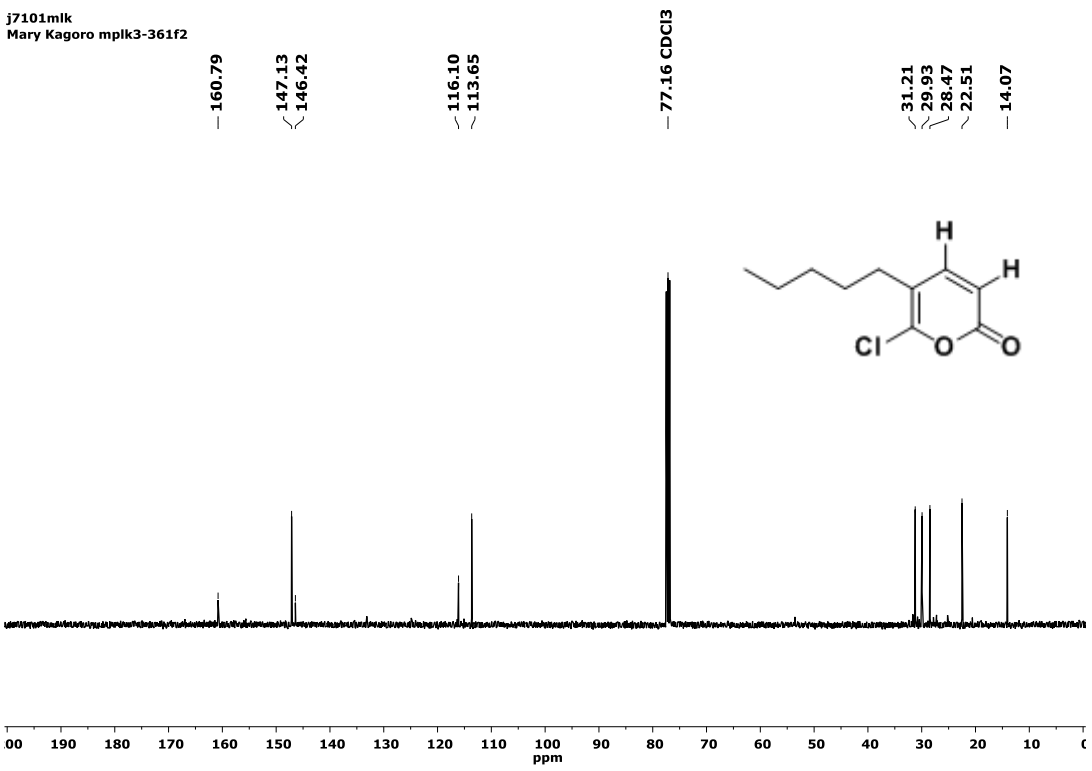
j7101mlk
Mary Kagoro mplk3-361f2
160.79
147.13
146.42
116.10
113.65
77.16 CDCl3
31.21
29.93
28.47
22.51
14.07
H
H
Cl
O
O
ppm

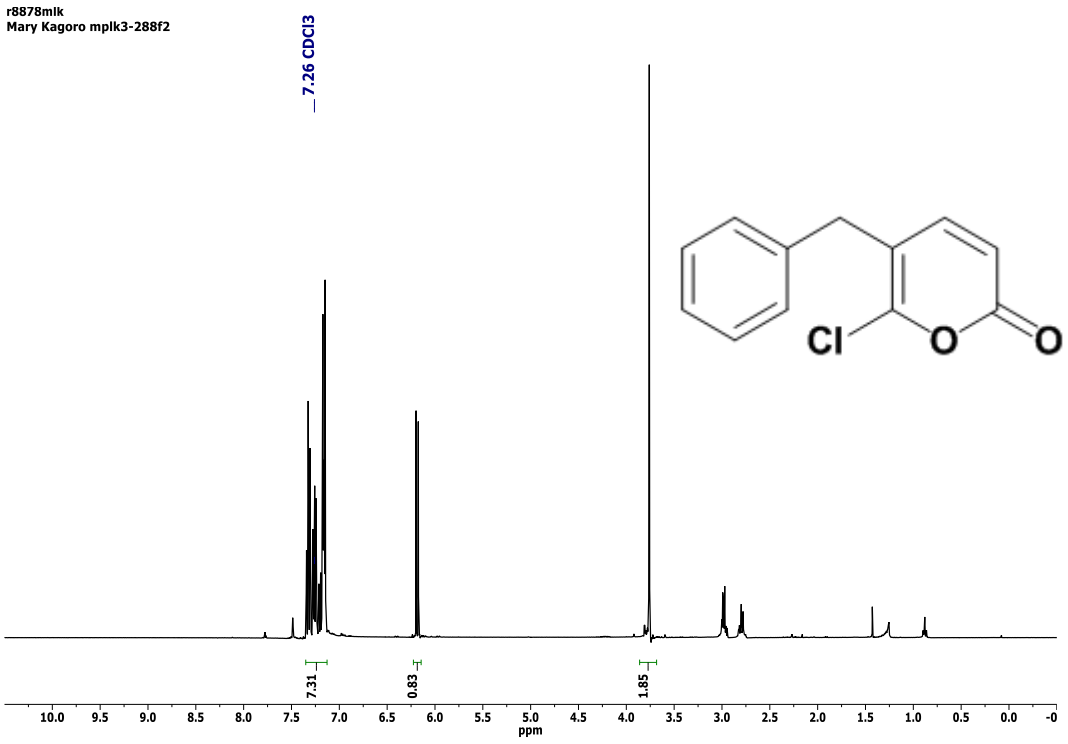
r8878mlk
Mary Kagoro mplk3-288f2
7.26 CDCl3
Cl
O
O
7.31
0.83
1.85
ppm

r8878mlk
Mary Kagoro mplk3-288f2

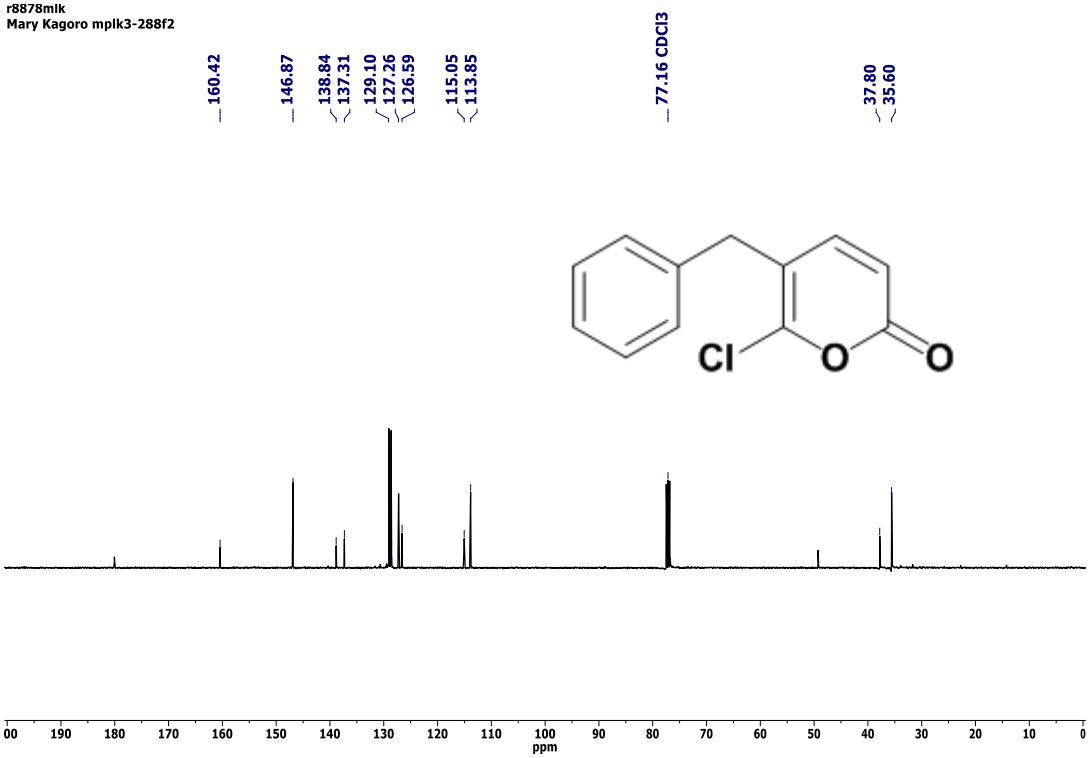

j1965mlk
Mary Kagoro mplk3-327f1

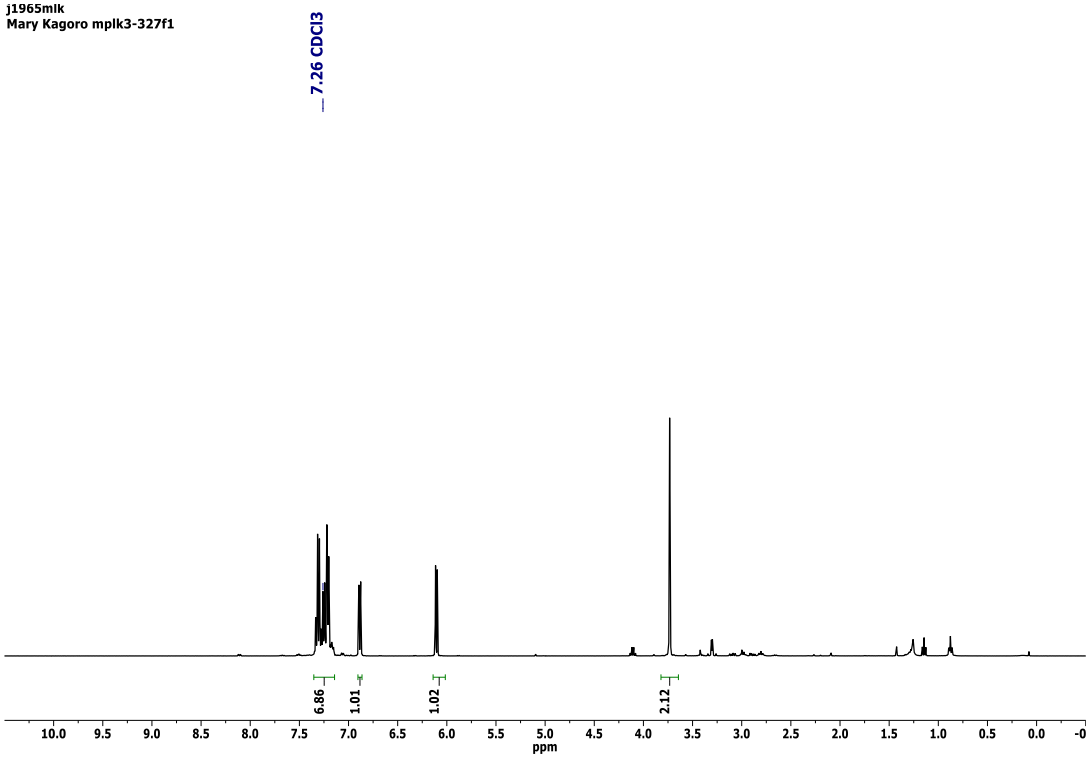

r4365mlk
Mary Kagoro mplk2-239

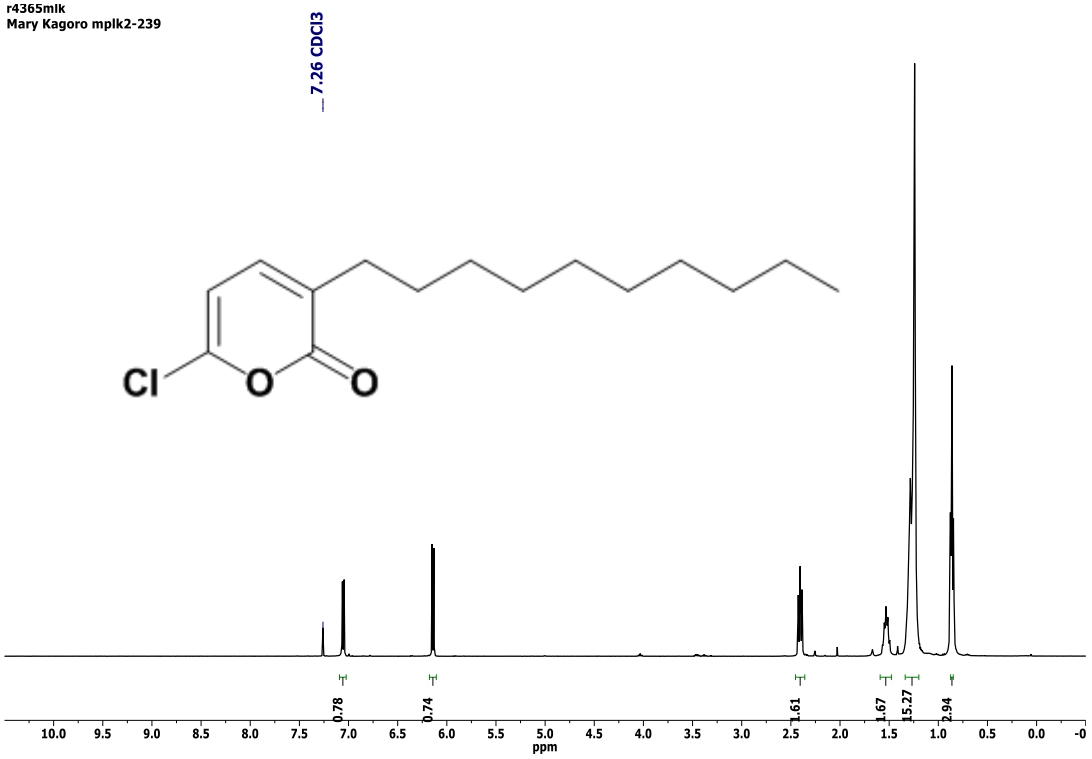

r9396mlk
Mary Kagoro mplk3-297f1

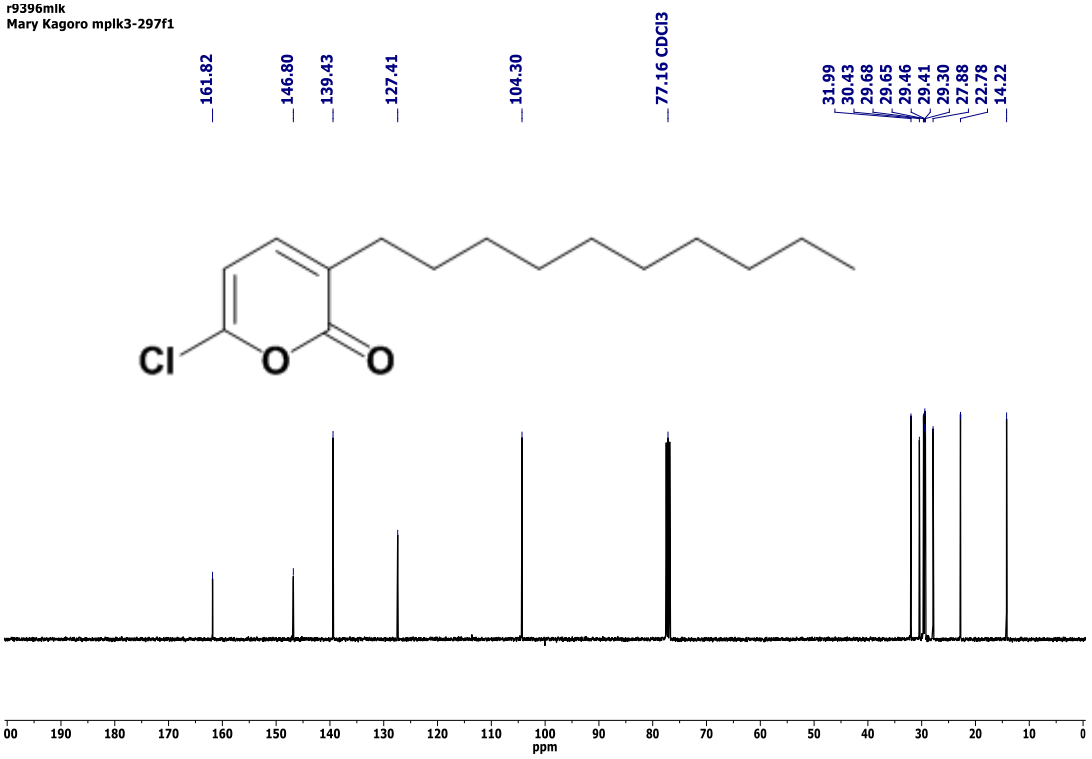

r9148mlk
Mary Kagoro mplk3-293f2

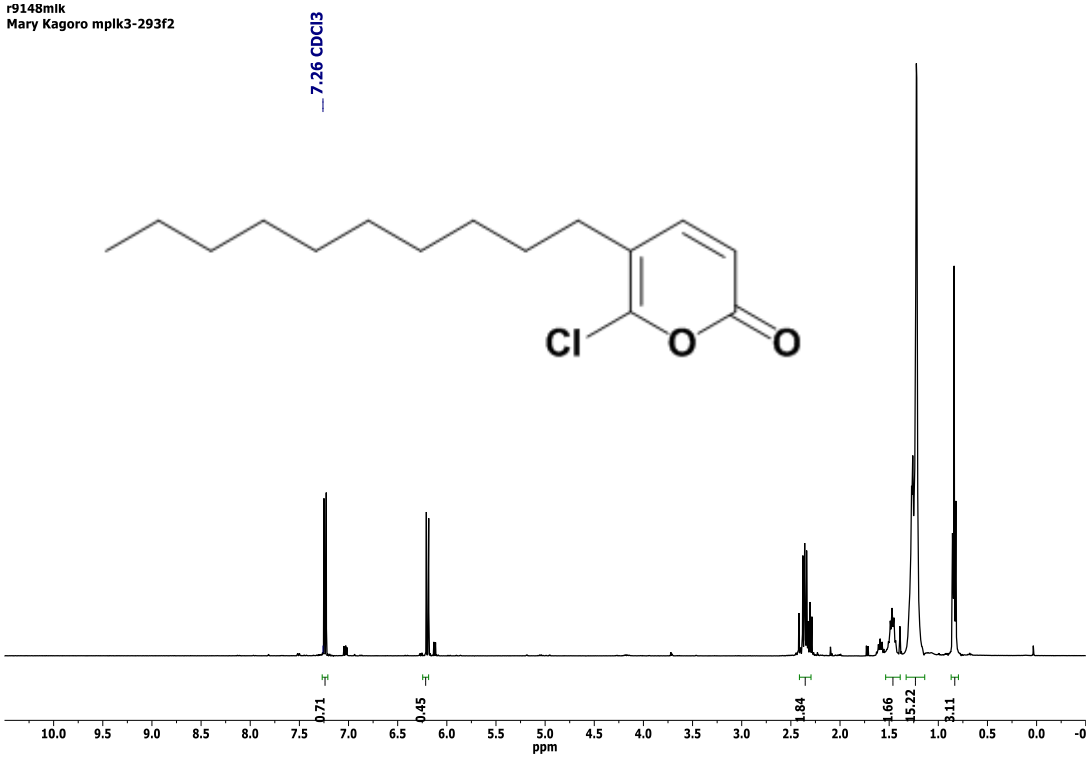

b4701mlk
Mary Kagoro mplk3-314f2

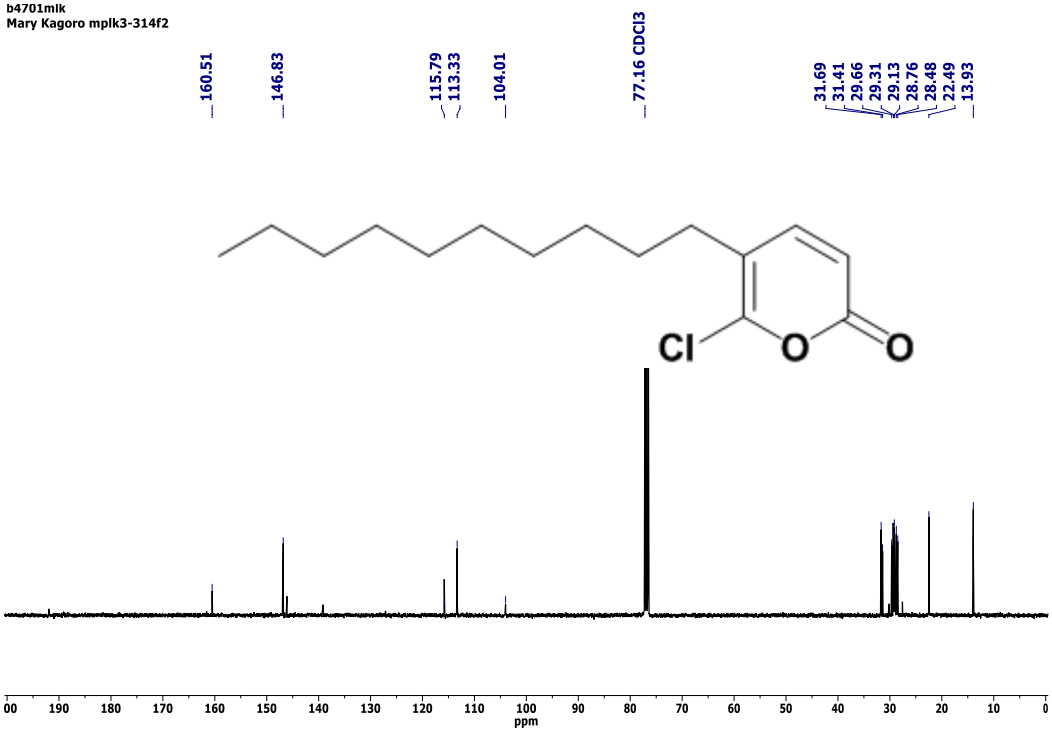

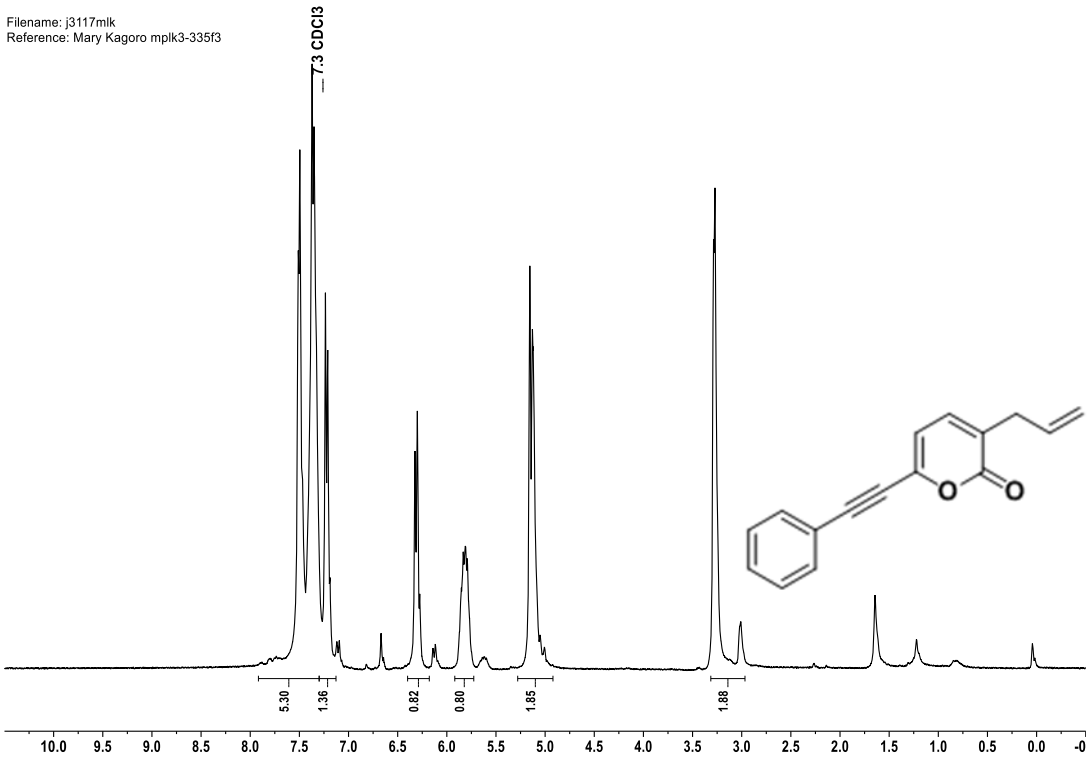
Filename: j3117mlk
Reference: Mary Kagoro mplk3-335f3
7.3 CDCl3
5.30
1.36
0.82
0.80
1.85
1.88
O
O
10.0 9.5 9.0 8.5 8.0 7.5 7.0 6.5 6.0 5.5 5.0 4.5 4.0 3.5 3.0 2.5 2.0 1.5 1.0 0.5 0.0 -0

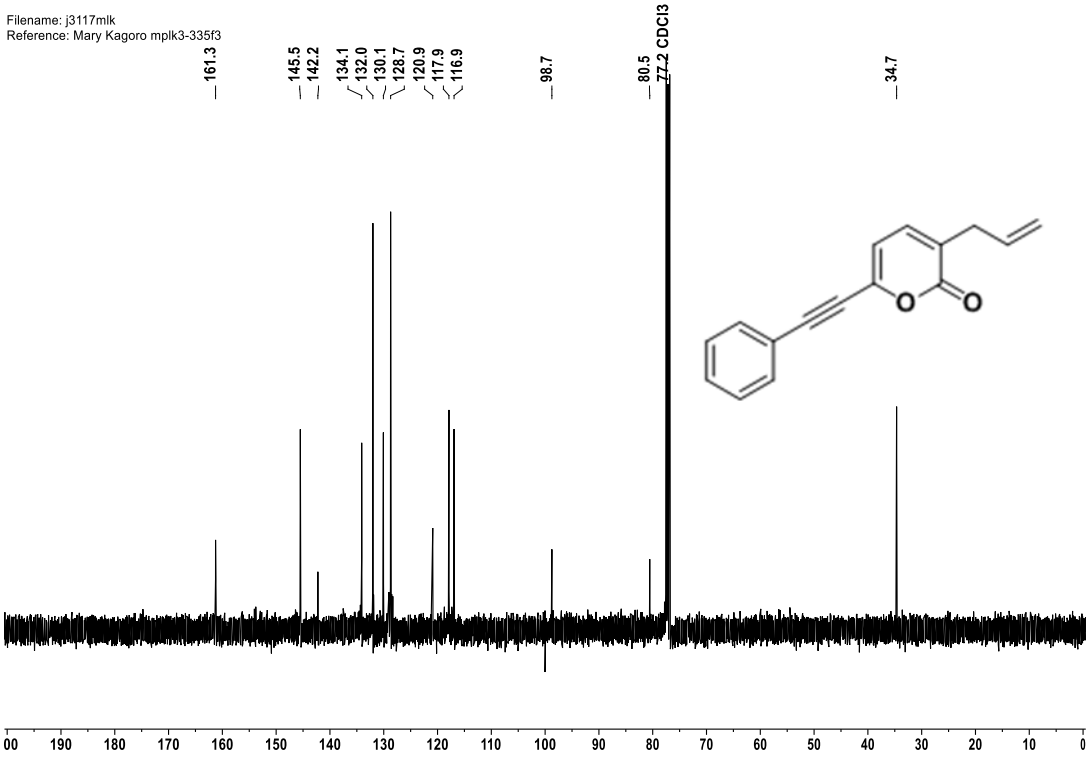
Filename: j3117mlk
Reference: Mary Kagoro mplk3-335f3
161.3
145.5
142.2
134.1
132.0
130.1
128.7
120.9
117.9
116.9
98.7
80.5
77.2 CDCl3
34.7
O
O
00 190 180 170 160 150 140 130 120 110 100 90 80 70 60 50 40 30 20 10 0

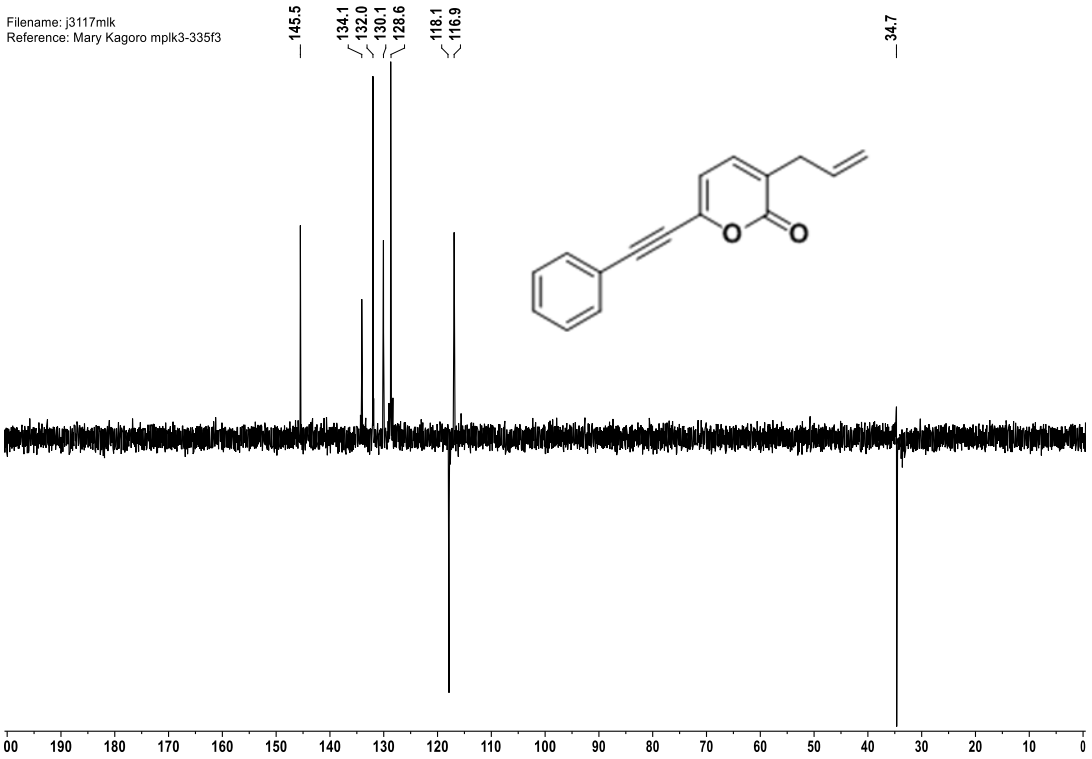
Filename: j3117mlk
Reference: Mary Kagoro mplk3-335f3
145.5
134.1
132.0
130.1
128.6
118.1
116.9
34.7
O
O
00 190 180 170 160 150 140 130 120 110 100 90 80 70 60 50 40 30 20 10 0

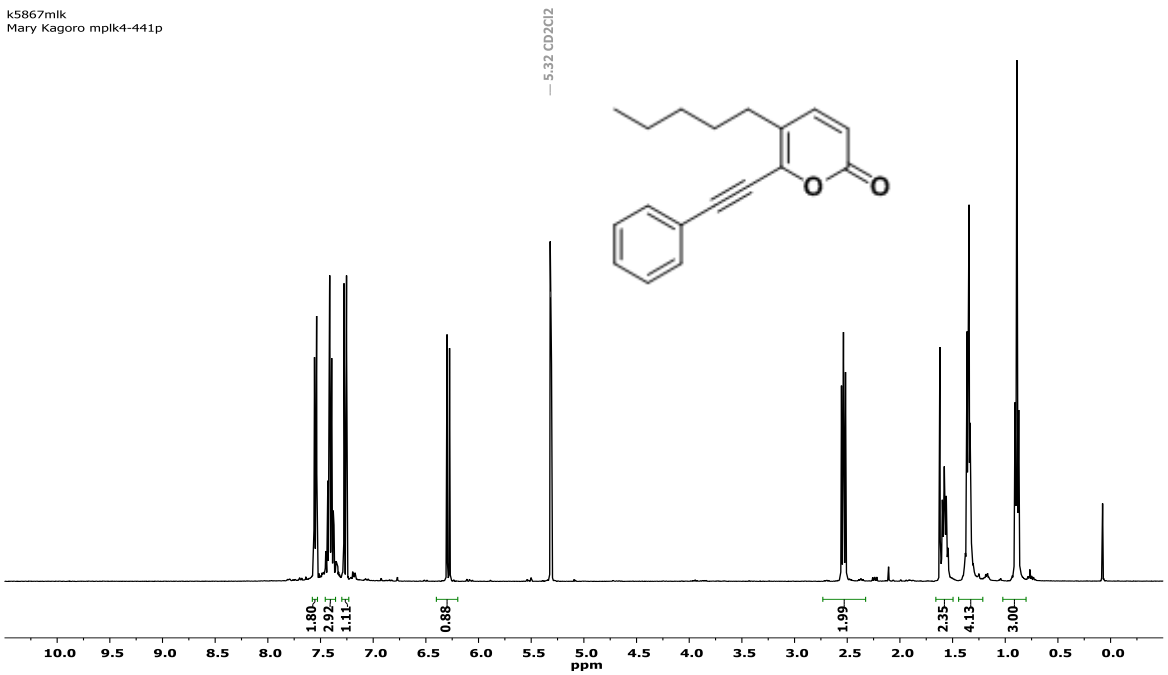
k5867mlk
Mary Kagoro mplk4-441p
5.32 CD2Cl2
O
O
1.80
2.92
1.11
0.88
1.99
2.35
4.13
3.00
10.0 9.5 9.0 8.5 8.0 7.5 7.0 6.5 6.0 5.5 5.0 4.5 4.0 3.5 3.0 2.5 2.0 1.5 1.0 0.5 0.0
ppm

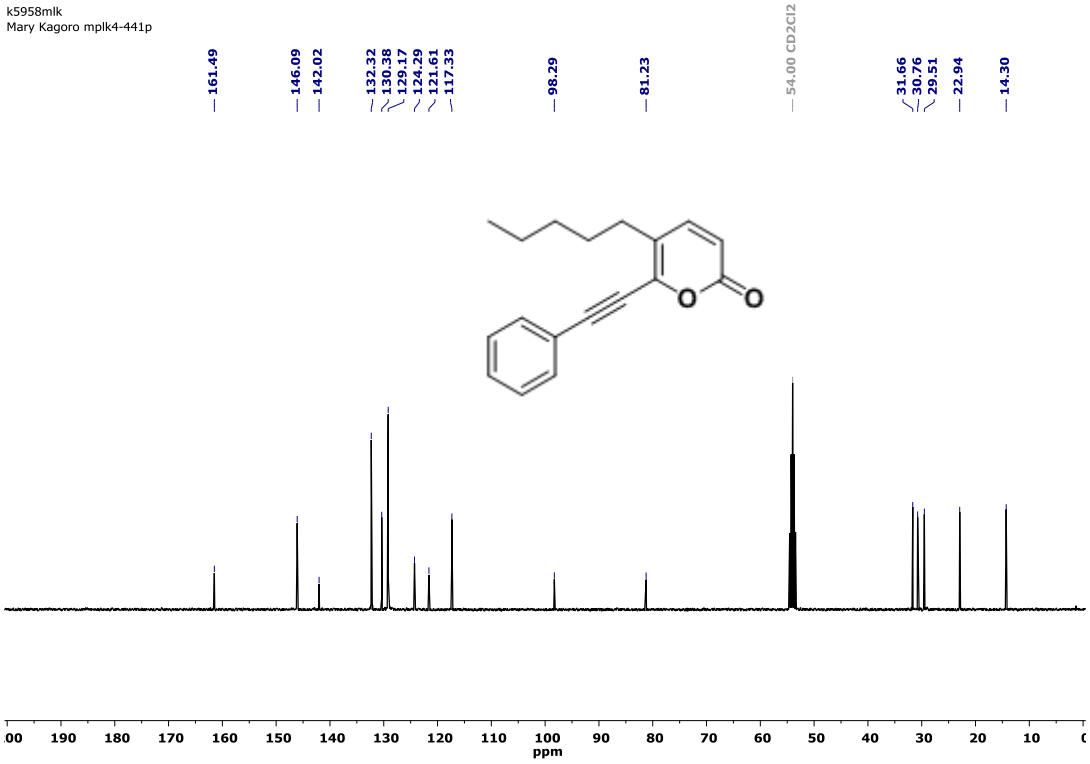
k5958mlk
Mary Kagoro mplk4-441p
161.49
146.09
142.02
132.32
130.38
129.17
124.29
121.61
117.33
98.29
81.23
54.00 CD2Cl2
31.66
30.76
29.51
22.94
14.30
O
O
ppm

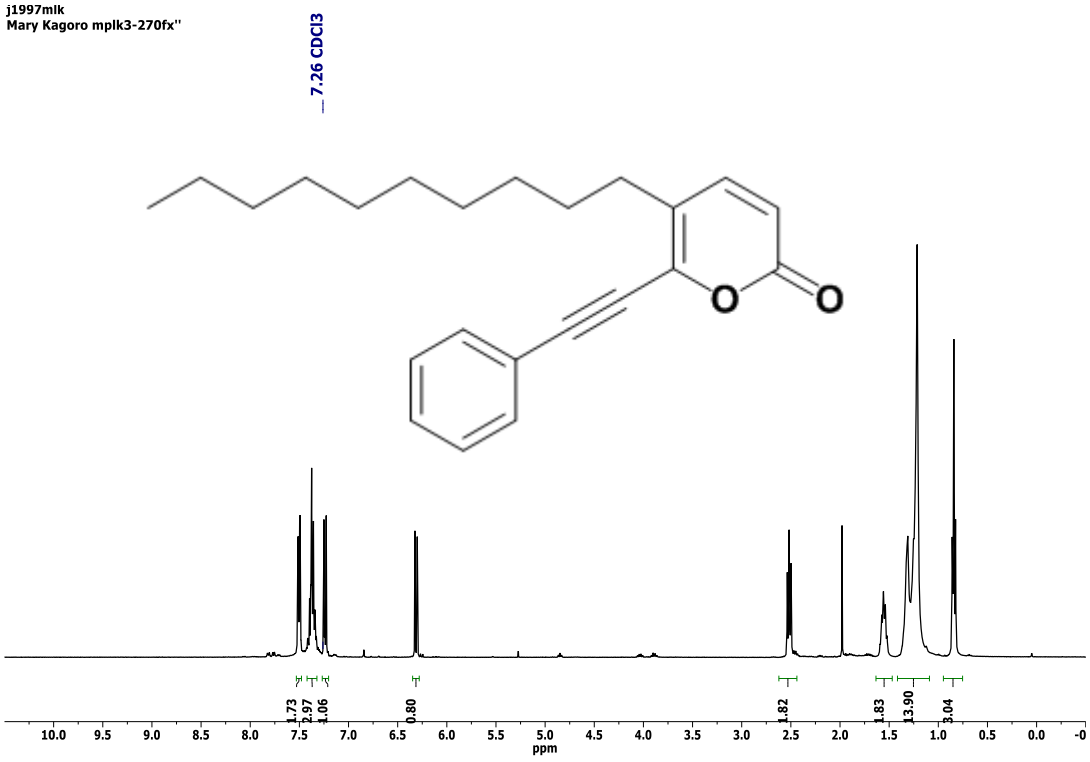
j1997mlk
Mary Kagoro mplk3-270fx''
7.26 CDCl3
O
O
1.73
2.97
1.06
0.80
1.82
1.83
13.90
3.04
ppm

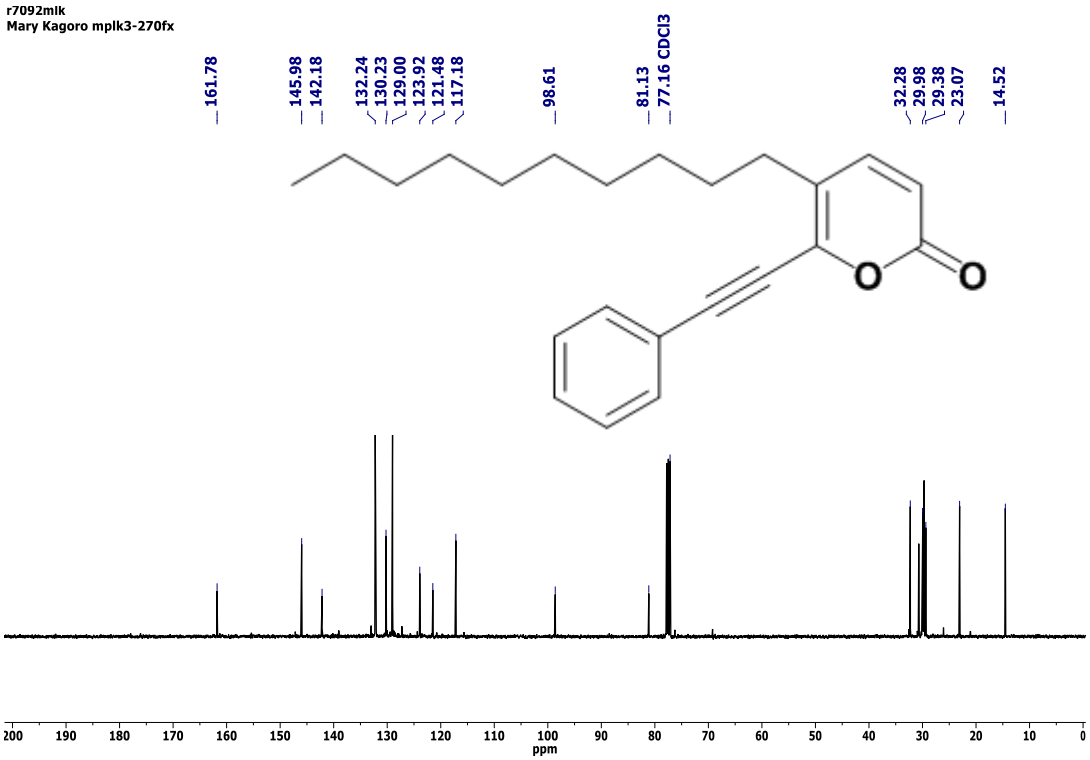
r7092mlk
Mary Kagoro mplk3-270fx
161.78
145.98
142.18
132.24
130.23
129.00
123.92
121.48
117.18
98.61
81.13
77.16 CDCl3
32.28
29.98
29.38
23.07
14.52
O
O
200 190 180 170 160 150 140 130 120 110 100 90 80 70 60 50 40 30 20 10 0
ppm


j3680mlk
Mary Kagoro mplk3-344
7.26 CDCl3
O
O
O
O
*
*
0.59
0.53
3.95
2.07
2.00
23.06
3.66
10.0 9.5 9.0 8.5 8.0 7.5 7.0 6.5 6.0 5.5 5.0 4.5 4.0 3.5 3.0 2.5 2.0 1.5 1.0 0.5 0.0 -0
ppm


j3680mlk
Mary Kagoro mplk3-344
172.09
169.39
144.48
122.35
77.16 CDCl3
61.91
51.81
35.44
31.94
29.81
29.57
29.27
22.72
14.15
O
O
O
O
*
*
ppm

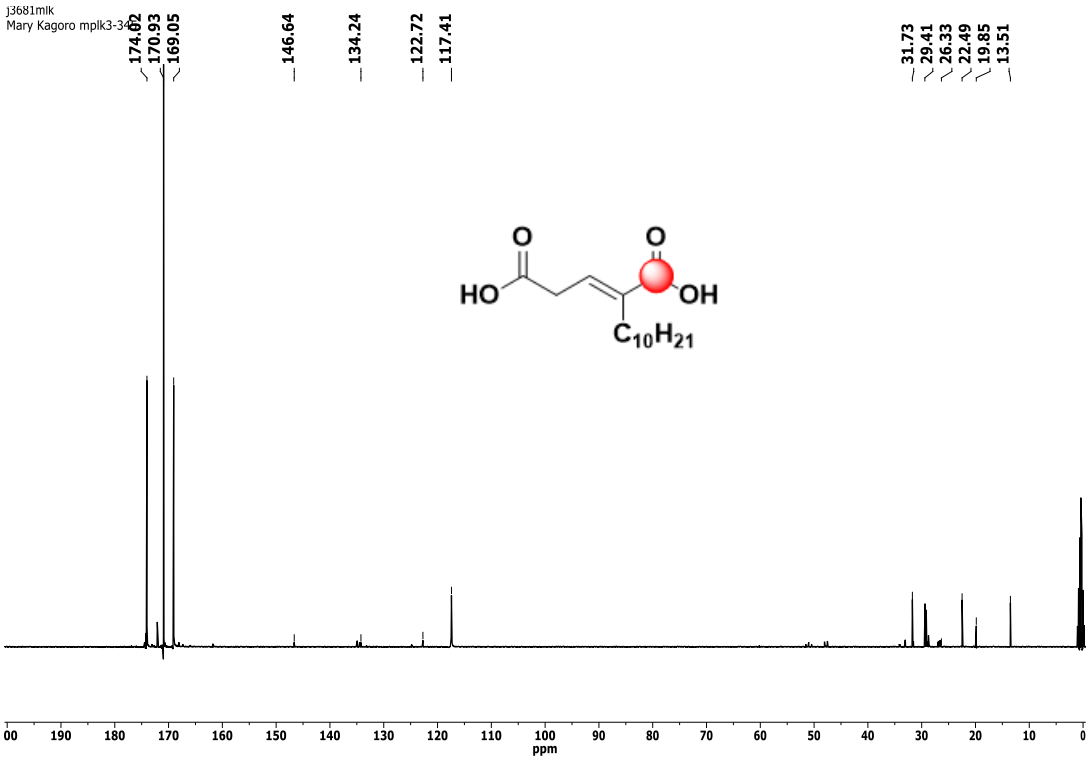
j3681mlk
Mary Kagoro mplk3-34
174.02
170.93
169.05
146.64
134.24
122.72
117.41
31.73
29.41
26.33
22.49
19.85
13.51
O
O
HO
OH
C10H21
ppm

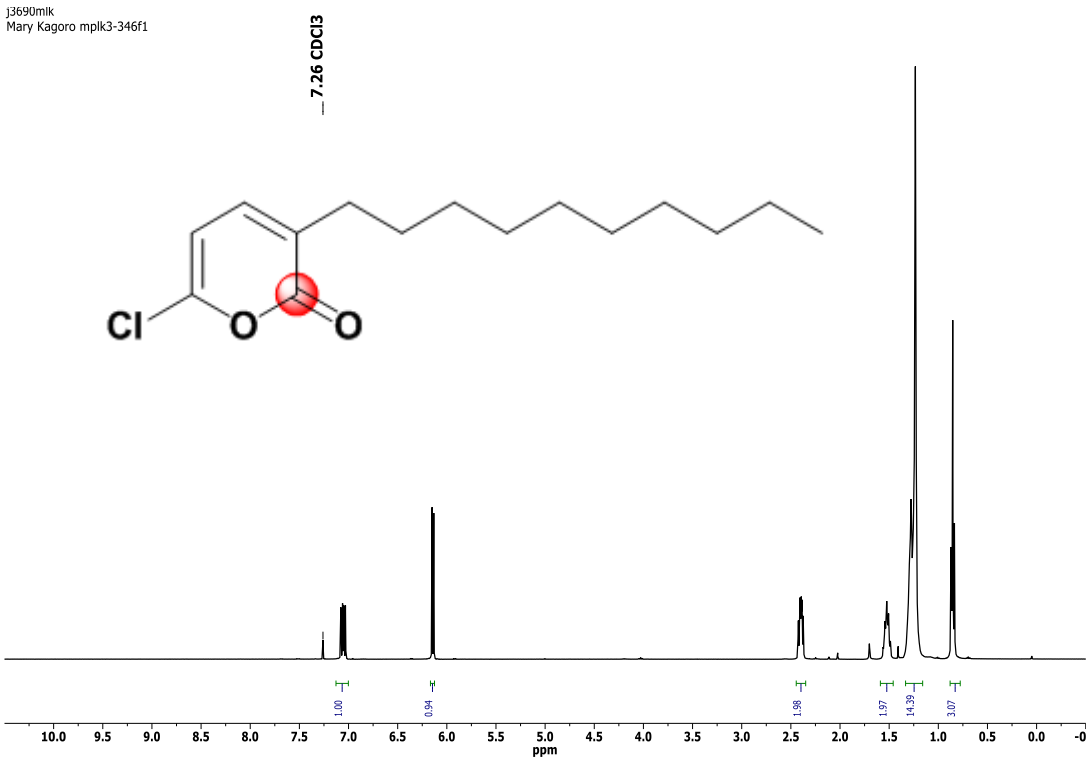
j3690mlk
Mary Kagoro mplk3-346f1
7.26 CDCl3
Cl
O
O
1.00
0.94
1.98
1.97
14.39
3.07
10.0
9.5
9.0
8.5
8.0
7.5
7.0
6.5
6.0
5.5
5.0
4.5
4.0
3.5
3.0
2.5
2.0
1.5
1.0
0.5
0.0
-0
ppm

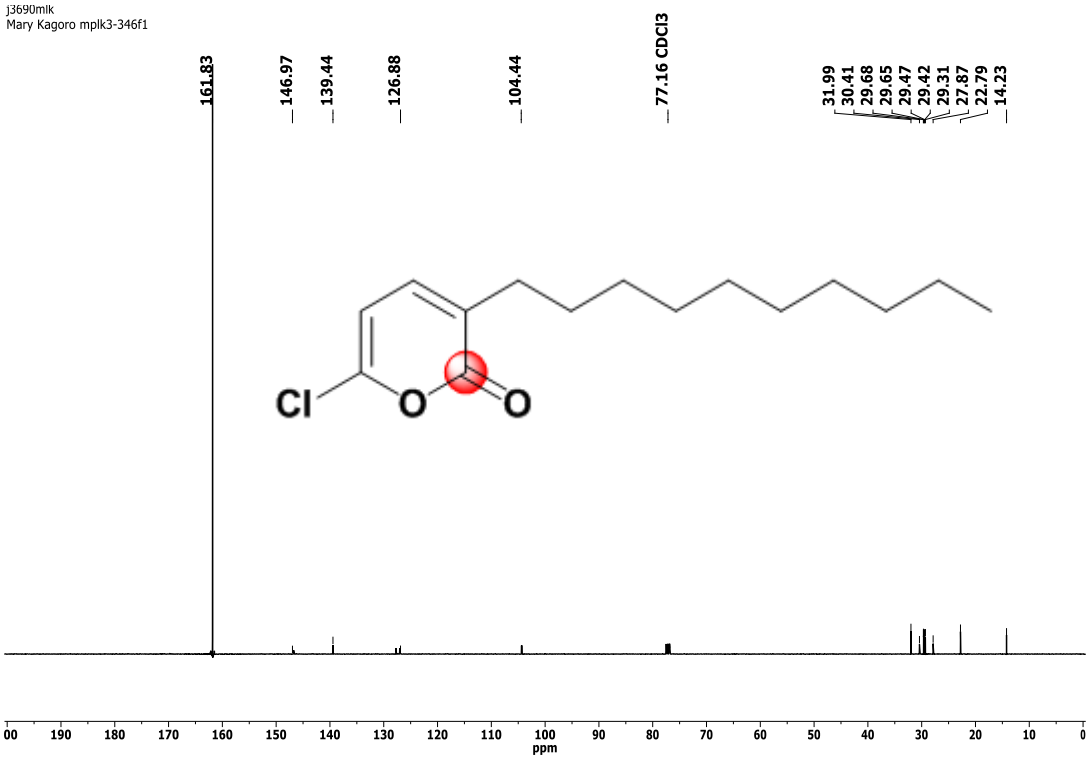
j3690mlk
Mary Kagoro mplk3-346f1
161.83
146.97
139.44
126.88
104.44
77.16 CDCl3
31.99
30.41
29.68
29.65
29.47
29.42
29.31
27.87
22.79
14.23
Cl
O
O
00
190
180
170
160
150
140
130
120
110
100
90
80
70
60
50
40
30
20
10
0
ppm

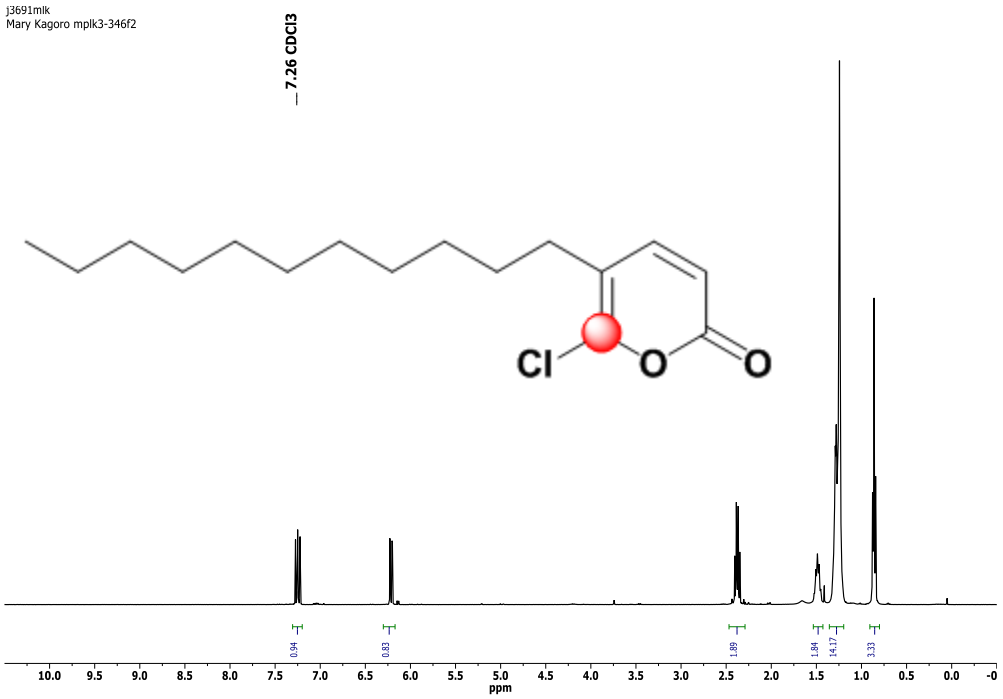
j3691mlk
Mary Kagoro mplk3-346f2
7.26 CDCl3
Cl
O
O
0.94
0.83
1.89
1.84
14.17
3.33
10.0 9.5 9.0 8.5 8.0 7.5 7.0 6.5 6.0 5.5 5.0 4.5 4.0 3.5 3.0 2.5 2.0 1.5 1.0 0.5 0.0 -0
ppm

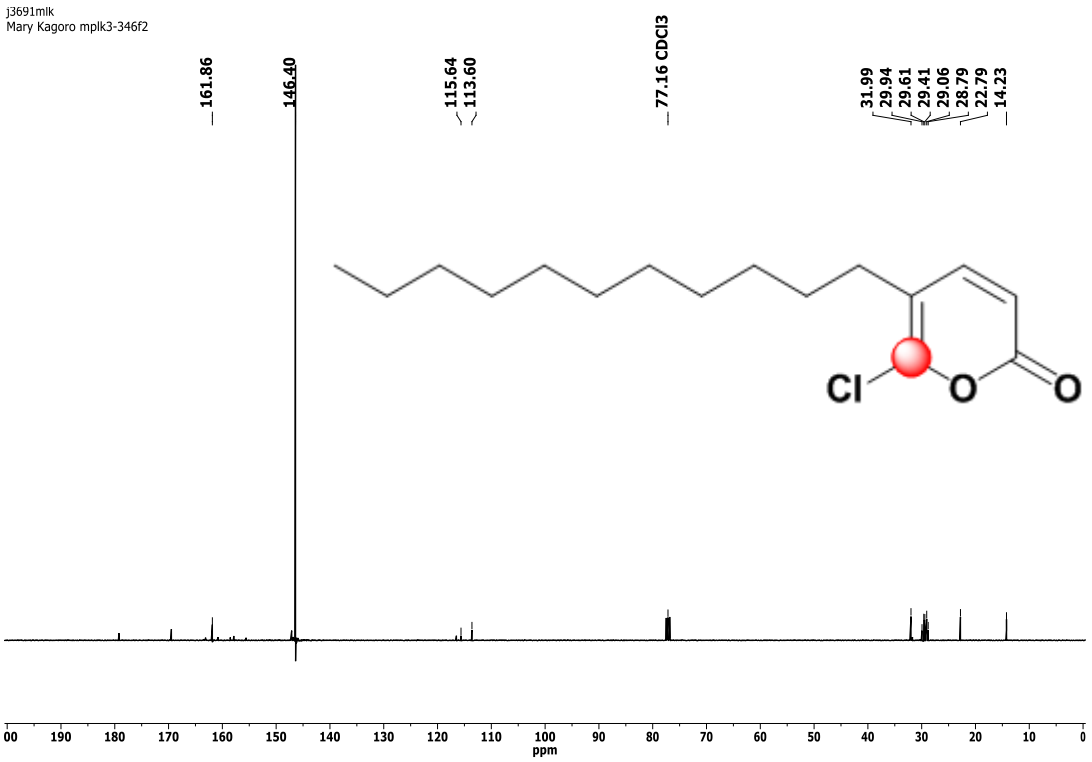
j3691mlk
Mary Kagoro mplk3-346f2
161.86
146.40
115.64
113.60
77.16 CDCl3
31.99
29.94
29.61
29.41
29.06
28.79
22.79
14.23
Cl
O
O
00 190 180 170 160 150 140 130 120 110 100 90 80 70 60 50 40 30 20 10 0
ppm

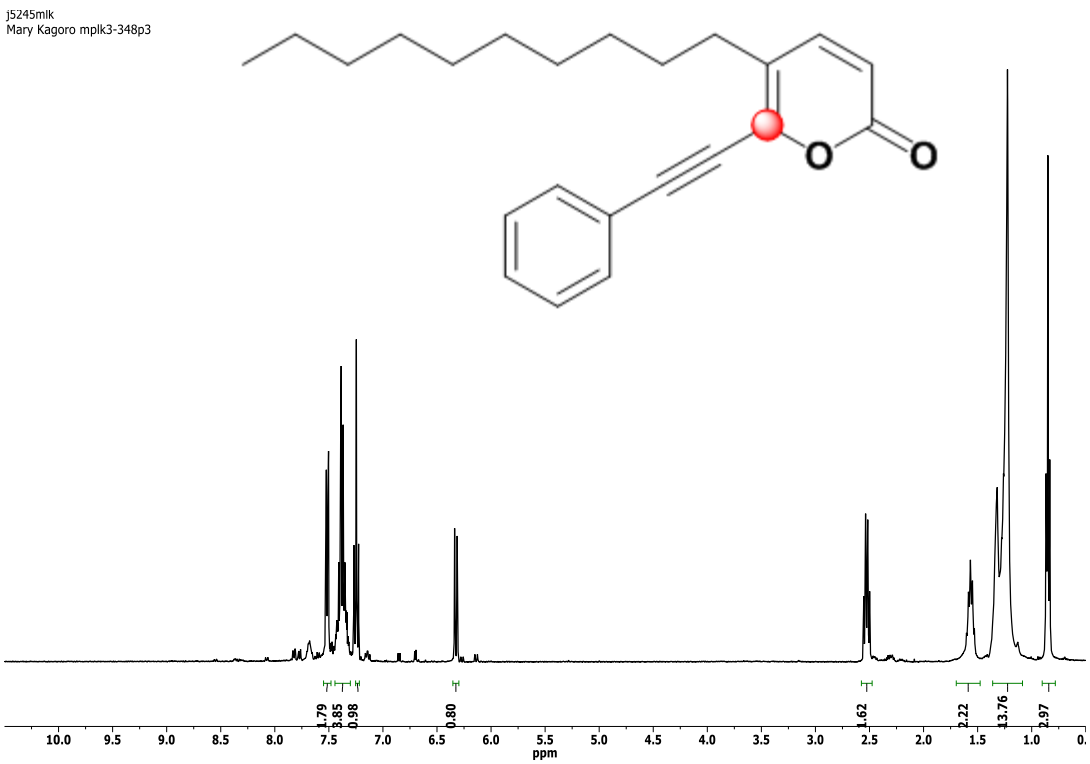
j5245mlk
Mary Kagoro mplk3-348p3
O
O
1.79
3.85
0.98
0.80
1.62
2.22
13.76
2.97
10.0
9.5
9.0
8.5
8.0
7.5
7.0
6.5
6.0
5.5
5.0
4.5
4.0
3.5
3.0
2.5
2.0
1.5
1.0
ppm

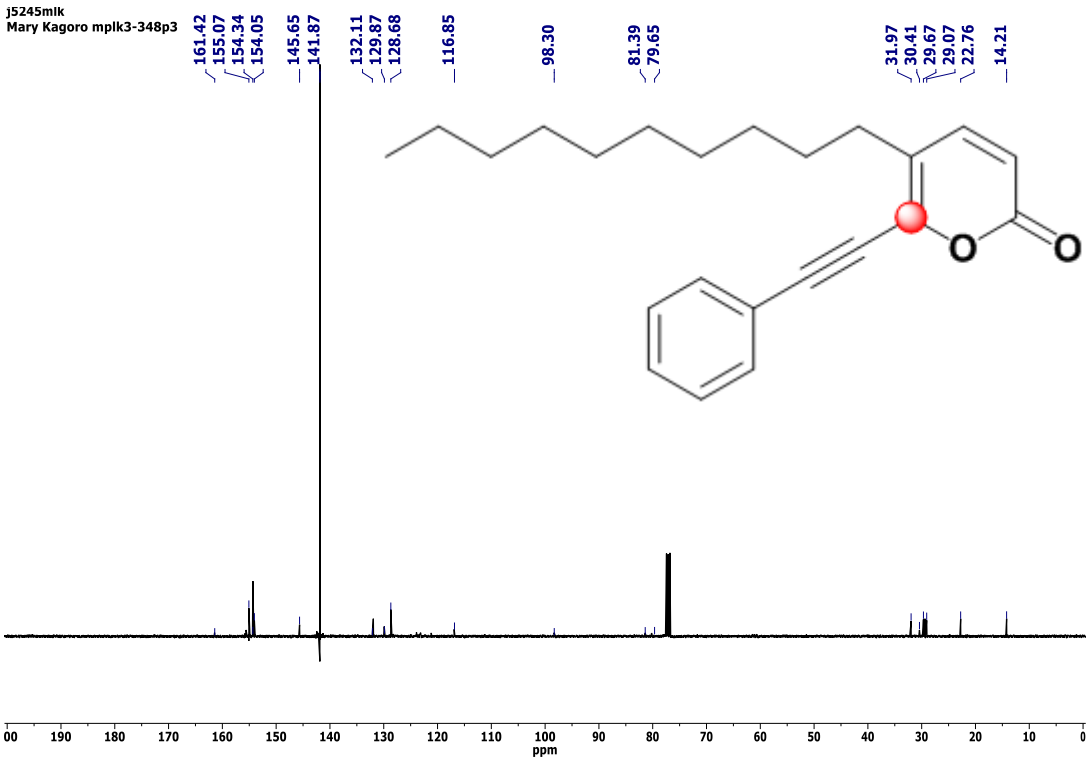
j5245mlk
Mary Kagoro mplk3-348p3
161.42
155.07
154.34
154.05
145.65
141.87
132.11
129.87
128.68
116.85
98.30
81.39
79.65
31.97
30.41
29.67
29.07
22.76
14.21
O
O
190
180
170
160
150
140
130
120
110
100
90
80
70
60
50
40
30
20
10
ppm

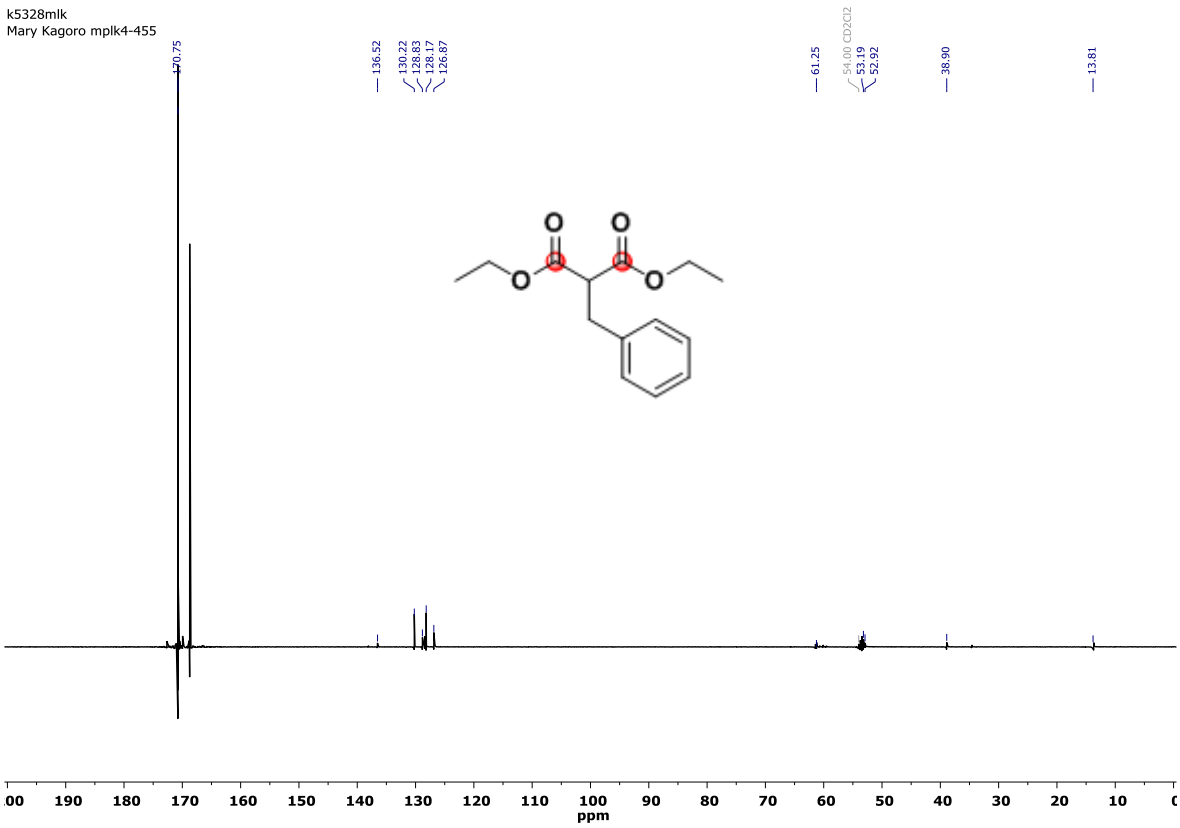
k5328mlk
Mary Kagoro mplk4-455
170.75
136.52
130.22
128.83
128.77
126.87
61.25
54.00 CD2Cl2
53.19
52.92
38.90
13.81
O
O
O
O
ppm

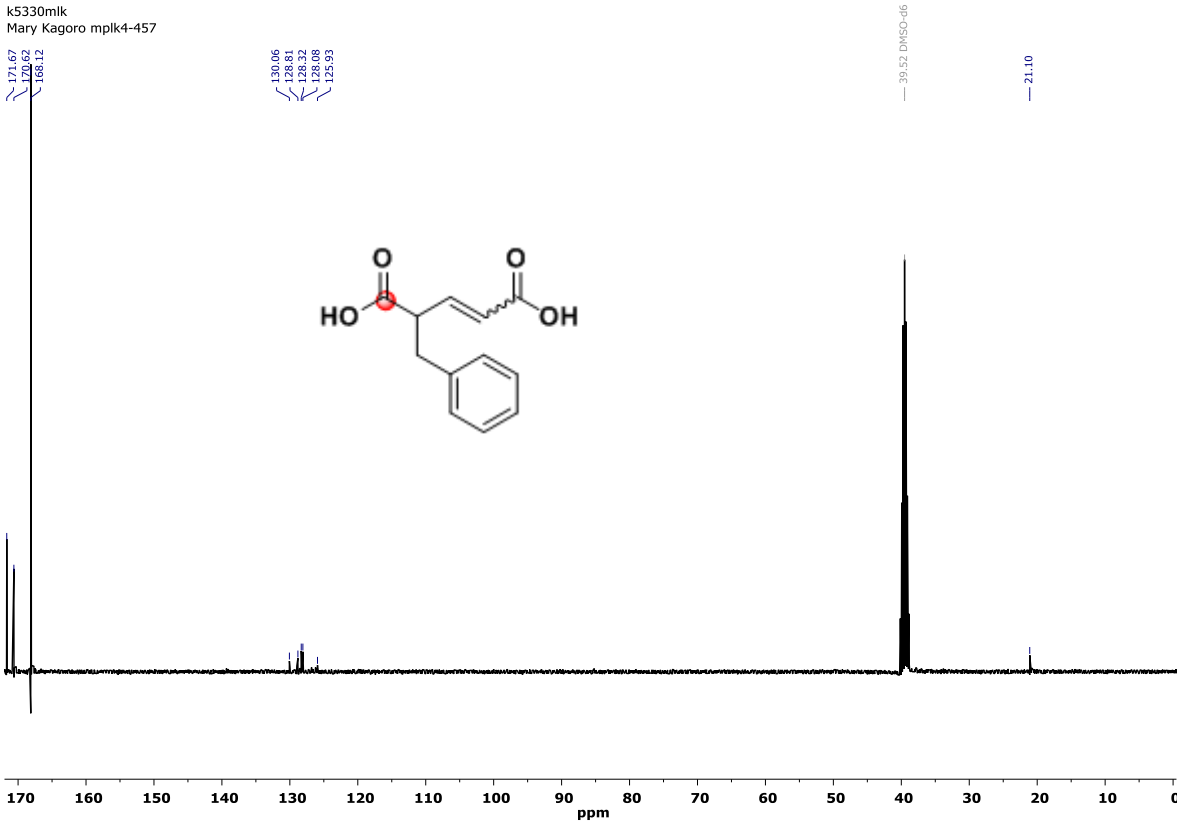
k5330mlk
Mary Kagoro mplk4-457
171.67
170.62
168.12
130.06
128.81
128.32
128.08
125.93
39.52 DMSO-d6
21.10
HO
O
O
OH
ppm

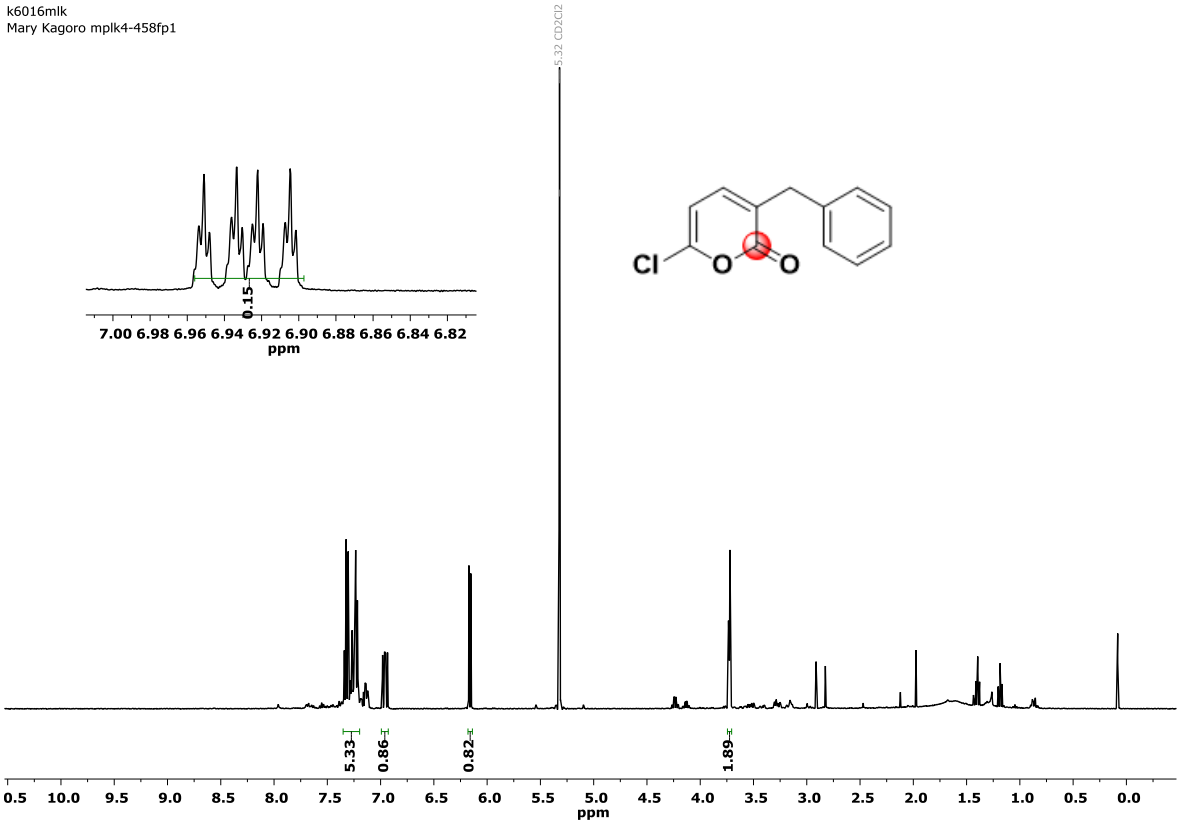
k6016mlk
Mary Kagoro mplk4-458fp1
5.32 CD2Cl2
0.15
7.00 6.98 6.96 6.94 6.92 6.90 6.88 6.86 6.84 6.82
ppm
Cl
O
O
5.33
0.86
0.82
1.89
0.5 10.0 9.5 9.0 8.5 8.0 7.5 7.0 6.5 6.0 5.5 5.0 4.5 4.0 3.5 3.0 2.5 2.0 1.5 1.0 0.5 0.0
ppm

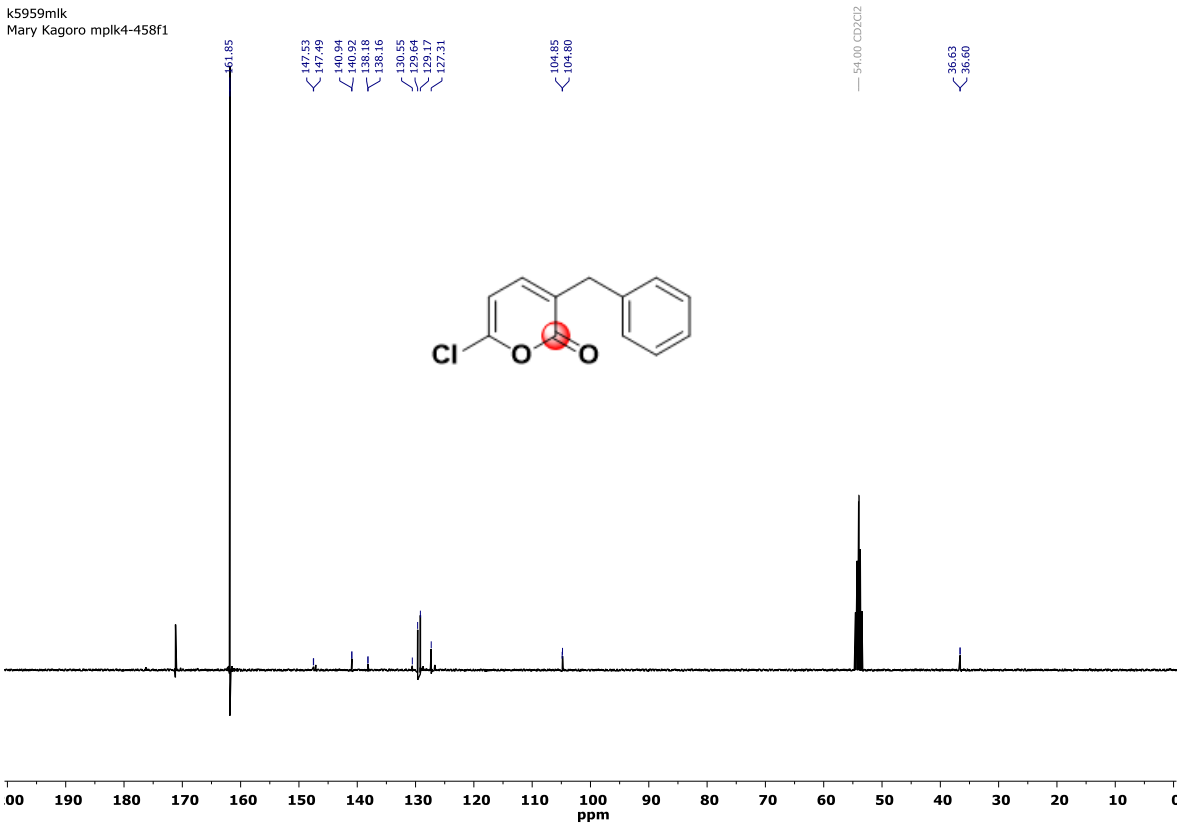
k5959mlk
Mary Kagoro mplk4-458f1
161.85
147.53
147.49
140.94
140.92
138.18
138.16
130.55
129.64
129.17
127.31
104.85
104.80
54.00 CD2Cl2
36.63
36.60
Cl
O
O
00 190 180 170 160 150 140 130 120 110 100 90 80 70 60 50 40 30 20 10
ppm

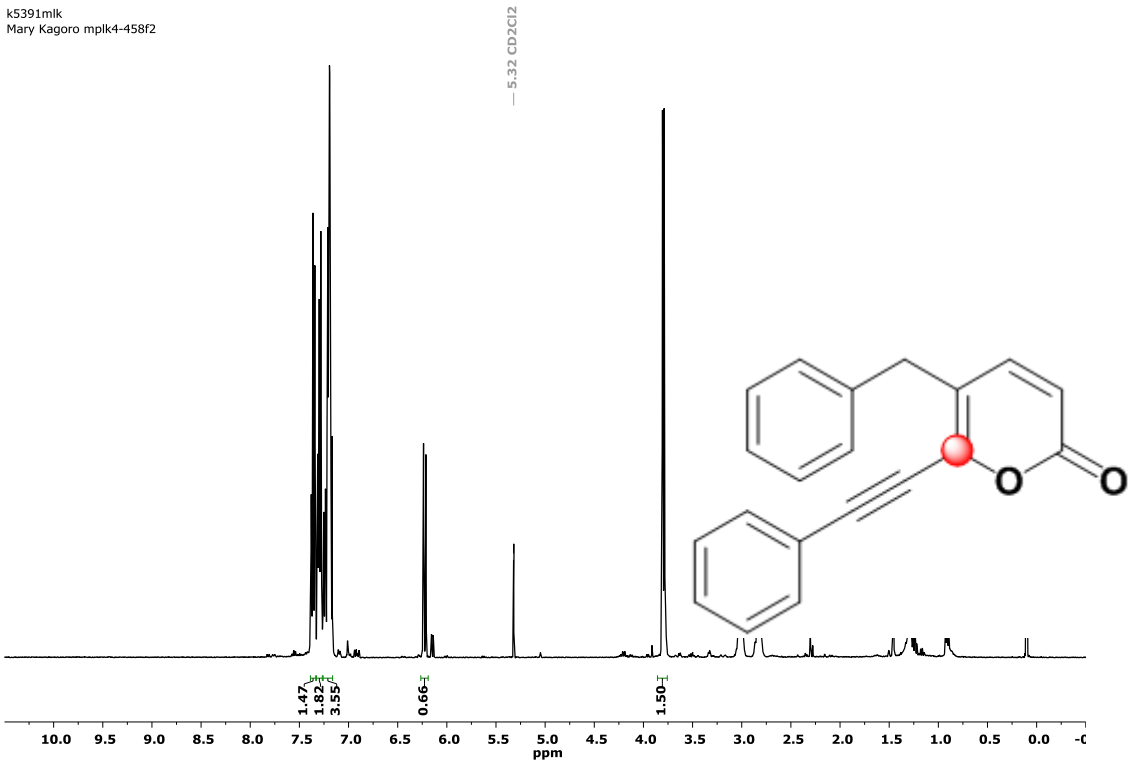
k5391mlk
Mary Kagoro mplk4-458f2
5.32 CD2Cl2
1.47
1.82
3.55
0.66
1.50
ppm

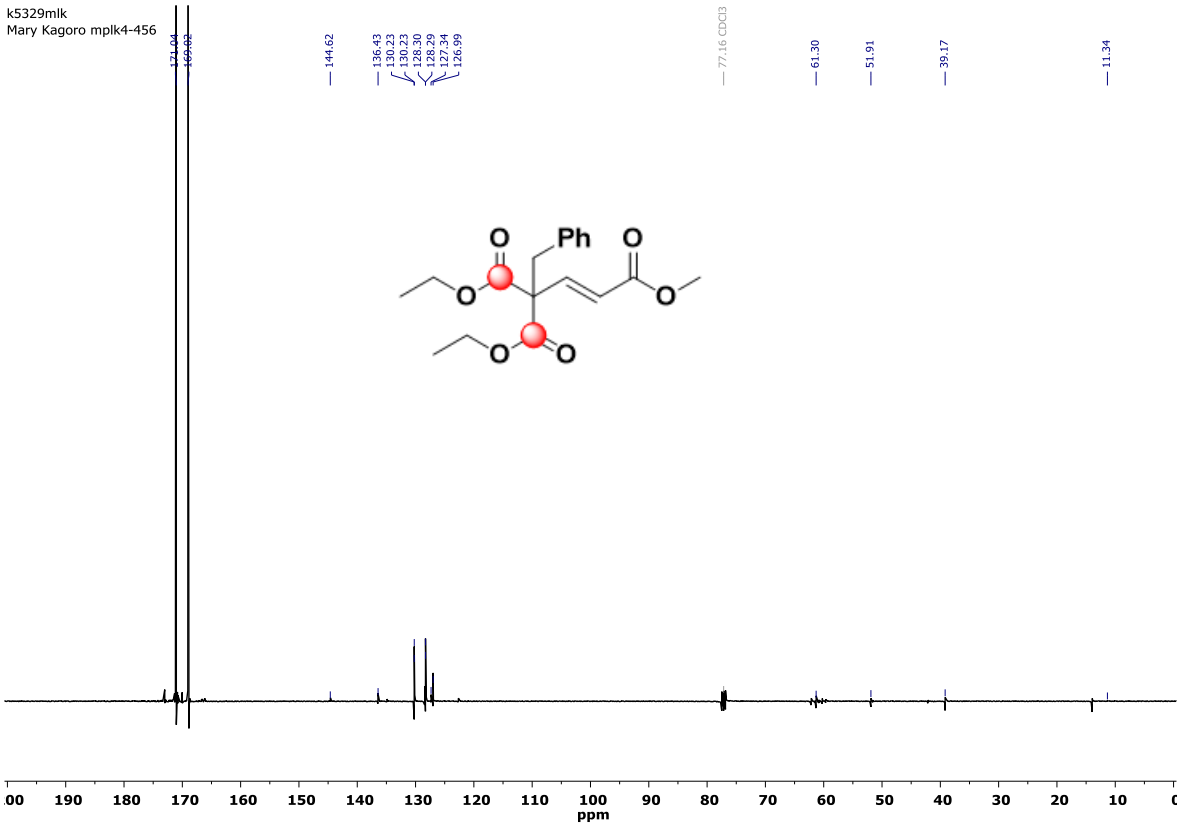
k5329mlk
Mary Kagoro mplk4-456
171.04
169.82
144.62
136.43
130.23
130.23
128.30
128.29
127.34
126.99
77.16 CDCl3
61.30
51.91
39.17
11.34
Ph
ppm

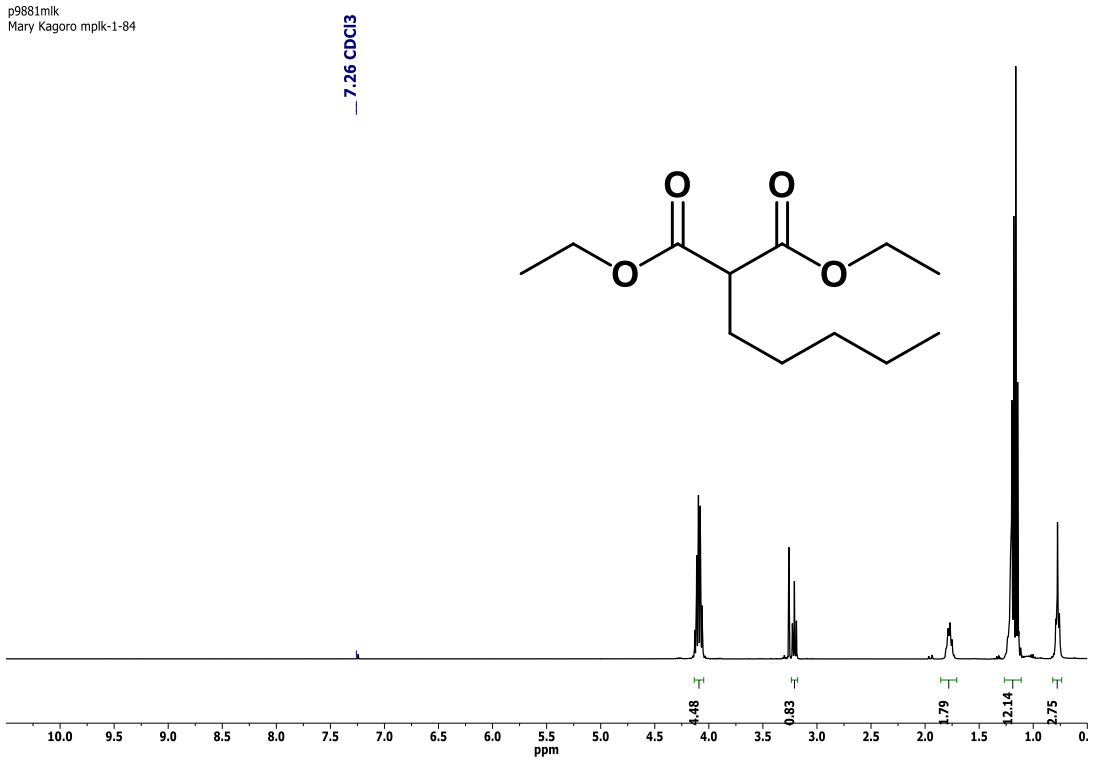
p9881mlk
Mary Kagoro mplk-1-84
7.26 CDCl3
O
O
O
O
4.48
0.83
1.79
12.14
2.75
10.0
9.5
9.0
8.5
8.0
7.5
7.0
6.5
6.0
5.5
5.0
4.5
4.0
3.5
3.0
2.5
2.0
1.5
1.0
ppm

Appendix 3: ATIR Spectra data for compounds

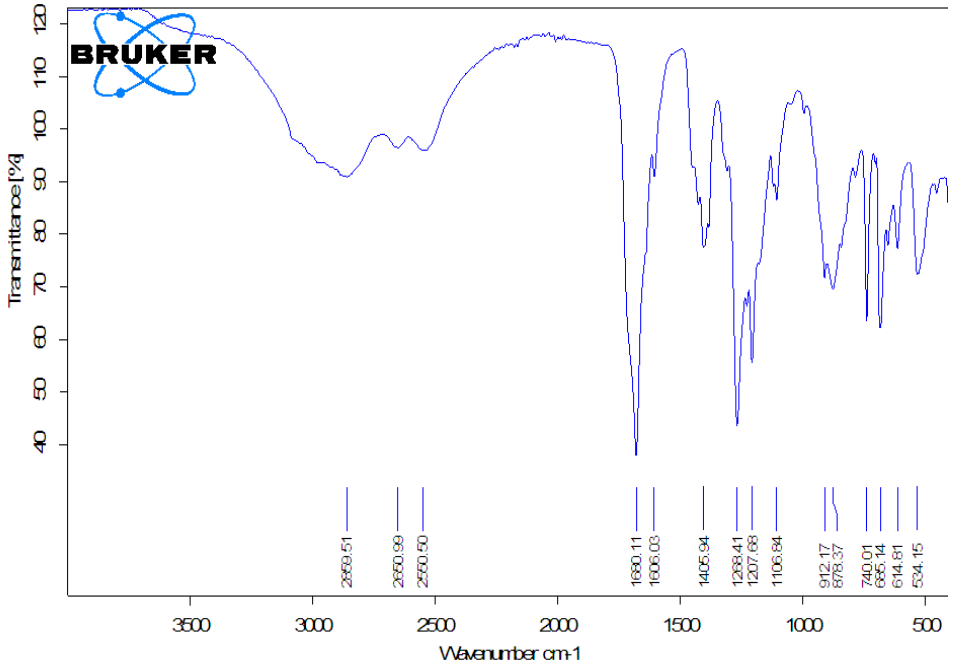

ATIR for 2-decyl glutaconic acid 141e.

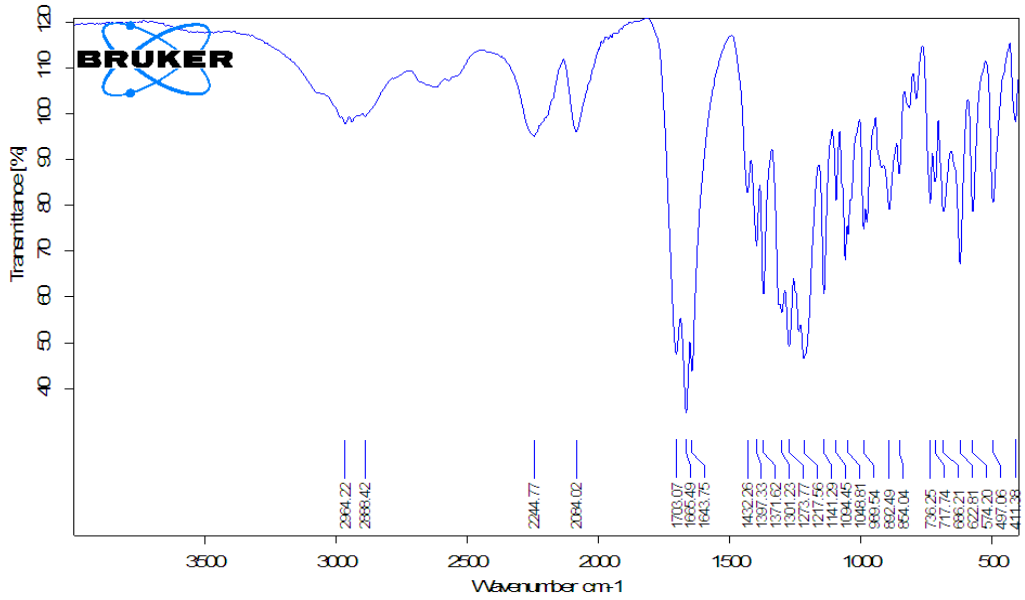

2-methylglutaconic acid 141a.

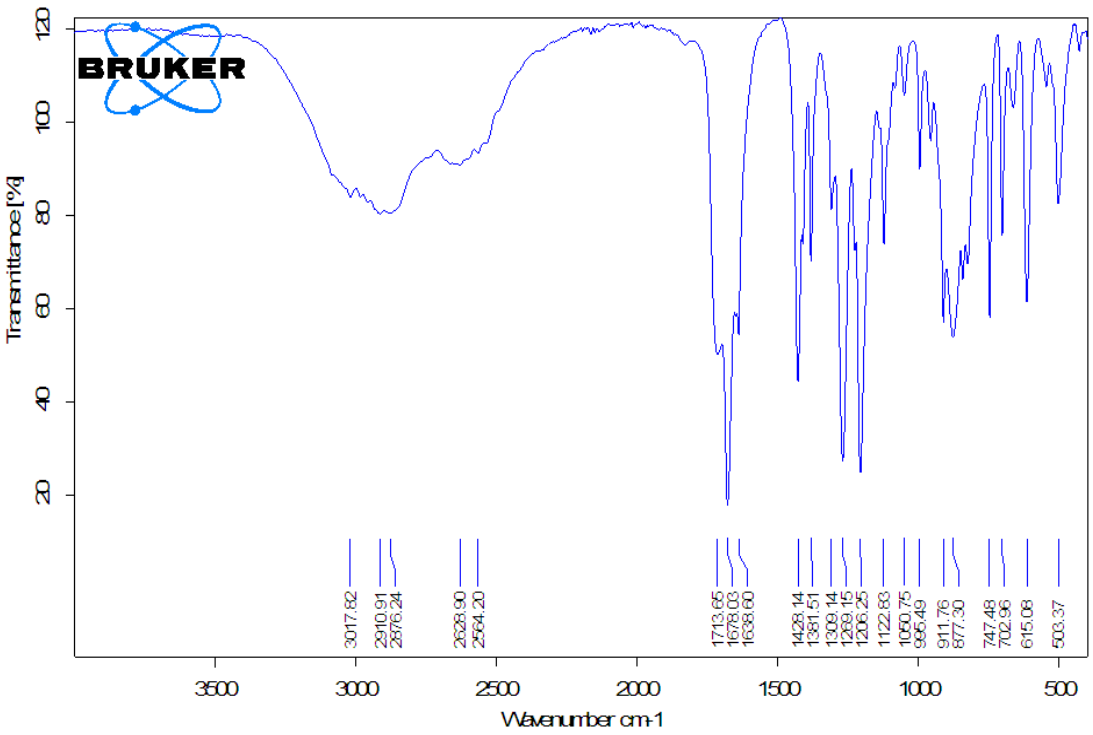

ATIR for 2-allyl glutaconic acid 141b.

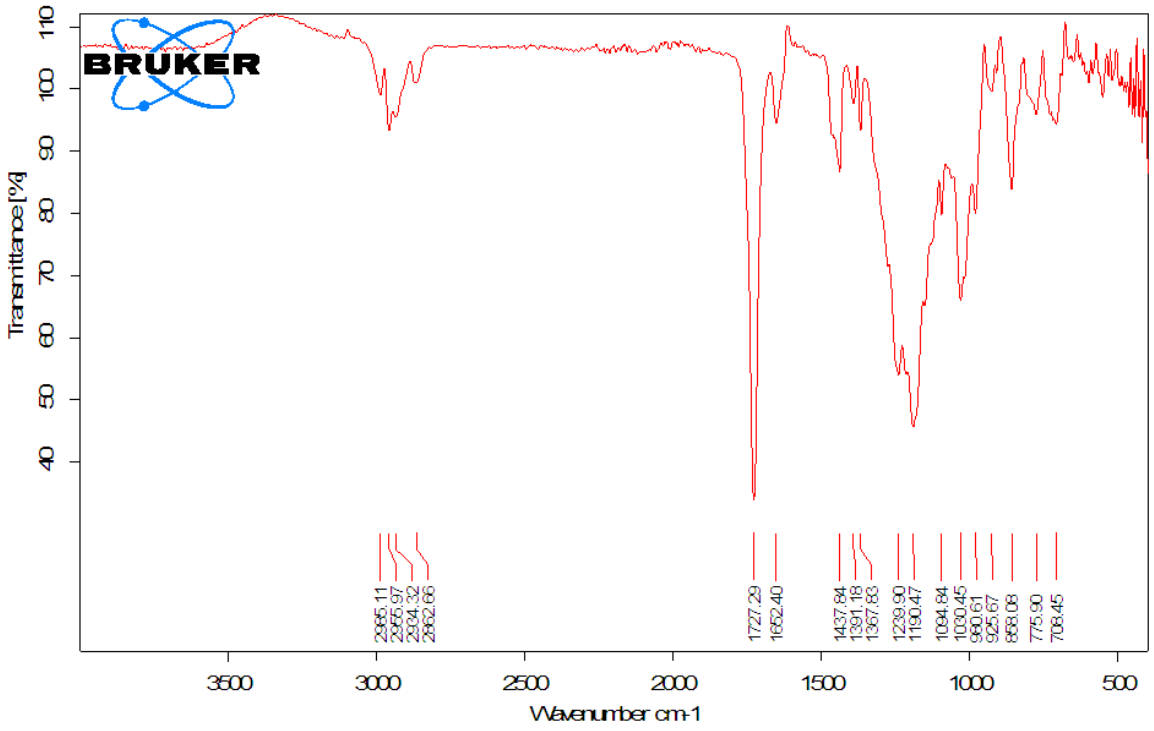

ATIR for compound 128c.

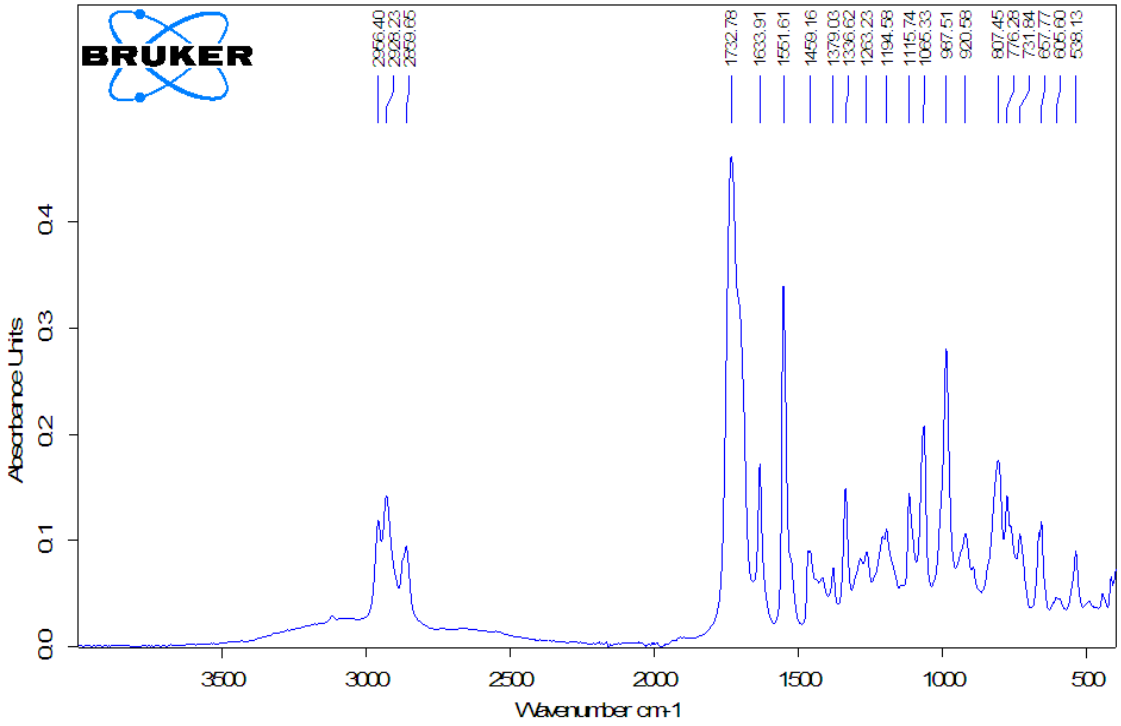

ATIR for compound 128b.

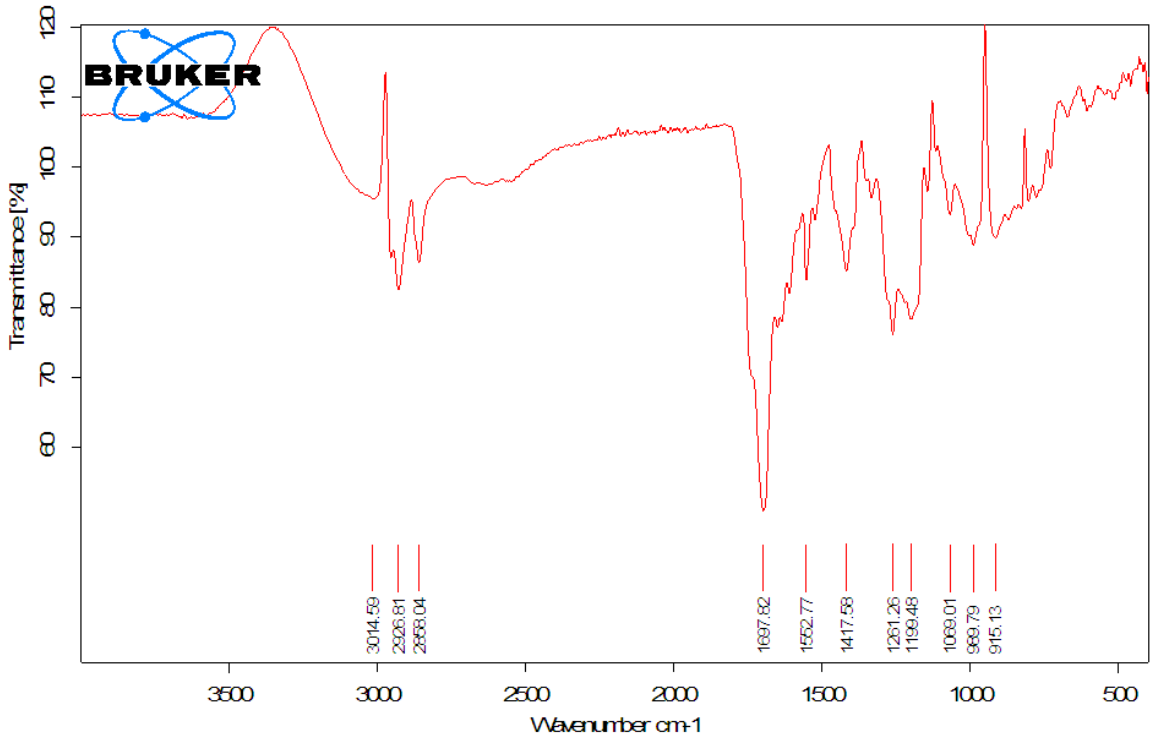

ATIR for compound 129b.

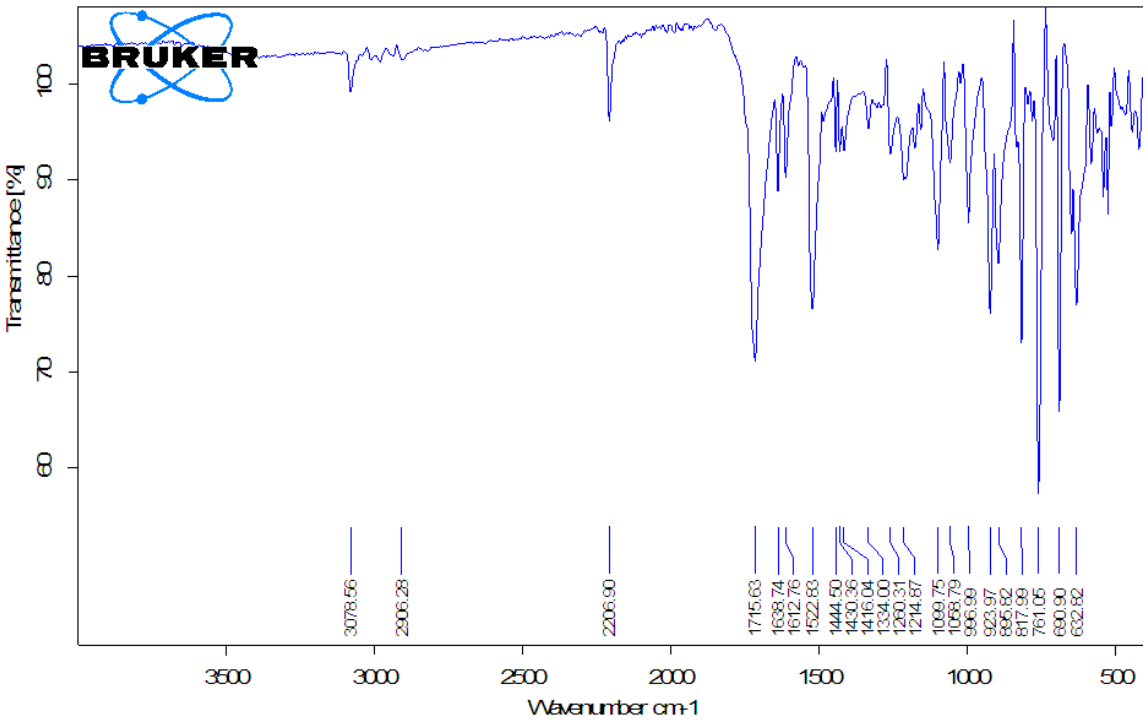

FTIR for compound 131b.

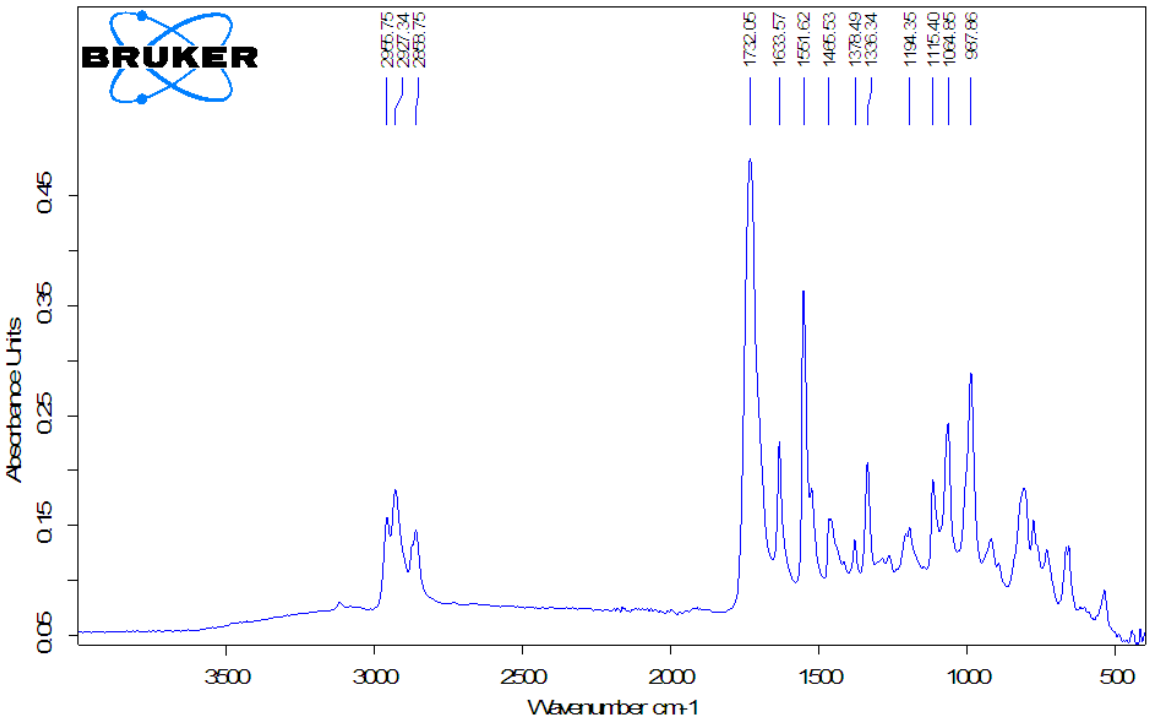

ATIR for compound 128c.

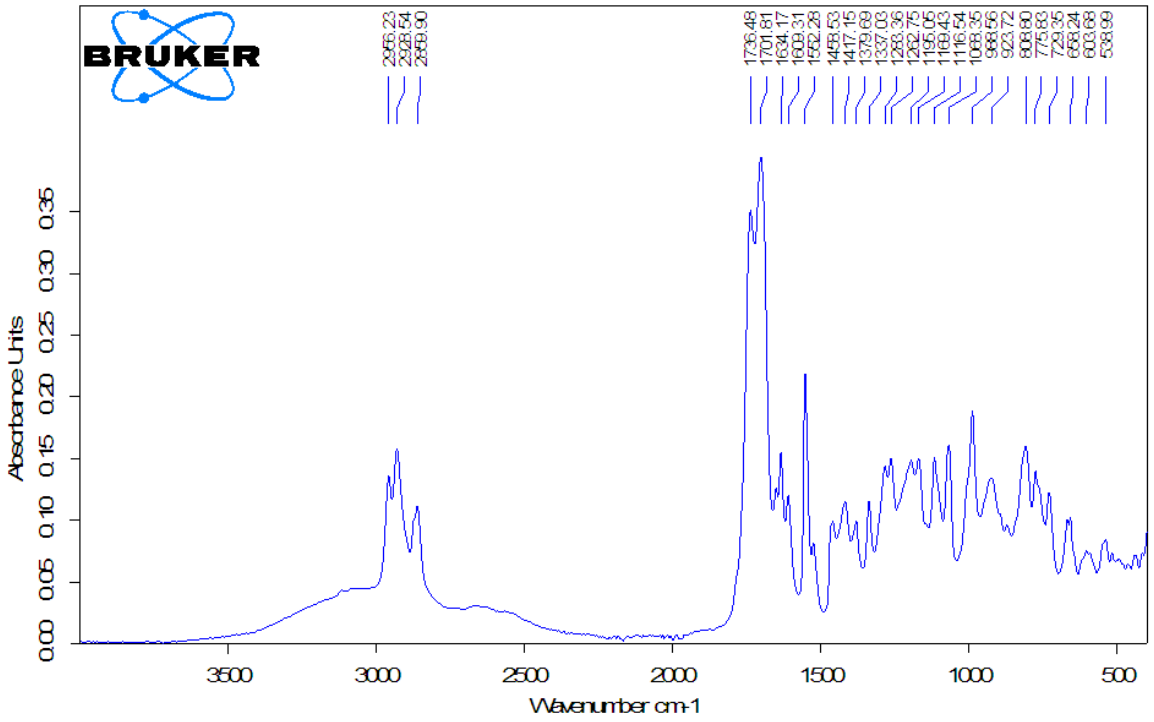

ATIR for compound 131b.

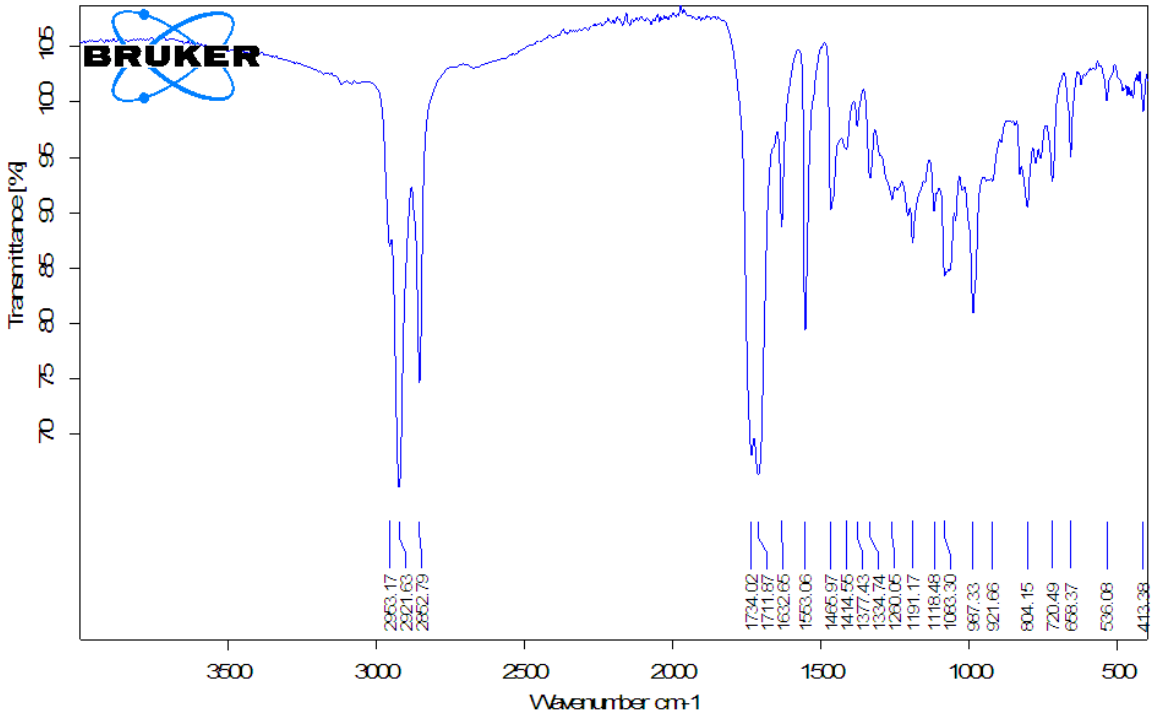

ATIR for compound 364f2.

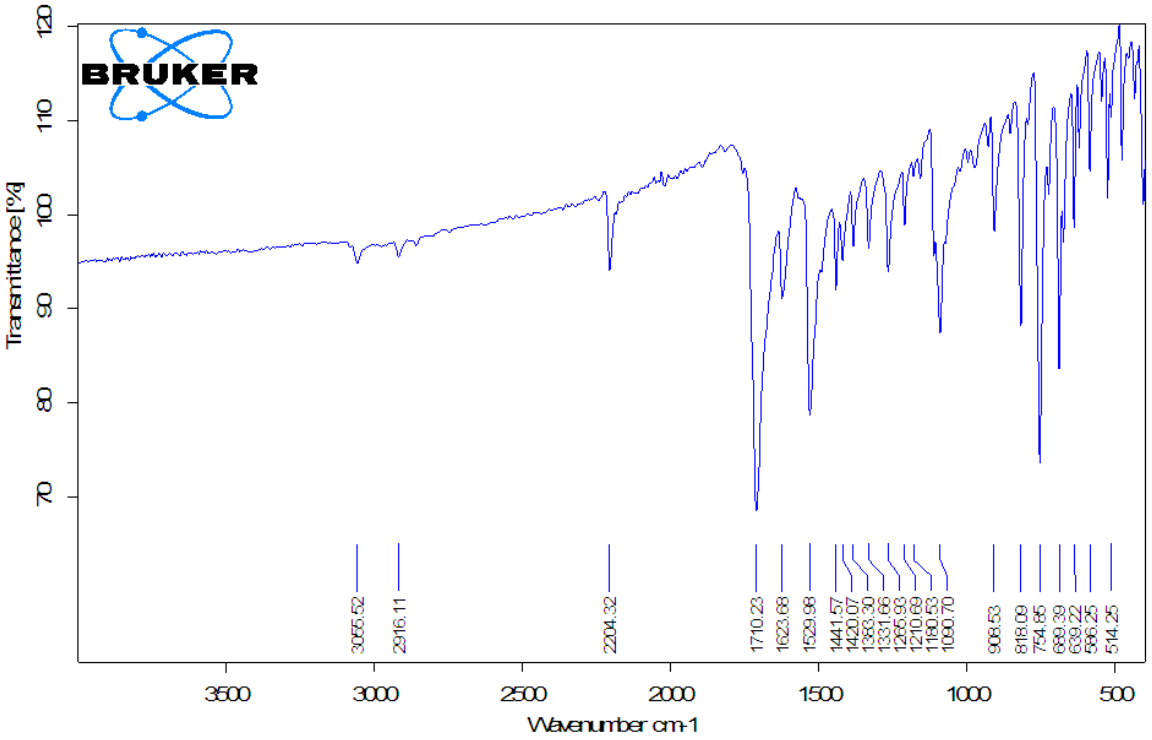

ATIR for compound 365f2.

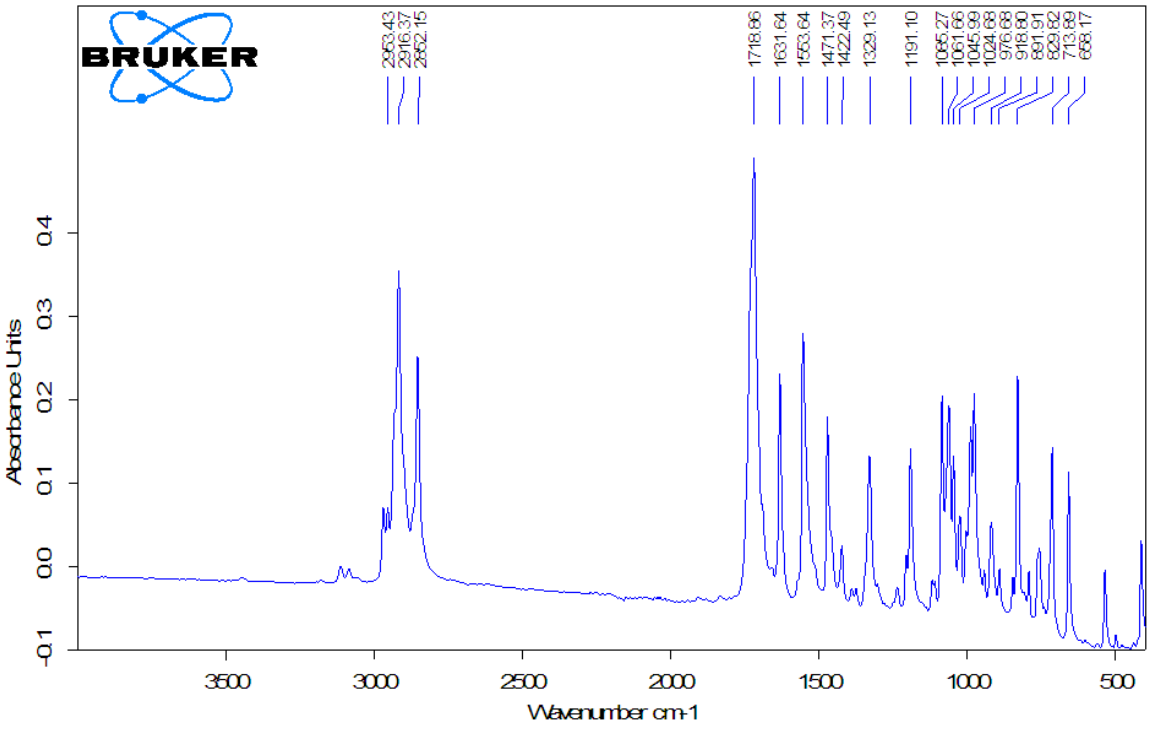

ATIR for compound 419f1.

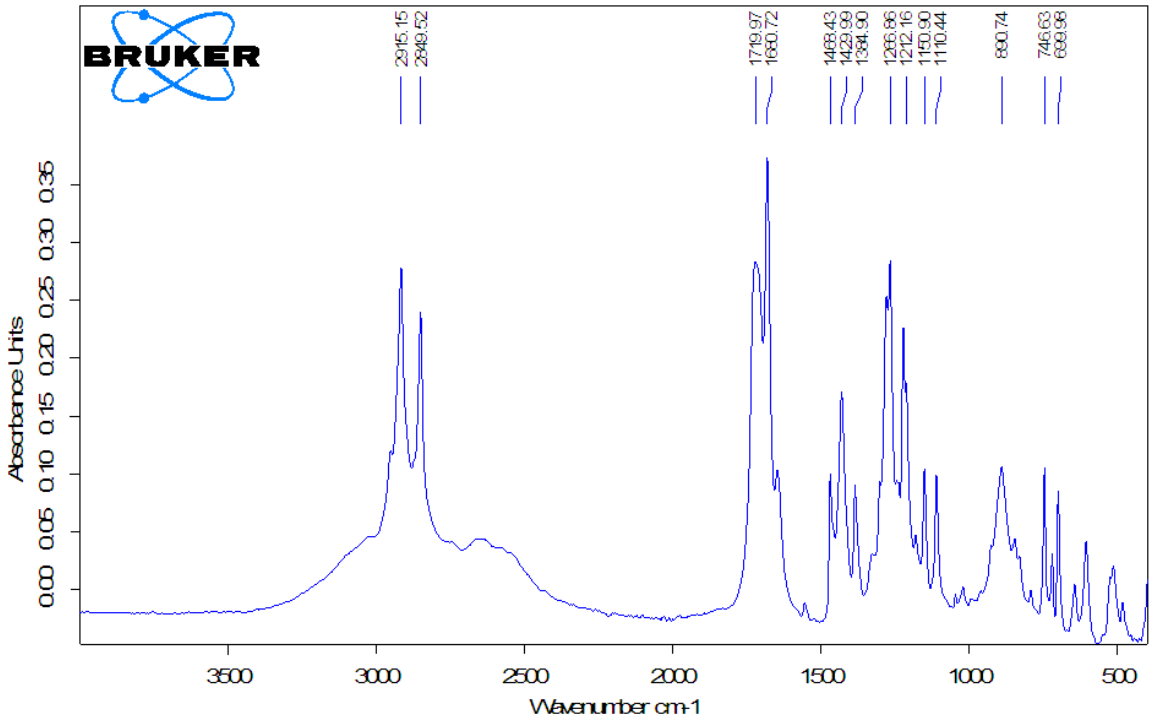

ATIR for compound 419f2.

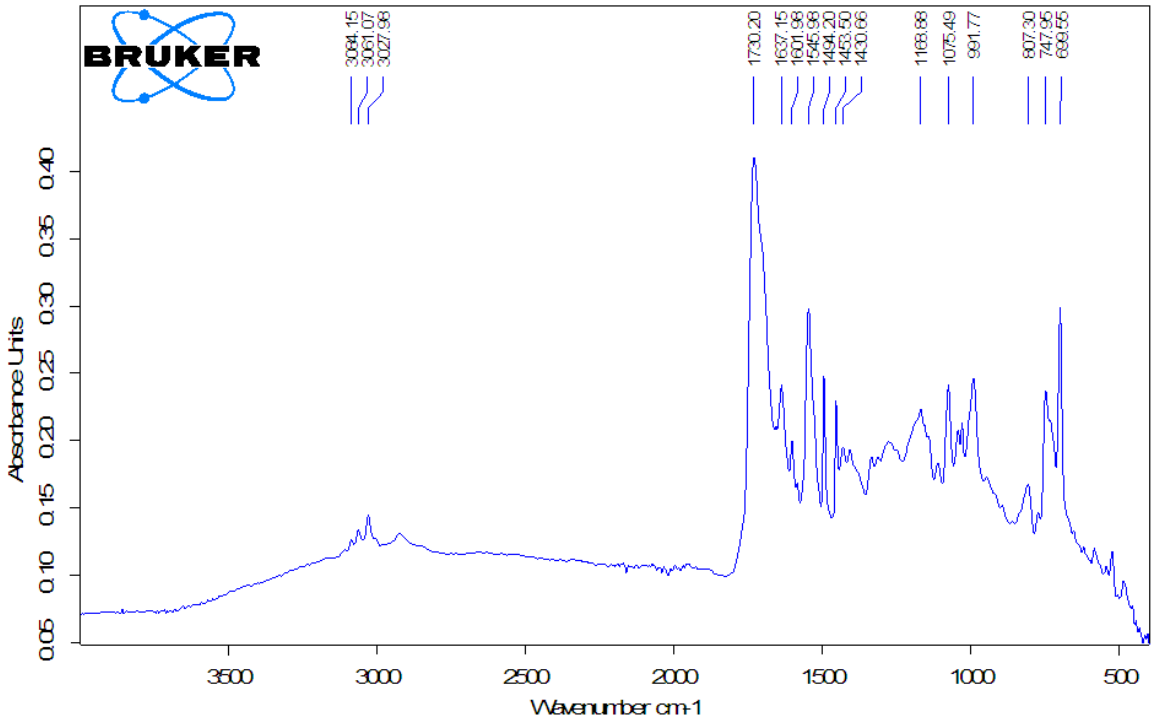

ATIR for compound 432f1

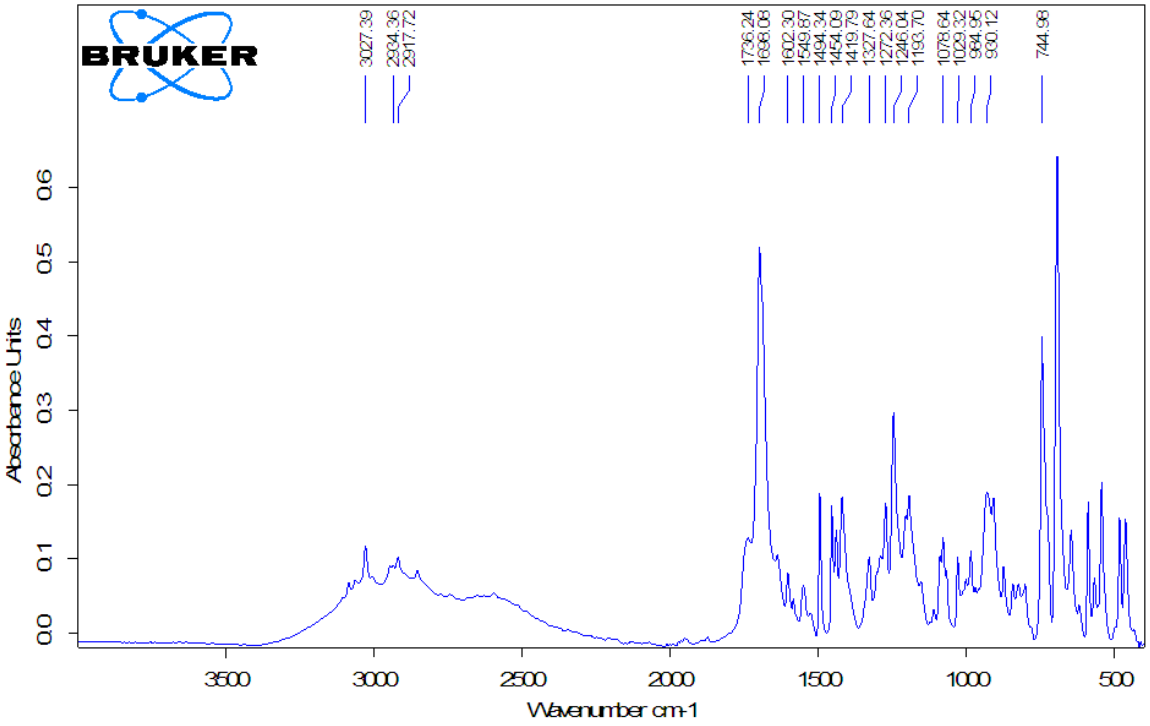

ATIR for compound 432f2.

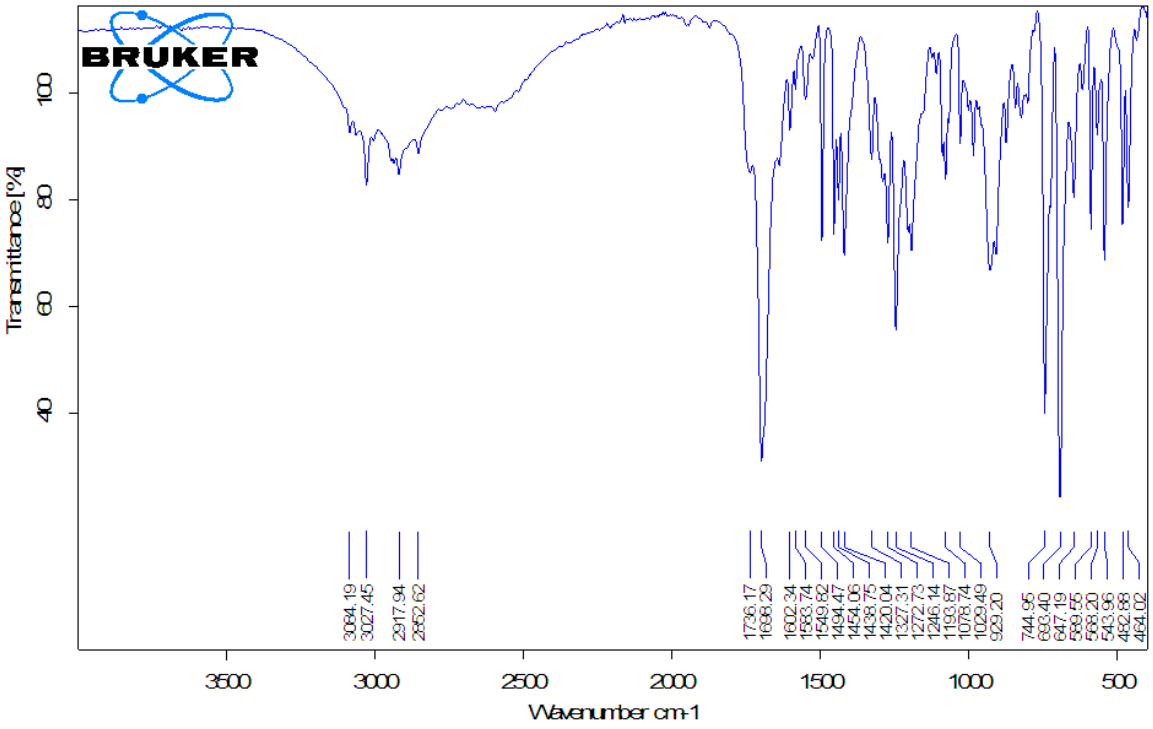

ATIR for compound 432f2.

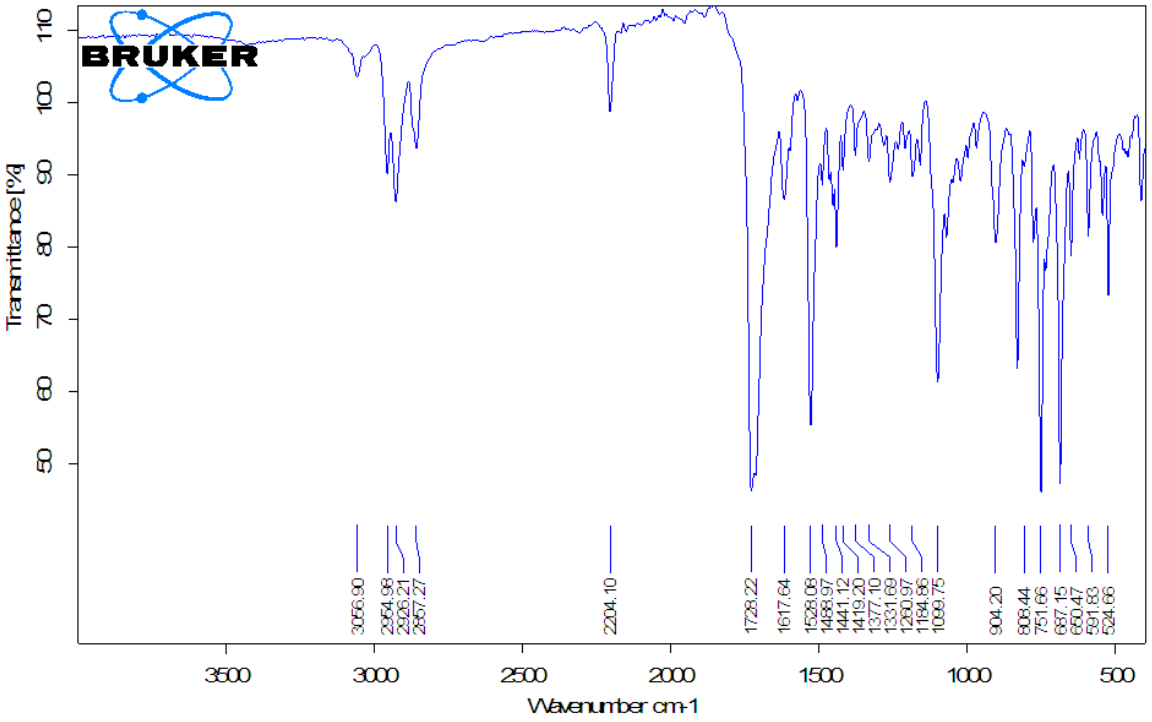

ATIR for compound 131a.

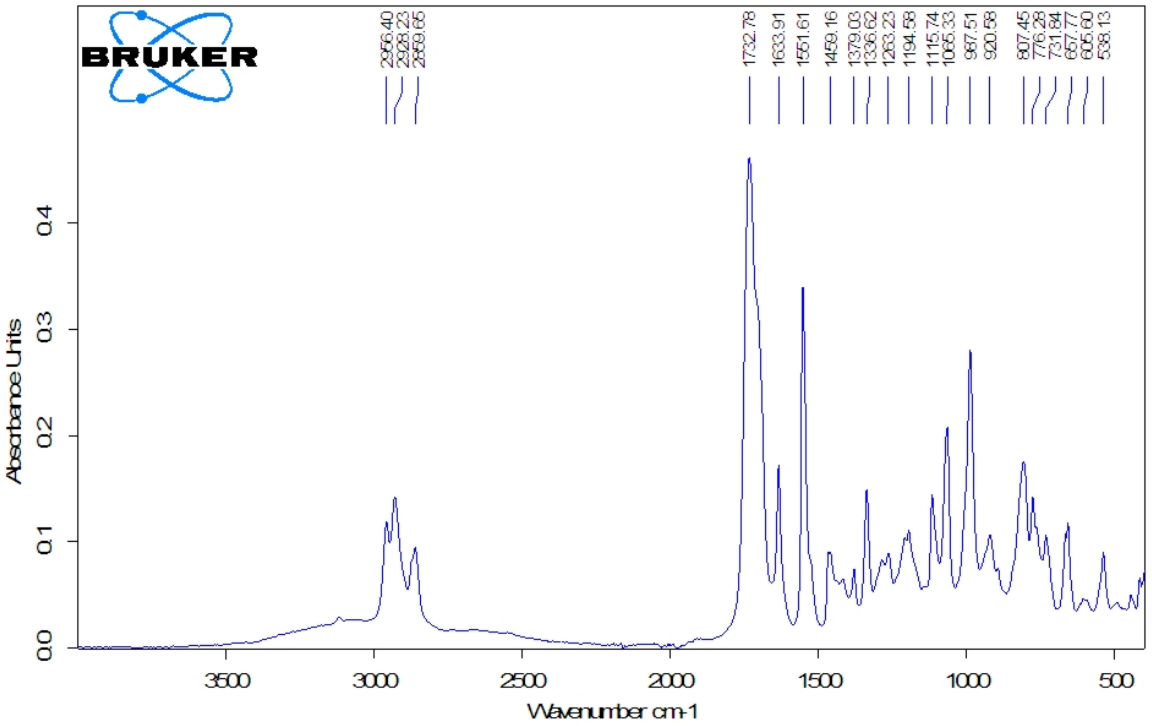

ATIR for compound 128c.

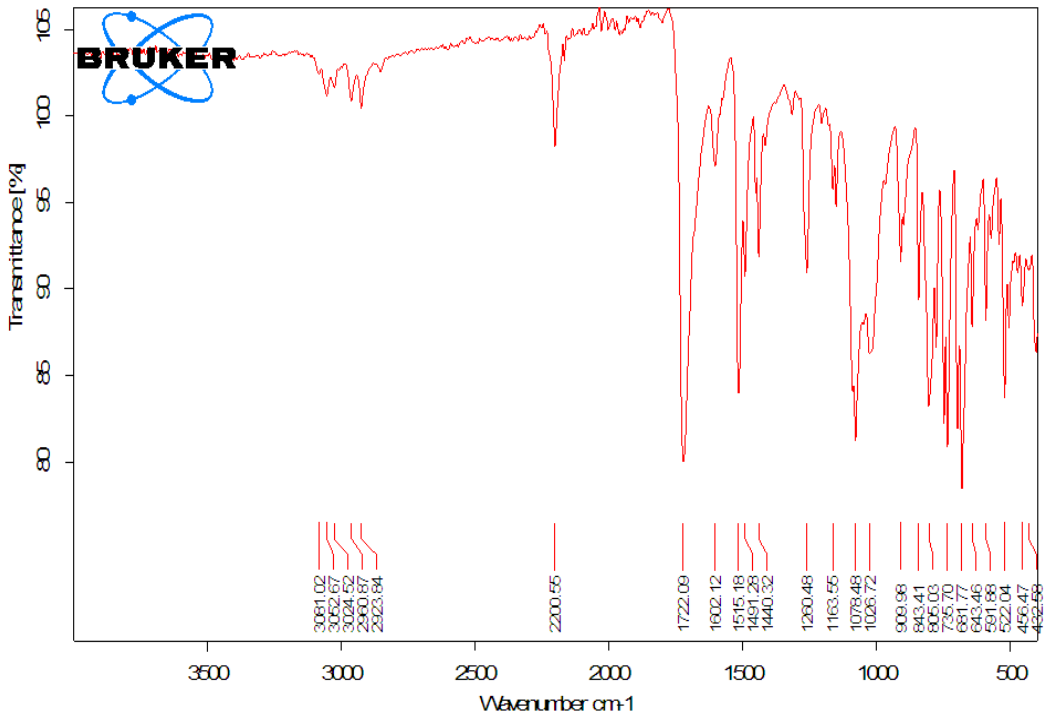

ATIR for compound 169a.

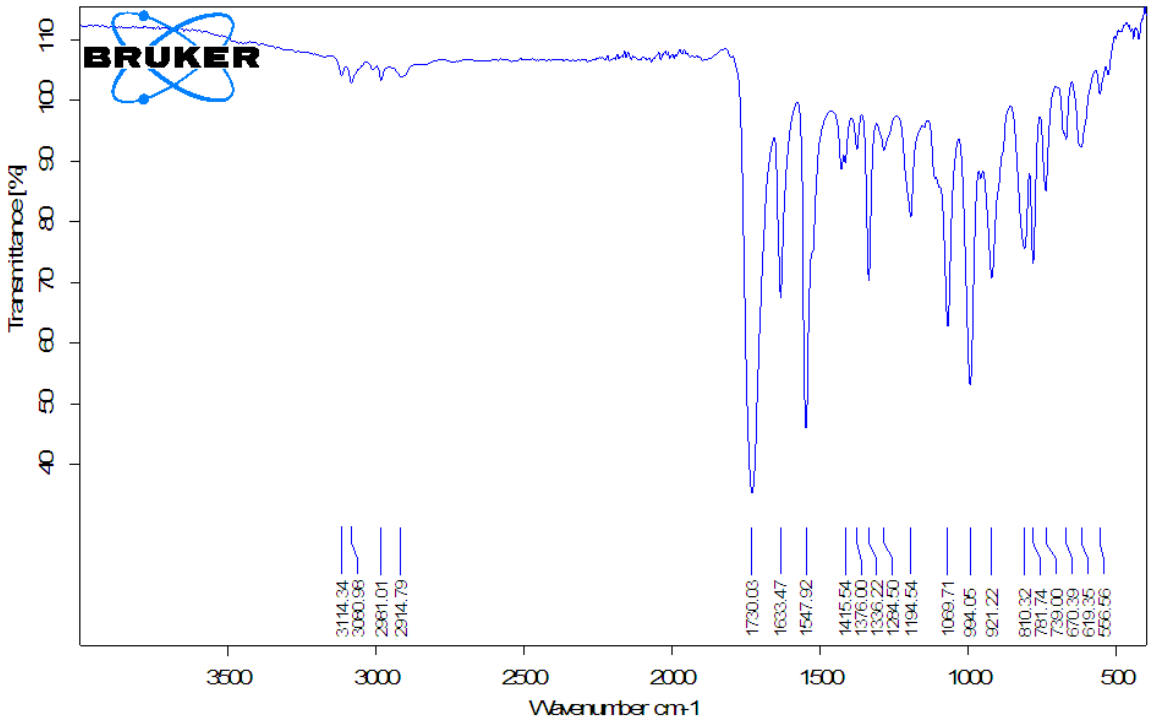

ATIR for compound 421f1.

Abbreviations

ABC Adenosine Triphosphate Multi-drug resistance Family

ADMET-absorption, distribution, metabolism, excretion and toxicology

AIDS-Acquired Immune Deficiency Syndrome

ALTADENA-adiabatic longitudinal transport after dissociation engenders nuclear alignment

AMR-Antimicrobial Resistance

Anti-TB-Anti-tuberculosis

ATIR-Attenuated transformed infrared

ADR-Adverse drug reactions

1AUJ- Bovine pancreatic protein, trypsin

BBB-Blood brain barrier

BDPA-Bis(Diphenylene)-2-phenylallyl

BLI-Bioluminescent imaging

CADD-computer-aided drug design

CC-Column chromatography

CDC-Centre for Disease control and Prevention

CDKR-Concentration-dependent killing rate

CHEMBL- ChEMBL is the welcome trust website for bioactive compounds

CLSI-Clinical and Laboratory Standards Institute

COSY- Correlation spectroscopy

CYP-Cytochrome P450

CS-Chemical shift

CT-Computed Tomography

CTRC-Chymotrypsin-C

DBSI-Drug-based similarity index

DBS-Drug-based similarity

DDI- Drug-drug interactions

DFT-Density functional theory

D-DNP-Dissolution dynamic nuclear polarization

DprE1-decaprenylphosphory D-ribose epimerase

E2- Elimination bimolecular

ETA-Ethionamide

EtaR- Ethionamide receptor

ESCs-Extended Spectrum Cephalosporin

ERO-Electrocyclic ring opening

ERC-electrocyclic ring closure

FBDD- Fragment-based drug discovery

FDA-American Food and drug administration

^{18}F-fluoro-DOPA-^{18}Fluoro dopamine neurotransmitter

ΔG- Change in free energy

HDAC -histone deacetylase

HIA-human intestinal absorption

HIV-Human Immune Deficiency Virus

hNMR-hyperpolarized NMR

h-PHIP-hydrogenative para-hydrogen induced polarization

HSQC-heteronuclear single quantum correlation

HTS- High Throughput Screening

Hz-Hertz

IGC_{50}-Growth inhibitory concentration when 50% of the bacteria is inhibited.

IR-Infrared

LE-Ligand efficiency

LDA-Lithium diisopropylamide

LBDS-Ligand-based drug screening

MFS- Major Facilitator Family

MI-Molecular Imaging LB- Lubia broth

MRI-Magnetic Resonance Imaging

MIC-Minimum inhibitory concentration

MICAD-Molecular imaging and contrast agents' database

MMP-Matched molecular pairs

MDR-Multi-Drug Resistant

MRS-Magnetic Resonance Spectroscopy

MRSA-methicillin resistant *Staphylococcus aureus*

M. tuberculosis-*Mycobacterium tuberculosis*

MDR-TB-multi-drug resistant tuberculosis

MS-ESI-Mass spectrometry by electron spray

MS-EI-Mass Spectrometry by electron ionization

MW-Molecular weight

N. gonorrhoeae- *Neisseria gonorrhoea*

NIR- Near infrared

NIRF-Near infrared fluorescent tag

NMR- Nuclear Magnetic Resistance

NP-Natural products

NOE-Nuclear overhauser effect

NOESY-Nuclear overhauser spectroscopy

OPSY-Only *para*hydrogen Spectroscopy

OD-Optical density

PASADENA- para-hydrogen and synthesis allow dramatically enhanced nuclear

PET-Positron Emission Tomography

PDT-Photodynamic therapy

P-gp-P-glycoproteins

PHIP-*para*hydrogen induced polarization

PPB-Plasma protein binding

PPM-parts per million

PS-Photosensitizer

P-type ATPase- Copper-transporting P-type ATPase

PTMS-Post-translational modification

QSTR-Quantitative Structure Toxicity relationship

QSAR-Quantitative structure-activity relationship

REDOR NMR- Rotational-echo double resonance

RND-Resistance-nodulation-division family

SAR- Structure-activity relationship

SARS-Severe Acute Respiratory Syndrome

SABRE- Signal amplification by reversible exchange

SBDS-Structure-based drug screening

S. aureus- *Staphylococcus aureus*

SMR-Small Multi-drug resistance Family

SPECT-Single Photon Emission Computed Tomography

STD- Saturation transfer difference NMR

STE-Stimulation edited echo

STI-Sexually transmitted Infection

S_N2- Substitution Bimolecular

ssNMR- Solid State NMR

T_1-Longitundinal Relaxation Rate

T_2-Spin-spin Relaxation Rate

TB-Tuberculosis

TBAB=Tetrabutylammonium bromide

THF-Tetrahydrofuran

TINS-target immobilized NMR screening

TP-Tetrahymena pyriformis toxicity

1D-one dimensional

2D-two-dimensional

3D-Three Dimension

4H4F-Human chymotrypsin-C

1QZQ- Human tyrosyl-DNA phosphodiesterase enzyme

1MU9-human tyrosyl-DNA phosphodiesterase

2E5C-Muscleblind-like protein 1

5TVP- human tyrosyl-DNA phosphodiesterase 2

2MZ2-Cannabinoid Receptor 1

3SN6-Beta-2 adrenergic G-protein receptor

5FIJ- HTH-type transcription regulator

VRE-Vancomycin resistant *Enterococcus*

XDR-Extensively Drug Resistant

ZA- Zymonic acid

References

[1] Franklin T. J. & Snow G. A. ‘’Biochemistry and Molecular Biology of Antimicrobial Action’’. 6th Edn. 2005, Springer, England.Pg.1-174.

[2] David van Duin, and David Paterson. *Infect Dis Clin North Am.* **2016**; 30(2): 377–390.

[3] Economou V and Gousia P. *Infect. Drug Resist*. **2015**; 8; 49-61.

[4] Sirijan Santajit and Nitaya Indrawattana. *BioMed. Research International* **2016**, Article ID 2475067, 8 pages.

[5] Rice LB, *Infection Control and Hospital Epidemiology*, **2010**; 31; S7–S10.

[6] Deguchi T, Nakane K, Yasuda M and Maeda S. *J. Urology* **2010**; 184: 851-858.

[7] Wright GD. *BMC Biology* **2010**, 8:123.

[8] Lewis K. *Nature Reviews Microbiology* 2007; 5 (1); 48–56.

[9] Balaban N.-Q., Gerdes K., Lewis K., and McKinney J. D., *Nature Rev. Microbiol.* **2013**, 11; 587-591. b.) Balaban, N.-Q., Merrin J., Chait R., Kowalik L., and Leibjer S., Science **2004**, 305.5690: 1622-1625.

c) Brown B. L., Lord D. M., Grigoriu S., Peti W., and Page R., J. Biol. Chem. 2013, 288: 1286-1294.

[10] international Statistical Classification of Diseases and Related Health Problems (ICD). b**)** Antimicrobial resistance: global report on surveillance **2014**. World Health Organization; **2014.** Global tuberculosis report 2016.

[11] Lozano R, Naghavi M, Foreman K, Lim S, Shibuya K *et al*., *Lancet* **2012**; 64: 357-372

[12] Markus Rudin and Ralph Weissleder. *Nat Rev. Drug Discov, **2003**,*2;123-131.

[13] Weissleder, R. *Nature Rev. Cancer* **2002**; 2, 11–18.

[14] Weissleder R. *Science* **2006**; 312:1168-1171.

[15] A. Quon, S. S. Gambhir, *J. Clin. Oncol*. **2005**, 23, 1664.

[16] Chen K.; and Chen X. *Current Topics in Medicinal Chemistry*, **2010**, 10, 1227-1236.

[17] Evelhoch, J. L., Gillies R. J., Karczmar G. S., Koutcher J. A., Maxwell R. J., Nalcioglu O., Raghunand N., Ronen S. M., Ross B. D., and Swartz H. M., *Neoplasia* **2000**. 2, 152–165.

[18] Cherry, S. R. *J. Clin. Pharmacol*. **2001**, 41, 482–491.

[19] Pilowsky, L. S. *Nucl. Med. Commun*. **2001**, 22, 829–833.

[20] Nicholson, J. K., Connelly, J., Lindon, J. C. & Holmes, E. *Nature Rev. Drug Discov.***2002**, 1, 153–161.

[21] Chen K and Conti P.S. *Adv. Drug Deliv. Rev.***2010**, 62, 1005-1022.

[22] Massoud T. F. and Gambhir S. S. *Nat. Biotech*. **2006**, 24, 905-908.

[23] MICAD-Molecular Imaging and Contrast Agent Database (MICAD). www.micad.nlm.nih.gov. National Centre for Biotechnology Information USA. Updated up to **2013**.

[24] Alauddin M. M., Shahinian A., Kundu R. K., Gordon E. M., and Conti P. S., *Med Biol* **1999**; 26:371-376.

[25] Macheda ML, Rogers S, Best JD. *J Cell Physiol*. **2005**; 202:654–662

[26] Lorberboym M, Feldbrin Z, Hendel D, Blankenberg FG, Schachter P. *J Nucl Med.* **2009**; 50: 534-537.

[27] Doss M, Kolb HC, Walsh JC, Mocharla V, Fan H, Chaudhary A, Zhu Z, Alpaugh RK, Lango MN, Yu JQ. *J Nucl Med*. **2013**; 54: 2087-2092.

[28] Kasina S, Rao TN, Srinivasan A, Sanderson JA, Fitzner JN, Reno JM, Beaumier PL, Fritzberg AR. *J Nucl Med.***1991**; 32: 1445-1451.

[29] Gary D. Luker Kathryn E. Luker. *J. Nucl. Med*. **2008**; 49, 1-4.

[30] Massoud TF, Paulmurugan R, Gambhir SS. *FASEB J.***2004**;18:1105–1107.

[31] Paulmurugan R, Gambhir S. *Cancer Res*. **2005**; 65:7413–7420.

[32] Remy I, Michnick SW. A. *Nat Methods*. **2006**; 3:969–971.

[33] Paulmurugan R, Gambhir S. *Anal Chem*. **2003**; 75:1584–1589. B) Paulmurugan R, Gambhir S. *Anal Chem*. **2005**; 77:1295–1302. C) Paulmurugan R, Gambhir S. *Anal Chem.***2007**; 79:2346–2353.

[34] Paulmurugan R, Gambhir S. *Proc Natl Acad Sci USA*. **2006**; 103:15883–15888.

[35] Zhang L, Lee C. K., Bhojani M. S., Khan A. P., Shilman A., Holland E. C., Ross B. D., and Rehemtulla A., *Nat Med*. **2007**; 13:1114–1119

[36] a) Luker KE, Hutchens M, Schultz T, Pekosz A, Luker GD. *Virology*. **2005**; 341:284–300. b) Luker GD, Pica CM, Song J, Luker KE, Piwnica-Worms D. *Nat Med*. **2003**; 9:969–973. c) Luker KE, Smith MCT, Luker GD, Gammon S, Piwnica-Worms H, Piwnica-Worms D. *Proc Natl Acad Sci* USA. **2004**; 101:12288–12293.

[37] Zhang G. J., Safran M., Wei W., Sorensen E., Lassota P., Zhelev N., Neuberg D. S., Shapiro G., and Kaelin Jr. W.G., *Nat Med.* **2004**; 10:643–648.

[38] Safran M., Kim W. Y., O'Connell F., Flippin L., Günzler Horner J. W., Depinho R. A., and Kaelin G. W., *Proc Natl Acad Sci USA.* **2006**; 103:105–110.

[39] Funovics M, Weissleder R, Tung C. *Anal Bioanal Chem*. **2003**; 377:956–963.

[40] Grimm J, Kirsch G. D., Windsor D. S., Kim B. F. C., Santiago M. P., Ntziachristos V., Jacks T., and Weissleder R., *Proc Natl Acad Sci USA*. **2005**;102: 14404–14409.

[41] Turk V, V Stoka, Vasiljeva O., Renko M., Sun T., Turk B., and Turk D. *Biochim Biophys Acta,* **2012**, 1824; 68-88

[42] Hernandez AA, WR. Roush. *Curr Opin Chem Biol*, **2002**, 6; 459-465

[43] Jiang T, Olson E, Nguyen Q, Roy M, Jennings P, Tsien R. *Proc Natl Acad Sci USA*. **2004**; 101:17867–17872

[44] Bingham J.P., Bian S., Tan Z.Y., Takacs Z., Moczydlowski E. *Bioconjug. Chem.* **2006**; 17:689–699. doi: 10.1021/bc060002u.

[45] Arnesano F, Banci L., Bertini I., Felli IC, Losacco M., Natile G. *J. Am. Chem. Soc.* **2011**, 133, 18361.

[46] Lange A, Giller K, Hornig S, Martin-Eauclaire MF, Pongs O, Becker S, and Baldus M. *Nature***2006**; 440:959. b) Lange, A., Becker, S., Seidel, K., Giller, K., Pongs, O., and Baldus, M. *Angew. Chem. Int. Ed. Engl.* **2005**; 44:2089–2092.

[47] Ali, N. A. A., Pilgrim, H., Liberra, K., Lindequist, U. & Jansen, R. *Phytochemistry* **1996**; 41:927–929.

[48] Mo, S., Wang S., Zhou G., Yang Y., Li Y., Chen X., and Shi J., *J. Nat. Prod*. **2004**; 67:823–828.

[49] Cragg, G.M.; Newman, D.J. *Pure Appl. Chem*. **2005**, 77, 7–24.

[50] Bozdogan B, Appelbaum PC. *Int. J. Antimicrob. Agents.* **2004**; 23: 113-119.

[51] Slee M. A., Wuonola M. A., McRipley R. J., Zajac I., Zawada M. J., Bartholomew P. T., Gregory W. A., Forbes M., *Antimicrob Agents Chemother*., **1987**; 31: 1791-1797.

[52] a) Avent A.G., Hanson J. R., and Truneh A., *Phytochemistry*, **1992**: 31: 3447 3449. b) Geiseler O., and Podlech J., *Tetrahedron* **2012**; 68: 7280-7287

[53] Abraham, W.-R., Knoch, I. and Witte, L. *Phytochemistry* **1990**; 29; 2877. B) Perrin, P. W. & Towers, G. H. N. *Phytochemistry* **1973**; 12: 589–592. c) Perrin, P. W. & Towers, G. H. N. *Phytochemistry* **1973**; 12:583–588.

[54] Ciavatta M. L., Manzo E., Nuzzo G., Villani G., Cimino G., Cervera J. L., Malaquias M. A. E., Gavagnin M., *Tetrahedron Lett.* **2009**; 50: 527–529

[55] Irschik H., Gerth K., Höfle G., Kohl, W., Reichenbach H., *J. Antibiot. (Tokyo)* **1983**; 36:1651–1658.

[56] Mukhopadhyay J., Das K., Ismail S., Koppstein D., Jang M., Hudson B., Sarafianos S., Tuske S., Patel J., Jansen R., Irschik H., Arnold E., and Ebright R. H., *Cell* **2008**; 135: 295– 307.

[57] Wang Y., Wang S.-J., Mo S.-Y., Li S., Yang Y.-C., and Shi J.-G, *Org. Lett.* **2005**; 7:4733–4736.

[58] a) Awadh Ali, N. A., Mothana, R. A., Lesnau, A., Pilgrim, H. & Lindequist, U. *Fitoterapia* **2003**; 74, 483–485. b) Tyagi S., Nuermberger E., Yoshimatsu T., Williams K., Rosenthal I., Lounis N., Bishai W., Grosset J., *Antimicrob. Agents Chemother*. **2005**; 49: 2289–2293.

[59] Stover C. K., Warrener P., VanDevanter D. R, Sherman D. R., Arain T. M., Langhorne M. H., Anderson S. W., Towell J. A., Yuan Y., McMurray D. N., Kreiswirth B. N., and Barry C. E., *Nature* **2000**; 405:962–966.

[60] Purtov K. V., Petushkov V. N., Baranov M. S., Mineev K. S., *Angew. Chem. Int. Ed*. **2015**; 54; 8124-8128.

[61] Stover, C. K., Warrener P., VanDevanter D. R.**,** *Nature* **2000;** 405:962-966.

[62] Park, I. H., Jeon, S. Y., Lee, H. J., Kim, S. I. & Song, K. S. *Planta Med*. **2004**; 70:143–146.

[63] McGlacken S.T., Kaiser M., Boshoff H.I., Boyd P. D. W., and Copp B. R., *Bioorg. Med. Chem.* **2012**, 20,1482-1493.

[64] Ndom JC, Mbafor JT, Kakam Z, Happi N, Vardamides JC, Mbaze Meva'a L, Mpondo TN, Fomum ZT. *Bol Latinoam Caribe Plant Med Aromaticas*, **2007**, 6:73– 80.

[65] Hamisi M. Malebo, Charles Kihampa, Clarence A. Mgina, Fortunatus Sung'hwa, Reiner Waibel, Stephan A. Jonker, and Mayunga H. H. Nkunya. *Nat Prod Bioprospect*. **2014**; 4: 129–133.

[66] Ronson T.O, Burns M. J, Voelkel M. H. H., Evans K. J., Jason L. M., Taylor R. J. K. and Fairlamb I. J. S., *Chem. Eur. J.* **2015**; 21;18905-18909.

[67] Brachmann A.O, Brameyer S., Kresovic D., Hitkova I., Kopp Y., C. Manske K., Schubert K., Bode H. B., Heermann R., *Nat. Chem. Biol*. **2013**; 9; 573–578.

[68] Suzie Park, Han-Shin Kim, Kiwon Ok, YunHye Kim, Hee-Deung Park, Youngjoo Byun, *Bioorg. & Med. Chem. Lett.* **2015**; 25: 2913–2917.

[69] Giovanni Appendino, Enrico Mercalli, Nicola Fuzzati, Lolita Arnoldi, Michael Stavri, Simon Gibbons, Mauro Ballero, and Andrea Maxia. *J. Nat. Prod.* **2004**, 67, 2108-2110.

[70] Kim, J. P., Yun, B. S., Shim, Y. K. & Yoo, I. D. *Tetrahedron Lett*. **1999**; 40, 6643–6644.

[71] Al-Yahya, M. A.; Muhammad, I.; Mizra, H. H.; El-Feraly, F. S. *Phytother. Res*. **1998**, 12, 335-339.

[72] Sucipto H., H. Sahner H., Prusov E., Wenzel S. C., R. W. Hartmann R. W., J. Koehnke J., and Müller R.**,** *Chem. Sci.*, **2015**, **6**, 5076-5085.

[73] Mukhopadhyay J., K. Das, S. Ismail, D. Koppstein, M. Jang, B. Hudson, S. Sarafianos, S. Tuske, J. Patel, R. Jansen, H. Irschik, E. Arnold and R. H. Ebright, *Cell*, **2008**, **135**, 295–307. Singh, S. B. et al. *J. Ind. Microbiol. Biotechnol*. **2003**; 30, 721–731.

[74] Belogurov G. A., Vassylyeva M. N., Sevostyanova A., Appleman J. R., A. X. Xiang, Lira R., Webber S. E., Klyuyev S., Nudler E., Artsimovitch I. and Vassylyev D. G., *Nature*, **2009**, 457, 332–335.

[75] Lira R., Xiang A. X., Doundoulakis T., Biller W. T., Agrios K. A., Simonsen K. B., Webber S. E., Sisson W., Aust R. M., Shah A. M., Showalter R. E., Banh V. N., Steffy K. R. and Appleman J. R., *Bioorg. Med. Chem. Lett.*, **2007**, 17, 6797–6800

[76] Erol Ö., Schäberle T. F., Schmitz A., Rachid S., Gurgui C., El Omari M., Lohr F.,

Kehraus S., Piel J., Müller R. And König G. M., *ChemBioChem*, **2010**, 11, 1235–1265.

[77] a) Atul Goel, Vishnu J. Ram. *Tetrahedron* **2009**; 65: 7865–7913. b) Pratap R. and Ram V. *Tetrahedron* **2017**; 73: 2529-2590

[78] Dobler D and Reiser O. *J. Org. Chem*. **2016**, 81, 10357−10365.

[79] Pirkle WH, Turner WV, *J. Org. Chem.* **1975**; 40:1617.

[80] Woodard BT, Posner G H. *Advances in Cycloaddition*. 1999; **5**: 47–83.

[81] Pirkle, W. H.; McKendry, L. H. *Tetrahedron Lett.* **1968**, 5279.

[82] Pirkle, W. H.; McKendry, L. H. *J. Ame. Chem. Soc.,* **1969**, *91*, 1179.

[83] Pirkle WH and Turner WV. *J. Org. Chem*., **1975**; 40:1617-1620

[84] Akilandeswari L. and Venuvanalingam P. *J. Theoretical and Computational Chem.,* **2007**; 6:233–243.

[85] a) Susana Breda, Leszek Lapinski, Rui Fausto, and Maciej J. Nowak. *Phys. Chem. Chem. Phys.*, **2003**, **5**, 4527-4532. b) Susana Breda, Leszek Lapinski, Rui Fausto and Maciej J. Nowak. *Phys. Chem. Chem. Phys*., **2003**, 5, 4527–4532

[86] Grigalunas M., West O., and Helquist P. *Org Lett*. **2016**; 18: 5724-5727.

[87] Dombray T., Blanc A., Weibel J.-M., Pale P. *Org. Lett.* **2010**; 12: 5362-5365.

[88] Manikandan R and Jeganmohan M., *Org Lett*. **2014**; 16: 652-655.

[89] Li-Chen Xu, Peng Zhou, Jia-Zhuo Li, Wen-Juan Hao, Shu-Jiang Tu and Bo Jiang. *Org. Chem. Front.*, **2018**, Advance Article.

[90] Marangoni MA, Bencke CE, Bonacorso HG, Martins MAP, and Nilo Zanatta. *Tetrahedron Lett.* **2018**; 59: 121–124.

[91] Horvath D. and Jeansdenas C. *J. Chem. Inf. Comput. Sci.* **2003**; 43: 680-690.

[92] McGlacken, G. P.; Fairlamb, I. J. S. *Nat. Prod. Rep*. **2005**, 22, 369−385.

[93] (a) Goel, A.; Ram, V. J. *Tetrahedron* **2009**, 65, 7865−7913. (b) Dickinson, J. M. *Nat. Prod. Rep*. **1993**, 10, 71−98.

[94] Weissleder R., Ross B. D., Rehemtulla A., and Gambhir S., S., Molecular Imaging: Principles and Practice, 2010; People's Medical Publishing House, USA, pgs. 1-9.

[95] Lipinski C.A; Lombardo F; Dominy B. W.; Feeney P.J. *Adv. Drug Delivery Rev*. **1997**, 23, 3-25.

[96] Talele TT, Khedkar SA, Rigby AC. *Curr Top Med Chem*. **2010**; 10:127–141.

[97] Halgren, T.A.; Murphy, R.B.; Friesner, R.A.; Beard, H.S.; Frye, L.L.; Pollard, W.T.; Banks, J.L. *J. Med. Chem*., **2004**, 47, 1750-1759.

[98] Shoichet B. K., Kuntz I. D., Bodian D. L., *J. Computational Chem*. **2004**; 13: 380–397.

[99] Leach, A.G.; Jones, H.D.; Cosgrove, D.A.; Kenny, P.W.; Ruston, L.; MacFaul, P.; Wood, J.M.; Colclough, N.; Law, B. *J. Med. Chem*., **2006**, 49, 6672-6682.

[100] Ripphausen P, Nisius B, Peltason L, Bajorath J. Quo Vadis, *J Med Chem.* **2010**;53:8461–8467.

[101] Colombo P., Cocconi D., Santi P., Bettini R., Massimo G., Catellani P. L., and Terazano C., (**2001**) in ''Pharmacokinetic Optimization in Drug Research: Biological, Physicochemical and Computational Strategies'' Eds. Testa, B., Van de Waterbeemd, H., Folkers, G. & Guy, R. Wiley-VCH, Zurich, pg 447-464. Conference: 2nd Lipophilicity Symposium.

[102] Fujita T., 'The extra-thermodynamic Approach to Drug Design.' In Hansch C., ed. Comprehensive Medicinal Chemistry. New York, Pergamon Press, **1990**; 4: 497-560.

[103] SwissADME: a free web tool to evaluate pharmacokinetics, drug-likeness and medicinal chemistry friendliness of small molecules. Sci. Rep. 2017, 7:42717. J. Chem. Inf. Model, 2016, 56, 1399-1404.

[104] Zoete V., Daina A., Bovigny C., and Michelin O., SwissSimilarity: A web tool for low to ultra-high throughput ligand-based virtual screening.

[105] ILOP: a simple, robust, and efficient description of n-octanol/water partition coefficient for drug design using the GB/SA approach. J. Chem. Inf. Model, 2014, 54; 3284-3301.

[106] Lemke T. L., Review of organic functional groups: introduction to medicinal organic chemistry'' 4th Ed, Philadelphia. Lippincott, Williams and Wilkins, 2003.

[107] Wadood A, Ahmed N, Shah L, Ahmad A, Hassan H, Shams S. *Drug Design & Delivery* **2013**; 1:3.

[108] A BOILED-Egg to predict gastrointestinal absorption and brain penetration of small molecules. ChemMedChem., 2016, 11: 1117-1121.

[109] Wang B., Yang L. P., Zhang X. Z., Huang S. Q., Bartlam M., Zhou S. F. Drug Metab. Rev. **2009**, 41, 573–643.

[110] Wójcikowski J., Maurel P., Daniel W. A. Drug Metab. Dispos. **2006**, 34, 471–476.

[111] Nishimura M, S. Naito*, Drug Metab. Pharmacokinet.* 20 **2005;** 20; 452–477.

[112] Gfeller D., Michielin O. and Zoete V. *Bioinformatics* **2013**, 29: 3073-3079.

[113] Chu X, K. Korzekwa, R. Elsby, K. Fenner, A. Galetin, Y. Lai, et al., *Clin Pharmacol. Ther*. **2013**; 94; 126–141.

[114] Lemke T. L., Williams D. A., Roche V. F., and Zito S. W., *''Foye's Principles of Medicinal Chemistry''* 6th Ed. Lippincott, Williams and Wilkins. Wolters Kluwer Health. Philadelphia. **2008**; pp 161-165.

[115] Giacomini K. M., Huang D.J., Tweedie L.Z., Benet L.Z., Brouwer K.L., Dahlin A., Hoffmaster K. A., Ishikawa T., Keppler D., Kim R. B., Niemi M.,

Sugiyama Y., Ware Y., Wright S. H., Yees W., and Zhang L., *Nat. Rev. Drug Discov.* **2010**; 9; 215–236.

[116] M.K. DeGorter, C.Q. Xia, J.J. Yang, R.B. Kim, *Annu. Rev. Pharmacol. Toxicol*. **2012**; 52; 249–273.

[117] Smith D., Di D. L., Kerns E. H., *Nat. Rev. Drug Discov*. **2010**; 9; 929–939.

[118] Koepsell H., Endou H., *Pflugers Arch.***2004**; 447; 666–676.

[119] Maeda K, Y. Tian, T. Fujita, Y. Ikeda, Y. Kumagai, T. Kondo, et al., *Eur. J. Pharm. Sci.* **2014**; 59; 94–103.

[120] David J. Wagner, Tao Hu, Joanne Wang, *Pharmacological Research* **2016**; 111; 237–246.

[121] Carpenter, T.S.; Kirshner, D.A.; Lau, E.Y.; Wong, S.E.; Nilmeier, J.P.; Lightstone, F.C. *Biophys. J.* **2014**, *107*, 630–641.

[122] Hochman, J.; Tang, C.; Prueksaritanont, T *J. Pharm. Sci.* **2015**, *104*, 916–929.

[123] Zsila, F.; Bikadi, Z.; Malik, D.; Hari, P.; Pechan, I.; Berces, A.; Hazai, E. *Bioinformatics* **2011**, *27*, 1806–1813.

[124] Bujak, R.; Struck-Lewicka, W.; Kaliszan, M.; Kaliszan, R.; Markuszewski, M.J. *J. Pharm. Biomed. Anal.* **2015**, *108*, 29–37.

[125] Race J. E., Grassl S. M., Williams W. J., Holtzman E. J., Biochem Biophys Res Commun **1999**; 255:508–514.

[126] Reid G., Wolff N. A., Dautzenberg F. M., Burckhardt G., Kidney Blood Press Res **1998;** 21:233–237.

[127] Roch-Ramel F., Besseghir K., Murer H., Renal excretion and tubular transport of organic anions and cations. *Handbook of Physiology. Renal Physiology.***1992** *Am. Physiol. Soc* Bethesda, MD, sect. 8, vol. II, chapt. 48, p. 2189–2262.

[128] Feng B., Hurst S., Lu Y., Varma M. V., Rotter C. J., El-Kattan A., Peter L., and Corrigan B., *Mol Pharmaceutics*. **2013**;10: 4207-4215.

[129] Yin J., Wang J., *Acta Pharmaceutica Sinica B*. **2016**; 6:363-373.

[130] Feng B., Varma M. V., *J Clin Pharmacol*. **2016**; 56: S110-S121.

[131] Imamura Y., Tsuruya Y., Damme K., Heer D., Kumagai Y., Maeda K., Murayama N., Okudaira N., Kurihara A., Izumi T., Sugiyama Y., and Kusuhara H., *Drug Metab Dispos*. **2014**; 42:685-694.

[132] Mathialagan S., Rodrigues A. D., Feng B., *J. of Pharm. Sci.***2017**, 106; 2535-2541.

[133] Thompson T. N., *Curr. Drug Metab*., **2000**, 1; 215-241.

[134] Guo H., Seet Q., Denkin S., Parsons L., Zhang Y.,*J Med Microbiol***. 2006**; 55:1527-31.

[135] Lepesheva, G. I., Hargrove T. Y., Kleshchenko, Y., Nes, W.D., Villalta, F. and Waterman, M.R. CYP51: a major drug target in the Cytochrome P450 superfamily. *Lipids*, **2008**, 43, 1117–1125.

[136] Lavender C, Globan M, Sievers A, Billman-Jacobe H, Fyfe *J: Antimicrob Agents Chemother*. **2005**:49:4068-74.

[137] DeBarber AE, Mdluli K, Bosman M, Bekker LG, Barry CE 3rd: *Proc Natl Acad Sci U S A.* **2000**; 97:9677-82. B) Rendic, S. and Di Carlo, F.J. *Drug Metab. Rev.,* **1997**; 29, 413–580.

[138] Maltarollo, V.G.; Gertrudes, J.C.; Oliveira, P.R.; Honorio, K.M. *Expert Opin. Drug Metab. Toxicol.* **2015**, *11*, 259–271. b) Nelson, D.R. Mining databases for cytochrome P450 genes. *Methods Enzymol.,* **2002***;* 357, 3–15.

[139] Colmenarejo, G. *Curr. Comput. Aided Drug Des.* **2005**, *1*, 365–376. Helma, C., *Curr. Opin. Drug Discov. Dev.* **2005**, *8*, 27–31.

[140] Guengerich F. P. *Drug Metab Pharmacokinet*. **2011**; 26: 3–14.

[141] Ajmani S., Jadhav K. and Kulkarni S. A., *QSAR Comb. Sci.,* **2009,** 28, 36–51.

[142] Dearden J.C*., IJQSPR*, **2016**, 1; 1-44.

[143] H. Yuan, Y.-Y. Wang, Y.-Y. Cheng. *J. Mol. Graph. Model*., **2007**, 26; 327-335.

[144] Cronin, M.T.D; Aptula A.O., Duffy J.C, T.I. Netzeva T.I; Rowe P. H., Valkova I.V; Wayne Schultz, T. Chemosphere, 2002; 49; 1201-1221. B) Mark Cronin T.D., and Schultz T. W. *Chem. Res. Toxicol*. **2001,** 14, 1284-1295.

[145] Kristien Mortelmans and Errol Zeiger. *Mutation Research* **2000**; 455:29–60

[146] Hansen, K.; Mika, S.; Schroeter, T.; Sutter, A.; TerLaak, A.; Steger-Hartmann, T.; Heinrich, N.; Muller, K. R. *J. Chem. Inf. Model.* **2009**, 49, 2077−2081.

[147] Cheng, F.; Li, W.; Zhou, Y.; Shen, J.; Wu, Z.; Liu, G.; Lee, P. W.; Tang, Y. admetSAR: a comprehensive source and free tool for assessment of chemical ADMET properties*. J. Chem. Inf. Model.* **2012**, 52, 3099−3105.b) Smith TF, Waterman MS. *J Mol Biol***1981**; 147: 195–197. b) Jie Shen, Feixiong Cheng, You Xu, Weihua Li, and Yun Tang. *J. Chem. Inf. Model.*, **2010**; 50; 1034-1041.

[148] Bender A., Glen R. C., *Org Biomol Chem.* **2004** ;2:3204–18.

[149] Maggiora G., Vogt M., Stumpfe D., Bajorath J., *J Med Chem.* **2014**; 57:3186–204.

[150] Kubinyi H. *Perspect Drug Discov Des.* **1998**;9-11:225–52.

[151] Eckert H., Bajorath J., *Drug Discov Today*. **2007**; 12:225–33.

[152] Bender A., Jenkins J. L., Scheiber J., Sukuru S. C. K., Glick M., Davies J. W., *J Chem Inf Model.* **2009**;49:108–19.

[153] Rogers D, Hahn M. *J Chem Inf Model*. **2010**;50:742–54.

[154] Cereto-Massagué A., Ojeda M. J., Valls C., Mulero M., Garcia-Vallvé S., Pujadas G. *Methods*. **2015**; 71:58–63.

[155] Reisen F., Zhang X., Gabriel D., Selzer P., *J Biomol Screen.* **2013**;18:1284–97.

[156] Holliday JD, Hu C-Y, Willett P. *Comb Chem High Throughput Screen*. **2002**;5:155–66.

[157] Chen X., Reynolds C. H., *J Chem Inf Comput Sci.* **2002**;42:1407–14.

[158] Salim N., Holliday J., Willett P., *J Chem Inf Comput Sci.* **2003**;43:435–42.

[159] Willett P., *Drug Discov Today.* **2006**;11:1046–53.

[160] Todeschini R., Consonni V., Xiang H., Holliday J., Buscema M., Willett P., *J Chem Inf Model.* **2012**;52:2884–901.

[161] Willett P., *J Chem Inf Model*. **2013**;53:1–10.

[162] Whittle M., Gillet V. J., Willett P., Alex A., Loesel J., *J Chem Inf Comput Sci.* **2004**;44:1840–8.

[163] Flower D. R., *J Chem Inf Comput Sci*. **1998**;38:379–86.

[164] Lajiness M. S., *Perspect Drug Discov Des*. 1997;7/8:65–84.

[165] Dixon S. L., Koehler R. T., *J Med Chem*. **1999**; 42:2887–900.

[166] Holliday J. D., Salim N., Whittle M., Willett P., *J Chem Inf Comput Sci.* **2003**;43:819–28.

[167] Godden J. W., Xue L., Bajorath J., *J Chem Inf Comput Sci*. **2000**;40:163–6.

[168] Congying Xu, Feixiong Cheng, Lei Chen, Zheng Du, Weihua Li, Guixia Liu, Philip W. Lee, and Yun Tang*., J. Chem. Inf. Model*. **2012**, 52, 2840−2847. B) Moroy G., Martiny V. Y., Vayer P., Villoutreix B. O., and *Miteva M. A. Drug Discovery Today* **2012;**17: 44-55

[169] **a)** Surade, S., Blaszczyk, M., Nikiforov, P.O., Abell, C., Blundell, T.L.., *Org Biomol Chem.* **2016**; 14: 2318–2326. b) Shen, J.; Cheng, F.; Xu, Y.; Li, W.; Tang, Y. Estimation of ADME properties with substructure pattern recognition. *J. Chem. Inf. Model.* **2010**, *50*, 1034–1041.

[170] a) DrugBankIophendylate. http://www.drugbank.ca/drugs/DB01187.

[171] Nikiforov, P.O., Surade, S., Blaszczyk, M., Delorme, V., Brodin, P., Baulard, A.R., Blundell, T.L., Abell, C**.** *Org. Biomol. Chem*. **2016**; 14: 2318-2326

[172] Tommaso A. Vannelli, Alina Dykman, and Paul R. Ortiz de Montellano. *J. Biol. Chem.* 2002; 277: 12824–12829.

[173] DeBarber, A. E., Mdluli, K., Bosman, M., Bekker, L.-G., and Barry, C. E., III. *Proc. Natl. Acad. Sci. U. S. A.* **2000**; 97: 9677–9682.

[174] Matsui H, Sakanashi Y, Oyama TM, Oyama Y, Yokota S, Ishida S, Okano Y, Oyama TB, Nishimura Y., *Toxicology*. **2008**; 27; 248(2-3)

[175] Fromtling RA: *Clin Microbiol Rev*. **1988**;1: 187-217.

[176] Source: Human Metabolome Database (HMDB). http://www.hmdb.ca/metabolites/HMDB0015318.

[177] Lee S. K., Kim D. H., Kim S. H., Lim D. J., *Eur Spine J*. 2013; 22 Suppl 3: S321-328.

[178] Gardner, G.: *Laryngoscope* **1980**; 90: 181–195.

[179] Britton, B. H., Hitselberger, W. E., Hurley, B. J.: *Arch. Otolaryngol*. **1968**; 88: 60–71.

[180] Warne T., Moukhametzianov R., Baker J. G., Nehmé R., Edwards P. C., Leslie A. G., Schertler G. F., Tate C. G., Nature. **2011**; 469: 241-244.

[181] Talevi A., *Front Pharmacol*. **2015**; 6: 205.

[182] https://www.ebi.ac.uk/chembldb.

[183] Lamb, J. *Nat. Rev. Cancer* **2007**, *7*, 54–60.

[184] Ahmed, J.; Worth, C. L.; Thaben, P.; Matzig, C.; Blasse, C.; Dunkel, M.; Preissner, R. FragmentStore–a comprehensive database of fragments linking metabolites, toxic molecules and drugs. *Nucleic Acids Res*. **2011**; 39: D1049−1054.

[185] Cheng, F.; Ikenaga, Y.; Zhou, Y.; Yu, Y.; Li, W.; Shen, J.; Du, Z.; Chen, L.; Xu, C.; Liu, G.; Lee, P. W.; Tang, Y., *J. Chem. Inf. Model*. **2012**; 52: 655−669.

[186] Merlot, C. *Drug Discovery Today* **2010**; 15: 16−22.

[187] Jonathan D. Tyzack, Hamse Y. Mussa, Mark J. Williamson, Johannes Kirchmair, and Robert C. Glen. *J Cheminform*. **2014**; 6: 29.

[188] Stefano Forli, Ruth Huey, Michael E. Pique, Michel Sanner, David S. Goodsell, and Arthur J. Olson. *Nat Protoc.* **2016**; 11: 905–919.

[189] Amy C. Anderson. David L. Mobley, and Pavel V. Klimvich. *J. Chem. Physics* 2012; 137:230901.

[190] Valère Lounnas, Tina Ritschel, Jan Kelder, Ross McGuire, Robert P. Bywater, and Nicolas Foloppe. *Comput Struct Biotechnol J.* **2013;** 5: e201302011.

[191] Alexander Scheer, Francesca Fanelli, Tommaso Costa, Pier G. De Benedetti and Susanna Cotecchia. *PNAS* **1997** February, 94 (3) 808-813.

[192] Xing Du, Yi Li, Yuan-Ling Xia, Shi-Meng Ai, Jing Liang, Peng Sang, Xing-Lai Ji, and Shu-Qun Liu. Int J Mol Sci. 2016; 17: 144.

[193] Nobuyuki Uchikoga and Takatsugu Hirokawar. *BMC Bioinformatics* **2010:** 11:236.

[194] Rasmussen, S.G., DeVree, B.T., Zou, Y., Kruse, A.C., Chung, K.Y., Kobilka, T.S., Thian, F.S., Chae, P.S., Pardon, E., Calinski, D., Mathiesen, J.M., Shah, S.T., Lyons, J.A., Caffrey, M., Gellman, S.H., Steyaert, J., Skiniotis, G., Weis, W.I., Sunahara, R.K., Kobilka, B.K. *Nature* **2011**; **477**: 549-555

[195] Rose AS, AR Bradley, Y Valasatava, JM Duarte, A Prlić and PW Rose. *Web-based molecular graphics for large complexes.* ACM Proceedings of the 21st International Conference on Web3D Technology (Web3D '16): 185-186, **2016**. doi:10.1145/2945292.2945324.

[196] Schellenberg, M.J., Lieberman, J.A., Herrero-Ruiz, A., Butler, L.R., Williams, J.G., Munoz-Cabello, A.M., Mueller, G.A., London, R.E., Cortes-Ledesma, F., Williams, R.S. *Science* **2017**; 357: 1412-1416.

[197] Ganjiwale, A., Eldeeb, K., Chandrashekar, I., Cowsik, S., Howlett, A. To be published.

[198] Takahashi, R., Nakamura, S., Nakazawa, T., Minoura, K., Yoshida, T., Nishi, Y., Kobayashi, Y., Ohkubo, T. *J. Biochem.* **2010**; 147: 95-107

[199] http://www.rcsb.org/pdb/.

[200] Rose A. S., and Hildebrand P. W., NGL Viewer: a web application for molecular visualization. *Nucl Acids Res*., **2015**; 43: W576-W579.

[201] a) Irina Kufareva and Ruben Abagyan. *Methods Mol Biol*. **2012**; 857: 231–257. b) Zemla A, Venclovas, Moult J, Fidelis K. *Proteins Suppl*. **2001**; 5: 13–21.c) Zhang Y, Skolnick J. *Bioinformatics*. **2004**; 57:702–710.

[202] http://autodock.scripps.edu/references. http://mgltools.scripps,edu/documentation/how-to/citing-pmv-adt-and-visit.

[203] Noel M O'Boyle, Michael Banck, Craig A James, Chris Morley, Tim Vandermeersch, and Geoffrey R Hutchison. Open Babel: An open chemical toolbox. *J. Cheminform*. **2011**; 3: 33.

[204] The Molecular Graphics Laboratory Forum; AutoDock, AutoLigand, MGLTools, Vina, PyRx and more.

[205] White R.L, Burgess D. S., Manduru M., and Bosso J. A., *Antimicrob. Agents Chemother.***1996;** 40;1914–1918.

[206] Patidar A.K., Selvam G., Jeyakandan R., Mobiya A. K., Bagherwal A., Sanadya G., and Mehta R. *Int. J. Drug Design and Discovery* **2011**; 2; 458-463.

[207] Davies, D.R., Interthal, H., Champoux, J.J., Hol, W.G.J**.** *J. Mol. Biol*. **2002**; **324**: 917-932

[208] Takahashi, R., Nakamura, S., Nakazawa, T., Minoura, K., Yoshida, T., Nishi, Y., Kobayashi, Y., Ohkubo, T**.***J. Biochem*. **2010**; **147**: 95-107

[209] Lee, S.L., Alexander, R.S., Smallwood, A., Trievel, R., Mersinger, L., Weber, P.C., Kettner, C. *Biochemistry* **1997**; **36**: 13180-13186

[210] Raymond, A.C., Rideout, M.C., Staker, B., Hjerrild, K., Burgin Jr., A.B. *J. Mol. Biol*. **2004**; **338**: 895-906.

[211] Gelb M., and Abeles R. H., *Biochem*. **1983**,

[212] Ringe D., Seaton B. A., Gelb M. H., Abeles R. H., *Biochem.* **1985**, 24;64-68.

[213] Abeles and Westkaemper, *Biochem.***1983**, 22, 3256.

[214] Konaté K, Mavoungou J. F., Lepengué A. N., Aworet-Samseny R. R., Hilou A., Souza A., Dicko M. H., and M'batchi B., *Ann. Clin. Microbiol. Antimicrob.* **2012**, 11;18.

[215] CLSI, ''Methods for Determining Bactericidal Activity of Antimicrobial Agents. Approved Guideline'', CLSI document M26-A. Clinical and Laboratory Standards Institute, 950 West Valley Road Suite 2500, Wayne, Pennsylvania 19087, USA, **1998**.

[216] Batra, J., Szabo, A., Caulfield, T.R., Soares, A.S., Sahin-Toth, M., Radisky, E.S. *J. Biol. Chem*. **2013**; **288**: 9848-9859.

[217] Boulanger WA and Katzenellenbogen JA. *J. Med. Chem*. **1986**, 29, 1159-1163.

[218] Ardenkjaer-Larsen J. H, Fridlund B, Gram A., Hansson G., Hansson L., Lerche M. H., Servin R., Thaning M., Golman K. *Proc Natl Acad Sci U S A.* **2003**; 100: 10158-63.

[219] Rossi FR, Ingold C. K. and Thorpe J. F. *J.Chem.Soc.***1923**,123,327

[220] a) Thorpe F.B., and Thole J.F. *J. Chem. Soc*. **1911**, 99,2187-2208.

[221] Ingold C. K., Powell W. J. *J. Chem. Soc*. 1**921**, 1222.

[222] Conrad M. and Guthzeit M. *Chem Ber*. **1882**, 15, 2841

[223] A) Mary Stoddard Hatch, William M. Brown, Jason A. Deck, Lucy A. Hunsaker, Lorraine M. Deck and David L. Vander Jagt. *Biochimica Biophysica Acta* **2002**, 1596, 381-392. B) Deck LM, Baca ML, Salas, SL, Hunsaker LA, and Vander Jagt DL. *J. Med Chem*.**1999,** 42, 4250-4256.

[224] Makozsa M. *Pure Appl. Chem.* **2000**, 27, 1399-1403.

[225] Wang Y.; Deng R.; Mi A.; and Jiang Y. *Synth. Commun.***1995**, 25, 1761-1764.

[226] Deng, R.; Wang, Y.; Jiang, Y. *Synth. Commun*. **1994,** 24, 1917–1921.

[227] Fedorynski, M.; Jezierska-Zieba, M.; Kakol, B. *Acta Pol. Pharm*. **2008**, 65, 647–654.

[228] A) Keglevich, G.; Novák, T.; Vida, L.; Greiner, I. *Green Chem*. **2006**, 8, 1073–1075. B) Keglevich, G.; Majrik, K.; Vida, L.; Greiner, I. *Lett. Org. Chem*. **2008**, 5, 224–228. C)

[229] Norman C. Craig, Anthony Chen, Ki Hwan Suh, Stefan Klee, Georg C. Mellau*, J. Am. Chem*. Soc. **1997**, 119, 4789-4790.

[230] Durst, H., and Liebeskind, L. *J. Org. Chem*. **1974**, 39,3271.

[231] Thompson D. L.; and Reeves P. C. *J. Chem. Ed*. **1985**, 62; 907-908.

[232] Shengming Ma and Lu Xiyan. Organic Syntheses Coll. **1998**, 9;415. B) Ma et al*., JCS. Chem Commun*. **1990**. c) Shengming Ma; Lu Xiyan. *Organic Syntheses Coll*. **1995**,72,112.

[233] Ma S; Lu X; Li Z. *J.Org. Chem. Commun*. **1992**, 57, 709.

[234] Ma S; Lu X. *J. Chem. Soc. Commun*, **1999**,1643

[235] Scotti F. and Frazza E.J., *J. Ame. Chem. Soc,***1968**, 29, 1800

[236] (a) Jones D. E., Morris R.O., Vernon C. A. and White R. F. M., I. *Chem. Soc*., **1960**, 2349; b) Jones D. E. and Vernon C., *Nature*, **1955**, 176, 791; C) Karel Topek, Vaclav Vsetecka and Milos Prochazka. *Collection Czech. techoslov. Chem. Commun.***1978**, 43,2395-2402.

[237] de Vries, B. *Chem. Ind. (London)*, **1962**, 1049-1050.

[238] Metternich J. B. and Gilmour R. *J. Am. Chem Soc.* **2015,** 137, 11254-11257.

[239] Paul J. Kropp, Edward J. Reardon, Jr., Zalman L. F. Gaibel, Kenny F. Williardy and James H. Hattaway, Jr. *J. Ame. Chem. Soc*. **1973**, 95, 7059.

[240] Christie, W.W., J. Chromatogr. **1988**, A, 454, 273-284.

[241] Kagan J.; Tolentino L., and Ettlinger M. G., *J. Org Chem*. **1975**, 40; 3085.

[242] a) Thole & Thorpe, *Annalen* **1912**, 101, 1739. b) Thorpe & Thole *Annalen*, **1912**, 101, 858, 861.

[243] Norman B and Thorpe J. F. ***J. Chem. Soc., Trans.,*****1912**,**101,** 871-891

[244] Pirkle W. H. and Dines M. *J. Heterocyclic Chemistry* **1969,** 6: 1-3.

[245] Fu, P.; Liu, P.; Qu, H.; Wang, Y.; Chen, D.; Wang, H.; Li, J.; Zhu, W. *J. Nat. Prod.***2011**, 74, 2219–2223.

[246] Bull J. E., Fitzgerald J.S.; Parker J.; Thorpe J. F. ***J. Chem. Soc.,*****1934**, 1653-1657.

[247] Kon G. A. R.; Nanji A. R. ***J. Chem. Soc.***, **1932**; **0**: 2426-2433.

[248] Biagetti M, Bellina F, Carpita A and Rossi R. *Tetrahedron Lett*. **2003**;44: 607-610.

[250] Lester R. M., Dickinson J. M., and Fairlamb I. J. S., *Bioorg. Med. Chem. Lett*. **2003**, 13, 12667.

[251] Fairlamb I. J. S., O'Brien C. T., Lin Z., and Lam K. C., *Org. Biomol. Chem*. **2006**, 4, 1213-1216.

[252] Fairlamb I. J. S., Lee A. F., Loe-Mie F. E. M., Niemela E. H., O'Brien C. T., and Whitwood C. A., *Tetrahedron* **2005**, 61, 9827-9838.

[253] Okuro, K.; Furuune, M.; Enna, M.; Miura, M.; Nomura, M. *J. Org. Chem.***1993**, 58, 4716.

[254] Gujadhur, R. K.; Bates, C. G.; Venkataraman, D. *Org. Lett*. **2001**, 3, 4315.

[255] Thathagar, M. B.; Beckers, J.; Rothenberg, G. *Green Chem*. **2004**, 6, 215.

[256] Ma, D, Liu, F. *Chem. Commun*. **2004**, 1934.

[257] a) Wang, Y. F.; Deng, W.; Liu, L.; Guo, Q. X. Chin. *Chem. Lett.***2005**, 16, 1197. b) Xie, Y.-X.; Deng, C.-L.; Pi, S.-F.; Li, J.-H.; Yin, D.-L. Chin*. J.*

Chem. **2006**, 24, 1290. C) LI j.-H, Li J.L, Wang D.-P, Pi S.-F, Xie Y.-X, Zhang M.-B and Hu X.-C. *J. Org. Chem*. **2007**, 72, 2053-2057.

[258] Li, J.-H.; Liu, W.-J. *Org. Lett.* **2004,** 6, 2809. (b) Li, J.-H.; Zhang, X.-D.; Xie, Y.-X. *Synthesis* **2005**, 804.

[259] Li, J.- H.; Hu, Q.-C.; Xie, Y.-X. *Tetrahedron Lett.* **2006**, 47, 9239.

[260] a) Li, J.-H.; Hu, X.-C.; Liang, Y.; Xie, Y.-X. *Tetrahedron* **2006**, 62, 31. b) J. F. Normant, Synthesis, 1972, 70.

[261] Akilandeswari L., Venuvanalingam P., *J. Theoretical and Computational Chem.* **2007**, 6, 233-243.

[262] Pirkle W. H., Turner W. V., *J. Org. Chem*. **1975**, 40, 1617.

[263] Birney D. M., *J. Org. Chem*. **1996**, 61, 243.

[264] a) Lemal D. *J. Am. Chem. Soc*. **1976**; 98:4325. B) Reva, I, Breda S, Roseiro T, Eusebio S, Fausto R, *J. Org. Chem.* **2005***,* 70, 7701-7710.

[265] Rainer K., Wong M. W., Wentrup C., *J. Org. Chem*. **1996**, 61, 6809-6813

[266] Fabian W. M. F., Bakulev V. A., Kappe C. O., *J. Org. Chem*. **1998**, 63, 5801-5805.

[267] Ross J. A., Seiders R. P., Lemal D. M., *J. Am. Chem. Soc.***1976**, 98, 4325-4327.

[268] Birney D. M., Ham S., Unruh G. R., *J. Am. Chem. Soc*. **1997,**

[269] Katzenellenbogen J., A., Roopa R., and Wei D., Bioorg. Med. Chem. Lett.,1992; 2: 1399-1404.

[270] Suguna K., Bottt R. R., Padlan E. A., E. Sheriff E. S. S, Gerson H. Cohen G. H., and Davies D. R., J. Mol. Biol.1987; 196: 877-900.

[271] a) Baker E. N., Hubbard, R. E., *Prog. Biophys. Mol. Biol.***1984**; 44: 97-179. B) Tang J. and Wong R. N. S. *J. Cellular Biochem*., **1987**; 33: 53-63.

[272] Enrico Di Cera. *IUBMB Life*. **2009**; 61: 510–515. b) Page M. J., Di Cera E. *Cell Mol. Life Sci*. **2008**; 65: 1220–1236.

[273] Almeida, P. C., Nantes, I. L., Rizzi, C. C., Judice, W. A., Chagas, J. R., Juliano, L., et al. *J. Biol. Chem.***1999**; 274: 30433–30438.

[274] a) Chieh Chang and Zena Werb. *Trends Cell Biol*. **2001**; 11: S37–S43. b) Vladimir Pelmenschikov and Per E. M. Siegbahn. *Inorg. Chem.***2002**; 41: 5659−5666. c) Ugalde, A. P.; Ordoń˜ ez, G. R.; Quiros, P. M.; Puente, X. S.; Lopez Otin, C. *Methods Mol. Biol*. **2010;** 622: 3.

[275] Steinmetzer, T.; Stuerzebecher, *J. Curr. Med. Chem*. **2004**, 11, 2297.

[276] Tanaka, K. A.; Key, N. S.; Levy, J. H. *Anaesth. Anal*. **2009**, 108, 1433.

[277] Hedstrom, L. *Chem. Rev*. **2002**, 102, 4501

[278] Chen, K. X.; Njoroge, F. G. *Curr. Opin. Invest. Drugs***2009**, 10, 821.

[279] Froelich, C. J.; Pardo, J.; Simon, M. M. *Trends Immunol*. **2009**, 30, 117

[280] Powers, J. C.; Asgian, J. L.; Ekici, O. D.; James, K. E. *Chem. Rev.***2002**, 102, 4639−4750.

[281] Boger, D. L.; Sato, H.; Lerner, A. E.; Austin, B. J.; Patterson, J. E.; Patricelli, M. P.; Cravatt, B. F*. Bioorg. Med. Chem. Lett.***1999**; 9: 265− 270.

[282] Koutek, B.; Prestwich, G. D.; Howlett, A. C.; Chin, S. A.; Salehani, D.; Akhavan, N.; Deutsch, D. G. *J. Biol. Chem.***1994**; 269: 22937−22940.

[283] a) Colombano G., Albani C., Ottonello G., Alison Ribeiro A., Scarpelli R., Tarozzo G., Daglian J., Jung K. M., Piomelli D., Bandiera T., *ChemMedChem* **2015**; *10*: 380-395. b) Otrubova, K.; Boger, D. L*. ACS Chem. Neurosci*. **2012**; 3: 340− 348.

[284] Parisi, M., and Abeles, R., *Biochemistry* **1992***; 31*: 9429.B) Cravatt, B. F.; Lerner, R. A.; Boger, D. L. *J. Am. Chem. Soc.***1996**; 118: 580−590.

[285] Kostka, V., and Carpenter, F., *J Biol Chem* **1964***; 239*: 1799. B) Patterson, J. E.; Ollmann, I. R.; Cravatt, B. F.; Boger, D. L.; Wong, C. H.; Lerner, R. A. *J. Am. Chem. Soc.***1996**; 118: 5938−5945.

[286] Powers, F., and Carroll, D., *Biochem Biophys Res Commun.* **1975***;* 67: 639.

[287] Alexander, J.P. and Cravatt, B.F. *Chem. Biol.* **2005**; 12: 1179–1187.

[288] Bottcher, T.; Sieber, S. A. *Angew. Chem., Int. Ed.* **2008**; 47: 4600−4603.

[289] a) Hoover, H. S.; Blankman, J. L.; Niessen, S.; Cravatt, B. F. *Bioorg. Med. Chem. Lett.***2008**; 18: 5838−5841. B) Kezdy, F., and Bender, M., *J Am Chem Soc* **1964***; 86*: 937.

[290] Boger, D. L.; Sato, H.; Lerner, A. E.; Hedrick, M. P.; Fecik, R. A.; Miyauchi, H.; Wilkie, G. D.; Austin, B. J.; Patricelli, M. P.; Cravatt, B. F. *Proc. Natl. Acad. Sci. U. S. A*. **2000**; 97: 5044−5049.

[291] Boger, D. L.; Miyauchi, H.; Hedrick, M. P. *Bioorg. Med. Chem. Lett*. **2001**; 11: 1517−1520.

[292] Anne F. Kornahrens, Armand B. Cognetta III, Daniel M. Brody, Megan L. Matthews, Benjamin F. Cravatt, and Dale L. Boger. *J. Am. Chem. Soc.* **2017**; 139: 7052−7061.

[293] Bachovchin, D. A.; Ji, T.; Li, W.; Simon, G. M.; Blankman, J. L.; Adibekian, A.; Hoover, H.; Niessen, S.; Cravatt, B. F. *Proc. Natl. Acad. Sci. U. S. A*. **2010**; 107: 20941−20946.

[294] Li, W.; Blankman, J. L.; Cravatt, B. F. *J. Am. Chem. Soc*. **2007**; 129: 9594−9595.B) Neumann U., Schechter M. N., Gütschow M., *Bioorg. Med. Chem.* **2001**; 9: 947-954.

[295] Antanasijevic A., Ramirez B., and Caffrey M., *J Biomol NMR*. **2014**; 60: 37–44.

[296] Mayer M, Meyer B. *J Am Chem Soc*. **2001**; 123: 6108–6117.

[297] Venkitakrishnan R. P., Benard O., Max M., and Markley J. L., *Methods Mol Biol.* **2012**; 914: 47–63.

[298] Corey E. J., and Streith J., *J. Amer. Chem. Soc*., **1964**; 86; 950.

[299] Ringe D, Seaton BA, Gelb MH, Abeles RH. *Biochemistry.* **1985**; 24: 64-8.

[300] Boulanger W. A., Katzenellenbogen J. A., *J Med Chem*. **1986** A; 29: 1483-7.

[301] Lee S. L., Alexander R. S., Smallwood A., Trievel R., Mersinger L, Weber P. C., Kettner C., *Biochemistry*. **1997**; 36: 13180-6.

[301] Huang R., Bonnichon A., Claridge T. D. W., Leung I. K. H., *Sci Rep*. **2017**; 7: 43727.

[302] Hayes C. E., Edelstein W. A., Schenck J. F., Mueller O. M., Eash M., *J. Magn. Reson.* **1985***;* 63: 622–628.

[303] Mugler J. P., 3rd, Driehuys B., Brookeman J. R., Cates G. D., Berr S. S., Bryant R. G., Daniel T. M., de Lange E. E., *et al.*, *Magn Reson Med*. **1997**; 37: 809-15.

[304] Theis T., Ganssle P., Kervern G., Knappe S., Kitching J., Ledbetter M.P, Budker D., Pines A. *Nature Physics* **2011**; 7: 571-575.

[305] Dana Schleyer, Heiko G. Niessen and Joachim Bargon. *New J. Chem.,* **2001**, 25, 423-426.

[306] Hu S, P.E. Larson, M. Vancriekinge, A.M. Leach, I. Park, C. Leon, J. Zhou, P.J. Shin, G. Reed, P. Keselman, C. von Morze, H. Yoshihara, R.A. Bok, S.J. Nelson, J. Kurhanewicz, D.B. Vigneron, *Magn. Reson. Imaging* 2013; 31: 490–496.

[307] Yoshihara H. A. I., Can E., Karlsson M., Lerche M. H., Schwitter J., A. Comment, High-field dissolution dynamic nuclear polarization of [1-^{13}C]pyruvic acid, in: 4th Intl. Workshop on Hyperpolarized Carbon-13 and Its Applications in Metabolic Imaging (2016, Philadelphia, PA, USA).

[308] Nelson SJ, Kurhanewicz J, Vigneron DB, Larson PE, Harzstark AL, Ferrone M, van Criekinge M, Chang JW, Bok R, Park I, et al. *Sci Transl Med.* **2013**;5 198-208.

[309] Golman K, Zandt RI, Lerche M, Pehrson R, Ardenkjaer-Larsen JH. *Cancer Res.* **2006**; 66: 10855–10860.

[310] Merritt ME, Harrison C, Storey C, Jeffrey FM, Sherry AD, Malloy CR. *Proc Natl Acad Sci U S A*. 2007;104:19773–19777.

[311] Yang C., Harrison C., Jin E. S., Chuang D. T., Sherry A. D., Malloy C. R., Merritt ME, DeBerardinis R. J., *J Biol Chem*. **2014a**; 289: 6212–6224.

[312] Gallagher FA, Kettunen MI, Hu D-E, Jensen PR, Karlsson M, Gisselsson A, et al. *Proc Natl Acad Sci U S A*. **2009**; 106: 19801–6.

[313] Chen A. P., Kurhanewicz J., Bok R., Xu D., Joun D., Zhang V., Nelson S. J., Hurd R. E., Vigneron D. B., *Magn Reson Imaging* **2008**; 26: 721–726.

[314] Gallagher F. A., Kettunen M. I., Day S. E., Lerche M., Brindle K. M., *Magn Reson Med.* **2008**; 60:253–7.

[315] Rodrigues T. B., Serrao E. M., B.W.C. Kennedy B. W. C., Hu D.-E; Kettunen M. I., Brindle K. M., *Nat. Med*. **2014**; 20: 93–97.

[316] Bouguet-Bonnet S˙, Reineri F., Canet D., *J. Chem. Phys*. **2009**;130: 234507.

[317] Buljubasich L., Franzoni M. B., and Mu¨nnemann K., *Top Curr Chem.* **2013**; 338: 33–74.

[318] Mata J. F., Altes T. A., Cai J., Ruppert K., Mitzner W., Hagspiel K. D., Patel B., Salerno M., Brookeman J. R., de Lange E. E., *J. Appl. Physiol.* **2007**; 102:1273–1280.

[319] Bhattacharya P., Chekmenev E. Y., Perman W. H., Harris K. C., Lin A. P., Norton V. A., Tan C. T., Ross B. D., and Weitekamp D. P., *J. Magn. Reson.* **2007**; 186: 150-155.

[320] Pravica M. G., and Weitekamp D. P., *Chem. Phys. Lett*. **1988**; 145; 255-258.

[321] Bowers C. R., and Weitekamp D. P., *J. Am. Chem. Soc*. **1987**; 109: 5541-5542.

[322] Kuhn L. T., and Bargon J., *Top. Curr. Chem.* **2007**; 276; 25-48.

[323] Adams R. W., Duckett S. B., Green R. A., Williamson D. C., and Green G. G., *J. Chem. Phys.* **2009**; 131:194505.

[324] Duckett S. B, and Mewis R. E. *Acc. Chem. Res*., **2012**; 45: 1247-1257

[325] Adams R. W., Aguilar J. A., Atkinson K. D., Cowley M. J., Elliott P. I., Duckett S. B., Green G. G., Khazal I. G., Lopez-Serrano J., and Williamson D. C., *Science* **2009**; 323: 1708–1711.

[326] Atkinson K. D., Cowley M. J., Elliott P. I., Duckett S. B., Green G. G., Lopez-Serrano J., and Whitwood A. C., *J. Am. Chem. Soc.* **2009**; 131: 13362–13368.

[327] Green R. A., Adams R. W., Duckett S. B., Mewis R. E., Williamson D. C., Green G. G. R., *Progress in Nucl Magn Reson Spectros.* **2012**; 67: 1–48.

[328] Wood N. J., Brannigan J. A., Duckett S. B., Heath S. L., and Wagstaff J. *J. Am. Chem. Soc*. **2007**; 129: 11012-11013.

[329] Gong Q., Gordji-Nejad A., Blumich B., and Appelt S., *Anal. Chem*. **2010**; 82: 7078-7082.

[330] Viale A., and Silvio A., *Current Opinion in Chemical Biology*, **2010**;

[331] Du¨wel S, Hundshammer C, Gersch M, Feuerecker B, Steiger K, Achim Buck A, Walch A, Haase A, et al., *Nat Commun* **2017**; 8: 15126.

[332] Mayer D, Levin Y, Hurd R, Glover G, Spielman D. *Magn. Reson. Med.* **2006**; 56: 932–7.

[333] Mayer D, Yen YF, Levin YS, Tropp J, Pfefferbaum A, Hurd RE, et al. *J. Magn. Reson.* **2010**; 204: 340–5.

[334] Schulte R, Wiesinger F, Fish K, Whitt D, Hancu I. *Magn. Reson. Med.* **2009**; 17: 2433.

[335] a) Gutte H., Hansen A. E., Larsen M. E., Rahbek S., Henriksen S.T., Johannessen H. H., Ardenkjaer-Larsen J., Kristensen A. T., Hojgaard L., and Kjaer A., *J. Nucl. Med.***2015**; 56:1786-1792. b) Golman K, Zandt I. R., Lerche M., Perhson R., Ardenkjaer-Larsen H., *Cancer Res.* **2006**; 66: 10855-10860.

[336] Menzel M. I., Farrell E. V., Janich M. A., Khegai O., Wiesinger F., Nekolla S., Otto A. M., Haase A., Schulte R. F., Schwaiger M., *J. Nucl. Med*. **2013**; 54: 1113–1119.

[337] Chekmenev E. Y., Hovener J., Norton V. A., Harris K., Batchelder L. S., Bhattacharya P., Ross B. D., and Weitekamp D. P., *J. Am. Chem. Soc.* **2008**; 130: 4212–4213.

[338] a) Bowers C. R., and Weitekamp D. P., *Phys. Rev. Lett.* **1986**; 57; 2645–2648. b) Bowers C. R., and Weitekamp D. P., *J. Am. Chem. Soc.* **1987**; 109, 5541–5542.

[339] Eisenberg, R.; Eisenschmid, T. C.; Chinn, M. S.; Kirss, R. U. Homogeneous Transition Metal Catalyzed Reactions; Moser, W. R., Slocum, D. W., Eds.; Advances in Chemistry 230; Washington, DC, **1992**; 45- 74.

[340] a) Eisenberg R. *Acc. Chem. Res*. **1991**,24, 110-116.b) Eisenschmid, T. C.; Kirss, R. U.; Deutsch, P. P.; Hommeltoft, S. I.; Eisenberg, R.; Bargon, J.; Lawler, R. G.; Balch, A. L. *J. Am. Chem. Soc.***1987**,109,8089.

[341] Zach Serber, Christian Richter, Detlef Moskau, Jean-Marc Bo¨hlen, Tobias Gerfin, Daniel Marek, Markus Ha¨berli, Ludivica Baselgia, Frank Laukien, and Alan S. Stern, Jeffrey C. Hoch, and Volker Do¨tsch, *J. Am. Chem. Soc*. **2000**, 122, 3554-3555

[342] Kurhanewicz j., Bok R., Nelson S. J., and Vigneron D. B., *J Nucl Med*. **2008**; 49: 341–344.

[343] [a] Ardenkjaer-Larsen J. H., Fridlund B., Gram A., Hansson G., Hansson L., Lerche M. H., Servin R., Thaning M. and Golman K., *PNAS* **2003**; 100: 10158-10163. [b] Golman K., Zandt R., and Thaning M., *Cancer Res.* **2006**; 66: 10855-10860. All in. Wilson D. M., R. E. Hurd R. E., Chen A. P., Van Criekinge M., Keshari K., Nelson S. J., Vigneron D. B., and Kurhanewicz J., *Proc. Intl. Soc. Mag. Reson. Med.* **2009**; 17: 538.

[344] a) Goldman M. *J. Magn. Reson.* **2001**; 149:160-187. b) Goldman M, Jóhannesson H, Axelsson O, and Karlsson M., *Magn. Reson. Imaging* **2005**; 23: 153–157.

[345] Aguilar J. A., Elliott P. I. P., López-Serrano J., Adams R. W., and Duckett S. B., Chem. Commun., 2007,0, 1183-1185

[346] Tang J. A., Gruppi F., Fleyser R., Sodickson D. K., Canary J. W., and Jerschow A., *Chem. Commun*. **2011**; 47: 958.

[347] Aguilar J. A., Adams R. W., Duckett S. B., Green G. G. R., and Kandiah R. J. *J. Magn. Reson*. **2011**; 208; 49.

[348] Falagas M. E., and Karageorgopoulous D. E., *Lancet* **2010**, 375: 248-251.

[349] Sukerkar PA, MacRenaris KW, Townsend TR, Ahmed RA, Burdette JE, and Meade TJ. *Bioconjugate Chem*., **2011**, 22,2304-2316.

[350] Deng L, Mikosova K., Robuck K., Scherman M., Brennan P. J., and McNeil M. R., *Antimicrob Agents Chemother*; **1995**; 39, 694 701.

[351] Ramaswamy S. V., Amin A. G., Goksel S., Stager E. C., Dou S.-J., El Sahly H., Moghazeh S. L., Kreiswirth B. N., and Musser J. M., *Antimicrob. Agents Chemother*. **2000**; 44, 326 36.

[352] Escuyer V. E., Lety M.-A., Torrelles J. B., Khoo K.-H., Rithner C. D., McNeil R. M., Brennan P. J., and Chatterjee D., *J Biol Chem* **2001**; 276, 48854 62.

[353] Berg S., Starbuck J., Torrelles J. B., Vissa V. D., Crick C. D., Chatterjee D., and Brennan P. J., *J Biol Chem* **2005**; 280, 5651-63.

[354] Dong CC; Styring P; Goodby JW, Chan LKM. *J. Mater. Chem*. **1999**; 9: 1669- 1677.

[355] Li Jun-Zhung, Shi-Ming Fan, Xuan-Fei and Shouxin Liu. *RSC Adv*., **2016,** 6, 1865.

[356] Ridvan L and Zavada J. *Tetrahedron* **1997**, 53, 14793-14806.

[357] Kolb N. and Michael A. R. Meier. *Green Chemistry*. **2012**, 14, 2429.

[358] Hewlins SA; Murphy JA; Lin J; Hibbs DE, Hursthouse MB. *J. Chem. Soc. Perkins Trans.* 1, **1997**;1559-1568.

[359] Sigma Adrich FT ^{13}C and ^{1}H-NMR data Library.

[360] MacInnes L, Schorstein DE and Suckling CJ, *J. Chem. Soc., Perkin Trans. I*, **1981**, 1103. E.

[361] Karel Topek, Vaclav Vsetecka and Milos Prochazka. *Collection Czech. techoslov. Chem. Commun.***1978**, 43,2395-2402.

[362] **I**tzia I. Padilla-Martinez, Irma Y. Flores-Larios, Efren V. García-Baez 1, Jorge Gonzalez, Alejandro Cruz and Francisco J. Martínez-Martinez, *Molecules* **2011**, *16*, 915-932; doi:10.3390/molecules16010915

[363] Sheena Y. Mary, Yohannan C. Panicker and Hema Tresa Varghese. *Oriental Journal of Chemistry* **2012**, 28, 1071-1075.